

## **ON-FOOD TECHNOLOGIES FOR IMPROVEMENTS IN FOOD SAFETY**

BIOACTIVE SYSTEMS FOR REAL-TIME FOOD QUALITY MONITORING AND  
PRESERVATION TO IMPROVE FOOD SAFETY AND REDUCE WASTE

BY SHADMAN KHAN  
B.H.Sc. (McMaster University, 2020)

A Thesis Submitted to the School of Graduate Studies in Partial Fulfilment of the Requirements  
for the Degree Doctor of Philosophy in Biomedical Engineering

McMaster University © Copyright by Shadman Khan, June 2024

McMaster University, Doctor of Philosophy (2024) Hamilton, Ontario (Biomedical Engineering)

**TITLE:** Bioactive Systems for Real-Time Food Quality Monitoring and Preservation to Improve Food Safety and Reduce Waste

**AUTHOR:** Shadman Khan, Bachelor of Health Sciences in Biomedical Discovery and Commercialization (McMaster University, 2020)

**SUPERVISOR:** Dr. Tohid Didar

**NUMBER OF PAGES:** 296

## Lay Abstract

With global food insecurity at crisis levels, the need for smart food technologies that offer improvements in food safety and reduce food waste is pronounced. Contamination monitoring, spoilage monitoring, and food decontamination represent three key mechanisms through which impact can be enacted in this space. In this dissertation, platforms that offer breakthroughs across all three of these avenues are presented. First, the sensing-relevant fluorescence properties of contamination-prone foods are assessed to inform the design of fluorescence-based detection platforms. These findings are applied towards contamination monitoring, where improvements are afforded by a novel food packaging system that facilitates the in-package sensing activity of any integrated optical sensor. The platform is validated using a newly developed *Salmonella* sensor, yielding completely hands-free, in-package sensing of the high-risk pathogen using a handheld reader and smartphone. Contrarily, efforts to improve spoilage monitoring took a consumer-centric approach, yielding an inexpensive, pH-responsive, colorimetric spoilage sensor for at-home use. The sensing platform can be employed as either a real-time food monitoring platform applied to sealed food packaging, or as a rapid test to evaluate food quality before consumption. With regards to food decontamination, a platform to facilitate bacteriophage delivery into the interior matrices of contamination-prone foods is presented. Finally, insights gathered through the technical, commercial, and regulatory engagements performed as a part of this dissertation are summarized into a situational assessment seeking to guide future works in the smart food technology space.



## Abstract

Despite extensive mitigative efforts, foodborne illness and food waste continue to impose significant burdens on both human health and on the economy. While technical efforts seeking to develop breakthrough technologies that improve food safety and reduce waste have been reported extensively in literature, real-world translation has been limited. Recognizing that contamination monitoring, spoilage monitoring, and food decontamination represent some of the most promising mechanisms for improvement, this dissertation details the development of technologies that meet each of these three objectives. Importantly, real-time monitoring efforts were all enacted through optical biosensing to ensure high real-world applicability. Accordingly, contamination-prone food products were first subjected to extensive fluorescence assessment to evaluate sensing-relevant properties that stand to educate sensor design. To this end, optical fluorophores for target food products were identified. These findings were then applied towards the development of a fluorescent nucleic acid probe (fNAP) surface sensor, as a tool for contamination monitoring. To actualize the in-package integration of this sensor, a revolutionary packaging technology was developed. The system addressed long-standing barriers in in-package food sampling and sensing reagent integration. By combining our fNAP sensor and packaging technologies, we demonstrated  $10^3$  CFU/g detection of *Salmonella* in sealed whole chicken products in a completely hands-free, real-time manner. Alongside its high specificity and stability, the platform showed effective readout *via* a handheld fluorescence reader paired with a smartphone, suggesting grocer-level use of the system. On the other hand, the development of an effective spoilage monitoring technology was enacted on a consumer-level through the development of an inexpensive, colorimetric pH-based spoilage sensor, validated using fish. The system embeds food-safe, pH-responsive sensing agents inside environment-responsive microneedles. These microneedles offer strong baseline mechanical properties that switch to hydrogel-like properties upon exposure to fluid-rich environments. When applied to sealed fish products for real-time monitoring, non-destructive penetration through packaging films was followed by hydrogel form enactment by the fluid-rich fish matrix. This transition triggered sensing activity. A defined shift from purple to blue reliably signaled spoilage in proof-of-concept studies. Moreover, the increased surface area afforded by the microneedles was employed towards rapid testing of opened fish products that had already spoiled. Here, colorimetric spoilage detection occurred within 45 minutes. Finally, food decontamination efforts sought to deliver bacteriophages into fluid-rich food products with difficult-to-permeate surface layers – such as fruit and skin-containing meat products. This marked the first effort to actively deliver bacteriophages into interior food matrices. Extensive on-food microneedle material characterization was used to identify the optimal base material. These microneedles were loaded with *E.coli*-targeting bacteriophages and applied onto contaminated ready-to-eat chicken breasts. The microneedles yielded a nearly 3-log improvement in target reduction compared to flat patches used to deposit bacteriophages onto the product's surface. Collectively, this dissertation presents several breakthrough on-food technologies that take unconventional approaches towards improving food safety and food waste. Experiences from operating in the smart food space were summarized into an assessment to guide future works.

## Acknowledgements

First, I would like to recognize my supervisor, Dr. Tohid Didar. Since the moment I approached him as an undergraduate student in 2019, he has provided me with unwavering guidance and support. He has taken every opportunity to mentor me in both my academic and professional journeys. Moreover, he has done his best to always push me to “focus” and truly shoot for the stars. My progress to date as a researcher would not be possible without him.

I would like to thank my committee members Dr. Carlos D.M. Filipe and Dr. Leyla Soleymani. Dr. Filipe has greeted me with pure joy and excitement at every opportunity, giving me the motivation to keep pushing on the toughest of days. His mentorship throughout my doctoral degree has been instrumental, pushing me to always think about real-world impact in my work. Dr. Leyla Soleymani’s guidance has also been foundational, teaching me the importance of critically assessing my work at every step. I would also like to thank Dr. Yingfu Li and Dr. Zeinab Hosseinidoust for their support at various stages throughout my degree.

I would like to recognize current and former lab colleagues. Dr. Amid Shakeri, Dr. Noor Abu Jarad, Akansha Prasad, Hannah Mann, Liane Ladouceur, Dr. Roderick Maclachlan, Kyle Jackson, Jimmy Gu, Jonathan Monteiro, Fatima Arshad, and Mahum Javed, thank you for both your technical support and friendship throughout this degree. The work presented in this dissertation would not have been possible without all of your contributions.

On a personal level, I would first and foremost like to acknowledge my parents, Jabid and Monowara. You have sacrificed every one of your dreams to give me the opportunities you did not have. I am eternally grateful for everything you two have done and continue to do for me. To my brother, Rayan, having you as my “infinity friend” will always be my greatest honour and I am forever grateful for the bond we have. To my best friends, Omaiike Sikder and Nikhil Nair, the friendship we have built over the past eight years has been beyond my wildest dreams. I am beyond grateful for the personal and professional support you have offered me. I am also looking forward to adding medical support to this list, as you become my two favourite MDs. To my friend, Mahum Javed, I am grateful for the comfort and support you have always given me, especially during some of the toughest periods of my life. To my friend, Misha Khawaja, I thank you for the never-ending laughter, support, and reassurance you have brought into my life.

Finally, I am grateful to God.

“With hardship comes ease” [94:7]. This promise from God has inspired me to persevere through many difficult times. As I appreciate the completion of this dissertation, I recognize that this was only possible through His will.

## Table of Contents

<b>LAY ABSTRACT .....</b>	<b>4</b>
<b>ABSTRACT .....</b>	<b>5</b>
<b>ACKNOWLEDGEMENTS.....</b>	<b>6</b>
<b>LIST OF FIGURES .....</b>	<b>10</b>
<b>LIST OF TABLES.....</b>	<b>16</b>
<b>LIST OF ABBREVIATIONS .....</b>	<b>17</b>
<b>DECLARATION OF ACADEMIC ACHIEVEMENT .....</b>	<b>18</b>
<b>CHAPTER 1: INTRODUCTION.....</b>	<b>19</b>
1.1    FOODBORNE ILLNESS AND FOOD WASTE.....	19
1.2    FOOD INEDIBILITY: CURRENT MEASURES FOR DETECTION AND REDUCTION .....	20
1.2.1 <i>Food contamination</i> .....	20
1.2.2 <i>Food spoilage</i> .....	21
1.3    APPROACHES TOWARDS IMPROVING FOOD SAFETY AND REDUCING FOOD WASTE.....	22
1.3.1 <i>Developments in contamination monitoring</i> .....	23
1.3.2 <i>Developments in spoilage monitoring</i> .....	24
1.3.3 <i>Developments towards food decontamination</i> .....	25
1.4    MOTIVATION .....	26
1.5    RESEARCH OBJECTIVES .....	28
1.6    THESIS OVERVIEW .....	32
<b>CHAPTER 2: MATERIAL BREAKTHROUGHS IN SMART FOOD MONITORING: INTELLIGENT PACKAGING AND ON-SITE TESTING TECHNOLOGIES FOR SPOILAGE AND CONTAMINATION DETECTION.....</b>	<b>34</b>
2.1    ABSTRACT .....	35
2.2    INTRODUCTION .....	35
2.3    SUBSTRATE MATERIALS FOR SMART FOOD SENSING PLATFORMS .....	39
2.3.1 <i>Metallic substrates</i> .....	40
2.3.2 <i>Polymeric substrates</i> .....	43
2.3.3 <i>Carbon-based substrates</i> .....	44
2.4    MATERIAL DEVELOPMENTS IN SMART FOOD SENSING PLATFORMS .....	45
2.4.1 <i>Biogenic amine monitoring</i> .....	45
2.4.2 <i>pH monitoring</i> .....	60
2.4.3 <i>Pathogen monitoring</i> .....	75
2.5    SITUATIONAL ASSESSMENT AND FUTURE DIRECTIONS.....	90
2.5.1 <i>Technical assessment and future directions for food spoilage monitoring</i> .....	90
2.5.2 <i>Technical assessment and future directions for pathogen monitoring</i> .....	93
2.5.3 <i>Regulatory considerations</i> .....	96
2.5.4 <i>Commercial considerations</i> .....	97
2.6    ACKNOWLEDGEMENTS .....	100
2.7    TABLES .....	101
<b>CHAPTER 3: DNAZYME-BASED BIOSENSORS: IMMOBILIZATION STRATEGIES, APPLICATIONS AND FUTURE PROSPECTIVE .....</b>	<b>108</b>

3.1	ABSTRACT .....	109
3.2	INTRODUCTION .....	109
3.3	DNAZYME IMMOBILIZATION STRATEGIES FOR BIOSENSING .....	112
3.3.1	<i>Covalent immobilization .....</i>	<i>113</i>
3.3.2	<i>Non-covalent immobilization .....</i>	<i>119</i>
3.4	DNAZYME APPLICATIONS IN BIOSENSING .....	128
3.4.1	<i>Detection of contaminants within food .....</i>	<i>129</i>
3.4.2	<i>Pathogen detection in biological samples .....</i>	<i>135</i>
3.4.3	<i>Heavy metal detection within water and the environment .....</i>	<i>137</i>
3.4.4	<i>Detection of clinically relevant biomarkers .....</i>	<i>141</i>
3.4.5	<i>Detection of cancer markers .....</i>	<i>145</i>
3.5	FUTURE DIRECTIONS .....	149
3.6	ACKNOWLEDGEMENTS .....	151
3.7	TABLES .....	153
<b>CHAPTER 4: COMPREHENSIVE FLUORESCENCE PROFILES OF CONTAMINATION-PRONE FOODS APPLIED TO THE DESIGN OF MICROCONTACT-PRINTED <i>IN SITU</i> FUNCTIONAL OLIGONUCLEOTIDE SENSORS .....</b>		<b>161</b>
4.1	ABSTRACT .....	163
4.2	INTRODUCTION .....	163
4.3	RESULTS AND DISCUSSION.....	167
4.3.1	<i>Establishing the fluorescence profiles of target food products .....</i>	<i>168</i>
4.3.2	<i>Monitoring changes in fluorescence profiles over product lifespans .....</i>	<i>170</i>
4.3.3	<i>Assessing fluorophore-biomolecule conjugate visibility on food backgrounds .....</i>	<i>172</i>
4.3.4	<i>Stability and functionality of microcontact printed fNAPs .....</i>	<i>176</i>
4.4	CONCLUSION .....	180
4.5	MATERIALS AND METHODS .....	181
4.6	ACKNOWLEDGEMENTS .....	185
4.7	SUPPLEMENTARY INFORMATION .....	186
<b>CHAPTER 5: ADVANCING <i>IN SITU</i> FOOD MONITORING THROUGH A SMART LAB-IN-A-PACKAGE SYSTEM DEMONSTRATED BY THE DETECTION OF SALMONELLA IN WHOLE CHICKEN.....</b>		<b>188</b>
5.1	ABSTRACT .....	190
5.2	INTRODUCTION .....	190
5.3	RESULTS AND DISCUSSION.....	193
5.3.1	<i>Lab-in-a-Package platform design .....</i>	<i>193</i>
5.3.2	<i>Test sample localization optimization .....</i>	<i>194</i>
5.3.3	<i>Absorption and diffusion-focused materials characterization.....</i>	<i>195</i>
5.3.4	<i>S. Typhimurium sensor development.....</i>	<i>199</i>
5.3.5	<i>Proof-of-concept testing of sensor-embedded packaging platform .....</i>	<i>202</i>
5.4	CONCLUSION .....	206
5.5	MATERIALS AND METHODS .....	208
5.6	ACKNOWLEDGEMENTS .....	214
5.7	SUPPLEMENTARY INFORMATION .....	216
<b>CHAPTER 6: FOOD-ACTIVATED, SPOILAGE SENSING MICRONEEDLES FOR REAL-TIME, CONSUMER-DIRECTED MONITORING OF PACKAGED FISH .....</b>		<b>223</b>
6.1	ABSTRACT .....	225
6.2	INTRODUCTION .....	225

6.3	RESULTS AND DISCUSSION.....	229
6.3.1	<i>Dehydrated gelatin microneedle fabrication and characterization.....</i>	229
6.3.2	<i>Anthocyanin integration and optimization.....</i>	234
6.3.3	<i>Analysis and testing of spoilage-sensing microneedles .....</i>	235
6.4	CONCLUSION .....	240
6.5	MATERIALS AND METHODS .....	241
6.6	ACKNOWLEDGEMENTS .....	244
<b>CHAPTER 7: ANTIMICROBIAL BACTERIOPHAGE-LOADED MICRONEEDLE PATCHES THAT COUNTERACT BACTERIAL PATHOGEN CONTAMINATION TO PREVENT FOODBORNE ILLNESS</b>		<b>245</b>
7.1	ABSTRACT .....	247
7.2	INTRODUCTION .....	247
7.3	RESULTS AND DISCUSSION.....	251
7.3.1	<i>Bacteriophage-loaded microneedles overview .....</i>	251
7.3.2	<i>Baseline microneedle material performance assessment.....</i>	251
7.3.3	<i>Comparison of microneedle materials for food-specific applications .....</i>	255
7.3.4	<i>Bacteriophage integration onto PMMA microneedles and system characterization.....</i>	258
7.4	CONCLUSION .....	260
7.5	MATERIALS AND METHODS .....	261
7.6	ACKNOWLEDGEMENTS .....	266
<b>CHAPTER 8: SMART FOOD PACKAGING COMMERCIALIZATION .....</b>		<b>267</b>
8.1	STANDFIRST .....	268
8.2	INTRODUCTION .....	268
8.3	TECHNICAL CHALLENGES.....	268
8.4	COMMERCIAL CHALLENGES .....	269
8.5	OPPORTUNITIES FOR IMPACT.....	270
<b>CHAPTER 9: CONCLUSION.....</b>		<b>273</b>
9.1	THESIS SUMMARY .....	273
9.2	THESIS CONCLUSIONS .....	274
9.3	CONTRIBUTIONS TO THE FIELD .....	278
9.4	FUTURE WORKS .....	282
9.5	FINAL REMARKS .....	284
<b>REFERENCES.....</b>		<b>285</b>

## List of Figures

<b>Figure 2.1. Current state of food spoilage and food contamination.</b> (a) Schematic illustration of food spoilage. (b) Key contributors to food spoilage and their impact on the organoleptic properties of food. (c) Schematic illustrations of the food contamination timeline, and stages at which pathogenic contamination can occur. (d) Annual global illness rates caused by respective pathogens obtained from the World Health Organization. Regulatory limits as defined by the Food and Drug Administration for ready-to-eat (RTE) products. <sup>[17,18]</sup> Infectious dose recorded in literature. Produced using BioRender. ....	38
<b>Figure 2.2. Commonly used substrate materials for food monitoring.</b> (a) Materials used as substrates within food sensors. (b) Summary of relevant properties and use cases of common substrate materials. Primary application refers to situations in which the described material is most commonly applied but should not be considered all-encompassing. Produced using BioRender. ....	41
<b>Figure 2.3 Strategies to detect biogenic amine accumulation in food.</b> (a) Structures of common biogenic amines produced during food spoilage. (b) Interactions that mediate the detection of biogenic amines. (c) Mechanisms for signal transduction in response to biogenic amine binding: (i) colorimetric nanoparticle aggregation, (ii) fluorescence shifts within metal-organic framework, and (iii) signal-inducing conformational changes within probes. Produced using BioRender. ....	50
<b>Figure 2.4. Intelligent monitoring of pH changes in food.</b> (a) Opposing pH changes in different subtypes of foods, mediated by distinct processes. (b) Anthocyanins, the predominant organic food dye used in pH-mediated monitoring of food spoilage, undergo chemical reactions that result in dramatic colour shifts. (c) Various organic materials used to derive intelligent pH-monitoring films, and parameters for optimization to enhance performance in situ. Produced using BioRender. ....	62
<b>Figure 2.5. Physical properties of intelligent pH-responsive films used to monitor spoilage.</b> (a) Common modifications made to films that alter their mechanical and thermal stability, including: (i) the addition of hydrophilic and (ii) anionic compounds to facilitate cross-linking of film materials, (iii) nano-encapsulation of pigments to increase long-term stability and prevent heat- or light-mediated degradation, and (iv) nanofillers that increase film density and strength. (b) A comparison of the properties of different pH-responsive organic dyes used in intelligent packaging. Produced using BioRender. ....	68
<b>Figure 2.6. Biorecognition probes used for on-site pathogen detection and in situ food monitoring.</b> (a) The common types of probes that are used to identify bacteria – antibodies, bacteriophages, DNAzymes, and aptamers. (b) Various probe-based strategies to detect bacterial contamination, including: (i) phage-mediated identification, transduced via amperometric monitoring of target-binding, or phage replication-induced resonant frequency shifts, (ii) aptamer-mediated recognition and resultant nanoparticle aggregation, (iii) DNAzyme-mediated detection, resulting in fluorescence changes, and (iv) antibody-based recognition, inducing colorimetric transduction via the use of dye-loaded, antibody-gated liposomes integrated into microneedles. Produced using BioRender. ....	76
<b>Figure 2.7. Material strategies for the improvement of foodborne pathogen sensors.</b> (a) Material structuring to induce higher probe density. (b) Material encapsulation for the preservation of probes over time in response to environmental stresses. (c) Antifouling coatings for the prevention of non-specific adhesion on the sensing surface. (d) Form factor manipulation to increase sensor contact with test matrix. Produced using BioRender. ....	87
<b>Figure 3.1. Immobilization of DNAzymes onto biosensing components using thiol-based attachment.</b> (a) Hemagglutinin-responsive DNAzymes immobilized onto porous AuNPs, which maximize available surface area for binding. Reprinted with permission from ref <sup>[246]</sup> . Copyright 2019 Elsevier. (b) Immobilization of thiolated DNAzymes hybridized with fluorophore-quencher construct onto AuNPs for uranyl ions detection. Reprinted with permission from ref <sup>[238]</sup> . Copyright 2013 American Chemical Society. (c) Pb <sup>2+</sup> -responsive DNAzymes hybridized with a quencher-containing fragment immobilized onto R-phycoerythrin using N-succinimidyl 3-(2-pyridyldithio) propionate (SPDP) as a crosslinking agent. Reprinted with permission under a Creative Commons CC-BY license from ref <sup>[261]</sup> . Copyright 2019 Multidisciplinary Digital Publishing Institute.....	115

**Figure 3.2. DNA hybridization-mediated immobilization of DNazymes for sensing applications.** (a) Uranyl ion-responsive DNazymes hybridized to a substrate strand for immobilization onto magnetic beads. Reprinted with permission from ref<sup>[291]</sup>. Copyright 2017 Elsevier. (b) Hybridization-based click chemistry for the detection of copper ions through fluorescence. Reprinted with permission from ref<sup>[292]</sup>. Copyright 2020 Taylor & Francis. (c) Hybridization of hemin/G-quadruplex DNazymes with lysozyme aptamers for immobilization onto carbon fibre composites. Reprinted with permission from ref<sup>[293]</sup>. Copyright 2019 Elsevier. .... 123

**Figure 3.3. DNzyme-based sensors for the detection of Escherichia coli.** (a) Antibody-mediated electrochemical sensing system for E. coli using rolling circle amplification for ultrasensitive limit of detection. Reprinted with permission from ref<sup>[305]</sup>. Copyright 2016 Elsevier. (b) Ultrasensitive fluorescence detection system for E. coli O157:H7 involving rolling circle amplification. Reprinted with permission from ref.<sup>[306]</sup> Copyright 2020 Elsevier. (c) RNA-cleaving fluorescent DNzyme sensor immobilized on flexible patch for on-package, real-time detection of E. coli. Associated images show sensor performance when in contact with spiked food samples. Reprinted with permission from ref<sup>[16]</sup>. Copyright 2018 American Chemical Society. .... 129

**Figure 3.4. Pathogen detection using immobilized DNazymes.** (a) Colorimetric detection of H. pylori through the immobilization and release of urease upon DNzyme-induced cleavage. Reprinted with permission from ref<sup>[247]</sup>. Copyright 2019 John Wiley and Sons. (b) Fluorescence-based detection of E. coli using RNA-cleaving DNazymes immobilized on graphene through  $\pi$ - $\pi$  stacking interactions. Reprinted with permission from ref<sup>[187]</sup>. Copyright 2018 Springer Nature. .... 136

**Figure 3.5. Metal ion detection using DNzyme-based biosensing platforms.** (a) A hybridization chain reaction-based horseradish peroxidase concatemer sensing system for Cu<sup>2+</sup> detection. Reprinted with permission under a Creative Commons CC-BY license from ref<sup>[326]</sup>. Copyright 2017 Springer Nature. (b) A nanoparticle-based lateral flow test strip for Pb<sup>2+</sup> detection. Reprinted with permission from ref<sup>[327]</sup>. Copyright 2018 Elsevier. (c) Gold nanoparticles for plasmonic detection of Pb<sup>2+</sup> ions. Reprinted with permission from ref<sup>[328]</sup>. Copyright 2020 American Chemical Society. .... 138

**Figure 3.6. Detection of circulating tumor cells using immobilized DNazymes.** (a) DNzyme-based platform for the capture and release of circulating tumor cells. Reprinted with permission under a Creative Commons Attribution 3.0 unported license from ref<sup>[356]</sup>. Copyright 2020 Royal Society of Chemistry. (b) Target cancer cells compete with nanocages to bind to nanotetrahedron-aptamer probes, triggering release from screen-printed gold electrodes. Reprinted with permission from ref<sup>[360]</sup>. Copyright 2018 Elsevier. .... 146

**Figure 3.7. MicroRNA detection using immobilized DNzyme-based platforms.** (a) A platform of miRNA-initiated and intracellular sodium fueled DNzyme-probes to differentiate lung cancer cell subtypes. Reprinted with permissions from ref.<sup>[370]</sup>. Copyright 2020 American Chemical Society. (b) DNazymes conjugated to gold nanoparticles for intracellular miRNA detection. Reprinted with permissions from ref.<sup>[372]</sup>. Copyright 2017 American Chemical Society. .... 148

**Figure 4.1. Schematic illustration of experimental approach.** (a) Establishing inherent fluorescence profiles of target food products. (b) Evaluation of array visibility using fluorophore-conjugated oligonucleotides to identify labels that offer high signal to noise ratios. (c) Mechanism of action of RNA-cleaving fluorescent nucleic acid probes. (d) Fluorescence shift in fNAP microarrays following target-mediated fNAP cleavage. Created using BioRender. .... 167

**Figure 4.2. Baseline fluorescence properties of target food products.** (a) Mean fluorescence intensities of produce products. (b and c) Mean fluorescence intensities of beef and chicken samples, respectively. All values consist of at least four data points. Error bars and dashed lines represent standard deviation. .... 169

**Figure 4.3. Changes in mean fluorescence intensity of target food products.** Graphical depiction paired with intensity ranges for each evaluated wavelength provided for (a) romaine lettuce, (b) spinach, (c) ground beef, (d) whole beef, (e) ground chicken, and (f) whole chicken. All values consist of at least four data points. Error bars represent standard deviation. .... 171

**Figure 4. 4. Visibility of contact-printed microarrays composed of fluorophore-labelled DNA oligonucleotides.** (a) Fluorescence images of DNA microarrays deposited onto polyethylene food packaging. (b) SNR values of

fluorescent DNA microarrays at baseline and with overlaid products. Each value consists of 30 data points. Error bars represent standard deviation. (c) Fluorescence images of DNA microarrays once overlaid with target food products. (d) Coefficient of variation of baseline DNA microarrays. Performance threshold identified with a dashed line. (e) Coefficient of variation of DNA microarrays overlaid on target food products. All scale bars depict 50  $\mu\text{m}$ ..... 174

**Figure 4.5. Stability and functionality of fNAP arrays deposited via microcontact printing.** (a) Schematic illustration of fNAP microcontact printing. (b) SNRs of fNAP arrays before and after wash cycle. (c) Fluorescence images of fNAP arrays before and after testing. (d) (i) SNRs and (ii) CVs of fNAP arrays before and after testing. (e) Fluorescence images of fNAP arrays overlaid with target food products. (f) (i) SNRs and (ii) CVs of positive and negative state fNAP arrays when overlaid with target food. Error bars show standard deviation. Significance is indicated via ns/\*\*\*\* markers, corresponding to no significance and  $P < 0.0001$ , respectively. Scale bars show 50  $\mu\text{m}$ . ..... 178

**Figure S4.1.** Photobleaching of romaine lettuce under the Cy5 channel over four minutes..... 186

**Figure S4.2.** Inkjet-printed RNA-cleaving fluorescent nucleic acid probe arrays. (a) Fluorescence images before and after positive and negative control treatments. Scale bars indicate 200 $\mu\text{m}$ . (b-c) SNR and CV values of resultant arrays, respectively. Error bars represent standard deviation. .... 187

**Figure S4.3.** Inkjet-printed RNA-cleaving fluorescent nucleic acid probe arrays overlaid with food products. (a) Fluorescence images of positive and negative control-treated arrays with overlaid food samples. Scale bars indicate 200 $\mu\text{m}$ . (b-c) SNR and CV values of resultant arrays, respectively. Error bars represent standard deviation. .... 187

**Figure 5.1. Schematic illustration of the Lab-in-a-Package platform.** (a) Complete Lab-in-a-Package in situ detection platform with inclined packaging tray, reagent-saturated membrane, and sensor incorporation shown for RTE chicken products. Imaging procedure involving fluorescence scanning also shown. (b) Inclined food packaging trays with angles ranging from 45° to 90° to optimize test sample localization. (c) Depiction of membrane saturation with reagent components, diffusion of buffer components and target analyte to sensor surface, and fouling prevention. (d) FNAP sensor development with corresponding material surface and biochemical modifications. .... 193

**Figure 5.2. Characterization of packaging models and membrane candidates based on application-relevant properties.** (a) CAD models for all packaging models with top, bottom, and orthogonal views shown. (b) Time required for water a droplet to fall down packaging edge. (c) Time required for 5 mL of buffer to reach sensing window when dispensed at a rate of 0.5 mL/s. (d) Percentage of original PBS volume localized on sensing window after 1 minute when dispensed at a rate of 0.2 mL/s. (e) Percentage of original chicken purge volume localized after 24h at 37°C. (f) SEM images of candidate membranes at 100X with overlays at 500X. (g) Mean background fluorescence of candidate membranes. (h) Absorption capacity of candidate membranes. (i) Volume of buffer diffused through candidate membranes after 2 minutes. (j) Membrane effects on bacterial growth following a 6h incubation with *E. coli*. (k-l) Bacterial diffusion through (k) unsaturated and (l) buffer-saturated membranes onto underlying substrates following a 6h incubation at 37°C with *E. coli*. (m) Membrane effects on bacterial growth following a 6h incubation with *S. Typhimurium*. (n-o) Bacterial diffusion through (n) unsaturated and (o) buffer-saturated membranes onto underlying substrates following a 6h incubation at 37°C with *S. Typhimurium*. All reported values represent the mean of all samples with error bars representing sample standard deviation. All asterisks represent significant differences at corresponding significance levels. .... 198

**Figure 5.3. *S. Typhimurium* sensor development and testing.** (a) Schematic illustration of *S. Typhimurium*-responsive nucleic acid probe cleavage activity within food matrices, with associated pre-cleavage, cleavage, and quencher separation states. (b) Sensitivity testing of nucleic acid probe using bacterial dilutions in chicken purge, with associated images with 100  $\mu\text{m}$  scale bars. (c) Temperature profile of nucleic acid probe with bacterial species of  $10^7$  and  $10^5$  CFU/mL at 4°C, 25°C, 37°C, and 45°C. (d) Covalent attachment confirmation of nucleic acid probe on substrate surface. (e) Stability testing of developed sensor tested with  $10^6$  to  $10^3$  CFU/mL of bacteria after storage for three months at 4°C. (f) Specificity testing of nucleic acid probe using various bacterial species at  $10^6$  CFU/mL, with



associated images with 100  $\mu\text{m}$  scale bars. All reported values represent the mean of all samples with error bars representing standard error of the mean. All asterisks represent significant differences at corresponding significance levels. .... 200

**Figure S5.4. Lab-in-a-Package platform development and testing.** (a) Schematic illustration of in situ sensing interface with FNAP-based *S. Typhimurium* detection. (b) Images of packaging platform assembly, involving (i) sensor implantation within sensing window, (ii) membrane incorporation, and (iii) food addition into the package. Scale bars represent 3 cm on printed packaging tray. (c) Inherent fluorescence of chicken purge at four fluorescence wavelengths. Mean fluorescent values of overlayed cotton membranes shown with grey boxes. (d)  $\text{MgCl}_2$  concentration optimization for membrane absorption and diffusion. (e) Sensitivity testing following in situ full platform testing of contaminated whole chicken sample, with associated images with 100  $\mu\text{m}$  scale bars. (f) Contamination of food products from (i) various avenues of contamination, introduced during (ii) stages of the production process. (g) Induced real-world contamination detection in situ with Lab-in-a-Package platform. (h) Optical image of experimental set-up for handheld fluorescence scanner with associated smartphone readout. (i) *S. Typhimurium* detection using FNAP sensor as visualized using a handheld scanner, and associated images with 3.33 mm scale bars. (j) Handheld fluorescence detection of *S. Typhimurium* in Lab-in-a-Package, with associated sensor images with 3.33 mm scale bars. All reported values represent the mean of all samples with error bars representing standard error of the mean. All asterisks represent significance differences at corresponding significant levels. (a) and (f) created using BioRender. .... 203

**Figure S5.1.** Top views of 45, 60, and 90 degree 3D-printed packaging models (left to right) with bottom view images overlayed. Scale bars represent 2.5 cm on printed packaging trays. Printed trays were smoothed according to previously reported acetone-based approaches. .... 217

**Figure S5.2.** 2D drawings of packaging trays with key dimensions shown in mm in isometric, side and bottom views. Sensor window dimensions are highlighted in the bottom view along with dimensions for the inner edges used to secure sensors in place. .... 217

**Figure S5.3.** Volume localization over time for all packaging models based on an original applied volume of 5 mL across 10 and 20 seconds and 10 mL across 30 to 60 seconds. Reported values represent mean of all samples with error bars representing sample standard deviation. .... 218

**Figure S5.4.** Microscopic images of tested membrane materials at 4X with overlays of 10X images. Scale bars represent 500  $\mu\text{m}$  at 4X and 100  $\mu\text{m}$  at 10X. .... 218

**Figure S5.5.** Membrane absorption capacity over time based on volume of buffer absorbed. (a) Carrying capacity of cotton-cellulose and cellulose membranes over 30 seconds. (b) Carrying capacity of cellulose-polyester, cotton, and polyester membranes over 10 seconds. (c) Carrying capacity of all five membrane materials over 30 minutes. Reported values represent the mean of all samples with error bars representing sample standard deviation. Graphs with different axes ranges were used based on the higher absorption capacities of cellulose and cotton-cellulose materials compared to cotton, polyester, and cellulose polyester. .... 218

**Figure S5.6.** Membrane buffer retention over 120 hours as a percent of the original volume of buffer applied for all five membrane materials. Membranes were submerged in excess PBS buffer for 1 minute and stored for 120 hours. Reported values represent the mean of all samples with error bars representing sample standard deviation. .... 219

**Figure S5.7.** Membrane porosity characterization based on percent area covered by pores compared to total sample area. Unmodified membrane SEM images (top) and analyzed SEM images with pores shown in red (below). Scale bars represent 500  $\mu\text{m}$ . .... 219

**Figure S5.8.** Characterization of membrane antifouling capabilities. (a) Optical density measurement of chicken purge, chicken purge filtered through a cotton membrane, and water (control). Asterisks represent a significant difference between OD of membrane-filtered chicken purge and unfiltered chicken purge at the corresponding significance level. (b) SEM image of cotton membrane saturated in chicken juice at 100X with 500X overlay. Scale bars represent 500  $\mu\text{m}$  at 100X and 100  $\mu\text{m}$  at 500X. .... 219

<b>Figure S5.9.</b> Calibration curve for the determination of probe density on sensing interface. TRITC-labelled single-stranded DNA molecules were used to establish calibration curve correlating fluorescence per unit area and oligonucleotide content. The resultant linear relationship was used to quantify immobilized sensing probe density based on NaOH-induced maximal fluorescence per unit area. Average of sensing probe values denoted as a unique data point. The calibration curve was developed using a previously described protocol. ....	220
<b>Figure S5.10.</b> Effect of chicken purge on bacterial growth. Comparison of bacterial concentration present in chicken purge contaminated with bacteria, bacteria resuspended in PBS buffer, and chicken purge. Reported values represent the mean of all samples with error bars representing sample standard deviation. MacConkey agar was used based on its selectivity for gram-negative bacteria. ....	220
<b>Figure S5.11.</b> Linear regression analysis on FNAP sensor sensitivity data (Figure 5.3b) with regression coefficient and model equation shown. Model significance was evaluated based on slope coefficient value ( $P < 0.001$ ). ....	220
<b>Figure S5.12.</b> Linear regression analysis on Lab-in-a-Package sensitivity (Figure 5.4e) with regression coefficient and model equation shown. Model significance was evaluated based on slope coefficient value ( $P < 0.05$ ). ....	221
<b>Figure S5.13.</b> Optical images of complete Lab-in-a-Package set-up. Whole, unprocessed RTE chicken product sample and polyolefin food wrap shown in top view. Saturated membrane, FNAP sensor, and inclined tray shown in bottom view. Scale bars represent 4 cm. ....	221
<b>Figure S5.14.</b> Overview of Lab-in-a-Package sensing window. (a) Optical image of sensing interface with membrane and FNAP sensor shown within the sensing window of the redesigned packaging tray. Scale bars represent 0.6 cm. (b) Zoomed-in optical image of FNAP sensor arrays with 2.5 cm scale bars. ....	221
<b>Figure S5.15.</b> <i>S. enterica</i> serovar Typhimurium growth study demonstrating exponential growth of an original $10^2$ CFU/mL sample over a 4 hour timespan. Reported values represent the mean of all samples with error bars representing standard error of the mean. ....	222
<b>Figure S5.16.</b> Full system specificity testing where samples were contaminated with a mixture of common food contaminants including <i>E. coli</i> O157:H7 (EC), <i>Listeria monocytogenes</i> (LM), and <i>S. enterica</i> serovar Typhimurium (ST). Reported values represent the mean of all samples with error bars representing standard error of the mean. Asterisks represent a significant difference at corresponding significance level. ....	222
<b>Figure S5.17.</b> Target verification study comparing the concentration of <i>S. enterica</i> serovar Typhimurium recovered from the sensor surface after an 8-hour incubation period compared to the initial contaminated purge sample. Reported values represent the mean of all samples with error bars representing standard deviation. ....	222
<b>Figure S5.18.</b> Full system testing with <i>S. enterica</i> serovar Typhimurium contaminated lettuce samples. (a) Optical image of experimental set-up. (b) Quantification of sensor signals from lettuce samples contaminated with $10^6$ CFU/mL of spiked produced washing water. Reported values represent the mean of all samples with error bars representing standard deviation. Asterisks represent a significant difference at corresponding significance level... ..	222

**Figure 6.1. Overview of gelatin-anthocyanin fish spoilage sensor.** (a) Schematic illustration of developed sensor applied to sealed fish product for real-time monitoring. (b) Food-activated hydration of gelatin-anthocyanin microneedles, inducing increase in microneedle diameter. (c) pH-induced colour change from purple to blue within microneedles as food product spoils. Some components produced using BioRender. .... 228

**Figure 6.2. Fabrication and characterization of dehydrated gelatin microneedles.** (a) **Schematic illustration of fabrication protocol.** (b) Optical images of gelled, frozen and dehydrated gelatin microneedles. Scale bar depicts 4 mm. (c) Optimization of gelatin concentration based on the mechanical strength of resultant microneedles. (d) Optimization of dehydration time based on the mechanical strength of resultant microneedles. (e) Baseline mechanical characterization of optimized gelled, frozen, and dehydrated microneedles. (f) Scanning electron microscopy images of (i) gelled and (ii) dehydrated microneedles. Main image scale bar depicts 150  $\mu\text{m}$ , while inset image scale bar depicts 10  $\mu\text{m}$ . (g) Optical images of food packaging films penetrated by dehydrated gelatin microneedles. Scale bar depicts 3 mm. (h) Percent penetration of dehydrated gelatin microneedles through food packaging films through ten uses. (i) Percent reusability of dehydrated gelatin microneedles through food packaging films through ten uses. All error bars depict standard deviation. All asterisks represent corresponding significance levels. .... 232

**Figure 6.3. Anthocyanin incorporation into dehydrated gelatin microneedles and corresponding performance testing.** (a) Absorbance shifts observed through fish spoilage using various anthocyanin concentrations and measurement wavelengths. (b) Correlation analysis of anthocyanin concentration-absorbance wavelength combinations. (c) Optical images of an anthocyanin-embedded dehydrated gelatin microneedle sensor, a single needle, and rehydrated patches following exposure to pH. 6.0, 8.0, and 10.0, from left to right. Coloured images have scale bars depicting 1 mm, while Brightfield image scale bar depicts 200  $\mu\text{m}$ . (d) Percent colour shift exhibited by sensors prepared using varying anthocyanin concentrations at different pH ranges. (e) Mechanical assessment of anthocyanin-embedded microneedle sensor. (f) Scanning electron microscopy images of (i) gelled and (ii) dehydrated anthocyanin-embedded microneedles. Main image scale bar depicts 150  $\mu\text{m}$ , while inset image scale bar depicts 10  $\mu\text{m}$ . (g) Quantification and associated images of real-time monitoring of sealed fish throughout its product lifespan. (h) Quantification and associated images of spoiled fish rapid test. (i) pH responsiveness of sensors after long-term storage. (j) Mechanical integrity of sensors after long-term storage. (k) pH responsiveness of sensors after storage at diverse temperature for 5 days. (l) Mechanical integrity of sensors after storage at diverse temperature for 5 days. All error bars depict standard deviation. All asterisks represent significant differences at corresponding significance levels. .... 238

**Figure 7.1. Schematic overview of bacteriophage-loaded microneedles.** (a) PMMA polymeric chains with bacteriophage incorporation applied to assorted food items as antibacterial additives. (b) Selective bacteriophage delivery only upon target presence to provide contaminant lysis and resultant bacterial clearance and bacteriophage propagation. Bacteriophage remain loaded in the presence of other food constituents including lipid molecules and non-pathogenic microbes to prevent nonspecific delivery. (c) Bacterial clearance and decontamination in food products to prevent foodborne illness and food waste. .... 250

**Figure 7.2. General microneedle characterization and material comparison.** (a) Overview of microneedle fabrication via micromolding process. (b) Optical images of microneedle array patches. (c) SEM images of microneedles at 350X with 10000X overlays. (d) Compression testing force-displacement curves of all material candidates with associated pre- and post-compression microneedle images. (e) Microneedle reusability across increasing forces for all candidate materials. (f) Short and long-term stability of all microneedle with asterisk representing significant differences at corresponding significant levels. (g-h) Continued microneedle stability testing through exposure to (g) pH levels and (h) sonication-based stressors. (i) Preliminary penetration assessment of all microneedle material candidates based on penetrative performance in agarose pucks of varying density with pictures showing penetration in 1.5% agarose. (j) Water absorbance of PMMA, PDMS, and gelatin overtime. All reported values represent the mean of all samples with error bars representing standard error of the mean. .... 254

**Figure 7.3. Food-specific microneedle characterization.** (a) Optical images of various food items post penetration from PMMA microneedle arrays. (b-c) Microneedle material assessment through (b) penetration and (c) reusability assessment at 2.5, 5, and 7.5 N of force. (d) Associated optical images of microneedle reusability after insertion into peach samples at 5 N. (e) Comparison of penetration and reusability through food-centric applications and tests. (f) Change in microneedle performance after 24h incubation in mushrooms (M), peaches (P), fish (F), RTE chicken (CN), and cheese (C). (g-h) Performance assessment with porcine skin through (g) penetration and (h) reusability analysis with associated images of PMMA and PVA penetration. .... 257

**Figure 7.4. Full-system assessment of bacteriophage-loaded PMMA microneedles.** (a) Baseline bacterial counts in mushrooms (M), peaches (P), fish (F), RTE chicken (CN), and cheese (C). (b) Effect of peach juice and chicken purge on bacteriophage populations compared to pure bacteriophage suspensions. (c) Bacteriophage delivery into peach and chicken pieces compared to control bacteriophage suspensions. (d) Bacteriophage delivery via flat and microneedle array patches to provide varying levels of bacterial clearance. (e) Quantification of bacterial reduction post bacteriophage delivery from flat and microneedle patches with high (left) and low (right) levels of contamination. .... 260

## List of Tables

<b>Table 2.1.</b> Recently developed platforms for biogenic amine detection in food samples. ....	101
<b>Table 2.2.</b> Relevant properties of base film materials and modifiers for in situ pH sensing. ....	103
<b>Table 2.3.</b> Recently developed sensing platforms for pathogen identification in food. ....	104
<b>Table 2.4.</b> Food monitoring technologies in the commercial pipeline. ....	106
<b>Table 3.1.</b> Comprehensive overview of existing DNAzyme immobilization techniques for biosensing. ....	153
<b>Table 3.2.</b> Overview of existing literature involving the use of DNAzymes for environmental detection. Studies segregated into subsections pertaining to food contaminant, pathogen, and metal ion detection. ....	156
<b>Table 3.3.</b> Overview of existing literature on the use of DNAzymes for clinical applications. Studies segregated into sub-sections pertaining to nucleic acid, protein, and cancer detection. ....	159
<b>Table S4.1.</b> Fluorescently labelled single stranded oligonucleotides used in the study. ....	186
<b>Table S5.1.</b> Summary of packaging tray model characterization. ....	216
<b>Table S5.2.</b> Summary of membrane materials characterization. ....	216
<b>Table S5.3.</b> Oligonucleotide sequences used for <i>S. enterica</i> serovar Typhimurium sensor. ....	217

## List of Abbreviations

<b>RFD</b>	RNA-cleaving fluorescent DNase
<b>fNAP</b>	Fluorescent nucleic acid probe
<b>DAPI</b>	4',6-diamidino-2-phenylindole
<b>FITC</b>	Fluorescein isothiocyanate
<b>TRITC</b>	Tetramethylrhodamine isothiocyanate
<b>TAMRA</b>	Tetramethylrhodamine
<b>NP</b>	Nanoparticle
<b>LOD</b>	Limit of detection
<b>SNR</b>	Signal-to-noise ratio
<b>CV</b>	Coefficient of variance
<b>SD</b>	Standard deviation
<b>RTE</b>	Ready-to-eat
<b>SEM</b>	Scanning electron microscopy
<b>PDMS</b>	Polydimethylsiloxane
<b>PVA</b>	Polyvinyl alcohol
<b>PMMA</b>	Polymethylmethacrylate
<b>BA</b>	Biogenic amine

## **Declaration of Academic Achievement**

This dissertation was written to fulfill the degree requirements for a Doctor of Philosophy in Biomedical Engineering at McMaster University. The work described was undertaken between September 2020 and July 2024.

The majority of experiments detailed in this work were conceived, conducted, analyzed, and written by the author of this dissertation, in consultation with supervisor Dr. Tohid Didar.

**Chapter 1:** *Introduction* – Drafted by Shadman Khan and reviewed by Dr. Tohid Didar.

**Chapter 2:** *Material Breakthroughs in Smart Food Monitoring: Intelligent Packaging and On-Site Testing Technologies for Spoilage and Contamination Detection* – Drafted by Shadman Khan in collaboration with Jonathan Monteiro, figure development by Akansha Prasad, and reviewed by Dr. Carlos D.M. Filipe, Dr. Yingfu Li, and Dr. Tohid Didar.

**Chapter 3:** *DNAzyme-Based Biosensors: Immobilization Strategies, Applications and Future Prospective* – Drafted by Shadman Khan with contributions from Brenda Burciu and Kristen Dellinger, and reviewed by Dr. Carlos, D.M. Filipe, Dr. Yingfu Li, and Dr. Tohid Didar.

**Chapter 4:** *Comprehensive Fluorescence Profiles of Contamination-prone Foods Applied to the Design of Microcontact-printed in situ Functional Oligonucleotide Sensors* – Shadman Khan performed experiments, data analysis, data visualization, and manuscript development with contributions from co-authors. The manuscript was reviewed by Dr. Carlos D.M. Filipe, Dr. Yingfu Li, and Dr. Tohid Didar.

**Chapter 5:** *Advancing in situ Food Monitoring Through a Smart Lab-in-a-Package System Demonstrated by the Detection of Salmonella in Whole Chicken* – Shadman Khan and Akansha Prasad collectively performed experiments, data analysis, data visualization, and manuscript development with contributions from co-authors. The manuscript was reviewed by Dr. Carlos D.M. Filipe, Dr. Yingfu Li, and Dr. Tohid Didar.

**Chapter 6:** *Food-Activated, Spoilage Sensing Microneedles for Real-Time, Consumer-Directed Monitoring of Packaged Fish* – Shadman Khan and Akansha Prasad collectively performed experiments, data analysis, data visualization, and manuscript development with significant contributions from Mahum Javed. Roderick Maclachlan performed scanning electron microscopy. The manuscript was reviewed by Dr. Tohid Didar.

**Chapter 7:** *Antimicrobial Bacteriophage-loaded Microneedle Patches that Counteract Bacterial Pathogen Contamination to Prevent Foodborne Illness* – Shadman Khan and Akansha Prasad collectively performed experiments, data analysis, data visualization, and manuscript development with contributions from co-authors. The manuscript was reviewed by Dr. Tohid Didar.

**Chapter 8:** *Smart Food Packaging Commercialization* – Drafted by Shadman Khan and reviewed by Dr. Zeinab Hosseinidoust, Dr. Yingfu Li, Dr. Carlos D.M. Filipe, and Dr. Tohid Didar.

**Chapter 9:** *Conclusion* – Drafted by Shadman Khan and reviewed by Dr. Tohid Didar.

## **Chapter 1: Introduction**

### **Preface**

This chapter provides an overview of foodborne illness and food waste, alongside currently enacted mechanisms for detection and mitigation. Emerging technologies are then presented, broadly categorized into efforts that detect food contamination, detect food spoilage, and yield food decontamination. These discussions act as a preliminary situational overview of the food technology space in anticipation of a more in-depth analysis in Chapters 2 and 3. The motivations that guide this thesis are then presented, which inform the subsequent research objectives. Finally, the structure of this dissertation is presented.

### **1.1 Foodborne Illness and Food Waste**

Despite extensive legislative efforts from government, the introduction of rigorous best practice guidelines from regulators, and the optimization of operations by producers and distributors, the prevalence of foodborne illness and the severity of food waste has not significantly decreased.<sup>[1]</sup> With regards to foodborne illness, there are 600 million cases per year, resulting in 420,000 deaths.<sup>[2,3]</sup> High rates of illness exist in developing and developed countries alike, with 4 million Canadians and 48 million Americans suffering from such ailments per year.<sup>[4,5]</sup> Annual hospitalizations in Canada and the United States total 12,000 and 128,000, respectively, while resulting respective deaths exceed 400 and 3000.<sup>[4,5]</sup> While the economic burden of foodborne illness has not been recently estimated for Canada, associated costs and lost productivity total well into the billions. Such values are corroborated by recent estimations for the United States, that suggest a total associated economic loss exceeding \$77 billion USD per year.<sup>[6]</sup>

In another vein, food waste across the developed world exceeds 40% of total food production, which has become especially unacceptable at a time of heightened food insecurity.<sup>[7]</sup> A significant portion of unnecessary waste is caused by ongoing societal reliance on inaccurate, static expiry dates, which do not account for variations in microbiological composition, storage, and handling. In cases where these predictions postdate the time of expiry, consumption can induce illness. In an

effort to limit such events, expiry dates are ultraconservative. Unfortunately, this means that they regularly predate spoilage, yielding the disposal of massive quantities of edible food products.<sup>[8,9]</sup>

Concurrently, complex food distribution networks are employed to meet the diverse needs of consumers today. Increased handling yields a greater risk of contamination, while longer networks result in food products spending significant portions of their lifespan in transport. While various chemical preservatives have been employed to increase product shelf life, a significant amount of food waste continues to occur at the grocer and consumer levels owing to products expiring soon after delivery and purchase, respectively.<sup>[7]</sup>

## **1.2 Food Inedibility: Current Measures for Detection and Reduction**

The inedibility of food can be induced through by a diverse range of changes on the microscopic level.<sup>[10]</sup> While the end result is the same – in that products must be tossed, the mechanism by which food transitions to an inedible state can be broadly categorized into one of two events: food contamination or food spoilage.

### **1.2.1 Food contamination**

Generally, food contamination refers to the presence of an externally sourced pathogenic agent on or within food matrices. Contaminants are most often pathogenic bacteria such as *Escherichia coli*, *Salmonella* spp., and *Listeria monocytogenes*.<sup>[11,12]</sup> Even when present in small concentrations, some of these bacterial pathogens are capable of inducing illness. Moreover, many microbes are capable of proliferating in the nutrient-rich environment found in food, meaning that contamination events that yield small degrees of bacterial loading are still dangerous. As such, regulatory guidelines are stringent, with bacterial thresholds of 100 colony-forming units (CFU)/g, 0 CFU/g, and 100 CFU/g for the three aforementioned pathogens, respectively.<sup>[13–15]</sup>

Given that there are no visual indications associated with food contamination, its detection relies solely on microbiological sensing efforts. To this end, traditional bacterial culturing remains the gold-standard approach used in industry. Unfortunately, culturing is extremely time-consuming



and laborious. Moreover, the need to open packaging for product sampling means that individual packages cannot be assessed.<sup>[16]</sup> The resultant lot-based approach – where one product is tested as a representation of thousands, offers significant opportunity for contaminated products to reach consumers. Products are also not monitored in real-time, rather only being evaluated at set points in the production timeline.<sup>[16,17]</sup> As such, contamination events occurring after testing go undetected. These shortcomings represent key drivers for the hundreds of food recalls that are retroactively enacted in Canada each year. To circumvent issues pertaining to time and labour, efforts have been made to develop rapid, on-site testing platforms that may be used by industry stakeholders *in lieu* of culturing approaches.<sup>[8]</sup> While such platforms offer significant value-add, they do not offer a mechanism for individual product monitoring or real-time assessment. Additionally, these systems generally employ complex sensing cascades that require expensive transduction devices, which are difficult to integrate at a grocer level and completely inaccessible at the consumer level.<sup>[8]</sup>

Efforts to reduce the occurrence of food contamination have largely involved legislative measures and operational changes in industry. While some foods – such as milk, go through decontamination processes, most products are not subjected to such measures. This because of the harsh conditions that most decontamination procedures induce, which would significantly degrade the organoleptic properties of most food products. Developing non-destructive decontamination approaches for contamination-prone produce and meat products represents an intriguing measure towards increased food preservation through post-contamination reclamation.<sup>[18]</sup>

### **1.2.2 Food spoilage**

Food spoilage is characterized by a multitude of changes in the food microenvironment, including the proliferation of inherently present microbes, the degradation of proteins, and the oxidation of lipids.<sup>[10]</sup> These changes are connected by a complex network of reactions that ultimately induce changes in the organoleptic properties of a given food product. While spoilage mechanisms vary significantly between food types, microbial growth can be considered the main

driver of spoilage. As microbes proliferate, they pose a risk both through both their own presence and through the increasingly large concentrations of harmful agents they produce.<sup>[10]</sup> Concurrently, they initiate various degenerative processes that deteriorate food quality. For example, spoilage bacteria are known to engage in the decarboxylation of amino acids, inducing the formation of biogenic amines (BA) that reduce both food quality and safety. On the other hand, lipid oxidation, which plays a key role in inducing rancidity and odour, is largely induced by air exposure. Importantly, air exposure also often promotes the proliferation of innately present microbes.<sup>[8]</sup>

Currently, food products are not assessed for spoilage at industry or consumer levels beyond simple visual inspection. While useful for contamination monitoring, sampling-based rapid detection at an industry level stands to offer very limited value in spoilage sensing. This is because spoilage does not occur at the same rate within every product in a lot. Moreover, spoilage largely occurs once products are with consumers, making industry level monitoring futile. Effective spoilage monitoring must occur at the consumer level, using markers that correlate well with spoilage events. As spoilage bacteria are innately present at considerable concentrations in fresh food products, microbe-based monitoring of spoilage offers a high risk of false positives. As an alternative, metabolites produced by microbes – namely BAs, provide an indirect measure of microbial growth, making them effective markers for food spoilage sensing.<sup>[19,20]</sup> In parallel, pH has also garnered significant attention as an effective food state marker, as the various compositional changes occurring during spoilage induce shifts between acidity and alkalinity.<sup>[21,22]</sup>

Technical efforts to mitigate food spoilage have centered upon the development of active packaging with preservative properties. Here, antioxidant and antimicrobial films have demonstrated an ability to increase product shelf-life by a considerable degree.<sup>[23]</sup> Such efforts have been reviews at length elsewhere but are outside of the scope of this dissertation.

### **1.3 Approaches towards Improving Food Safety and Reducing Food Waste**

Improving food safety and reducing food waste can be enacted through the two key mechanisms discussed in Section 1.2: effective detection and adverse process reduction. Given the

suboptimal contamination and spoilage detection platforms that exist today, improved contamination and spoilage detection systems stands to offer substantial benefit towards both improving food safety and reducing waste. Adverse process reduction through the induction of increased preservative activity also presents value towards increasing safety and reducing waste but may be more reasonable to enact on the food safety front. This is because food decontamination presents a slightly more intriguing value proposition to industry stakeholders who would be responsible for enacting efforts towards improved preservation. Specifically, decontamination stands to benefit industry stakeholders through a reduced likelihood of expensive food recalls and a lower demand for food testing, yielding a high cost tolerance towards developed technologies. The value-add of decontamination is also very clear, in that rendering a food product safe to eat would significantly reduce waste. On the other hand, the mix of microbial and oxidative processes that govern spoilage makes the value-add of systems seeking to alleviate singular mechanisms of food spoilage difficult to discern.

### **1.3.1 Developments in contamination monitoring**

While inexpensive, accurate rapid tests for pathogenic contamination would be useful to industry stakeholders and consumers alike, in-package integration of contamination sensors offers the greatest value-add. Such an approach enacts real-time individual product monitoring in a hands-free manner throughout a given product's lifespan. In-package contamination sensing relies on three key functions: the collection of a test sample that is representative of the bulk food matrix, the detection of pathogenic targets, and the transduction of an easy-to-interpret signal. Most research efforts have focused on the latter two functions. Here, antibodies, aptamers, and bacteriophages have all been employed towards the detection of foodborne pathogens, with systems offering optical readout holding the most potential for real-world translation.<sup>[8,9]</sup>

Namely, Yousefi *et al.* detailed the covalent integration of *E. coli*-responsive RNA-cleaving fluorescent DNazymes (RFDs) microarrays onto food packaging films, through the employment of non-contact piezoelectric printing.<sup>[17]</sup> RFDs are composed of an enzymatic strand with target-

induced catalytic activity, paired with a substrate strand hosting a fluorophore-quencher pairing. In the presence of the target bacterial species, cleavage between the fluorophore and quencher yields separation between the two entities, resulting in a defined increase in fluorescence. The smart packaging developed by Yousefi *et al.* offered detection at concentration as low as  $10^3$  CFU/mL.<sup>[17]</sup> Other recent efforts towards in-package contamination sensing include liquid-infused RFD sensors and antibody-based microneedle sensors with colorimetric transduction.<sup>[24,25]</sup>

### 1.3.2 Developments in spoilage monitoring

In-package spoilage sensors must be designed for specific use-cases, as the initial microbial composition, rate of growth, and thresholds for spoilage vary significantly between food products. Recognizing that products such as produce are quite easily distinguished as spoiled, developing spoilage sensors for high risk products such as meat have been prioritized. Specifically, several studies have evaluated the intricacies of spoilage progression in products such as chicken, beef, and fish to identify appropriate BA and pH spoilage thresholds.<sup>[26–28]</sup> In-package BA-mediated monitoring has largely involved the design of electrochemical noses that quantify the buildup of gaseous BAs. While capable of ultrasensitive offering ultrasensitive, such systems would be difficult to integrate into individual products in the real-world due to cost.<sup>[29,30]</sup>

Contrarily, pH monitoring can be enacted in a much more cost-effective manner through the use of anthocyanins.<sup>[21,31]</sup> These food-derived dyes are non-toxic and inexpensive, with pronounced shifts in colour in response to single logarithmic unit pH shifts. There is an extensive body of literature describing the integration of anthocyanins within soft polymer films to be used as food packaging.<sup>[32]</sup> While the spoilage sensing properties of such films are considered robust, they offer low mechanical integrity, preventing their real-world use. Recent research efforts have centered upon the integration of various nanofillers and chemical modifiers into these films to induce improvements in their mechanical properties. While a diverse range of approaches have been explored to date, improvements in performance have been minimal.<sup>[32]</sup>

Even if such improvements in anthocyanin film properties are enacted, the real-world use of such films is hindered by commercial considerations. While industry stakeholders are incentivized to integrate contamination sensing systems into packaging to reduce the incidence of expensive food recalls, they are not incentivized to actualize in-package spoilage sensing to the same degree. In fact, unnecessary food waste at the consumer level results in increased product sales. This, alongside the risk associated with the adaptation of a new packaging film, makes such systems less attractive to private industry stakeholders.

### **1.3.3 Developments towards food decontamination**

The role of traditional chemical antimicrobial preservatives in food is well-established, wherein they offer improvements in product shelf life. Their efficacy against pathogenic contamination is limited however, due to their limited potency and non-specific activity. Decontamination ultimately requires agents that exhibit targeted antimicrobial activity in a potent manner. To this end, food-approved, lytic bacteriophages – which are bacteria-infecting viruses, exhibit significant promise.<sup>[33]</sup> These agents are extremely specific to their host bacteria, meaning that their deposition onto food does not yield any significant off-target effects. Moreover, bacteriophage infection is succeeded by the lysis of the host bacterium, which results in the release of hundreds of progeny bacteriophages that induce further antibacterial activity. Such target-induced amplification ensures that bacteriophages are only propagated to high concentrations throughout a given food matrix when necessary.<sup>[33,34]</sup>

These advantages have garnered significant interest towards highly concentrated liquid suspensions of bacteriophages – many of which are commercially available.<sup>[35,36]</sup> Such suspensions have been proposed for use within food processing as either an immersion bath or a spray. Immersion yields a more pronounced decrease in target bacteria count, but also tends to alter the organoleptic properties of the food product. This makes it unfeasible for real-world use. On the other hand, spray deposition leaves the food matrix largely intact, but does not exhibit bacterial load reduction to the same degree. In an effort to make sprayed bacteriophage suspensions more

effective, Tian *et al.* developed microgels composed entirely of *E. coli* O157:H7-targeting bacteriophages, with each gel hosting over  $10^5$  PFU/mL bacteriophages.<sup>[37,38]</sup> When used to treat lettuce and meat products that had been artificially contaminated with *E. coli* O157:H7 on their surface, the sprayed suspension induced target bacteria load reductions of up to 9-logs.<sup>[37]</sup> This study – alongside several works that detail the development of bacteriophage-embedded packaging films, demonstrate the potential of phage-based biomaterials in the food safety space.<sup>[39,40]</sup>

## 1.4 Motivation

Despite extensive literature detailing the development of various smart packaging systems that offer real-time food monitoring and food decontamination, real-world translation has been limited. Ultimately, the offerings of these systems do not effectively meet the technical, commercial, and operational expectations of food industry stakeholders. With the repercussions of foodborne illness and food waste becoming increasingly pronounced, there is a clear need for platforms that better exhibit the characteristics necessary for real-world use.

With regards to in-package contamination sensing, many of the drawbacks of existing platforms stem from a lack of real-world consideration in system design. Namely, while mechanisms for effective pathogen detection have been studied at length, strategies towards the in-package collection of test samples that are representative of a bulk food product are non-existent.<sup>[16]</sup> To overcome this oversight, most proof-of-concept studies have employed small food samples contaminated at localized sites directly adjacent to the in-package sensor. This eliminates the need for pathogen transport to the sensing site. Of course, the likelihood of an in-package sensor – measuring a few square centimeters, aligning perfectly with the exact site of contamination on a bulk food product is small.<sup>[8]</sup> The lack of a mechanism for the stable in-package incorporation of sensing-relevant reagents (i.e., buffers) represents another application-specific oversight. These agents are necessary for the function of many in-package sensors. Within proof-of-concept testing, they are broadly dispensed onto food products to ensure widespread

availability. While buffers used in this space are food-safe, such an approach induces alterations in the organoleptic properties of the food product being tested.<sup>[8]</sup>

Application-specific oversights are also made with regards to accessible signal transduction. Namely, many developed platforms rely on complex signal readout systems that are not accessible outside of a laboratory setting.<sup>[8,9]</sup> To this end, colorimetric sensing platforms that can be analyzed *via* the naked eye offer the greatest use-case at both industry and consumer levels. Recognizing however, that many sensing cascades cannot adopt a colorimetric signal transduction mechanism, developing electrochemical and fluorescence platforms that can at least be transduced by relatively affordable, handheld devices is imperative. In such a case, these devices can be used by food distributors and grocers to check for food contamination prior to the point-of-sale.

It is important to recognize that such handheld devices would likely yield a notable decrease in sensor sensitivity. That being said, tuning sensor design to better match the desired application would stand to counteract this effect to a degree. Specifically, in-package fluorescence sensors have rarely considered the background fluorescence of a given food product when selecting the signalling fluorophore – yet another common oversight. With a better understanding of both the inherent fluorescence exhibited by target foods and the visibility of candidate fluorophores on such food textures, sensor design stands to be significantly improved.

Motivations for the development of inexpensive, food-safe spoilage sensors stem from a need to reduce food waste. As end-user food waste is not a priority for food producers and distributors, the industry-led integration of in-package spoilage sensors that would come with added packaging costs proves difficult to justify. To this end, developing inexpensive spoilage sensors that can be purchased and used directly by consumers may be the best way to reduce the disposal of edible food products. There are two use cases for such sensors, each with unique requirements. The first involves sensors that can offer real-time monitoring of sealed food products to be consumed at a later date, without opening the package. If packaging needs to be opened for sensing, the resultant air exposure would counteract the benefits afforded by spoilage sensing. The second use case

involves the rapid testing of food products prior to consumption, wherein readout would have to be available within minutes. Both platforms would stand to bring significant value to consumers.

As inexpensive, food-derived pH-responsive agents that offer colorimetric signal transduction, anthocyanins are positioned as an optimal sensing agent in the food spoilage sensing space.<sup>[21,32]</sup> While they exhibit some chemical instability as standalone molecules, their integration into polymer matrices have been shown to afford them significant protection. As such, while anthocyanin packaging films may not offer strong real-world translation, the extensive body of literature that details the impact of various polymer materials and modifications on anthocyanin sensing proves extremely useful towards informing sensor design and development.

Finally, efforts towards developing better pathogenic decontamination mechanisms for food are motivated by recent progress in bacteriophage-based technologies.<sup>[41]</sup> These agents are primed for use against pathogens in food, where they stand to offer highly efficient, targeted elimination of bacteria implicated in foodborne illness. While bacteriophage suspensions and bacteriophage-incorporating biomaterials are effective against products that have a high sprayable surface area and low interior volume – such as produce, they cannot effectively treat high volume food matrices such as meat. In fact, several studies have reported that bacteriophages struggle to penetrate and disperse through dense food matrices.<sup>[42–44]</sup> As such, effective antibacterial activity against pathogens present deep within food matrices has not yet been enabled in a manner that preserves the organoleptic properties of the product. This is especially true when the product is protected by a peel or skin. This has created a need for improved bacteriophage dissemination strategies. This is especially relevant for pathogen elimination, as the localized nature of contamination means that effective decontamination required bacteriophages to be well-distributed within the food matrix.<sup>[42]</sup>

## **1.5 Research Objectives**

The aforementioned motivations for smart food-targeting material development guide the objectives of this thesis. Broadly, efforts seek to address longstanding barriers that have prevented meaningful progress towards real-world translation. This includes objectives towards better



understanding the sensing-relevant properties of target foods, actualizing real-world in-package pathogen sensing, designing consumer-level sensors for spoilage monitoring, developing systems for improved pathogen-targeting bacteriophage dissemination, and creating a framework to guide translational work in this space going forward.

**Objective 1: Perform sensing-relevant fluorescence analysis of contamination-prone food products throughout their lifespan**

Recognizing the oversights that have been made in prior works with regards to fluorophore selection, a better understanding of the fluorescence properties of foods commonly implicated in pathogenic outbreaks is sought. To this end, lettuce, spinach, chicken, and beef have been noted as products of interest. Baseline fluorescence properties of the target foods, as observed under sensing-relevant imaging conditions, stand to offer an understanding which fluorescence wavelengths are suitable for the respective food products, with regards to biosensing. Employing wavelengths where a given product exhibits a high degree of inherent fluorescence would stand to reduce the sensitivity of the resultant sensor. Changes in fluorescence over time also need to be considered, to account for spoilage-related shifts that could induce a change in background noise. Moreover, while baseline fluorescence offers some context, a stronger understanding of how such backgrounds influence the visibility of fluorescently-labelled sensing agents requires overlaid imaging. Such efforts would better inform fluorescence sensor design for on-food applications.

**Objective 2: Actualize and validate in-package contamination sensing through the development of mechanisms for hands-free sampling and buffer integration**

While many in-package pathogen detection mechanisms have real-world potential, a platform technology that facilitates in-package detection is lacking. This objective seeks to develop an in-package sample collection system that is simple and cost-effective, wherein real-world industry integration would be feasible. Moreover, a mechanism for the localization of food-safe reagents necessary for sensing needs to be developed. The non-toxic nature of these agents means that

localization does not have to be 100% effective. Rather, the mechanism must simply provide a better alternative to the reagent dispensing approach that has been employed to date. The developed platform must be validated using an in-package pathogen sensor. The employed sensor must be compatible with a handheld signal transduction device. Collectively, this objective stands to provide the first actualization of hands-free in-package contamination monitoring.

**Objective 3: Develop an inexpensive, consumer-centric spoilage sensor for real-time monitoring of a high-risk perishable food product**

The development of inexpensive spoilage sensors for consumer use marks a key objective of this thesis. Anthocyanins present an intriguing sensing foundation, owing to their inexpensive, pH-responsive, and food-safe properties. Tools for both the real-time monitoring of sealed foods and the rapid testing of opened products are sought. Real-time monitoring of sealed products requires the design of a food sampling mechanism that is non-destructive to the surrounding packaging. Recognizing that anthocyanin-embedded materials generally offer low mechanical integrity to ensure anthocyanin availability, this presents a premise within which a soft sensing material must penetrate through packaging films with limited disruption of their sealing properties. On the other hand, rapid testing of open products seeks to build upon existing literature that detail anthocyanin films with efficient pH-responsive capabilities. Recognizing that anthocyanin-based sensing requires contact between these molecules and the underlying food matrix, efforts to accelerate food testing will involve exploring sensor form factors that offer a larger sensing interface. To mitigate costs to consumers, both these use cases are to be fulfilled by a single inexpensive sensing tool.

**Objective 4: Design a platform that offers improved bacteriophage dissemination within meat products for food decontamination**

The dissemination of bacteriophages within dry food matrices requires the integration of external mechanical energy sources, which is beyond the scope of this thesis. Rather, the presented objective centers upon the enactment of improved bacteriophage delivery into fluid-rich foods that

are encased by a protective layer. This includes fruits, vegetables, as well as ready-to-eat meat products with oil-rich skins. The tool used for delivery must offer effective bacteriophage delivery without relying on any additional equipment. It must also be inexpensive to promote widespread industry and consumer-scale use. Material selection is expected to be a key factor in system design, to ensure effective food-safe delivery of bacteriophages in a manner that does not compromise their antibacterial viability. Assessment of the developed platform requires comparison against conventional liquid suspension spraying as a baseline control. Importantly, the efficacy of bacteriophages within externally-protected, fluid-rich foods has not been explored. Successfully meeting this objective would thus support new food applications for bacteriophages.

**Objective 5:** Employ experiences in this research space towards creating a framework for improved real-world translation of smart food-targeting materials

A significant quantity of literature is published annually detailing developments in smart food monitoring and food decontamination. The accompanying lack of real-world developments suggests that there is a disconnect between stakeholders in this space. While in pursuit of the diverse objectives presented in this thesis – in partnership with industry stakeholders, a comprehensive understanding of the operational landscape will also be sought. Such findings can then act as a framework for future efforts in the space, with key emphasis placed on barriers that continue to hinder real-world translation and opportunities that stand to evoke meaningful, widespread process. Stakeholder needs in this space are summarized in **Table 1.1**.

**Table 1.1. Stakeholder priorities in the food smart food sensing space**

Stakeholder	Key Priorities
Innovators	<ul style="list-style-type: none"><li>• Regulatory support towards increased real-world implementation (i.e., higher testing frequency requirements, defined spoilage thresholds)</li><li>• Clear roadmap towards commercial translation</li></ul>
Food Industry Players	<ul style="list-style-type: none"><li>• Maximized profit per unit item</li><li>• Reduced product lost to contamination, avoidable waste</li><li>• Limited exposure to legal ramifications in case of smart systems failure</li></ul>
Government	<ul style="list-style-type: none"><li>• Reduced incidence of foodborne illness</li><li>• Reduced avoidable food waste</li></ul>
Consumers	<ul style="list-style-type: none"><li>• Ease of access to food products (affordability, inclusive selection)</li><li>• Reduced risk of foodborne illness</li><li>• Comprehensive evidence towards the safety of smart packaging systems</li></ul>

## 1.6 Thesis Overview

The chapters of this dissertation are as follows:

**Chapter 2:** *Material Breakthroughs in Smart Food Monitoring: Intelligent Packaging and On-Site Testing Technologies for Spoilage and Contamination Detection* – A review of smart food monitoring technologies from a material-centric perspective. Both on-site and in-package sensing platforms are discussed, and critically assessed based on their real-world viability. This work was published in *Advanced Materials*.

**Chapter 3:** *DNAzyme-Based Biosensors: Immobilization Strategies, Applications and Future Prospective* – A review of DNAzyme-based biosensors, with a focus on surface-based immobilization mechanisms and mechanisms employed towards their diverse applications. This work was published in *ACS Nano*.

**Chapter 4:** *Comprehensive Fluorescence Profiles of Contamination-prone Foods Applied to the Design of Microcontact-printed in situ Functional Oligonucleotide Sensors* – A research article detailing the sensing-relevant fluorescence profiles of select contamination-prone foods, quantified through direct comparisons with surface-printed fluorescence oligonucleotide microarrays. This work was published in *Scientific Reports*.

**Chapter 5:** *Advancing in situ Food Monitoring Through a Smart Lab-in-a-Package System Demonstrated by the Detection of Salmonella in Whole Chicken* – A research article detailing the development of a novel packaging system to enable real-time, in-package contamination monitoring. The system was validated using a novel *Salmonella* fluorescence sensor, where  $10^3$  CFU/g detection of the target pathogen was demonstrated within sealed whole chicken products. This work was published in *Advanced Materials*.

**Chapter 6:** *Food-Activated, Spoilage Sensing Microneedles for Real-Time, Consumer-Directed Monitoring of Packaged Fish* – A research article detailing a spoilage sensor composed of dehydrated gelatin microneedles with environment-responsive mechanical properties and a food-safe anthocyanin sensing agent that exhibits pH-responsive colour change. Real-time spoilage monitoring was enabled on sealed fish products throughout their lifespan and rapid contamination detection was demonstrated on opened fish products. This work is unpublished.

**Chapter 7:** *Antimicrobial Bacteriophage-loaded Microneedle Patches that Counteract Bacterial Pathogen Contamination to Prevent Foodborne Illness* – A research article detailing extensive microneedle material characterization for on-food application, followed by bacteriophage loading onto the best-performing material for in-food delivery. The resultant platform exhibited a near 3-log improvement in antibacterial efficacy relative to flat substrates that only offered surface-based delivery of the loaded agent. This work is unpublished.

**Chapter 8:** *Smart Food Packaging Commercialization* – This down-to-business article details barriers to smart food packaging commercialization, alongside opportunities for widespread impact. An emphasis is placed on approaches that have proven successful in our work. This work is published in *Nature Reviews Bioengineering*.

**Chapter 9:** *Conclusion* – This chapter provides a final overview of this dissertation *via* main conclusions and contributions to the field, alongside a discussion of future works.

## Chapter 2: Material Breakthroughs in Smart Food Monitoring: Intelligent Packaging and On-Site Testing Technologies for Spoilage and Contamination Detection

### Preface

This chapter provides an in-depth assessment of the food sensing space presented in Chapter 1, with an emphasis on the material properties of emerging systems. The food contamination and spoilage sensing systems presented here are enabled through the detection of either biogenic amines, pH, or microbes, all of which have a defined relationship with food quality. Sensors and their underlying materials are evaluated with regards to their technical capabilities and real-world viability. This is followed by a summary of the technical and commercial considerations that govern the food sensing landscape. Material-centric proposals that may overcome key barriers in the space are then proposed.

### Authors

Shadman Khan<sup>†</sup>, Jonathan K. Monteiro<sup>†</sup>, Akansha Prasad, Carlos D.M. Filipe, Yingfu Li, Tohid F. Didar

<sup>†</sup>These authors contributed equally.

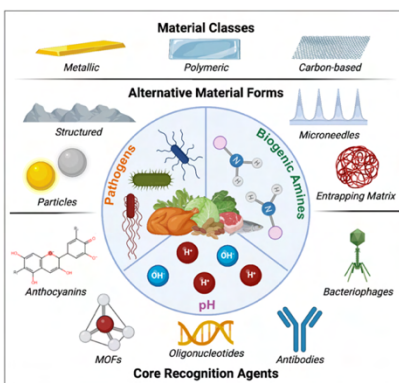
I was responsible for defining the scope of this review and performing extensive literature review to define sub-sections. I authored all sections with Jonathan K. Monteiro, with Akansha Prasad contributing through manuscript review and figure development. Carlos D.M. Filipe, Yingfu Li, and Tohid F. Didar supervised and reviewed the work.

### Publication

Advanced Materials, 2023, 36, 2300875

### Publication Date

April 2023



## 2.1 Abstract

Despite extensive commercial and regulatory interventions, food spoilage and contamination continue to impose massive ramifications on human health and the global economy. Recognizing that such issues would be significantly eliminated by the accurate and timely monitoring of food quality markers, smart food sensors have garnered significant interest as platforms for both real-time, in-package food monitoring and on-site commercial testing. In both cases, the sensitivity, stability, and efficiency of the developed sensors are largely informed by underlying material design, driving focus towards the creation of advanced materials optimized for such applications. Herein, we provide a comprehensive review of emerging intelligent materials and sensors developed in this space, through the lens of three key food quality markers – biogenic amines, pH, and pathogenic microbes. Each sensing platform is presented with targeted consideration towards the contributions of the underlying metallic or polymeric substrate to the sensing mechanism and detection performance. Further, the real-world applicability of presented works is considered with respect to their capabilities, regulatory adherence, and commercial potential. Finally, we provide a situational assessment of the current state of intelligent food monitoring technologies, discussing material-centric strategies to address their existing limitations, regulatory concerns, and commercial considerations.

**Keywords:** food packaging materials, food spoilage, food contamination, biogenic amines, pH monitoring, pathogen detection, food sensors

## 2.2 Introduction

Despite significant technological and regulatory efforts, issues pertaining to food waste and foodborne illness continue to persist globally.<sup>[45]</sup> With regards to food waste, societal reliance on predicted, static expiry dates is the primary contributor, as it generates the disposal of significant volumes of edible food each year.<sup>[46]</sup> While efforts to better map out the spoilage patterns of individual food types have been made, spoilage is heavily influenced by environmental conditions, making it a non-standardized process.<sup>[27,47]</sup> Strategies to monitor spoilage in real-time are currently

not applied commercially, specifically because conventional means of food monitoring – such as bacterial culturing, are time-consuming, tedious, and futile on an individual product monitoring basis – a prerequisite for spoilage monitoring given its variable nature.<sup>[48]</sup> This has yielded significant interest towards the development of sensors that can monitor spoilage-related changes within food in real-time. While food spoilage is mediated by many different biochemical and microbial changes, shifts in biogenic amine concentration, pH, microbial content, and lipid oxidation have been identified as main contributors (**Figure 2.1a**).<sup>[48,49]</sup> These changes heavily influence the organoleptic properties of food, as detailed in Figure 2.1b. From a sensing perspective, changes in the former two have garnered the most interest, largely due to the diverse means by which these shifts can be tracked using relatively simple reaction cascades.

On the other hand, foodborne illness is largely caused by pathogenic bacteria that contaminate food products at various stages during the food production pipeline (2.1c).<sup>[50]</sup> The consumption of such contaminated foods often results in illnesses with potentially severe prognoses. While several regulatory measures are in place to mitigate the likelihood of such contamination events, pathogenic outbreaks remain rampant. Many pathogenic bacteria are responsible for such ailments, with *Escherichia coli* O157:H7, *Salmonella* spp., *Listeria monocytogenes*, and *Campylobacter jejuni* being four of the most common culprits (Figure 2.1d).<sup>[51–53]</sup> Efforts to proactively detect contamination on a commercial scale currently involve time-consuming and expensive processes that require complex sample processing and shipment to external facilities. Common evaluation strategies include chromatographic and spectroscopic techniques, as well as *in vitro* bacterial culturing and sequencing.<sup>[54]</sup>

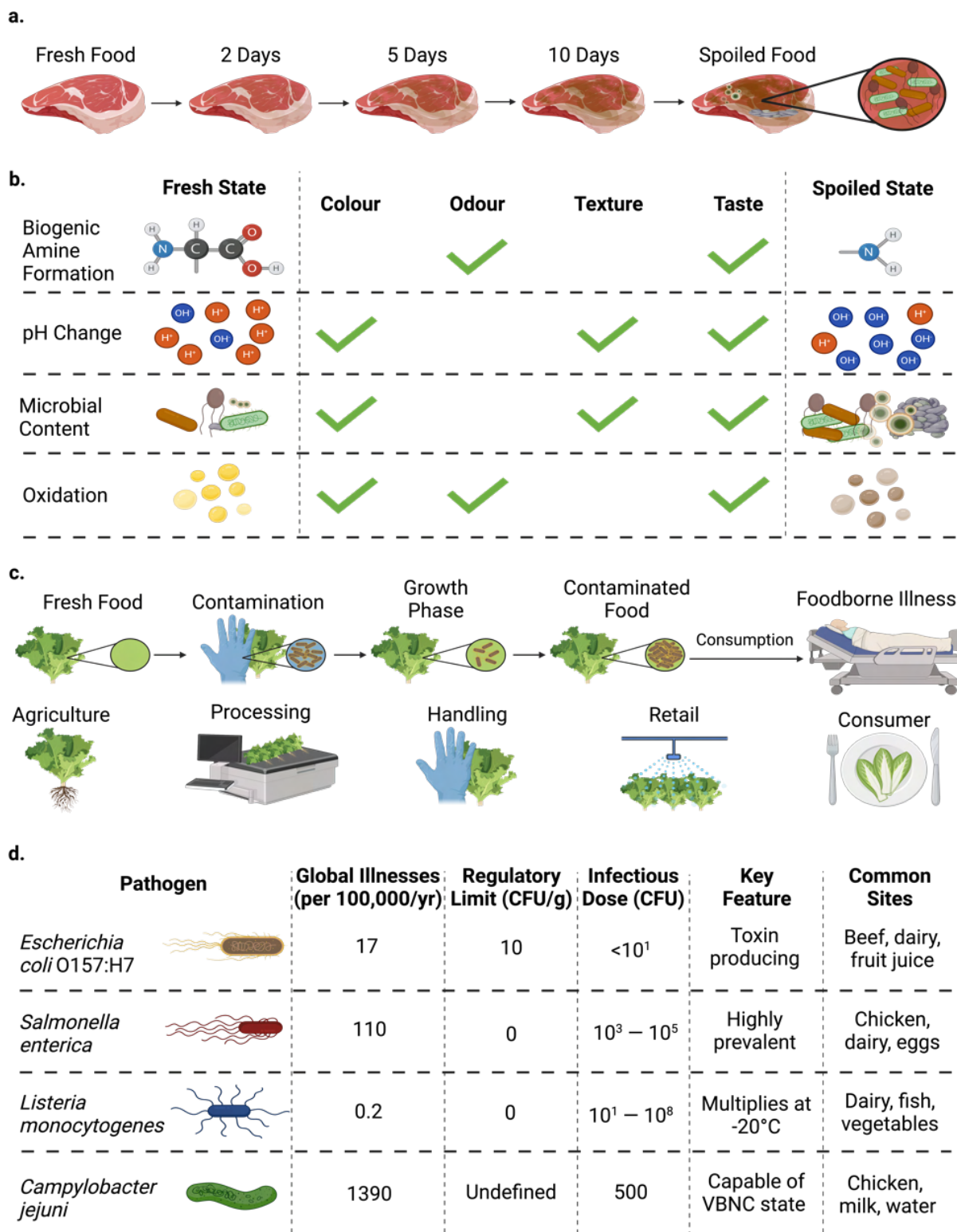
Studies exploring the development of biosensors that enable the monitoring to spoilage and contamination have been widespread.<sup>[17,55–58]</sup> Such sensors target one of two key avenues to real-world implementation: on-site use or in-package integration. On-site use requires sensing platforms with high sensitivity, that can offer output signals within a short period of time. These systems are permitted greater flexibility regarding sample manipulation, as test samples can be



readily processed prior to evaluation. Oppositely, in-package integration requires low cost, autonomous platforms that use biocompatible reagents, which can be applied *in situ*. Such platforms represent a gold standard in food monitoring, as their integration onto packaging materials yields smart food packaging – materials that monitor products over their entire lifespan.

Given that spoilage monitoring requires such constant evaluation, efforts in this space have largely centered upon the creation of *in situ* platforms. These sensors report shifts in biogenic amine concentration and pH *via* electrochemical, fluorescent, or colorimetric means. That being said, some on-site systems have been developed for spoilage monitoring, in hopes of creating commercial scale means of rapid, ultrasensitive testing that can be used as needed. Oppositely, efforts to enable the monitoring of pathogenic contamination in food have yielded both on-site and *in situ* sensors that offer value at different stages of the food production pipeline. Specifically, on-site platforms are extremely valuable within commercial environments, where rapid, ultrasensitive platforms offer significant value over conventional techniques. On the other hand, *in situ* platforms – while usually less sensitive, offer a means by which contamination can be monitored within individual products at a consumer level.

The vast majority of food-targeting sensors are composed of sensing agents immobilized onto or within an associated substrate, as free-state sensors are largely unfeasible in this space.<sup>[16]</sup> Thus, while the capabilities of the incorporated sensing agents undoubtedly influence resultant sensor performance, application-informed material selection is equally contributory. To this end, the material properties, mechanical stability, and biocompatibility of candidate substrates represent key considerations that determine their suitability for particular platforms. While a wide range of metallic and polymeric materials have shown applicability in the food monitoring space, a critical review of the real-world viability and optimal use cases of reported substrates is absent.



**Figure 2.1. Current state of food spoilage and food contamination.** (a) Schematic illustration of food spoilage. (b) Key contributors to food spoilage and their impact on the organoleptic properties of food. (c) Schematic illustrations of the food contamination timeline, and stages at which pathogenic contamination can occur. (d) Annual global illness rates caused by respective

pathogens obtained from the World Health Organization. Regulatory limits as defined by the Food and Drug Administration for ready-to-eat (RTE) products.<sup>[2,59]</sup> Infectious dose recorded in literature. Produced using BioRender.

With consideration towards the rapid progress being made in the smart food monitoring space, this review discusses recent advancements in the development of intelligent sensors designed for on-site and *in situ* detection of food spoilage and contamination. First, an overview of substrate materials used within smart food sensors is provided and their unique material offerings are established. The use of these material in food sensing is then contextualized through a critical review of recently reported sensing platforms. Specific emphasis is placed on the impact of selected substrates on resultant sensor performance. In parallel, recognizing the plethora of different approaches being explored in food sensing, the limitations of presented platforms are highlighted, to assess their real-world viability. Finally, an assessment of the current state of smart food monitoring technologies is provided and future directions aimed at yielding real-world sensors with regulatory and commercial potential are discussed.

### **2.3 Substrate Materials for Smart Food Sensing Platforms**

Materials used in the smart food sensing space can be broadly categorized into metallic, polymeric, or carbon-based in nature, where their vastly different characteristics yield distinctive use cases (**Figure 2.2a**). Specifically, while functional surface chemistry or agent entrapment potential are instrumental for all such sensing platforms, other desirable traits are informed by the target application. In general, on-site testing technologies prioritize material contributions to sensing signal transduction to actualize ultrasensitive, rapid target detection. Oppositely, *in situ* platforms generally target substrates that offer long-term stability in food-relevant environmental conditions and high biocompatibility, to combat concerns pertaining to material leaching. Emphasis on such traits has yielded the development of various emerging materials produced through modifications to established base materials with favourable characteristics. While the value of such materials is best understood in the context of specific applications – as described in

Section 3 of this review, this section provides an introductory overview to base substrates used in this space and their respective properties (Figure 2.2b).

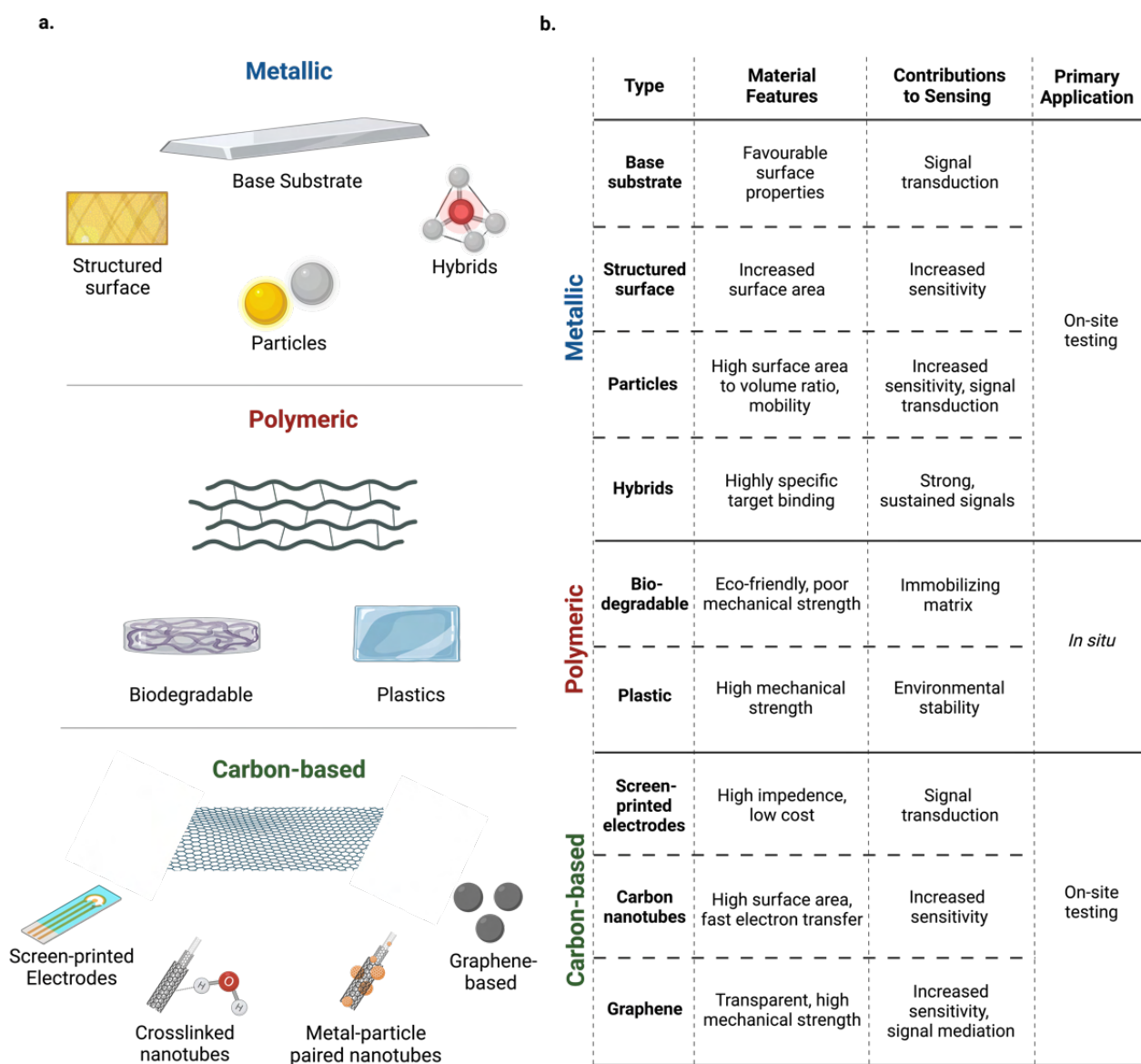
### **2.3.1 Metallic substrates**

While many metallic agents have been established as biocompatible, approval for use within food packaging is stringent.<sup>[60]</sup> Recognizing that they are also quite expensive, commercial incorporation of such materials as sensing substrates within individual products is largely unfeasible. As such, metallic substrates can be considered best suited for on-site testing technologies, where they offer several optical and chemical properties that can be exploited for rapid, ultrasensitive detection of target entities.<sup>[61]</sup>

Gold (Au) is by far the most commonly used metallic substrate in this space. Its high dielectric constant, molecular weight, conductivity, and surface energy have all been exploited within biosensing to increase the sensitivity, stability, and selectivity of the resultant sensing platform.<sup>[62–64]</sup> Yet, the value of Au substrates is most clearly demonstrated through their ease of functionalization.<sup>[65]</sup> While Au is largely inert, it is readily functionalized with thiol-modified agents through the formation of Au-S bonds. In this way, well-established self-assembled monolayers of sensing agents can be immobilized onto the substrate without the introduction of a crosslinking agent.<sup>[62,66]</sup> These densely packed probe monolayers resultantly contribute to high detection sensitivity. That being said, the stability of this crosslinking approach is somewhat questionable given the relatively weak nature of the Au-S bond.<sup>[67]</sup>

The density of detection probes can be further increased per unit area using the diverse Au form factors available. Specifically, aside from a base flat substrate, micro- and nanoscale structures – namely wrinkles and flowers, are well-established in literature.<sup>[68]</sup> Such structural modifications offer higher functional surface area – mediating increased probe density, while also offering antibiofouling properties in certain circumstances, which improves detection performance.<sup>[69]</sup> Concurrently, particle-based form factors are also commonly employed, as they are particularly valuable within in-solution platforms, where they pair high surface area-to-volume

ratios with mobility within the test sample, increasing the likelihood of probe-target interactions.<sup>[70–73]</sup> Further, their size confinement effect yields electronic and optical properties that facilitate their use as electrostatic target detectors and colorimetric transducers, respectively.<sup>[70]</sup> Namely, Au nanoparticles (AuNPs) are well noted for their ability to both quench or enhance the signal of fluorescent molecules, based on their size and specific characteristics of a given system.<sup>[71,74]</sup>



**Figure 2.2. Commonly used substrate materials for food monitoring.** (a) Materials used as substrates within food sensors. (b) Summary of relevant properties and use cases of common

substrate materials. Primary application refers to situations in which the described material is most commonly applied but should not be considered all-encompassing. Produced using BioRender.

Recognizing the high cost of pure metallic substrates, there has been continued emphasis on the development of hybrid platforms that employ metallic agents as a component of the sensing substrate. Namely, recent works in the food sensing have employed Au and silver (Ag) nanoparticles as substrate components within plasmonic sensors.<sup>[75]</sup> Similar to Au, Ag offers high plasmon resonances at the visible-near infrared region of interest, making it a suitable substrate for such sensors.<sup>[75]</sup> Importantly, Ag also shows a propensity for thiol binding, presenting a simple strategy for surface functionalization. Other nanoscale structural forms of Ag have also been employed, with nanodendrites and nanowires both being used for food-related sensing applications for higher surface area and faster electron transfer, respectively.<sup>[76,77]</sup> The latter innovation has yielded significant improvements in the efficiency of sensing cascades, reducing detection times to less than two hours in some cases.<sup>[76]</sup> On a more macroscale, the combination of Ag with polymers and other metals to create composites has also been explored, yielding materials with unique sensing capabilities.<sup>[78–80]</sup> Cost considerations have also yielded increasing interest towards aluminum and silicon-based substrates for plasmonic sensors, but such efforts have not been presented in food sensing.<sup>[75]</sup>

Concurrently, there has been a growing interest in the use of metal-organic frameworks (MOFs) for food biosensing. MOFs are hybrid structures of metal ions conjugated to organic ligands.<sup>[78,81]</sup> Based on the component type and number of ions, as well as the structure of the organic ligand, these MOFs have unique selectivity for target analytes based on shape and size. Typically, these MOFs are composed of lanthanide ions or other fluorophores, that exhibit strong, sustained signalling upon target binding.<sup>[82]</sup> MOFs have been explored extensively in the sensing space as their structure is easily fine-tunable and modifiable, which permits optimization of structural porosity and target specificity.<sup>[81]</sup> Extensive work has been conducted to synthesize MOFs responsive to cues of spoilage and contamination in food. In the intelligent packaging space,

MOFs are convenient as they can be synthesized on packaging materials themselves to make nanocomposite films, often with limited intervention.<sup>[83]</sup> These MOFs act as nanofillers within the film matrix, enhancing the structural performance of the polymer while acting as analyte receptors and signal transducers. Optimized incorporation of these MOFs into various materials is ongoing to maximize their sensing functionality within resultant intelligent films.

### 2.3.2 Polymeric substrates

Principally, polymeric substrates dominate the food sensing space, owing to their low cost and high tunability.<sup>[75]</sup> Such substrates are frequently used for both on-site sensors and *in situ* package sensors. As such, considerations towards material viability are largely defined by the target application. Most prominently, biodegradable polymers – such as cellulose, starch, and chitosan, and plastics – such as polystyrene and polyethylene, have been used in this space.<sup>[61,84]</sup>

Interest in biodegradable polymers is largely driven by environmental concerns surrounding conventional food packaging materials, making such substrates a focus within *in situ* detection platforms.<sup>[85]</sup> Such polymers exhibit high biocompatibility and can be embedded with biosensing agents relatively easily due to their tunable porosity.<sup>[84]</sup> However, they have historically offered poor stability in food-relevant conditions, limiting their real-world applicability.<sup>[86]</sup> To this end, the introduction of various modifications has produced several emerging substrates that are detailed in Section 3. Briefly, recently developed materials have aimed to strike a balance between environmental resilience – largely through the maximization of mechanical and thermal stability, and sensing performance, wherein the incorporation of sensing agents within polymer substrates has reduced film strength at times.<sup>[87,88]</sup> In parallel, efforts have also been made to improve the stability of polymer-entrapped, volatile sensing agents. The use of nanofillers and nanoencapsulation for each of these two objectives, respectively, has garnered significant interest in particular.<sup>[89–91]</sup> With regards to on-site detection platforms, cellulose paper-based substrates have been commonly employed, owing to their low cost and versatility.<sup>[92]</sup> Here, poor stability is of limited concern given the significantly shorter use time.

Despite their detrimental environmental impact, conventional packaging plastics are often favoured for *in situ* applications due to their high environmental stability and barrier capabilities.<sup>[93]</sup> Direct incorporation of biosensing agents onto such polymers can prove comparatively tedious however, requiring surface activation steps using various physical or chemical strategies that offer varying degrees of consistency – especially when applied on a commercial scale.<sup>[94]</sup> Emerging platforms that employ such substrates have thus developed means by which probe immobilization can be simplified and the sensitivity of the resultant platforms can be maximized. Such strategies are also detailed at-length in Section 3.

### 2.3.3 Carbon-based substrates

Carbon-based substrates are heavily used in on-site electrochemical biosensors, where they function as effective signal transducers. Compared to metallic substrates, carbon substrates offer high surface impedance for electrochemical detection at a much lower cost.<sup>[95]</sup> The use of carbon is further substantiated by its successful deployment within screen-printed electrodes, which have been noted for their compact form factor and high detection sensitivity.<sup>[61,84]</sup> Efforts to further improve the performance of these substrates have yielded significant focus towards carbon nanotube substrates, which offer high surface area, antifouling properties, and rapid electron transfer – characteristics that all act to improve detection sensitivity.<sup>[96]</sup> Other nanostructures – namely nanohorns, have also been explored due to similar advantages.<sup>[97]</sup> While carbon substrates offer limited functional surface chemistry, conventional crosslinkers can be used for the biofunctionalization of these substrates with target-specific recognition molecules.<sup>[96]</sup> The pairing of such substrates with metallic particles has also yielded improvements in biofunctionalization.<sup>[84]</sup>

Concurrently, graphene-based substrates have also established themselves as keystone carbon-based substrates for biosensing applications. Alongside their high mechanical strength, favourable surface properties, and high electron transfer capabilities, these substrates are cost-effective and optically transparent.<sup>[98]</sup> This latter property mediates compatibility with various optical transduction strategies. Such optical strategies can be further supported by the inherent



quenching activity of graphene, which has been exploited in fluorescence sensing.<sup>[98]</sup> From a manufacturing perspective, laser-induced graphene producers have found the use of graphene as a base substrate very attractive. In fact, laser-induced graphene has been formed on existing food packaging in recent works.<sup>[99]</sup> Outside of conventional layered graphene-based substrates, the use of graphene quantum dots is also increasing, owing to their tunable photoluminescence and photostability, enabling them to act as transducers.<sup>[100]</sup> Further, combinatorial approaches that pair such agents and metallic nanoparticles have yielded materials with unique properties.<sup>[101]</sup>

## **2.4 Material Developments in Smart Food Sensing Platforms**

With growing demand for improvements in food safety, biogenic amine, pH, and pathogen monitoring have all experienced significant material-driven progress in detection performance, mechanical stability, and commercial potential in recent years. In this section, we detail emerging platforms, with specific consideration towards their real-world viability.

### **2.4.1 Biogenic amine monitoring**

An important mediator of spoilage in food is the growth of bacteria and other microorganisms.<sup>[27]</sup> This growth is influenced by the environmental conditions in which food is stored, including temperature and humidity. Food handling can also introduce extrinsic bacteria into food that then alter the spoilage process. The tracking of bacteria-mediated changes in food has been identified as a potential avenue for the real-time monitoring of food quality. Specifically, tracking compounds produced by the proteolytic breakdown of animal tissue has garnered significant interest. These entities are often toxic when consumed at high levels, further substantiating their use as a detection target. Biogenic amines are one such class of organic by-products, formed by the decarboxylation of amino acids and other nitrogenous compounds.<sup>[102–104]</sup> Histidine, tyrosine, lysine, and ornithine are common sources of biogenic amines during spoilage, forming histamine, tyramine, cadaverine, and putrescine, respectively (**Figure 2.3a**).<sup>[102]</sup>

Importantly, not all bacterial species contain the decarboxylase enzymes necessary to produce these amines, meaning that spoilage and contamination are not universally correlated with

their presence.<sup>[105,106]</sup> Thus, the application of biogenic amines as an indicator of food quality is limited to certain food products, and to the bacteria that typically contaminate them. To this effect, fish and other seafood have been identified as a prime target for biogenic amine monitoring. These products exhibit high concentrations of histidine within their muscles, which is converted into histamine – an agent that can induce poor clinical outcomes, by microbes naturally present within the fish.<sup>[107,108]</sup> Similarly, dairy products also exhibit high biogenic amine formation as they begin to spoil, with tyramine being the most prevalent amine in these foods.<sup>[109]</sup>

Current methods to measure biogenic amines in food include gas and high-performance liquid (HPLC) chromatography, as well as capillary electrophoresis, which all identify specific amine compounds based on their unique structural properties.<sup>[109]</sup> Alternatively, real-time quantitative PCR (qPCR) can also be used to detect the increased expression of decarboxylase enzymes in processed food samples.<sup>[110]</sup> Efforts have been made to improve laboratory techniques for analyte detection, but these methods involve complex equipment, extensive sample processing, and readout analysis, making them unfeasible for on-site, *in situ* detection. While these methods are generally useful for the detection of biogenic amines, an ideal sensor for food monitoring would exhibit high sensitivity and specificity to biogenic amines present within complex food matrices, without the need for sample processing. A variety of systems have been explored under this premise, based on their selective reactivity with different basic/nitrogenous organic compounds. Three common platforms used within this space are nanoparticles, reactive organic compounds (ROCs), and biorecognition probes with specificity for biogenic amines. These platforms interact with biogenic amines *via* electrostatic, covalent, and conformational interactions that transduce into detectable signals (Figure 2.3b). While they are produced within the food matrix as a by-product of protein degeneration, biogenic amines are quickly emitted from food as gaseous compounds as they are volatile in nature. As such, an important physical consideration in the design of these platforms includes the ability of materials to sequester and retain these volatile amine molecules.

#### 2.4.1.1 Nanoparticle-mediated detection

Nanoparticles have become a staple in the biosensing space due to their diverse physical and chemical properties, ease of functionalization, and high surface area-to-volume ratio.<sup>[111]</sup> These are all properties that have been leveraged in the development of electrochemical and colorimetric biogenic amine sensors. Colorimetric detection usually involves the induction of nanoparticle aggregation in response to target binding, resulting in an observable change in colour. For real-world application, an observable colorimetric threshold can be set in accordance with by-product levels indicative of food spoilage, but the qualitative nature of this approach limits system accuracy. In contrast, electrochemical sensors use electrodes or other probes to measure impedimetric and conductive changes in response to nanoparticle-target binding. Within electrochemical biogenic amine sensors, targeted binding of these compounds permits their quantification in real-time. Both systems have been explored heavily in recent years and offer unique benefits and drawbacks, that tailor their use towards varying circumstances.<sup>[112]</sup>

With regards to colorimetric sensing, AuNPs are used extensively, owing to their vivid transition from deep red to purple when shifting from an aggregated to non-aggregated state (Figure 2.3c.i). Such an approach has been applied most commonly in solution, where the free movement of both the target and the nanoparticles maximizes binding events. For biogenic amine detection, these binding events are most easily induced *via* electrostatic interactions that occur between positively charged target amines and negatively charged citrate groups functionalized onto the nanoparticles. These interactions induce aggregation *via* various hydrophobic interactions or the electrostatic binding of multiple nanoparticles to a single target molecule, which brings them closer together in proximity. The precise mechanism of individual systems is often left unclear. El-Nour *et al.* used this strategy in the development of a histamine sensor for chicken, where binding to the target resulted in AuNP aggregation.<sup>[20]</sup> The resultant sensor demonstrated a limit of detection of 0.6  $\mu\text{M}$  but required solid test samples to be homogenized prior to evaluation. Unfortunately, target detection *via* electrostatic interactions means that the system does not

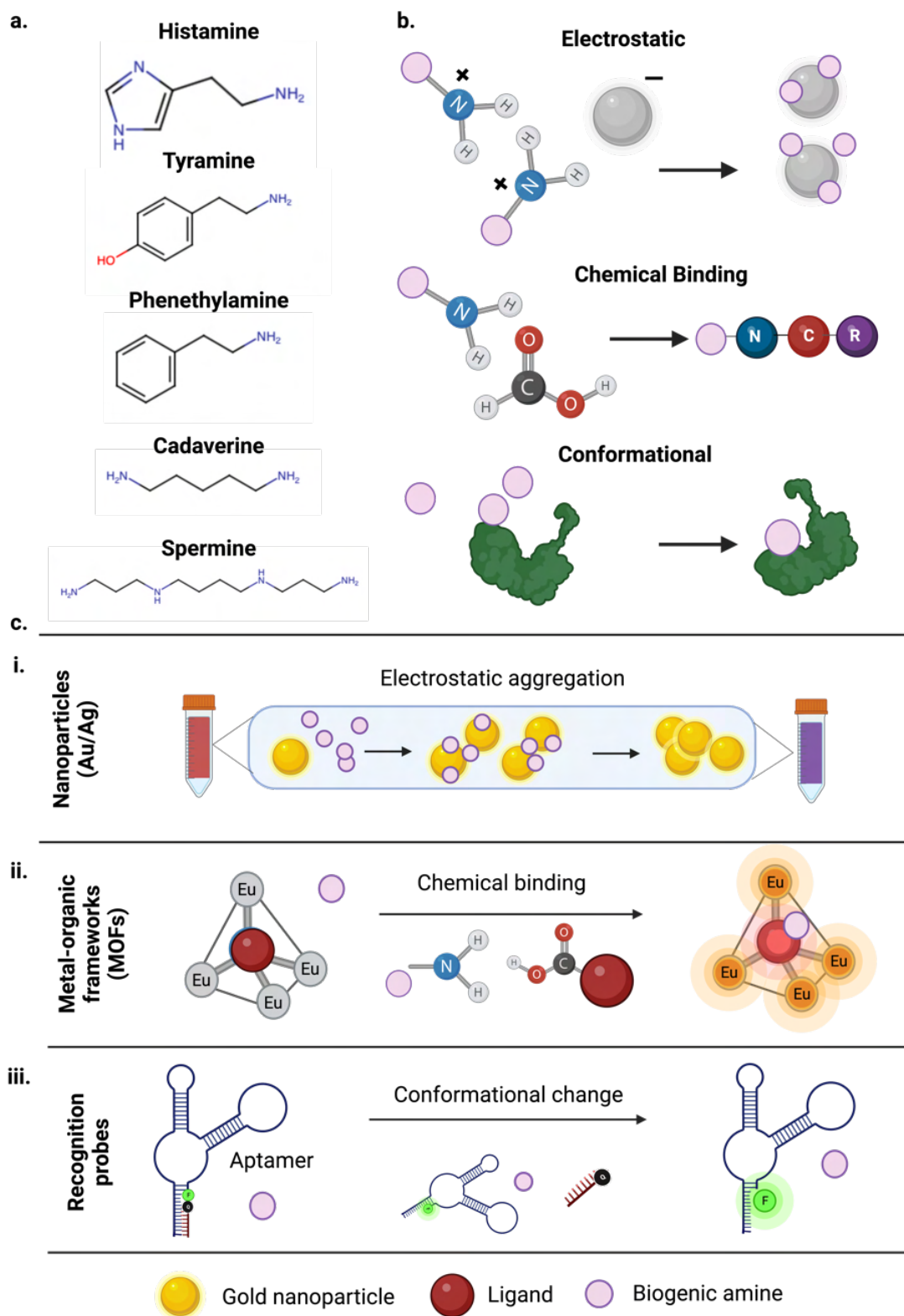
respond to the target with high specificity. Rather, the nanoparticles can react with any similarly charged compounds present in the test matrix, leading to false positives. The existence of a plethora of organic compounds and proteins in complex food matrices makes this a significant concern. In an effort to create a colorimetric histamine sensor with higher specificity, Lapenna *et al.* investigated unmodified AuNPs, that lacked the typically incorporated citrate groups.<sup>[113]</sup> They found that the aliphatic amino group and the imidazole ring of histamine were both capable of binding to the gold surface. As such, histamine can act as a crosslinker between AuNPs in the absence of capping agents such as citrate. The resultant sensor was assessed in wine and showed a limit of detection of 0.2  $\mu\text{M}$ . Ultimately, while the colorimetric nature and high sensitivity of these platforms are intriguing, their in-solution nature and need for sample homogenization prevents their use *in situ*.

Aiming to eliminate processing and homogenization steps, many recent works have developed biogenic amine-targeting intelligent noses.<sup>[114,115]</sup> These intelligent noses often use nanoparticle-based reaction cascades to monitor gas production, which can lead to colorimetric signals in a solid-state format. Further, some approaches use closed systems to retain volatile amines for prolonged amounts of time – a strategy that offers improvements in detection sensitivity. By overcoming the need for direct contact with food, these platforms eliminate concerns pertaining to sensor surface fouling and limit the likelihood of cross-reactivity with non-target compounds. There is significant diversity in the mechanisms these systems use to yield accurate signals, but food-targeting systems demand specific emphasis on use of ease to enable widespread deployment.

Under this premise, Gholampour *et al.* (2021) developed a colorimetric intelligent nose that employed a cadmium (II) ion-embedded polyethylene-glycol (PEG) and polylactic acid (PLA) copolymer that released the immobilized ions in response to gaseous pH increases induced by the accumulation of vaporized amines.<sup>[116]</sup> PEG-PLA copolymers are commonly used in controlled-release systems, with slow degradation of the copolymer over time leading to the release of

nanoparticles or drugs into a biological matrix.<sup>[117,118]</sup> Such a system offers control over the rate of  $\text{Cd}^{2+}$  ion release into foods over time to interact with anionic amines. This triggers colour changes that correlated with increases in amine vapours. To make their system applicable to *in situ* detection in food, they incorporated their polymer into agarose hydrogels, which permitted the permeation and increased retention of trimethylamine vapour into the detection system. The system showed successful colorimetric detection of spoilage at room temperature, but minimal change was observed after 24 days at 3°C. The spoilage state of this sample was not specified, and thus the efficacy of the system remains unclear. While intriguing, the system is quite complex, limiting its commercial viability. Further, the toxic nature of cadmium poses a hurdle for real-world use.

Similarly seeking to create an alternative intelligent nose, Tseng *et al.* (2017) developed a nanoparticle-based paper sensor for the detection of putrescine and spermidine.<sup>[119]</sup> Here, a mold was used to print silver (Ag) and Au nanoparticles onto paper substrates using reversal nanoimprint lithography. Nanoparticle immobilization onto solid substrates to create films for biosensing, rather than using them in an in-solution format reduced the level of user interference required. This strategy yielded over 85% transfer efficiency from the mold to the substrate. Using lithography to imprint the nanoparticles onto papers is cheap and efficient, as it eliminates the need for chemical modifiers. In the resultant sensing platform, interactions between the immobilized nanoparticles and the targeted amines led to a measurable wavelength dip shift as measured by localized surface plasmon resonance (LSPR). This same shift did not take place when the sensors were exposed to other common gases in the air. This system was evaluated as a spoilage detection platform for salmon and demonstrated a limit of detection of 13.8 ppm. From an application perspective, the authors argued that this system is well situated as a rapid, low cost, on-site detection tool. However, the need for LSPR measurements is likely to severely hinder widespread commercial use and eliminates the possibility of consumer level monitoring. This is common with the use of nanoparticles as a biosensing platform, as they do not elicit significant visual signals upon aggregation when immobilized onto materials.



**Figure 2.3 Strategies to detect biogenic amine accumulation in food.** (a) Structures of common biogenic amines produced during food spoilage. (b) Interactions that mediate the detection of

biogenic amines. (c) Mechanisms for signal transduction in response to biogenic amine binding: (i) colorimetric nanoparticle aggregation, (ii) fluorescence shifts within metal-organic framework, and (iii) signal-inducing conformational changes within probes. Produced using BioRender.

Ultimately, the use of nanoparticles for biogenic amine detection is largely driven by their high surface area, ease of functionalization, and contributions to signal transduction within both colorimetric and electrochemical platforms. In comparison to other platforms, nanoparticles are also cost-effective as they are relatively easy to synthesize and functionalize.<sup>[63,73]</sup> Moreover, sensing cascades can be designed to activate nanoparticle aggregation at a predefined biogenic amine concentration, without any user interference.<sup>[20]</sup> Yet, while some recent works have shown an ability to differentiate target biogenic amines from chemically similar non-target compounds, nanoparticle-based systems offer limited specificity. Further, the incorporation of nanoparticle-based platforms *in situ* is difficult to implement due to regulatory hurdles. While some nanoparticles are FDA-approved for usage as therapeutics and drug-delivery agents for disease treatment, their use in consumables requires further investigation. As such, concurrent research has applied alternative agents that – in some cases, offer more specific interactions with biogenic amines, to maximize sensor accuracy.

#### 2.4.1.2 Reactive organic compound-mediated detection

Various reactive organic compounds (ROCs) carry inherent reactivity with biogenic amines, offering a promising avenue for their detection. This reactivity can be non-specific, and mediated generally by positive charge, or can be specific for the structures of distinct biogenic amines. Changes in the electron distribution and the creation of new reactive by-products following ROC–biogenic amine reactions enable detection *via* electrochemical, colorimetric, or fluorometric transduction. A benefit to the use of such compounds is the relative ease with which they can be fine-tuned and modified to increase their target selectivity. While enhanced reactivity with amines and other basic compounds could also lead to an increase in background signals, incorporation into intelligent noses can limit such effects. Prevalent ROCs used for the detection

of biogenic amines include pyrylium salts, donor- $\pi$ -acceptor conjugation structures, metal-organic framework structures, and metallocomplexes.

Pyrylium salts are aromatic compounds that react with biogenic amines to derive pyridine, or similar conjugated analogs. This conversion changes the fluorescence profile of the compounds, enabling their use as chameleon labels (ChLs) – labels that change in colour or fluorescence upon interacting with biological molecules. One study recently explored the use of pyrylium salts in crafting ChLs to detect putrescine and trimethylamine.<sup>[120]</sup> In this platform, the salts were deposited onto silica gel-coated aluminum strips to create amine-responsive ChLs. Other convenient material candidates for the development of ChLs include organic polymeric matrices such as cellulose, that readily absorb reactive probes. These labels underwent fluorescence quenching over time owing to increased binding of target amines. An LOD of 0.1  $\mu\text{M}$  was obtained for both biogenic amines in a gaseous state. When stored with fish samples at room temperature, the platform demonstrated an 85% quenching efficiency in 18 hours, validating its use as an *in situ* monitoring system. Qi *et al.* (2021) developed a similar fluorescent sensor by immobilizing a pyrazine compound (PD-6) onto edible gelatin films.<sup>[121]</sup> Due to the entrapment of the sensing agent within the substrate matrix, a high density of the compound could be introduced relative to two-dimensional surface immobilization. The sensor exhibited strong changes in fluorescence in response to target amine exposure, while displaying minimal reactivity with non-target amine-based compounds. These films were also reusable, as the addition of conjugate acids reversed biogenic amine binding and mediated the reproduction of the PD-6 derivative. Ultimately, pyrylium salts offer an easy-to-incorporate tool for biogenic amine detection. However, considering that fluorescence signalling is difficult on a consumer scale, colorimetrically signalling ROCs have been studied in parallel.

To this end, donor- $\pi$ -acceptor (D- $\pi$ -A) conjugation structures are similar compounds that can be co-opted for use in intelligent films, changing in fluorescence or colour in response to a variety of toxins and compounds present in food. Prosthetic substitution of D- $\pi$ -A compounds can be used to induce changes in responsiveness to specific compounds. Duan *et al.* evaluated the use



of a D- $\pi$ -A structure substituted with benzoic acid (DPABA), which exhibited sensitivity to both solid and gaseous state amines released from fish during spoilage.<sup>[122]</sup> The formulation of DPABA ChLs involved simply soaking cellulose films in DPABA solution. In response to target exposure, DPABA exhibited changes in both colour and fluorescence. When incorporated into packaging in the form of food ChLs, these sensors showed a limit of detection as low as 0.3-0.6 ppm of ammonia, fading in colour from red to pink, and then to yellow in response to decreased freshness. A toxicity assay confirmed that DPABA had no cellular toxicity at the concentrations being used in the developed system. However, further toxicity studies are required for reactive compound-incorporating ChLs, including time-course studies that evaluate leaching into foods. The practicality of this system is hindered by the limited selectivity of DPABA though, which exhibits a degree of cross-reactivity with non-target agents present within food. The evaluation of alternative prosthetic groups that offer higher specificity represents a viable next step, warranted by the colorimetric transduction these compounds offer.

As an alternative means of achieving optical signals, MOFs have been explored extensively.<sup>[29,123–125]</sup> These compounds are composed of coordinately bonded organic ligands and metal ions, that collectively form complex multi-dimensional structures. When these compounds are paired with porous coordination polymers, hybrid polymers with distinct reactive properties are produced (Figure 2.3c.ii). These properties are easily tunable *via* manipulation of the constituent MOFs with different metals ions and organic groups. The use of MOFs for biogenic amine detection is substantiated by the structural voids they possess, which enable entrapment of gaseous compounds. Retention of these compounds does not permanently alter MOF structure, allowing each framework to sequester volatile compounds multiple times for enhanced detection. Based on their nature, these MOFs can undergo changes in luminescence, fluorescence, and electric potential upon target binding, offering flexibility in system design. Lanthanides are commonly used as the metallic element of MOFs as they can undergo photobleaching-resistant increases in luminescence.<sup>[82]</sup> With regards to biogenic amines in particular, these MOF-

incorporating polymers have demonstrated responsiveness to amines present in both solid and gaseous states with high sensitivity. Modifications to the MOF structure using prosthetic ligands that selectively bind to the imidazole rings or aromatic groups of biogenic amines can be used to fine-tune system performance. Namely, Xu *et al.* (2017) developed amine-detecting cellulose hydrogels composed of methyl red (MR)-conjugated europium MOFs (EuMOFs).<sup>[19]</sup> Both MR and Eu ions exhibited fluorescence shifts in response to the presence of biogenic amines, owing to a pH-induced energy transfer. This was paired with a pH-induced colorimetric shift of MR. System evaluation using histamine gas demonstrated a limit of detection of 100 nM. That being said, the specificity of this platform remains unclear. Further, the use of pH indicator compounds such as MR raises concerns pertaining to toxicity. While the platform does not require direct contact with the food matrix, implementing such compounds within food packaging is unlikely to be regulatorily approved.

Rather than using such pH-responsive compounds, Yao *et al.* (2021) described a similar tetrahedron cage composed solely of lanthanide ions and a tris-beta-diketone ligand, the shape of which was optimized for the permeation of biogenic amines.<sup>[126]</sup> This system used the stabilizing ligand within the MOF structure itself to engage in covalent target binding, which subsequently enabled an inherent luminescent shift. Using spin-coating, a film composed of this MOF was produced, demonstrating an optical response to amine exposure within seconds. While this rapid response offers significant promise, the ligand binds target molecules through a simple carbonyl-amine reaction. The generalized nature of this reaction makes the system susceptible to false positives induced by other volatile nitrogenous, non-target small molecules.

A MOF-based platform with higher specificity was developed by Jindal *et al.* (2020), who used a cadmium MOF that exhibited fluorescence quenching upon reacting with biogenic amine vapours. Rather than using luminescence, this approach co-opts changes in autofluorescence that take place with chemical bonding. This shift is induced by the deprotonation of imidazolium cations within the MOF structure.<sup>[127]</sup> The structure showed ultrasensitive detection towards

aliphatic biogenic amines to the order of 56 ppb owing to their higher compatibility with the system's reaction mechanism. A degree of affinity was also observed against aromatic biogenic amines, permitting generalized biogenic amine detection. Ultimately, such studies that fine-tune MOFs with more specific reactivity to distinct biogenic amine subtypes are required for the development of more applicable platforms.

The last commonly used ROC-based biogenic amine detection strategy involves the use of metallocomplexes. These are heterocyclic compounds that carry natural reactivity with positively charged amine-based species, which ligate their metal groups to change compound structure. In relation to biogenic amine detection specifically, Sahudin *et al.* recently developed sensing films by conjugating Zn to salphen, *N, N'*-phenylenebis (salicylidene) – a Schiff base, to form stable metal complexes.<sup>[128]</sup> These structures were then immobilized onto transparent silica microparticles, which bonded selectively to histamine vapour secreted from food and subsequently exhibited an increase in autofluorescence. These microparticles are both anionic and hydrophilic in nature, improving the ease of functionalization of the Schiff base, as well as the retention of cationic amines. When immobilized onto glass slides, these particles achieved a detection limit of 4.4 pM with histamine-spiked shrimp, increasing up to 73% in fluorescence after exposure. Importantly, the Zn-salphen complexes demonstrated binding selectivity for histamine and biological amines over other common amine-containing organic compounds, ensuring strong signal correlation with spoilage. The system also demonstrated increased selectivity towards histamine – an aromatic amine, relative to other aliphatic amines, ensuring a degree of specificity towards the target structure. Lai *et al.* (2021) applied a similar strategy to create fluorescent nanofilms that enable non-destructive, direct-contact detection of spoilage in food. They derived nanofilms on glass by condensing a Calix [4] pyrrole derivative (CPTH), which promoted metallocomplex self-assembly with a tetraphenethylene derivative (TPEBA) at an air/DMSO interface. TPEBA exhibits innate fluorescence that quenches after binding to volatile amines.<sup>[129]</sup> To increase system specificity towards aliphatic amines, the films were nanostructured, and

yielded a limit of detection of 0.89 ppm. The effect of the nanostructures on specificity remained unclear however, as the study did not evaluate sensing performance in the presence of non-target, volatile organic compounds, which could competitively bind the nanofilms.

A variety of chemical probes thus exist that can be leveraged as intelligent noses for biogenic amine detection. D- $\pi$ -A conjugation structures, MOFs, and similar metal-complex platforms carry the advantage of being highly tunable in terms of shape, specificity, chemical nature, and signal transduction, offering several avenues for performance optimization. Large-scale manufacturing strategies for MOFs as biosensors are currently being developed. A significant benefit of using these chemical probes is that they can often be recycled and reused within biosensing films.<sup>[130]</sup> Typically, treatment with acids and bases can cause a restoration of the structure of the parent compound, permitting repeated use. The primary limitation to their use for *in-situ* monitoring thus becomes their long-term retention within packaging films. Recognizing that specificity towards subtypes of target biogenic amines remains the most prominent limitation of existing systems, such optimization represents the focus of future works in this space.

#### 2.4.1.3 Probe-based detection

Like the aforementioned chemical agents, many biological macromolecules also carry inherent affinity for biogenic amines. Examples of such molecules include enzymes and antibodies, and functional oligonucleotides, all of which can be used in biogenic amine detection as biorecognition probes. Such systems have been explored extensively, owing to their high long-term stability, specificity, and selectivity.

DNA aptamers are a class of functional oligonucleotides that selectively bind specific molecular targets (Figure 2.3c.iii).<sup>[131]</sup> In contrast to antibodies, which offer similar functionality, aptamers are cheaper to synthesize, as they do not require the generation of hybridomas or the use of animals. They are also less prone to degradation and highly specific in their target recognition abilities, with limited cross-reactivity to related molecules.<sup>[132,133]</sup> Such probes can also be multiplexed within biosensors with relative ease, enabling the detection of an array of biogenic

amines in parallel.<sup>[134]</sup> Considering these advantages, Lerga *et al.* described the derivation of H2, a DNA aptamer with high binding affinity for histamine, as quantified by its low dissociation constant ( $K_D = 3\text{-}34\text{ nM}$ ).<sup>[135]</sup> The authors subsequently incorporated the developed aptamer into a solution-based, on-site platform for histamine detection. By pairing biotinylated aptamers with streptavidin-horseradish peroxidase, colorimetric detection limits of 18 pM and 76 pM in buffer and urine was reported, respectively, with little competitive binding from other biomolecules. This efficacy of this system is somewhat reduced by the immobilization of histamine onto magnetic beads, as this restricts their orientation, limiting their interactions with aptamers. Nonetheless, the system remained highly sensitivity, showing high applicability as a sensor for liquid test matrices. Unfortunately, the use of such a reaction cascade for solid food matrices would likely prove unfeasible. Seeking to evaluate solid samples nonetheless, the same authors (2020) immobilized the H2 aptamer onto AuNPs to colorimetrically detect spoilage in fish samples *via* NaCl addition.<sup>[136]</sup> While the system showed no *in situ* value, given that it required substantial sample homogenization and processing prior to testing, this study sought to substantiate its use within complex food matrices. In this system, dispersed AuNP-H2 complexes – appearing red, withstood nonspecific NaCl-mediated aggregation due to the presence of aptamers. Upon biogenic amine exposure, the aptamer bonded selectively to histamine and the free AuNPs aggregated, appearing blue. A limit of detection of 8 nM was reported.

In another instance, Dwidar *et al.* used a previously derived A1-949 RNA-histamine aptamer to develop a fluorescent biogenic amine monitoring system with a detection limit of 1  $\mu\text{M}$ .<sup>[137]</sup> They first constructed a fluorescently labelled L-DNA version of their aptamer, more stable than its RNA counterpart. This was then coupled with a complementary oligonucleotide that contained a quencher which was released following substrate binding, yielding a fluorescent signal. The A1-949 aptamer is less sensitive than the H2 aptamer with a dissociation constant of 370 nM, contributing to the system's lower limit of detection. Fluorescent aptamer labelling is more convenient than an HRP-conjugated system, as it does not require the addition of any external

reagents. Again however, this system required sample homogenization and processing prior to testing, making it unfeasible for *in situ* use.

In contrast to DNA, the advantage of using certain peptides is the abundance of existing candidates that react with amine-based compounds physiologically. Antibody probes are one such peptide-based biorecognition element for monitoring amine production in food. Namely, Zeng *et al.* recently used histamine-binding antibodies within a lateral flow assay aimed at monitoring fish products.<sup>[138]</sup> The sensor was capable of detecting 0.25 mg/kg of histamine within complex test matrices within 15 minutes. Alternatively, Parate *et al.* developed a similar chip-based sensor consisting of histamine-specific antibodies conjugated to interdigitated electrodes for electrochemical detection of the target.<sup>[139]</sup> These sensors demonstrated a limit of detection of 30  $\mu\text{M}$  in tuna broth. Ultimately though, these platforms have limited *in situ* applications, as they require a liquid interface to be able to capture histamine ions for effective detection. They do, however, offer some perspective on the viability of antibody-based lateral flow and electrochemical sensing, respectively, for on-site food monitoring.

Aside from amine-specific antibodies, other peptides – namely monamine and diamine oxidase enzymes, also exhibit biogenic amine responsiveness. These enzymes are useful as they not only bind to biogenic amines as antibodies do, but rather produce reactive by-products that can be used for detection. These enzymes also have many free carboxyl and amine groups, which mediate their functionalization onto surfaces with limited impact on enzyme activity. Under this premise, Kacar *et al.* immobilized both enzymes onto indium tin oxide nanoparticles, which were then coated onto electrodes to develop amperometric amine sensors.<sup>[140]</sup> These electrodes displayed high sensitivity towards biogenic amines – particularly putrescine, histamine, and cadaverine, *via* Prussian blue-mediated reduction of the  $\text{H}_2\text{O}_2$  by-product formed by the oxidase enzyme. Further, the sensor showed effective detection when tested with homogenized fish and cheese samples. Importantly, while the functionality of using amine oxidase enzymes can be called into question because of non-specific reactions with non-target amino-based biological

compounds, the study filtered for biogenic amine-triggered reactions by employing a low potential. Similarly, Torre *et al.* (2019) described the cross-linking of diamine oxidase onto a screen-printed electrode using bovine serum albumin and glutaraldehyde, which showed responsiveness to histamine present within liquid fish extracts.<sup>[103]</sup> While some interference was seen from other amines – namely phenylethylamine and spermine, the high prevalence of histamine within spoiling fish samples was noted to limit the impact of non-specific signals. Another electrochemical enzyme-based approach was presented by Vanegas *et al.* (2018), who coated graphene surfaces with copper nanoparticles conjugated with diamine oxidase for biogenic amine detection.<sup>[141]</sup> They used a liquefied fish paste to show highly selective detection of histamine, with a limit of detection of 11.6  $\mu\text{M}$ . Seeking to the biogenic amine detection capabilities of these enzymes with one another, Boka *et al.* (2012) compared their efficacy for amperometric electrode sensing.<sup>[142]</sup> They showed that diamine oxidase can be used to measure total BA content because of its limited specificity, monoamine oxidase could be used for tyramine, tryptamine, and phenylethylamine, and putrescine oxidase could be used to selectively measure putrescine in isolation. Ultimately, the use of these systems continues to be limited by the questionable *in situ* compatibility of such reaction cascades and the need for complex readout equipment.

A variety of biosensing approaches continue to be explored for the detection of biogenic amines in food as markers of spoilage. Strategies for using biogenic amines to detect spoilage should vary between different types of foods. For some foods, specific detection of certain biogenic amines that are produced only during spoilage is convenient. Multiplexed detection is an advantageous strategy for monitoring spoilage in other foods, where parallel sensing would provide a more comprehensive assessment of spoilage. The synthesis of multiplexed biogenic amine sensors is possible with highly specific and selective biorecognition probes, such as aptamers or MOFs. Given the magnitude of food waste globally, the need for such real-time, food quality sensors are well-established. While many of the discussed platforms are well-situated as on-site detection tools, *in situ* detection remains the gold standard to allow for monitoring

throughout the entire food production and consumption pipeline. Many of the biogenic amine-based sensors lack *in situ* compatibility in their current form due to issues surrounding system cost and detection specificity, but significant advancements have been made towards this objective, as detailed above. Concurrent evaluation of other systems that offer increased viability for *in situ* spoilage monitoring has yielded significant focus on pH sensors.

### 2.4.2 pH monitoring

As an alternative to tracking highly specific entities, pH monitoring has been used as a more generalized means of real-time food quality assessment.<sup>[143]</sup> pH changes in food are induced by an accumulation of metabolic products such as lactic acid, and the aforementioned biogenic amines, largely formed through bacterial growth and protein degradation. Given that such activities encompass the main contributors to food spoilage, changes in food pH are considered to be reflective of food quality.<sup>[143–145]</sup> Importantly, given that bacteria actively contribute to changes in food pH, real-time pH detection can be considered to account for adverse changes in microbial population introduced by poor storage conditions and contamination – a characteristic that increases the utility of such platforms. Concurrently, environment-induced fluctuations in pH can directly promote microbial growth and compromise the integrity of biomolecules within food itself, promoting rancidity.<sup>[144,146]</sup> Such events make the tracking of pH itself advantageous.

Yet, as opposed to biogenic amines or bacteria, where elevations directly correlate with deteriorating food quality, the relationship between pH and food quality is much more variable. Specifically, food products exhibit diverse baseline pH values, and the direction in which spoilage and contamination shift these values is not universal (**Figure 2.4a**). For example, fruit exhibits a decrease in pH over time due to an accumulation of organic acids during the ripening process. Contrarily, meat displays an increase in pH, largely induced by the production of bacterial by-products. This variability means that each food product must be evaluated independently to characterize correlations between spoilage and pH. Until now, studies seeking to report such



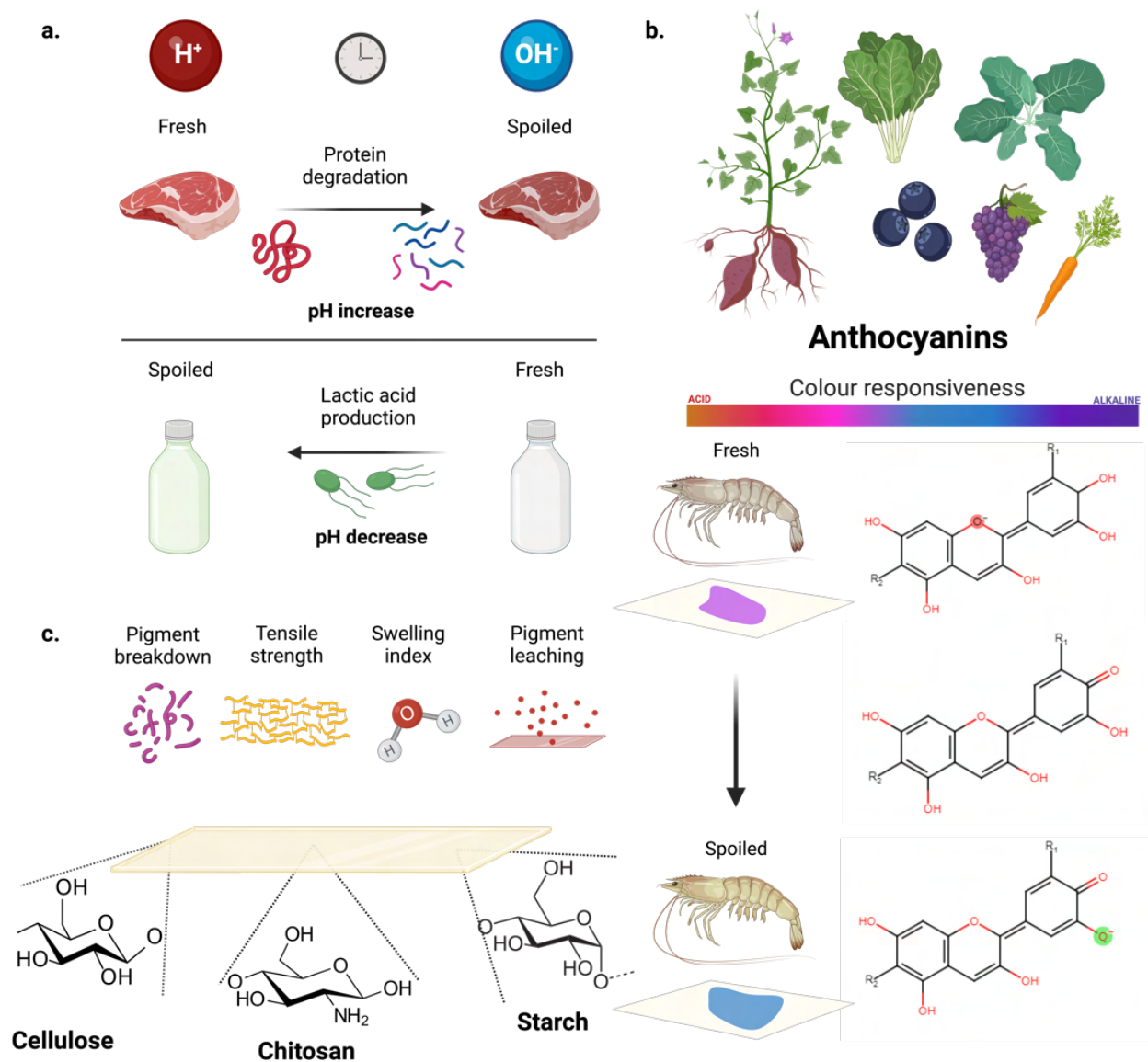
relationships have largely focused solely on fruits and meat due to their perishable nature and high dietary consumption.

Further, considering its generalized nature, correlating pH values to the point at which a given food product becomes inedible has proven difficult. To substantiate the use of pH-based sensors as real-time food quality indicators, the establishment of well-defined spoilage thresholds is necessary. Nonetheless, the plethora of food-targeting pH sensors reported thus far offer a significant improvement over existing industry-standard, static expiry dates, by allowing users to gain some insight into the general quality of a given product in real-time. These pH sensors have historically involved the use of chemical dyes that undergo colour changes as pH fluctuates. While several agents can be used for this purpose, an important consideration in food monitoring is the biocompatibility of the dyes, to ensure safe applicability onto food samples. To this end, non-toxic, organic, dye-based compounds are used.<sup>[147,148]</sup>

#### *2.4.2.1 Anthocyanin-based pH sensors*

Innately present within different types of fruits, flowers, and vegetables, anthocyanins are a class of such non-toxic, dye-based compounds that function as pigmenting agents (Figure 2.4b).<sup>[147,148]</sup> These compounds are typically pH responsive, which they transduce *via* a colour change. Most often, they are red at acidic pH levels (<7), purple under pH-neutral conditions, and blue at basic pH levels (>7). This colour scheme is not universal however, with many anthocyanins exhibiting notably different signal transduction spectra. Importantly, the pH response signals of anthocyanins are often reversible, enabling sensor reusability. This has been demonstrated within various studies, where anthocyanin-embedded packaging that was stored on spoiled food samples reverted to their initial colour state following open air incubation. Concurrently, anthocyanins also boast innate antimicrobial and antioxidant capacities – characteristics that have yielded interest into their value as therapeutic candidates for cardiovascular disease and neurodegeneration.<sup>[149,150]</sup>

Within the scope of food packaging, these antioxidant and antimicrobial properties make anthocyanins viable candidates for food preservation – a growing area of research, but outside the scope of this review.



**Figure 2.4. Intelligent monitoring of pH changes in food.** (a) Opposing pH changes in different subtypes of foods, mediated by distinct processes. (b) Anthocyanins, the predominant organic food dye used in pH-mediated monitoring of food spoilage, undergo chemical reactions that result in dramatic colour shifts. (c) Various organic materials used to derive intelligent pH-monitoring films, and parameters for optimization to enhance performance in situ. Produced using BioRender.

A variety of different plants have been used to source anthocyanins for pH sensing, with common targets including black carrot, red cabbage, purple potato, pigmented berries and corns, eggplant, and other richly coloured fruits and vegetables.<sup>[151–153]</sup> All of these sources have been found to yield anthocyanins with good pH responsiveness in buffer. The use of anthocyanins and other such organic dyes are also convenient for pH detection as they enable reagentless sensing, and intrinsically change colour in response to pH changes. Within more complex environments however, these compounds have exhibited poor stability. Thus, recent efforts in the food monitoring space have centered upon maximizing stable anthocyanin incorporation into packaging films, to enable *in situ* detection. Specifically, anthocyanins have been successfully incorporated into polymeric films composed of natural polymers such as cellulose, chitosan, and various starches, as well as synthetic polymers such as polyvinyl alcohol (PVA).<sup>[153]</sup> Synthesis of these films is simple, and involves blending of component starches or polymers, followed by mixing with plant-extracted anthocyanins.<sup>[152]</sup> Stabilizing agents such as glycerol or other plasticizing agents are also added prior to casting. Film preparation is usually conducted at low humidity and temperature, to limit film hydration and subsequent anthocyanin degradation.<sup>[152]</sup> While natural polymers have been explored heavily due to their biodegradability and limited toxicity, their use within *in situ* pH sensing systems is further driven by their chemical properties.

Specifically, an important consideration in the development of pH-monitoring films is low susceptibility to fluctuations in pH. Significant changes in pH can compromise the integrity of some materials, impairing their ability to act as functional sensors. To this end, organic polymers are relatively resistant to such degradation, thus acting as a stable interface for anthocyanin-pH interactions.<sup>[88,154]</sup> The exploration of such a diverse range of materials has also been necessitated by the need to limit the rapid degradation of anthocyanins, to induce improvements in pH responsiveness.

Simultaneously, it is important to consider the effect anthocyanin incorporation has on the stability of the polymer matrix. To this end, the swelling index (SI), water solubility (WS), and

tensile strength (TS) of developed films are commonly assessed, to consider their viability for *in situ* use over the duration of a given product's lifespan (Figure 2.4c).<sup>[155]</sup> Low SI and WS values are imperative in ensuring that films do not expand exponentially over time within fluid-rich food matrices. Such expansion risks leeching of incorporated anthocyanins, which can result in ambiguous and inconsistent colorimetric signals.<sup>[156]</sup> Unfortunately, anthocyanin incorporation often induces higher SI and WS values because of their propensity for interactions with water molecules.<sup>[157]</sup> The existence and magnitude of such interactions depend on the chemical nature of a given anthocyanin.<sup>[158]</sup> Anthocyanins that exhibit defined colour changes while exhibiting relatively lower affinity for water are thus optimal. Efforts to further improve system stability are focused on film material optimization. Concurrently, TS provides a measure of the mechanical strength of a given film – a consideration that is vital for real-world applicability, given the manner in which food packaging materials are handled.

#### *Material optimization of anthocyanin films*

Most recently developed anthocyanin films have reported polymer blends that yield properties superior to the constituent materials alone. To this end, cellulose-chitosan films have shown significant promise, owing to improvements in the mechanical and chemical characteristics of resultant films. Namely, Alizadeh-Sani *et al.* created a matrix composed of chitosan nanofibers and methyl cellulose *via* a solution casting approach that entrapped saffron petal anthocyanins within the polymeric matrix.<sup>[159]</sup> Compared to a pure cellulose substrate, the study noted a significant reduction in moisture content within the film following the incorporation of chitosan nanofibers and anthocyanins. This was attributed to the replacement of water molecules by these entities within the film matrix. While a promising development, these hybrid films offered limited anthocyanin carrying and retention capacity due to the larger size of the constituent polymers. Concerns surrounding anthocyanin retention are further amplified by the system's reliance on physical entrapment for anthocyanin immobilization.

Comparatively, PVA can form direct interactions with embedded anthocyanins. Such interactions stabilize their immobilization within resultant films and limit interactions with water molecules in the environment, which can accelerate their degradation. Under this premise, Kuswandi *et al.* created red cabbage anthocyanin-embedded bacterial cellulose-PVA films, *via* a simple protocol that involved the immersion of cellulose films in a 1% PVA-anthocyanin solution.<sup>[160]</sup> As expected, anthocyanin incorporation alone yielded an increase in the SI and WS, but this was counteracted by PVA, resulting in properties comparable to the cellulose base film. Unfortunately, PVA incorporation did not yield any improvements in TS and resultantly failed to counteract the plasticizing effects of anthocyanins. As such, a reduction in TS was observed from 65.2 MPa to 39.5 MPa. These sensors were used to detect pH decreases in milk colorimetrically, displaying a transition from blue-gray to pink as the milk spoiled. The authors argued that the improved anthocyanin stability afforded by these sensors qualified their use for *in situ* spoilage monitoring, as the films could be embedded onto milk and juice bottle caps. Such a set-up would limit mechanical stress on the film, limiting concerns pertaining to the decreased TS.

Operating under a similar premise, Vo *et al.* successfully used anthocyanin-embedded, PVA-infused chitosan films for the pH monitoring of pork samples.<sup>[161]</sup> Sodium tripolyphosphate (TPP) was added into the polymer matrix to improve film strength *via* the induction of increased intermolecular interactions. While the optimized 35/65 PVA to chitosan blend offered some improvements in performance, the TS of the developed film remained suboptimal. Ultimately, further material interventions are needed to overcome the poor mechanical strength of such films.

Compared to chitosan, starch films offer significantly worse mechanical properties. Nonetheless, studies seeking to improve their material properties for food packaging applications are widespread.<sup>[162]</sup> These efforts are largely driven by the inexpensive nature of the material. Here, PVA has also been used, namely by Zhang *et al.* (2020), who detailed the production of anthocyanin-embedded packaging films composed of cornstarch and PVA.<sup>[163]</sup> While the resultant film exhibited strong pH monitoring performance when applied to shrimp samples, its TS was only

7.3 MPa. Anthocyanins were seen to slightly increase the strength of these films – likely due to the replacement of water within the film matrix, but only to a maximum of 11.3 MPa. The films also exhibited very poor stability, with a WS of 40.3%. As such, widespread use of starch films for food packaging requires changes in film composition outside of PVA to induce significant improvements in strength and stability.

Ultimately, film material optimization has been shown to increase the overall stability and functionality of *in situ* pH sensors substantially. However, resultant sensors are still limited by the sub-optimal film properties and poor anthocyanin stability, specifically over extended periods of time and in varying environmental conditions. This has substantiated the need for secondary film modifications that improve film and/or anthocyanin stability, yielding more reliable *in situ* detection platforms.

#### *Chemical modifiers*

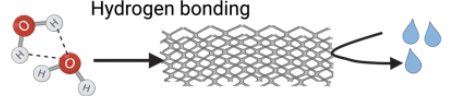
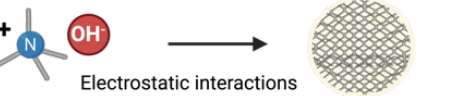
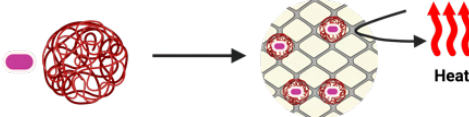

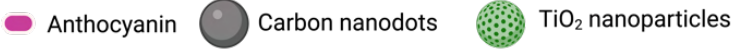

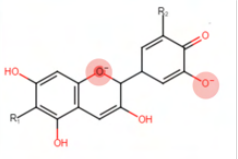
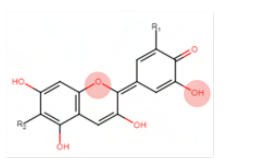
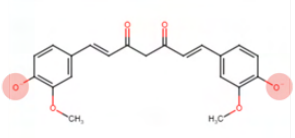
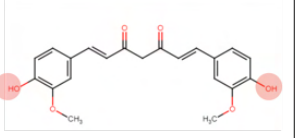
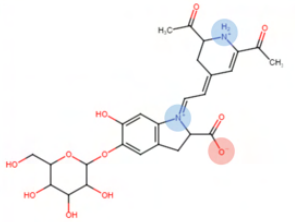
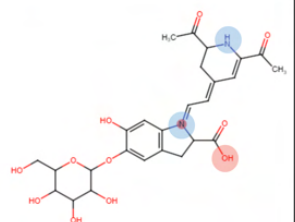
While the induction of denser film matrices is the most common strategy for the development of more stable films – as presented in many of the aforementioned studies, modifications that induce improved chemical compatibility within the film matrix have also been explored. Namely, Eze *et al.* incorporated riceberry phenolic extract (RPE) into anthocyanin-containing chitosan films as a means of increasing hydrophilic interactions (**Figure 2.5a.i**) and thus promoting hydrogen bonding with chitosan.<sup>[164]</sup> Increased cross-linking was seen within these modified chitosan films, effectively decreasing WS and SI. In addition, improved preservation of the stored food was also observed, due to the reduced porosity and permeability of the developed film, which limited the introduction of moisture, oxygen, and other external gases into the packaging. This phenomenon was supported by the innate antioxidant activity of RPE.

Seeking a similar chemically-induced improvement in physical stability, Wen *et al.* stabilized 2,2,6,6-tetramethylpiperidine-1-oxyl (TEMPO)-oxidized bacterial cellulose films with thymol, to increase the resultant film's TS and hydrophobicity – the latter of which also minimized

sensor surface fouling.<sup>[165]</sup> Subsequent functionalization with anthocyanins from purple potato extract showed pH responsiveness as expected. TEMPO oxidation introduced anionic carboxylate crosslinkers (Figure 2.5a.ii) into the cellulose films, enhancing their associations with embedded anthocyanins, thus improving physical stability. These films were functional at pH sensing for shrimp *in situ* when applied as a packaging material over stored shrimp samples at room temperature for 6 hours and extended shelf-life preservation, which was attributed to the film surfaces' resistance to microbial colonization and water vapour permeability.

Such chemical approaches have also been applied to improve anthocyanin stability in response to environmental stimuli. Heat degradation is of concern given that various food products undergo thermal processing post-packaging. Such treatment causes the polymerization of anthocyanins, which impairs their ability to respond to pH and causes dye browning. The latter may be interpreted as false positives within colorimetric pH monitoring. Qin *et al.* reported that the heat instability of anthocyanins can be reduced *via* coupling with Maillard reaction products of whey protein isolates (WPI).<sup>[166]</sup> Maillard reactions change the glycation state of WPIs, allowing them to readily conjugate with other compounds. When such WPIs were coupled with anthocyanins, reduced anthocyanin degradation and better color stability was observed. Similarly, Wu *et al.* (2021) developed gellan gum packaging films embedded with anthocyanins stabilized by heat-treated soy-protein isolates. The films demonstrated enhanced stability and lowered water vapour permeability, owing to the increased intermolecular interactions. Evaluation of the film with shrimp samples confirmed strong *in situ* pH monitoring capabilities.

Ultimately, chemical modifiers are a promising avenue for film optimization given the diverse range of improvements they provide. That being said, they only offer limited improvements in terms of anthocyanin stability, another key factor for *in situ* use.

a.					
Modification	Tensile Strength	Water Solubility	Pigment Stability	Function	Mechanism
i. Hydrophilic compounds	↑	↑	↑	Physical stability	Hydrogen bonding 
ii. Anionic cross-linkers	↑	↑	↑	Physical stability	Electrostatic interactions 
iii. Nano-encapsulation	—	—	↑	Thermal stability	
iv. Nano-fillers	↑	—	—	Physical stability	
					
b.					
Dye	Photo-stability	Visibility	Physical Stability	pH spectrum 	
Anthocyanin	↑↑↑↑	↑↑↑↑	↑↑↑↑		
Curcumin	↑	↑	↑↑↑↑		
Betanin	↑↑↑↑	↑↑	↑↑↑↑		

**Figure 2.5. Physical properties of intelligent pH-responsive films used to monitor spoilage.** (a) Common modifications made to films that alter their mechanical and thermal stability, including: (i) the addition of hydrophilic and (ii) anionic compounds to facilitate cross-linking of film materials, (iii) nano-encapsulation of pigments to increase long-term stability and prevent heat- or light-mediated degradation, and (iv) nanofillers that increase film density and strength. (b) A comparison of the properties of different pH-responsive organic dyes used in intelligent packaging. Produced using BioRender.



### *Anthocyanin nanoencapsulation*

Efforts to protect anthocyanins from environmental disturbances have been explored by non-chemical means as well, using approaches that both induce improved film stability and limit the leaching of anthocyanins from carrier films. To this end, the nanoencapsulation of anthocyanins has garnered significant interest, largely through the use of protein-polysaccharide complexes (Figure 2.5a.iii).<sup>[167]</sup> These complexes prevent the heat-based degradation of anthocyanins, enhancing their potential use in long-term pH monitoring. Many variations of these food-grade complexes have been evaluated for their ability to act as protective nanocarriers for anthocyanins, while maintaining their ability to interact with the greater food matrix.<sup>[168]</sup> One such strategy involved the incorporation of anthocyanins into ovalbumin-propylene glycol alginate nanocomplexes, which were deposited onto PVA and glycerol matrices to make intelligent films.<sup>[169]</sup> This approach increased the stability of embedded anthocyanins, resulting in improved performance against pH buffers. That being said, the study noted that alginate nanocomplex incorporation increased water vapour permeability, yielding an increase in the film's WS, from 12.26% to 29.34% – a shift that compromises the long-term stability of the film.

To better understand the effect of anthocyanin nanoencapsulation on film stability, Qin *et al.* tested anthocyanins incorporated into sago starch films stabilized with PVA, both in a free and nanoencapsulated form.<sup>[170]</sup> Both forms were immobilized into the starch matrix *via* hydrogen bonding. While both films maintained the pH-responsiveness of anthocyanins and demonstrated effective real-time monitoring of fish, nanoencapsulation was found to improve the performance of the resultant film across several metrics. Specifically, decreases in water vapour permeability and moisture content, as well as improvements in TS were observed. Given this finding, modifications to the polysaccharides used to develop nanoencapsulating films have also been explored to improve system performance. In a recent work, Cheng *et al.* (2022) developed a “dual-modifying” cassava starch films incorporated with red cabbage anthocyanin.<sup>[171]</sup> These “dual modifications” refer to multiple chemical modifications that increase electrostatic interactions

between anthocyanins and starches, inducing improved immobilization. Several modifications were tested, including the addition of oxidized hydroxypropyl starch, acetylated di-starch phosphate, and oxidized acetylated starch, which all increased the anionic strength of the starch substrate, resulting in increased electrostatic interactions. All these modifications increased film stability, water resistance, and tensile strength. Modified cassava starch films were also thicker than native, starch-only films because of the increase in intermolecular interactions, which also led to increased density and rigidity. However, the potency of the colorimetric responses were not changed by any modification, as native and modified films had similar biosensing capacity.

#### *Micro- and nanoscale modifiers*

Lastly, micro- and nanoscale modifiers have been explored extensively.<sup>[172,173]</sup> While most of these modifications involve particles, Koshy *et al.* recently reported they use of carbon nanodots (CNs) as a packaging film modifier (Figure 2.5a.iv).<sup>[174]</sup> CNs are organic, biocompatible entities that are often used as fillers within pH monitoring films, inducing improvements in film stability. In their study, they embedded CNs alongside anthocyanins into starch films for real-time food monitoring. Despite the incorporation of CNs, the resultant film had a relatively low TS of approximately 10 MPa. Similarly, minimal improvements in stability were observed, with CN incorporation yielding a WS of 27.2%. While these films showed good detection of pH changes occurring in pork during spoilage, the subpar mechanical properties of starch films were not overcome through the incorporation of CNs. The incorporation of CNs into anthocyanin-embedded chitosan and cellulose packaging films is yet to be explored. It is possible that CN incorporation into these film matrices may yield more substantial improvements in film properties.

On the other hand, micro- and nanoparticles have been explored heavily as both anthocyanin carriers and as filler materials that induce improvements in film stability. With regards to anthocyanin carrier particles, chitosan-cellulose microparticles have been explored for their anthocyanin loading and retention capacity. Specifically, Wang *et al.* contrasted cellulose as an anionic cross-linking agent with sodium tripolyphosphate (TPP) when coupled with chitosan in

the form of microparticles.<sup>[175]</sup> They found that the chitosan-cellulose particles exhibited high loading efficiency, as indicated by evenly distributed anthocyanins throughout the particles, while the chitosan-TPP particles only displayed anthocyanin on their surfaces. The improvement in distribution induced by cross-linking with cellulose increased retention of anthocyanins over time. This stability was facilitated by interactions between negatively charged cellulose and positively charged chitosan. While effective, these interactions simply entrap anthocyanins. The lack of anthocyanin immobilization raises concerns surrounding long term stability.

As an alternative, chitosan-based anthocyanin nanoparticles have also been applied as anthocyanin carriers.<sup>[176]</sup> Alongside high retention capacity through surface immobilization of anthocyanins, this system demonstrated high thermal protection of the dyes by minimizing their hydration from the surrounding environment. Protection from pH fluctuations and light was also reported. With regards to the latter, the study found a 20% loss in anthocyanin functionality after 10 days when incorporated onto the chitosan nanoparticles, as opposed to an 86% loss with free anthocyanins stored in the same conditions. Further work is required to investigate whether the induction of such effective anthocyanin protection compromises the pH-sensing capabilities of the anthocyanins. Similar approaches investigated thus far have signaled minimal limitations.

The use of particles as filler materials largely centers upon inducing a denser film matrix, yielding improved stability. In a recent study, Zhang *et al.* used TiO<sub>2</sub> nanoparticles as a filler material within anthocyanin-embedded chitosan films for food-based applications.<sup>[177]</sup> The incorporation of TiO<sub>2</sub> alone did not significantly alter the WS of the chitosan film. However, chitosan films incorporated with both TiO<sub>2</sub> nanoparticles and black plum anthocyanins showed reduced WS in comparison to either agent alone. This improvement was attributed to interactions between the nanoparticles and hydrophilic anthocyanins, which prevented hydrophilic interactions with water molecules.

#### 2.4.2.2 Other compounds used for pH monitoring

Aside from anthocyanins, a variety of pH-responsive organic compounds have also been explored for integration into intelligent food packaging, although at a lower frequency. Current approaches have largely moved away from the use of chemical pH indicators, such as methyl red and bromocresol blue, because of their toxicity. That being said, Kim *et al.* overcame this issue by incorporating bromocresol blue into highly absorbent materials that reduced the likelihood of leaching.<sup>[178]</sup> The interface between the compound and food samples, however, was maintained to allow for effective sensing. In their approach, the indicator was embedded into filter papers and stabilized with PVA. Polyethylene terephthalate film were used as a physical barrier to limit compound leeching into the bulk matrix. While it is difficult to assess the extent of leeching of the indicator into the meat and any subsequent cytotoxicity that results, the study reported no visual migration of the purple dye onto a chicken matrix after 10 days of storage. Ultimately however, given the increasing prevalence of organic, non-toxic pH-responsive compounds, this approach has limited applications for *in situ* detection for food, where biocompatibility is a paramount concern. The search for non-toxic alternatives has yielded several viable compounds.

In particular, compounds native to plants have shown promise – namely, curcumin, alizarin, and betanin (Figure 2.5b). Curcumin is well-documented for its pH-responsive ability, and curcumin nanoparticles have been explored outside the food space as well, namely in improving signal readout from pH-responsive ELISAs.<sup>[179,180]</sup> Curcumin has been used heavily in the development of intelligent packaging films, as both a pH-responsive compound and a film stabilizer.<sup>[162]</sup> Typically found in the turmeric plant, curcumin gains a phenoxide group upon interaction with increasing concentrations of hydroxyl ions – as seen within meat spoilage, yielding a colour change. Moreover, curcumin functions as a film stabilizer when complexed with other pH-responsive compounds, because of its hydrophilic nature. This function was reported in a recent study, that showed that a combination of curcumin and anthocyanins yielded a packaging

film with improved mechanical stability than either agent in isolation.<sup>[181]</sup> However, the mechanism by which this combination of agents yielded improved performance was not reported.

Compared to curcumin, alizarin offers an additional benefit in that it can be used as a reusable pH indicator. This is due to the reversibility of the compound's protonation state – the parameter that influences the colour of the compound. Ezati *et al.* incorporated alizarin dye into cellulose-chitosan films.<sup>[182]</sup> Given alizarin's hydrophobic nature, its incorporation yielded a decrease in WS from 16.13% to 12.89%. The SI of the developed film remained unchanged relative to a base cellulose-chitosan film. Interestingly, a decrease in film stability was noted when stored at room temperature. From a functionality standpoint, these films exhibited responsiveness from pH 2 to 11 – a range that ensures widespread applicability with different food products. Tests with beef samples stored in the fridge confirmed effective pH detection in accordance with sample spoilage. In related works, the same research group showed that alizarin can also be incorporated into cellulose and chitosan films, offering similarly promising results.<sup>[182]</sup>

Seeking to evaluate how such alternative compounds compare with anthocyanins, Etxabide *et al.* compared anthocyanins, curcumin, and betanin – another natural pigmenting agent, based on their pH-responsiveness and stability under both light and heat exposure.<sup>[183]</sup> The study found that in isolation, curcumin pigment was the strongest of the three as a colorant but lost its colour intensity when under light exposure for prolonged periods of time. Oppositely, anthocyanins and betanin retained adequate intensity for up to a month. The long-term stability of these colorimetric agents is crucial for *in situ* detection to ensure viability throughout a food product's lifespan. With consideration towards the high background turbidity of food products, this brings the reliability of curcumin into question. Anthocyanins and betanin did exhibit less thermostability under warmer conditions, but this was considered to be a low priority consideration given that various material strategies have been shown to induce improved thermal stability, as detailed previously. Following extensive evaluations, Etxabide *et al.* concluded that anthocyanins remain the most viable class of agents for *in situ* pH-responsive intelligent packaging, owing to their dramatic colour changes,

wide pH detection range, and amendable stability.<sup>[183]</sup> However, while a largely comprehensive study, this work only analyzed the viability of tested compounds in solution, not in a film embedded format. To this end, Tirtashi *et al.* showed that immobilization and entrapment of these compounds influences their pH responsive properties, both in accuracy and magnitude of colour change.<sup>[184]</sup> Given the diverse range of materials being used to prepare *in situ* films and the wide range of compounds being explored for their pH-responsive behaviour, generalized claims surrounding the viability of a given entity have thus proven difficult to support.

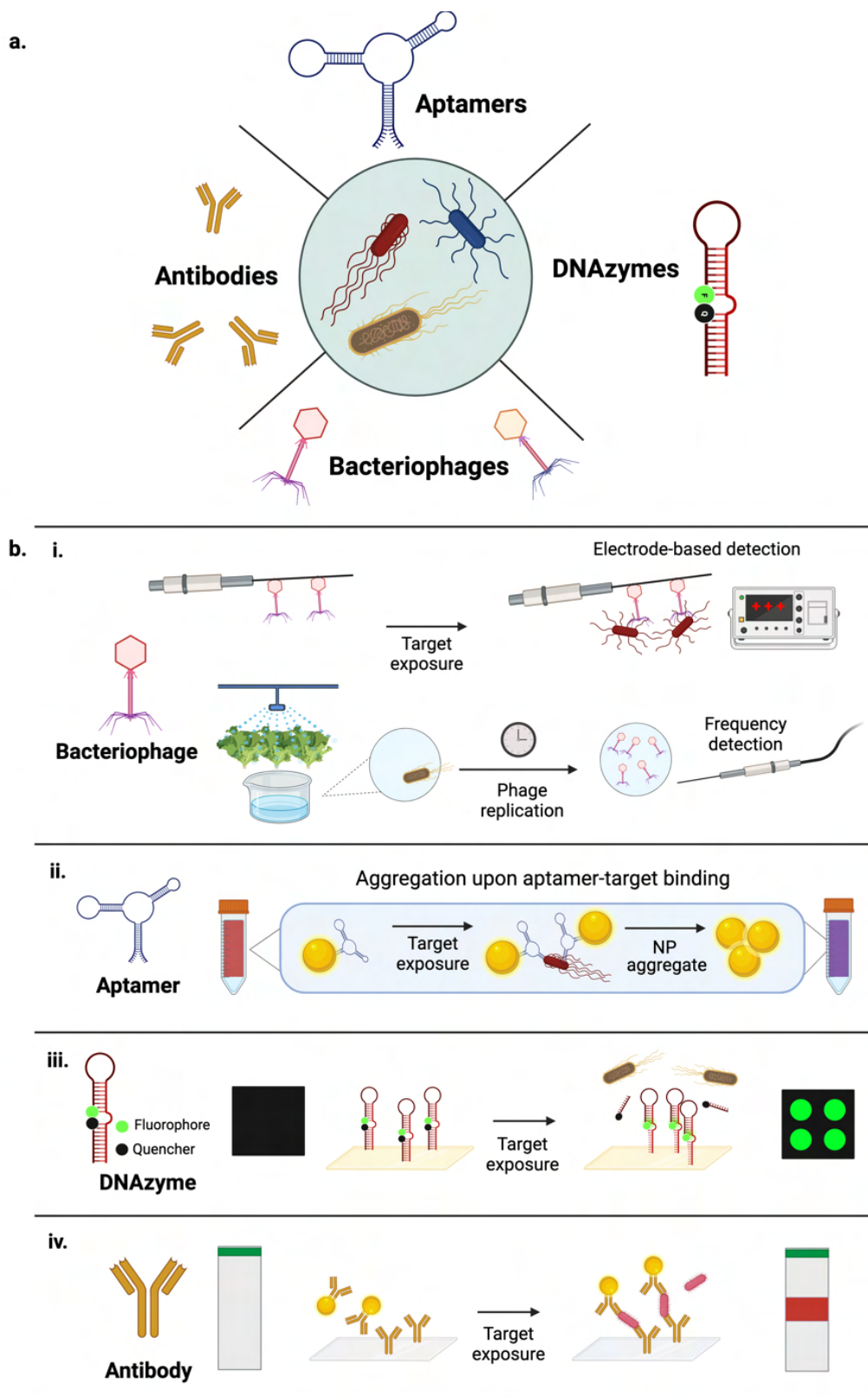
Ultimately, existing *in situ* pH sensors offer significant promise as spoilage monitoring systems, but their use continues to be limited by poor dye and film stability, preventing their widespread commercial use. As most pH sensors are designed by incorporating reactive plant-based dyes into simple organic polymers, they are cheap and cost-effective for spoilage detection, and are also convenient for commercial usage as they lead to obvious visual changes without requiring complicated signal readout methods.<sup>[152]</sup> As they are relatively simple in design, they are also easy to mass produce at a relatively low cost, and to store in liquid-free environments to prevent dye release and degradation. Nanoencapsulation of dyes further increases the long-term stability of these films during storage. Alongside this, there also exists the potential to multiplex different types of anthocyanins with similar color-responsiveness in pH labels, to enhance sensor performance. However, the relationship between pH and spoilage lacks the objective consistency that is offered by biogenic amine or pathogen monitoring, which raises some concerns regarding the viability of such systems. Intrinsic differences in the degree of pH fluctuation between foods during spoilage, as well as other compounds produced during shelf storage, can also make pH unreliable as a metric for spoilage. Resultingly, there continues to be a defined need for studies that evaluate this relationship comprehensively on a large sample scale. Lastly, given that food spoilage is typically accompanied by discernible colour and odour changes, it is imperative that such sensors report spoilage at a timepoint where consumption is harmful, but not apparent. Evaluation of how well existing pH monitoring films identify this timepoint is necessary.

Nonetheless, pH monitoring of food continues to be an active area of research with frequent developments that yield confidence towards commercial applicability in the future.

### 2.4.3 Pathogen monitoring

The contamination of food products by pathogenic bacteria usually arises from improper practices during livestock handling, food processing, and product packaging.<sup>[185]</sup> Timely identification of food contamination is paramount in minimizing the incidence of food-borne illness. However, contamination detection typically requires multiple days, as it involves food processing, culturing, and genomic analysis to evaluate the presence of pathogenic bacterial strains. All these steps cannot be done *in situ* and require export outside of processing facilities and commercial grocery stores – an expensive and time-consuming process. Moreover, some bacterial strains can enter a viable but non-culturable (VBNC) state that prevents accurate identification and quantification *via* typical microbiological culture methods.<sup>[186]</sup> As such, there is a growing demand for *in situ* biosensors for bacterial detection that enable the on-package detection of pathogenic contamination within a few hours of sample incubation, with minimal user processing. This section discusses recent advancements in this space.

Functional biorecognition probes are the predominant bacterial detection platform, due to their high sensitivity and specificity.<sup>[187]</sup> Various types of probes can be used to detect bacterial contamination in food by harnessing their natural binding affinity for bacterial compounds. In comparison to the detection of fluxes in biogenic amine concentration and pH, pathogen detection demands significantly higher specificity, to ensure that non-pathogenic microbial populations that are naturally present in food products do not induce false positive signals. Candidates for the development of biorecognition probe-based sensors for *in situ* pathogen detection are thus chosen primarily due to their high target binding specificity. Promising probes include bacteriophages, functional oligonucleotides, and antibodies (**Figure 2.6a**). These probes are incorporated into detection platforms that signal pathogenic contamination through diverse transduction methods.



**Figure 2.6. Biorecognition probes used for on-site pathogen detection and in situ food monitoring.** (a) The common types of probes that are used to identify bacteria – antibodies,



bacteriophages, DNazymes, and aptamers. (b) Various probe-based strategies to detect bacterial contamination, including: (i) phage-mediated identification, transduced via amperometric monitoring of target-binding, or phage replication-induced resonant frequency shifts, (ii) aptamer-mediated recognition and resultant nanoparticle aggregation, (iii) DNzyme-mediated detection, resulting in fluorescence changes, and (iv) antibody-based recognition, inducing colorimetric transduction via the use of dye-loaded, antibody-gated liposomes integrated into microneedles. Produced using BioRender.

#### 2.4.3.1 Bacteriophage-based probes

Bacteriophages, commonly referred to as phages, are bacteria-targeting viruses with intrinsic specificity to their host species, which makes them reliable biorecognition probes.<sup>[188]</sup> Upon binding to the host bacterium, lytic phages replicate exponentially in host cells until they induce lysis, which destroys the bacterium and allows for further phage propagation within nearby host cells.<sup>[189]</sup> Because of the natural predatory relationship that exists between bacteriophages and bacteria, these viruses act as a promising type of probe for application in food biosensing – an application that is further supported by their biocompatible nature. With consideration towards real-world applicability, bacteriophage production is easily scalable, and the viruses demonstrate high stability under diverse environmental and chemical conditions, as discussed by Ahovan *et al.* in a recent review.<sup>[190]</sup>

A predominant approach for developing bacteriophage-based biosensors involves phage incorporation into electrochemical-based platforms that exhibit detectable changes in electrical current upon binding target proteins. For example, Quiton *et al.* developed an impedimetric electrochemical biosensor that exhibited changes in impedance following phage-mediated binding of *Salmonella* cells onto graphene-modified screen-printed electrodes (Figure 2.6b.i).<sup>[191]</sup> Phage immobilization is accomplished by pre-activating carboxyl groups on screen-printed electrodes prior to incubation with bacteriophage. Interestingly, this leads to sufficient immobilization of the bacteriophage onto the electrodes in the right conformation, as this sensor demonstrated a limit of detection of 12 CFU/mL following a 40-minute incubation with test samples. In such a sensor, impedance of electron transfer takes place upon phage-bacteria binding, leading to a change in

signal output. The system showed specificity towards *S. typhimurium* – the most common source of foodborne *Salmonella* infection, over other non-target *Salmonella* strains. Mechanistically, this was due to phage specificity for strains of *Salmonella*, as there were no changes in impedance upon incubation with other common pathogens. Yet despite the high sensitivity and specificity of the developed platform, the widespread applicability of the system was limited by its reliance on electrochemical impedance spectroscopy, a complex lab-based technique performed by trained experts. Similarly, Wang *et al.* (2022) also explored *Salmonella* detection using AuNPs to enhance the sensitivity of an electrochemical bacteriophage-based sensors.<sup>[192]</sup> AuNPs were absorbed onto gold disk electrodes to increase the sensor's specific surface area and conductivity (**Figure 2.7a**) . Subsequently these nanoparticles were crosslinked with SEP37 *Salmonella* bacteriophages using cysteamine. This probe showed a limit of detection of as low as 1 CFU/mL within contaminated chicken. However, higher bacterial concentrations that increased bacterial lysis rates impeded sensor performance due to the release of intracellular ions from cells, which alters the electron transfer potential of the system.

In another study, Zolti *et al.* described the immobilization of a P100 bacteriophage onto carbon nanotubes with high sensitivity for *Listeria monocytogenes*, detecting as low as 8.4 CFU/mL of bacteria.<sup>[193]</sup> The bacteriophages were first functionalized with quaternized polyethylenimine which then enabled charge-directed immobilization onto the carbon nanotubes, increasing interaction and infection with target bacteria. This approach is used to immobilize bacteriophages as polyethylenimine is positively charged at neutral pH, enabling electrostatic interactions with the bacteriophage head.<sup>[194]</sup> They reported a similar detection strategy for *E. coli* and other pathogenic bacteria as well. Interestingly, these sensors efficiently retain phage and allow them to retain their performance for up to two weeks. Similar to other studies, they show that the high specificity of bacteriophage strains for species-specific bacterial receptors leads to low cross-reactivity with other bacteria. Other surface modifications have also been coupled with phage to help enhance the sensitivity of electrochemical biosensors.

Seeking to develop a platform with more applicability in the food industry, Sultan *et al.* incorporated bacteriophages onto a millimetre-wave based antennae sensor, which was used to detect *E. coli* within produce wash water (Figure 2.6b.i).<sup>[195]</sup> Rather than using phages for detection, they instead use antennae to detect changes in resonant frequency that result with increases in phage replication, which take place in the presence of bacteria. This strategy also allows for very sensitive detection at low levels of contaminant pathogen, with phage fluctuation detectable within 40 minutes from sample incubation. However, detection would work significantly better with higher bacterial levels, which lead to more profound production of phages. The use of wash water instead of food for the substrate to detect changes in resonant frequency reduces the presence of competitive signals that could lead to false positives. While antenna-based detection is extremely sensitive to changes in resonant frequency, direct application of bacteriophages to food is a non-viable approach for reagentless sensing and for prolonged monitoring. An ideal approach would incorporate these bacteriophage into food packaging to enable monitoring without interfering with packaged food products.

Overarchingly, electrochemical-based bacteriophage systems offer excellent sensitivity and specificity, ensuring rapid, accurate detection. Efforts are now being made to optimize such platforms, as the stability of bacteriophages on electrochemical surfaces remains questionable. Yet, while valuable tools, sensor measurements largely require the use of complex apparatuses that are not readily adoptable to *in situ* environments, limiting the applicability of such platforms to processing facilities. Consumer-level monitoring requires an *in-situ* platform with signal readouts that are easily acquired and interpreted.

To this effect, fluorescent and luminescent transduction systems are being explored to address some of the drawbacks within conventional electrochemical bacteriophage sensors. Namely, Wisuthiphaet *et al.* paired a genetically engineered T7 phage that overexpresses alkaline phosphatase (ALP) following successful *E. coli* infection.<sup>[196]</sup> A non-fluorescent ALP substrate was then introduced into test solutions. Cleavage of this substrate by ALP yielded a fluorescent

precipitate that was tracked optically. This platform was shown to successfully detect  $10^4$  CFU/mL in various beverages. Ultimately, the use of such homogenous test matrices raises concerns regarding this system's viability for complex food samples, especially given its limited sensitivity.

Similarly, Nguyen *et al.* engineered *Salmonella*-responsive bacteriophages with NanoLuc, a luciferase enzyme, that produced luminescent signals following successful infection of target cells.<sup>[197]</sup> This platform was able to detect as low as 1 CFU *Salmonella* in 25 g of inoculated ground turkey and 100 g of powdered infant formula after as low as 2 hours, owing to the high optical intensity of NanoLuc. However, it should be noted that the turkey and infant formula samples were enriched for 7 and 16 hours, respectively, and the samples were subsequently homogenized prior to testing. Enrichment and homogenization of samples limits the *in situ* application of this sensor, but the use of engineered bacteriophage luminescence represent an interesting avenue that could be explored within the *in situ* space. Overarchingly, such synthetic bacteriophage-based sensors suggest easier *in situ* incorporation compared to pure electrochemical platforms. One current limitation to their usage is that they require the addition of external reagents to produce signals as these phages are usually engineered with enzymes that require substrates to generate signals. Engineering phages with genetic circuits that use substrates found in food, or ones produced as an effect of bacterial contamination itself, would increase the convenience of using these sensors. Biosensors designed around the premise of phage replication could also use phages engineered to express reporter molecules themselves, as replication in the presence of bacteria would lead to an increased positive signal. Such genetic circuits are also advantageous because they can be used to facilitate multiplexed detection of contaminants within samples. By engineering different bacteriophage strains with unique reporter molecules, contamination by a number of prevalent pathogens can be analyzed.

While these studies have shown that bacteriophages act as prime candidates for the detection of pathogenic bacteria, few studies have manipulated them into functional, intelligent materials that can be applied to food. Bacteriophages are fairly easy to propagate, making them

easy to mass produce.<sup>[198,199]</sup> However, this production process also has significant risks for biosafety, as continuous propagation of phages through the bacterial strains they infect favours the evolution of resistant strains of these bacteria.<sup>[199]</sup> Beyond production, the storage of these phages post-production is also challenging. Unlike other probes, bacteriophages are composed of complex assemblies of protein and genetic material, making them more difficult to store long-term.<sup>[164,165]</sup> The recent development of new approaches to engineering bacteriophages into functional nanomaterials themselves warrants further exploration into how these probes can be deployed to create intelligent packaging for food monitoring.<sup>[37]</sup>

#### *2.4.3.2 Oligonucleotide probes*

DNA and other nucleic acid-based nanotechnologies have been increasingly explored for their biomedical applications, from clinical therapeutics to biosensing. The characteristic advantage of using such probes lies in the intrinsic programmability of nucleic acids, which can be used to synthesize oligonucleotides that display high binding affinity and specificity towards a diverse range of ligands. There are two main types of oligonucleotide probes: (1) aptamers, which are single-stranded oligonucleotides that fold into secondary structures with high binding affinity to target biomolecules, and (2) DNazymes, which are oligonucleotides that exhibit catalytic activity upon binding to a target.<sup>[132,200]</sup> These are both synthesized via systematic evolution of ligands by exponential enrichment – a methodical approach involving the selection of responsive nucleic acid probes from large DNA libraries that are exposed to targets.<sup>[132]</sup> Both aptamers and DNazymes can be functionalized *via* their DNA backbones using a variety of different prosthetic groups that enable their use in fluorescent, colorimetric, and electrochemical-based detection systems.<sup>[201]</sup> These nucleic acid probes have been explored in the development of pathogen-detecting biosensors, by coupling their binding activity with a signal reporting cascade. These probes have then been immobilized onto various sensing substrates. Evaluation of existing probes is well-documented in literature: Li *et al.* (2019) reviewed electrochemical aptamer-based

pathogen detection methods and Khan *et al.* (2021) reviewed the development of DNAzyme-based biosensors for widespread applications, with a defined focus on surface immobilization.<sup>[133,200]</sup>

Aptamer-based pathogen detection is not as common as DNAzyme-based methods given that a greater number of pathogen-responsive DNAzymes have been reported thus far. For the aptamer-based sensors that do exist, a key consideration is signal transduction. While DNAzymes have enzymatic, reactive activity that enables the activation of a reporting entity following target-induced cleavage, DNA and RNA aptamers only have binding affinity. As such, aptamer-based sensors must co-opt structural changes to the aptamer upon target binding, with colorimetric, fluorescent, or electrochemical additions to the DNA backbone.<sup>[137]</sup> Once coupled with signalling entities, aptamers are powerful detection tools.

For many years, antibodies have been used in the biosensing space for the development of lateral flow assays such as the pregnancy test, which incorporates the specificity of antibody binding with a colorimetric signal provided by AuNPs. Given their high binding affinity, aptamers can also be used to develop such nanoparticle-based assays for pathogenic bacteria (Figure 2.6b.ii). Tasbasi *et al.* described the development of a lateral flow assay to identify *Listeria monocytogenes*.<sup>[202]</sup> They synthesized silica nanoparticles entrapped with TMB, a substrate for HRP, and capped them with *Listeria*-specific aptamers. When these sensors are exposed to as low as  $10^2$  cells, the aptamer is released, leading to a colour change in the sensor upon the addition of HRP. Reagent entrapment is efficient as it limits the degree of external tampering required, as such reactions typically require sequential addition of HRP and TMB. Typically, colorimetric systems that incorporate TMB in active food packaging are limited by the high reactivity of redox reagents. The aptamer-gated silica particles developed in this work provide an innovative incorporation strategy. Future investigation into the efficacy of this system when coupled with food is necessary for *in situ* detection.

A study by Hasan *et al.* described the development of a *Salmonella*-specific DNA aptamer used for electrochemical pathogen detection in chicken, with a limit of detection of 55 CFU/mL

and high specificity.<sup>[96]</sup> They modified their aptamer with an amine group, which permitted immobilization onto carbon nanotube surfaces that were enriched with carboxylic acid groups. An impedimetric electrochemical readout was obtained upon binding of bacterial proteins in samples of homogenized chicken. However, given that this device requires electrochemical impedance spectroscopy to measure aptamer-target binding, this system is faced with many of the same commercial challenges previously described for electrochemical platforms. Accordingly, aptamers with commercially translatable fluorescent mechanisms have been developed for pathogen detection. Namely, Tian *et al.* (2021) immobilized *Alicyclobacillus acidoterrestris*-specific aptamers onto magnetic nanoparticles to isolate target bacteria within juice samples, and subsequently used *A. acidoterrestris*-binding antibodies labelled with fluorescent quantum dots for fluorescence visualization.<sup>[203]</sup> The study reported a limit of detection of 10<sup>3</sup> CFU/mL within 90 minutes, with high specificity. While the optimization of such a system for *in situ* use is yet to be reported, the incorporation of similarly designed antibody-nanoparticles into nanocomposite packaging films may offer a platform of notable value.

Concurrently, DNAzymes have been applied within a wide array of pathogen-detecting systems.<sup>[204]</sup> Their recognition and reporter molecules, these oligonucleotides offer simple reaction cascades in which they are the only application in the food industry has only recently been explored and is an intriguing application of this technology. Given that DNAzymes can be designed with a built-in reporter, allowing them to offer dual functionality as both recognition and reporter molecules, these oligonucleotides offer simple reaction cascades in which they are the only functional entity.<sup>[200]</sup> This standalone nature has inspired direct incorporation onto a wide array of substrates, to develop functional packaging materials. To this end, a key consideration is the technique by which DNAzymes are deposited onto the sensor surface, as proper DNAzyme deposition is critical for sensor stability and subsequent *in situ* use.

One simple technique involves depositing DNAzyme solutions onto the target substrate and drying to induce noncovalent attachment. Qin *et al.* (2021) utilized this method to develop a

fluorescent DNAzyme sensor responsive to *Pseudomonas aeruginosa*, PAE-1.<sup>[205]</sup> They dried the DNAzymes onto polystyrene boards to create stable, non-covalently immobilized sensors. This system demonstrated high selectivity for *P. aeruginosa* based on cross-testing against seven other bacterial species. Furthermore, it boasted a limit of detection of  $10^2$  CFU/mL after 10 minutes of incubation with contaminated black tea. Concurrently, the viability of this deposition method was also assessed by Ali *et al.* in a platform designed for *in situ* use.<sup>[206]</sup> This study showed that DNAzymes can be incorporated onto paper-based sensors alongside stabilizing agents to create sensors for *in situ* *E. coli* detection. Specifically, they deposited solutions of an *E. coli*-fluorogenic DNAzyme dried onto wax-coated nitrocellulose paper stabilized with trehalose and pullulan sugars (Figure 2.7b). Lysozymes were also printed onto the paper sensors in parallel to lyse target bacteria. This increased target availability for DNAzyme binding, thus triggering faster detection. The resultant platform demonstrated a limit of detection of  $10^2$  CFU/mL after 30 minutes. Successful detection was also observed within diluted apple juice and milk samples.<sup>[206]</sup> Lastly, Ma *et al.* (2021) developed a fluorescent *Aeromonas hydrophila*-responsive DNAzyme, which they called DAh1, immobilizing it onto polystyrene using trehalose/pullulan stabilizers and drying to deposit the probes onto the surface.<sup>[207]</sup> DAh1 sensors remained stable for 6 months in comparison to freshly prepared sensors and were used to obtain a limit of detection of 36 CFU/mL in milk. Ultimately though, while DNAzyme deposition *via* drying is fast and requires no additional reagents, the lack of covalent immobilization threatens the integrity of the sensor when applied to complex, solid food matrices. This concern is not addressed within the presented studies, given that the reported sensors were assessed solely in liquid test matrices. Considering the harsh handling and environmental conditions food products are exposed to, other DNAzyme deposition techniques that offer better stability and detection in complex food matrices have gained traction for *in situ* pathogen detection.

Comparatively, covalent DNAzyme immobilization using chemically modified DNAzymes and/or substrate surfaces yields more robust and durable sensors that are better fitted

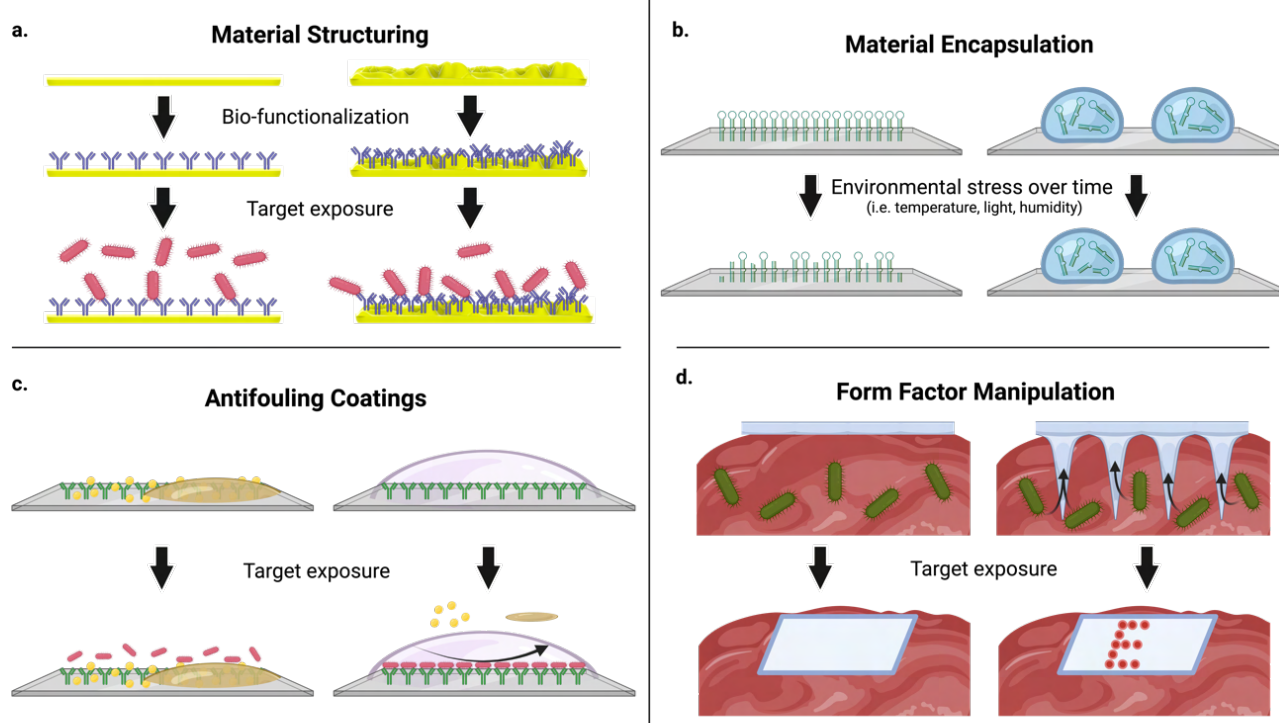


for *in situ* applications compared to simple drying. In a foundational study, Yousefi *et al.* (2018) used epoxy-mediated immobilization to develop an *in situ*-compatible *E. coli*-responsive DNAzyme patch with a limit of detection of  $10^3$  CFU/mL in buffer within 4 hours (Figure 2.6b.iii).<sup>[17]</sup> Specifically, 5' amine-modified DNAzymes were deposited onto epoxy-coated cycloolefin polymer substrates. Importantly, these flexible substrates were also incubated with unprocessed, contaminated solid food samples for 2 hours, and demonstrated successful detection of 1 CFU/mg *E. coli* on contaminated lettuce and beef samples. The same group later showed that the performance of such sensing systems can be improved by lubricant infusion of the sensor surface (Figure 2.7c).<sup>[208–210]</sup> Such a modification limits sensing interference through the prevention of surface fouling – specifically within complex liquid matrices, which have free-flowing proteins that can impede detection.<sup>[211–213]</sup> An increase in DNAzyme sensor sensitivity was observed in milk using this approach, with successful detection of  $10^2$  CFU/mL *E. coli* within an hour. This improvement was attributed to lubricant-mediated redirection of DNAzyme-binding entities away from the sensor substrate, and towards the oligonucleotides, yielding an increase in signal-inducing binding events. This indicated the scope for DNAzyme-based sensors to have anti-biofouling, repulsion, and signal amplification features incorporated within an *in situ* device.

A few concerns still exist in relation to the incorporation of DNAzymes *in situ*, much of which centers upon their dependency on specific metal ions for catalytic functionality. This can become a hindrance to DNAzyme-based sensor designs as it becomes important to incorporate these metal ions as aqueous solutions, which is a challenge when working with physical food samples. The platform used by Yousefi *et al.* addressed this obstacle by pre-treating food samples with a non-toxic magnesium ion-containing reaction buffer solution.<sup>[17]</sup> While effective, such treatments can influence the organoleptic properties of given food products. As such, better means of buffer incorporation remain a need in this space. A related concern was well-established by Qin *et al.* during the development of their PAE-1 sensor, where they noted that DNAzyme performance peaks at certain metal ion concentrations.<sup>[205]</sup> As such, while some highly effective DNAzymes

exhibit excellent sensitivity and specificity, requirements for high concentrations of metals ions for functionality limits their viability in the food sector. Increasing the presence of these ions past food-safe thresholds introduces regulatory concerns pertaining to toxicity. The metal ion requirement of a given DNAzyme thus must be considered during probe selection. Lastly, pH can also be a restrictive factor for DNAzyme activity, as it can cause DNA denaturation or trigger metal ion precipitation. However, while certain foods like meat do increase in pH during spoilage, these increases are usually insignificant towards DNAzyme functionality.

Yet, while DNAzymes effectively detect and report pathogens, they often lack the high target binding affinity of aptamers – a property that can yield higher sensitivity and specificity. As such, some works have coupled these two probes to harness both the binding activity of aptamers and the catalytic activity of DNAzymes. For example, Liu *et al.* constructed a coupled DNAzyme-aptasensor detection system for the detection of *Cronobacter sakazakii* in liquid solution.<sup>[214]</sup> This sensor used a split-DNAzyme-aptamer that assembled in the absence of *C. sakazakii* to produce a DNAzyme-mediated colorimetric signal. In the presence of *C. sakazakii*, the aptamer's affinity for the bacteria prevented DNAzyme assembly, resulting in no development of colour. This study reported a limit of detection of 1.2 CFU/mL. Since most *C. sakazakii*-related deaths result from infant formula, this system holds value despite its lack of viability as an *in situ* system, as it can be used to evaluate liquid test matrices with ease. Nonetheless, the split-DNAzyme-aptamer system is evidently promising for the detection of other pathogens in solid foods, making *in situ*-centric optimization a valuable area of future work. That being said, turn-off platforms yield an increased risk of false positives induced by colorimetric systems experiencing substrate depletion, and fluorescent probes experiencing photobleaching, which is inevitable during long-term monitoring. Transitioning towards a turn-on platform is thus a potential next step.



**Figure 2.7. Material strategies for the improvement of foodborne pathogen sensors.** (a) Material structuring to induce higher probe density. (b) Material encapsulation for the preservation of probes over time in response to environmental stresses. (c) Antifouling coatings for the prevention of non-specific adhesion on the sensing surface. (d) Form factor manipulation to increase sensor contact with test matrix. Produced using BioRender.

Overall, the customizability, sensitivity, and practicality that DNA-based systems offer makes them strong platforms for *in situ* food contamination detection. With growing efforts to improve sensor stability for long-term use, alongside the discovery of probes with higher sensitivity and specificity, the value of such systems can be expected to increase.

#### 2.4.3.3 Antibody-based probes

Analogous to DNA probes, antibodies are advantageous because they can be generated with high specificity and selectivity for certain target bacteria. As peptides, their abundance in free reactive amino and carboxyl groups can be used for covalent linkage to a variety of sensing platforms. This represents a key advantage over DNA-based probes, which are artificially functionalized with limited reactive groups. Another advantage of antibodies is that they do not

typically require external reagents to maintain their secondary structure. However, their widespread use is limited by several key disadvantages. Namely, antibodies are complex proteins that offer less environmental stability, showing denaturation in response to harsh changes in pH and temperature. Antibodies are also less refined compared to DNA-based probes, the latter of which undergo multiple rounds of *in vitro* selection to ensure optimal binding efficacy. Lastly, antibodies are more expensive to synthesize than DNA-based probes, which decreases their commercial viability. Despite these drawbacks, some antibody-based sensors have been developed using colorimetric and electrochemical transduction methods.

In a recent work, Zeng *et al.* (2022) demonstrated that antibodies specific to *Yersinia enterocolitica*, a pathogen commonly found in raw pork, can be used to develop a paper-based colorimetric sensor to directly monitor contamination in meat samples.<sup>[215]</sup> This method involved linkage of antibodies with colloidal gold nanoparticles to develop a lateral-flow based assay on paper strips for contaminant detection (Figure 2.6b.iv). A secondary detection antibody was subsequently introduced to produce a colorimetric signal, yielding a limit of detection in the range of  $10^2 - 10^3$  CFU/mL. The system successfully detected the target bacteria in both milk and pork samples down to a limit of detection of 5 CFU/mL, but only following sample enrichment with growth media and after incubations of 4 to 6 hours. Assessment of contaminated samples without growth media was not presented, limiting proper understanding of sensor functioning at real-world levels of contamination.

Recognizing that target pathogens are often located within solid food matrices, Kim *et al.* used a slightly different approach that involved the incorporation of *E. coli*-specific immunoglobulin G (IgG) antibodies into a microneedle-based platform (Figure 2.7d).<sup>[216]</sup> Specifically, porous silk microneedle substrates were functionalized with polydiacetylene liposomes that underwent colorimetric changes in response to mechanical stressors such as binding events between the immobilized antibodies and target *E. coli* cells. Owing to the porous nature of the needles, capillary action mediated the collection of test solution onto the surface of the

functionalized microneedle patch. Paired with the ease of colorimetric readout, this platform's ability to sample pathogens from within food samples rather than just the surface presents an intriguing approach for future works to explore. These microneedles also exploit encapsulation of their colorimetric dye to limit the degree of external manipulation required for sensor functioning. High antibody specificity also ensured no cross-reactivity with non-target bacteria, based on evaluations with *Salmonella*-contaminated fish. However, a comprehensive assessment of the platform's limit of detection was not completed.

Antibodies can also be used for impedance-based detection in other ways, usually following gold nanoparticle-based conjugation. For example, Vu *et al.* (2021) developed an electrochemical sensor by modifying screen-printed electrodes with AuNPs, which were then further conjugated to *E. coli* specific antibodies.<sup>[95]</sup> The resultant system exhibited a limit of detection of 15 CFU/mL within 30 minutes. *E. coli*-specific antibodies introduced specificity, which reduced AuNP-mediated non-specific reactivity. However, basal responses to other bacteria still existed. Greater potential for interference exists by bacteria that are closely related to *E. coli* but are not pathogenic strains themselves. Using a similar approach, Chiriaco *et al.* (2018) developed a portable microfluidic platform for the detection of *Listeria monocytogenes*.<sup>[217]</sup> Specifically, gold microelectrodes within the microfluidic chip were functionalized with *L. monocytogenes*-specific antibodies using protein A – a peptide that mediates immobilization orientation, thus maximizing functionality. The resultant system demonstrated a limit of detection of ~6 CFU/mL in artificially spiked milk samples. This study, however, went a step further, addressing issues pertaining to on-site electrochemical detection. Specifically, this work employed a portable electrochemical impedance spectroscopy device that was connected to a portable impedance analyzer for measurements – a setup that may be applicable on a commercial scale. Unfortunately, the sensor is limited to liquid test matrices, due to its microfluidic nature. Nonetheless, further development of platforms compatible with such portable technologies

may enable the widespread commercial use of such highly sensitive electrochemical sensors in the food industry.

Antibodies offer high specificity and easier immobilization compared to DNA-based probes. Antibodies are also widely produced for the development of commercial biosensors, such as pregnancy tests, and as such are easy to translate. However, they are less researched due to their disadvantages which include their high cost and difficulties pertaining to functionalization due to their complex structural nature. Despite these disadvantages, interesting antibody-based sensing platforms are being developed. These works require improvements for *in situ* package detection but are nonetheless intriguing devices with scope for future developments.

Ultimately, these three main biorecognition probes offer high sensitivity and specificity, making them good choices for use within food contamination detection sensors. Consequently, these probes offer significant promise in terms of actualizing *in situ* contamination detection for specific pathogens, given the large body of work supporting future developments.

## **2.5 Situational Assessment and Future Directions**

Despite the material-driven development of a plethora of food spoilage and contamination sensing systems – each with its own set of benefits and drawbacks, no platform has achieved widespread commercial acceptance as of yet. A wide range of issues continue to hinder real-world viability of individual platforms – such as inadequate sensitivity, lack of specificity, insufficient material stability, poor *in situ* compatibility, and cost. The objectives of future works will resultantly center upon addressing these shortcomings.

### **2.5.1 Technical assessment and future directions for food spoilage monitoring**

While promising, the real-world applicability of biogenic amine sensors remains uncertain, given the unclear quantitative relationship that exists between biogenic amine levels and food spoilage. Specifically, while the production of these compounds is indicative of spoilage, threshold values that indicate the specific point at which a given product has expired are difficult to establish.

Such thresholds are necessary for the effective elimination of food waste. Future works that seek to define these values will significantly substantiate the use of such technologies by mediating the design of sensors that exhibit positive signals at the point at which a given food product becomes inedible. pH-based monitoring similarly struggles with a lack of concrete threshold values indicative of spoilage, as various biochemical changes in food can induce fluctuations in pH, making the relationship between pH and spoilage difficult to define. As such, future studies that comprehensively evaluate this relationship within different foods are needed. While severe changes in pH can confirm food spoilage, this is meaningless to the consumer as such changes are paired with alterations in odour and visual properties that are easily observed. Better understanding the relationship between spoilage and both biogenic amine concentration and pH may also substantiate the need for ultrasensitive detection – an objective that will be supported by highly responsive probes such as aptamers.

As it currently stands, monitoring biogenic amine production remains the best indicator of the spoilage state of many different kinds of foods in real-time owing to a more concrete quantitative relationship. Intelligent noses represent perhaps the most promising class of biogenic amine sensors because of their high sensitivity, tunable specificity, *in situ* compatibility, and vapour-responsive nature – which eliminates the need for food sample manipulation. The diverse range of material approaches applied in this space yields several avenues of future exploration. Next steps pertaining to the design of *in situ* pH sensors are more ambiguous given that most platforms reported thus far continue to suffer from the same issues – limited film strength and poor dye stability. Nanoencapsulation of pH responsive dyes is currently positioned as the most promising avenue for platform improvements. On a different front, Riaz *et al.* (2019) recently showed that wild-cabbage-sourced anthocyanins can be crosslinked to poly-2-hydroxyethyl methacrylate contact lenses to detect pH changes in the eye.<sup>[218]</sup> Given that improvements to cellulose, chitosan, and starch films have yielded limited improvements, the exploration of such alternative polymers may be justified.

A second consideration for pH sensor design pertains to a growing focus on multi-functional intelligent food packaging systems. pH monitoring platforms are well-positioned to contribute to this space given that many organic pH responsive dyes and film modifiers offer relevant secondary functions. Specifically, the antioxidant and antimicrobial functions of anthocyanins may have significant implications for food preservation and contamination response. Ma *et al.* (2019) reviewed the possible implications of these dyes for pathogen control in food.<sup>[114]</sup> A few recent studies have brought increased focus towards this preservative measure. Namely, Chen *et al.* (2020) developed a pH-responsive cellulose film through the incorporation of purple sweet potato anthocyanin that exhibited strong antimicrobial properties, with up to 99.99% reduction of *E. coli* and *L. monocytogenes*.<sup>[219]</sup> Further development of such systems is warranted.

While many of the discussed secondary modifiers also offer a degree of antimicrobial activity, films may also be embedded with antimicrobial agents directly. For example, Mustafa *et al.* (2020) explored the incorporation of propolis extract (PE) into PVA/starch films cross-linked with boric acid.<sup>[220]</sup> Embedded PE exhibited antimicrobial activity against both *E. coli* and methicillin-resistant *Staphylococcus aureus*. PE incorporation was also shown to prolong the shelf-life of milk, as the antibacterial activity exhibited by the films was sufficient to delay milk spoilage. Perhaps more intriguingly though, bacteriophages present a class of safe, antimicrobial agents that can also be used to preserve foods and prevent contamination. These entities are already used in the food space commercially, and several studies have reported their encapsulation into films for improved stability and performance. The incorporation of bacteriophages into pH-responsive films may offer significant benefits.

While many developed platforms appear promising within a controlled, experimental context, commercial application will require consideration towards real-world environment-induced variations in signaling performance. This is likely to incite the comprehensive analysis of sensing interferences within diverse food products, multiplexing of different probes for improved reliability, and a focus on reagentless design. This latter consideration is especially important, as



many of the complex sensing cascades presented in this work require a range of reagents that may influence food spoilage. Finally, with improvements in sensor design, artificial intelligence, image analysis, and machine learning are expected to become key pillars in spoilage monitoring. Through the neural network-mediated training of intelligent signal processing systems, the risk of false positives can be expected to be negated to commercially acceptable levels. The massive advantages afforded by such technologies has already become clear in existing literature.<sup>[221–223]</sup>

### **2.5.2 Technical assessment and future directions for pathogen monitoring**

The need for improved real-time pathogen detection in food is well-established given the high prevalence of foodborne illness worldwide. The aforementioned developments have led to substantial gains in both on-site and *in situ* detection platforms for targeting bacteria within complex food matrices in real-time. The objective of future works will center upon addressing remaining shortcomings – namely improving the sensitivity of *in situ* platforms.

Making improvements to *in situ* sensitivity has proven difficult considering that most conventional signal amplification strategies do not have the necessary characteristics for incorporation. Ideally, they must function autonomously with no user interference, use biocompatible reagents, and be able to contribute to the reaction cascade while in an immobilized, solid-state form. As such, future efforts must rather look towards improving base probe sensitivity and incorporating novel signal amplification strategies.

Using bacteriophage as a sensing probe for bacterial detection in food has been reported sparingly, offering significant flexibility in terms of pathways for improvement. With more established oligonucleotide and antibody probes, one simple approach aimed at improving probe sensitivity involves modifying the means by which they are incorporated onto a sensing substrate. Specifically, improper orientation or restrictive immobilization can induce low functionality, yielding poor sensor sensitivity. This premise was explored by Liu *et al.*, who non-covalently immobilized *E. coli*-responsive DNAzymes into graphene sheets and found that such a system permitted single cell detection – partially due to the free nature of the DNAzyme.<sup>[224]</sup> There are a

plethora of different immobilization strategies that can be used for probe integration, each with unique characteristics that make them optimal for particular platforms. Such incorporation strategies have been reviewed by our group previously.<sup>[200]</sup> With the integration of new sensing substrates, novel immobilization strategies can be implemented. Alternatively, whole cell biosensing represents another viable avenue of exploration, with proven efficacy within other biosensing applications. To date, use in food sensing has been limited to very few studies.<sup>[225]</sup> Their complex nature and reliance on living bacteria likely limits these platforms to on-site detection, but their excellent performance garners future interest.

While many studies have evaluated bacteriophages, nucleic acids, and antibodies as probes for bacterial detection, they have so far been evaluated in isolation. As different probes carry distinct reactivity for different species of bacteria, these probes can be coupled with one another to create multiplexed sensors for bacterial detection. This is especially true for nucleic acids and antibodies, which can be functionalized with different types of fluorescent and colorimetric signal molecules, allowing for efficient multiplexing. In contrast, bacteriophages cannot be so easily chemically functionalized without permanently modifying their survival and their ability to detect bacteria.<sup>[226]</sup> However, genetically edited bacteriophages encoding different types of visible reporters present one possible path forward. Additionally, multiplexing is also possible using a mix of these different probes. As bacteriophages induce bacterial lysis, they cause the release of bacterial proteins, which may aid in nucleic acid probe and antibody-mediated detection.

Considering that bacterial contaminants cannot be detected in vapour – as biogenic amines and pH often are, but rather require direct contact with the sensing substrate, the detection of contamination *in situ* is limited to the food surface to which they are applied. Most of a given food product is thus left untested. Microneedle-based biosensors present an interesting opportunity to the development of intelligent packaging because of their unique ability to penetrate the biological matrix of solid foods, allowing them to collect more robust liquid test samples – which are drawn out by capillary forces, that are representative of both the food surface and the underlying matrix.

Aside from the study by Kim *et al.* (2020), microneedles have also been used in the food industry in the context of allergen detection by sampling DNA from complex food matrices.<sup>[216]</sup> Given their ease of fabrication and use however, this represents perhaps one of the most defined future directions for pathogen sensing work. A variety of distinct compounds – such as anthocyanins and antibodies, could also be functionalized onto the interior and exterior surfaces of these microneedles to elicit measurable signals.

On a broader scale, many of the presented *in situ* sensing systems require access to defined volumes of liquid test samples and have reaction cascades that require buffer solutions. For example, DNazymes, which require metal ions to properly adopt a secondary structure, require the addition of metal-ion reaction buffers to sensors for their proper functioning.<sup>[17]</sup> It is optimal that biosensors that are incorporated into packaging materials are able to function without external reagents as they can act as sentinels for bacterial growth and spoilage over time. Novel approaches are required to design reagentless biosensors for this purpose, or to allow the incorporation of such buffers into packaging materials. A packaging system that mediates collection of released juices and meat purge onto a sensing interface and facilitates stable incorporation of biocompatible buffers would thus substantially increase the reliability of many developed platforms. Printing probes onto organic polymers that also embed required reagents provides another potential alternative. With improved consistency, artificial intelligence can be better applied in food sensing, as complementary signal reading and processing devices would be easier to calibrate.

Finally, while spoilage and pathogen monitoring largely remain separated in research given the complex nature of each in isolation, it is anticipated that combined technologies will soon emerge. The need for such multiplex systems is apparent, given that only with spoilage and pathogenic contamination considered together, can we attain a comprehensive assessment of food safety. With continued emphasis on new avenues of detection, recognition towards areas of overlap are expected to drive such work forward. Material-driven innovation can be expected to be at the center of such efforts, as the incorporation of two different sensing cascades into a signal platform

will require various physical, chemical, and biological consideration. To this end, smart material advances that enable the development of both *in situ* and on-site platforms for use at the production, distribution, and consumer levels will define food safety going forward.

### 2.5.3 Regulatory considerations

Significant barriers continue to limit the translation of the presented *in situ* platforms from promising prototypes to approved products. Specifically, while many of the platforms discussed in this paper have significant potential in terms of their sensing ability, they incorporate materials that are not approved for food-contacting applications and are potentially harmful to the environment. Few studies have evaluated the extent of material leaching and the impact that these materials may have on human health and the environment. Overarchingly, regulatory approval of on-package labels and other on-food sensors usually involves ensuring that the leaching of immobilized compounds into foods stays below a threshold of 0.5 ppb.<sup>[227]</sup> It is unclear if the presented *in situ* biosensors meet these guidelines.

The regulatory requirements for approving new nanomaterial-based materials for intelligent food packaging applications are stringent, with comprehensive clinical and environmental toxicology profiles required by many governmental agencies – namely the Food and Drug Administration (FDA) and the European Union (EU).<sup>[228,229]</sup> EU regulations go a step further, requiring packaging nanomaterials to be listed as ingredients on food products, given the possibility of leaching.<sup>[228]</sup> Improper regulatory management has led to the recall of packaging materials in the past, making such considerations a priority during commercial development.<sup>[229,230]</sup> Regulations mediating relevant performance metrics are also important to consider when evaluating the design and efficacy of intelligent food monitoring systems. In terms of microbial contamination, critical thresholds for pathogenic bacteria have been set by various global agencies. Namely, the FDA limit for generic strains of *E. coli* is often as low as  $10^2$  CFU/g.<sup>[231,232]</sup> Pathogenic *E. coli* strains such as O157:H7 are limited to even lower thresholds, as they pose a significantly greater threat to human health.<sup>[233]</sup> Similarly, levels of *Salmonella* contamination in pork are as

low as 10 CFU/g.<sup>[234]</sup> With regards to chicken, cooked products have a zero tolerance 0 CFU/g threshold. The rational design of ultrasensitive biosensors that consider these thresholds can inform the creation of relevant intelligent sensors for food safety. As mentioned previously, such thresholds have not been set for spoilage, yielding ongoing societal reliance on pre-determined expiry dates that lack accuracy.

Finally, regulatory approval of performance claims requires significant consideration towards sensing interference. This includes thorough evaluation of developed sensing platforms within diverse food product to eliminate concerns pertaining to food matrix-induced false positives. The ability of these platforms to function throughout the food distribution pipeline, which involves significant variations in temperature, humidity, and duration of storage, is also of particular importance when considering claims centered around real-world viability.

#### **2.5.4 Commercial considerations**

Yet, while a plethora of promising on-site and in-package sensing platforms have been presented here, commercial success in this space has been scarce. To this end, Table 2.4 highlights some of the presented platforms that have made some progress towards commercialization. While the specific factors that hinder the real-world use of a given platform are specific to its design, overarching barriers include limited real-world consideration, high cost, and consumer hesitancy.

##### *2.5.4.1 Limited real-world consideration*

While the aforementioned Table 2.4 highlights select platforms that have positioned themselves as commercially promising products, many platforms in the food space do not adequately account for real-world considerations. Namely, food products are regularly oversimplified, treated as homogenous matrices with sensing studies. In reality, a single product offers several different microenvironments – all with varying properties that can undermine biogenic amine, pH, and pathogen monitoring.<sup>[235]</sup> This makes *in situ* platforms suited for real-world use extremely difficult to design, drawing attention towards on-site sensing platforms that can incorporate a product homogenization step prior to testing. Alongside failing to enable

individual product monitoring, such measures do not account for the diverse farming and processing practices employed today, that yield compositional differences among individual food products.<sup>[235]</sup>

Even with all such factors considered, the controversy surrounding the existence of consistent biogenic amines and pH baseline and spoilage values complicates real-world use. While many works have reported baseline and spoilage values, other studies have found large degrees of variation within individual products.<sup>[236]</sup> Such variations make the universal calibration of such platforms difficult. Ultimately, there exists a defined need for studies that comprehensively evaluate large numbers of food products sourced from different supplies, to provide a concrete situational assessment. In the event that baseline and spoilage values are largely inconsistent, the presented platforms can still offer significant value, but will require significant modifications in their reporting structure. For example, percent change in signal may be more useful than objective values. Of course, all such efforts will be supported by the anticipated development of more sensitive and specific sensing cascades, as detailed in 4.1 and 4.2. The development of such performance metrics will also help identify technologies with the greatest potential in a currently crowded area of study.

With regards to pathogen detection, the use of artificially spiked food products lowers the translatability of the results to the real world. Specifically, the distribution of bacterial contaminants on whole food products following real-world contamination has not been comprehensively studied. As such, artificial contamination involves the homogeneous distribution of bacterial targets across the surface of a test matrix – a protocol that makes consistent detection more attainable. Contaminated food samples sourced from industry must thus be incorporated in future studies.

#### *2.5.4.2 High cost*

The commercial viability of many developed food sensors are also hindered by unclear value propositions. *In situ* platforms in particular, can be expected to add noticeable cost to food

packaging – an industry in which very minimal increases in cost are often considered too dramatic to implement. While increased packaging costs can be partly justified through the prevention of food recalls, it has been estimated that *in situ* sensing platforms would account for over 50% of the cost of such smart food packaging.<sup>[237]</sup> The food industry expects that packaging should not account for more than 10% of the cost of goods sold, meaning that such a significant markup is unrealistic.<sup>[237]</sup> Ultimately, developing a compelling commercial case for *in situ* sensing platforms involves a greater focus on the cost of resultant platforms – a shift that has been observed within some recent works. Further, there exists a need for accurate estimations of the expected economic benefit of incorporating such sensors into packaged foods, to ensure that the cost of implementation is significantly lower than the anticipated savings. Such efforts must also account for the start-up costs associated with the development and mass manufacturing of such sensors.

On-site sensors offer a stronger commercial case as a replacement for culture-based methods that are expensive and logistically complex – largely owing to their need for off-site processing and reliance on sophisticated laboratory equipment. Acting as a first line of defense, such platforms can function as rapid tests that can replace some – if not all, culture-based testing protocols. Here, several presented works have shown promise, owing to their rapid detection and high sensitivity.<sup>[29,206,216]</sup> Given that testing is done periodically on select food products, a compelling cost-benefit ratio is much more achievable with such platforms. Nonetheless, minimizing cost is instrumental, to justify the significant capital required to develop and mass produce such platforms. Concurrently, ensuring that the approaches used for the fabrication of a given platform are suitable for commercial-scale manufacturing is also a defining consideration.

#### 2.5.4.3 Consumer hesitancy

Numerous studies have evaluated the willingness-to-pay (WTP) of consumers for *in situ* food monitoring technologies.<sup>[238,239]</sup> Consumers have a higher WTP and general interest in such products when they pose a greater societal benefit with minimal risks toward health. To this end, labels embedded with reactive, food-derived agents such as anthocyanins are especially

compelling. While various synthetic nanoscale agents have been categorized as food-safe, perceptions surrounding their incorporation in food remain largely negative.<sup>[238,239]</sup> A mix of consumer education and technological adaptation in response to consumer feedback can be expected to yield improvements in this space.

Concurrently, the environmental implications of such packaging platforms are of great interest to consumers.<sup>[239]</sup> The integration of biodegradable materials such as cellulose and chitosan – as discussed in this review, can thus be expected to aid in consumer acceptance. In comparison, the use of metals and plastics can generate runoffs that pose a threat to both environmental and human health. For platforms that require such agents, devising sustainable strategies for disposal are essential for large-scale distribution. Considering such factors proactively when designing food monitoring technologies is a necessary shift in this space, to ensure that more developed platforms achieve commercial success.

## **2.6 Acknowledgements**

S.K. is a recipient of the Vanier Canada Graduate Scholarship awarded by the Natural Sciences and Engineering Research Council of Canada. J.K.M. is a recipient of the Undergraduate Student Research Award from the Natural Sciences and Engineering Research Council of Canada. A.P. is a recipient of the Canada Graduate Scholarship – Master’s from the Natural Sciences and Engineering Research Council of Canada. This work was supported by the NSERC Discovery Grant, Ontario Early Researcher Award and Mitacs grants to TFD. T.F.D. is a Tier II Canada Research Chair in Nanobiomaterials.

## **Conflict of Interest**

The authors claim no conflicts of interest.



## 2.7 Tables

**Table 2.1.** Recently developed platforms for biogenic amine detection in food samples.

	Detection Mechanism	Signal Transduction	Limit of Detection	Advantages	Disadvantages	Ref
Electrostatic binding	AuNPs + citrate	Colorimetric	0.6 μM	Rapid target binding and signal generation	Non-specific target binding, requires extensive sample processing	[20]
	AuNPs without citrate	Colorimetric	0.2 μM			[113]
	AuNPs + AgNPs	Colorimetric	150 μM			[119]
Covalent binding	PD-6 pyrazine derivative	Fluorescent	Unspecified	Reactive specificity for biogenic amines, non-contact detection method	Poor translatability of readout method, non-specific signal generation	[121]
	DπA compounds	Colorimetric	3-5 μM	Fine-tunable via chemical modification, non-contact detection method	Non-specific target binding	[122]
	Methyl red-EuMOFs	Fluorescent	0.1 μM	Fine-tunable affinity via choice of MOF ligand, non-contact detection method	Poor translatability of readout method	[19]
	Tris-beta-diketone – lanthanide MOF	Luminescent	Unspecified		Non-specific target binding	[126]
	Cadmium-MOF	Fluorescent	10 μM		Poor translatability of readout method	[127]
Table continued						

Biorecognition probes	H2 DNA aptamer	Colorimetric	$1.8 \times 10^{-5} \mu\text{M}$	High specificity, fine-tunable affinity, and surface binding via chemical modification	Poor translatability of readout method, requires extensive sample processing	[135]
	A10949 RNA aptamer	Fluorescent	$0.37 \mu\text{M}$			[137]
	Antibody	Colorimetric	$2.25 \mu\text{M}$			[138]

**Table 2.2.** Relevant properties of base film materials and modifiers for in situ pH sensing.

Base Polymeric Materials Applied as Film Substrates						
Material	Tensile Strength (MPa)		Water Vapour Permeability (x10 <sup>-11</sup> gm/m <sup>2</sup> sPa)	Pigment Retention	Biocompatibility	Ref
Cellulose	20-30		10-20	Poor	Yes	[159]
Cellulose-PVA	35-45		5-15	Moderate	Yes	[160]
Chitosan	15-20		10-15	Poor	Yes	[161]
Chitosan-PVA	25-35		5-10	Moderate	Yes	[161]
Cellulose-chitosan	35-45		5-10	Moderate	Yes	[159]
Starch	5-10		15-25	Poor	Yes	[240,241]
Starch-PVA	7.5-12.5		10-20	Moderate	Yes	[163]
Secondary Modifications for Performance Improvements						
Modifiers	Base Material	Tensile Strength (MPa)	Water Vapour Permeability (x10 <sup>-11</sup> gm/m <sup>2</sup> sPa)	Pigment Retention	Biocompatibility	Ref
Riceberry phenolic extract	Chitosan	Increased (28.66)	Decreased (1.32)	Increased	Yes	[164]
TEMPO oxidation	Cellulose	Increased (95.09)	Decreased (4.14)	Increased	Yes	[165]
Alginate nanoencapsulation	PVA-glycerol	Not reported	Increased (29.34%)	Decreased	Yes	[169]
Nanocomplexes	Starch-PVA	Increased (23.03)	Decreased (3.1)	Increased	Yes	[170]
Nanoencapsulation + oxidation/acetylation of base material	Starch	Increased (10.37)	Decreased (9.2)	Increased	Yes	[171]
Carbon nanodots	Starch	Increased (10.22)	Negligible change (27.2%)	Decreased	Yes	[143]
TiO <sub>2</sub> nanoparticles	Chitosan	Increased (23.98)	Reduced (5.12)	Increased	Mostly biocompatible	[177]

**Table 2.3.** Recently developed sensing platforms for pathogen identification in food.

	Probe	Target	Deposition Method	Substrate	Limit of Detection	Signal Transduction	Ref
Bacteriophages	Bacteriophage	<i>Salmonella</i> spp.	EDC/NHS	Screen printed electrodes	12 CFU/mL (40 mins)	Electrochemical impedance spectroscopy	[191]
	Bacteriophage ZCEC5	<i>Escherichia coli</i>	Free flowing	No immobilizing substrate	Not reported (20 mins)	Antennae-mediated wave detection	[195]
	<i>PhoA</i> engineered-T7 bacteriophage	<i>Escherichia coli</i>	Free flowing	No immobilizing substrate	100 CFU/mL (<6h)	Fluorescence	[196]
	SEA1, TSP1 bacteriophages	<i>Salmonella</i> spp.	Free flowing	No immobilizing substrate	10-100 CFU/mL (2h)	Luminescence	[197]
Oligonucleotides	<i>Salmonella typhimurium</i> DNA aptamer	<i>Salmonella</i>	Not specified	Carbon nanotube modified-ITO electrode	55-67 CFU/mL (10 mins)	Electrochemical impedance	[96]
	Alicyclobacillus DNA aptamer	<i>Alicyclobacillus acidoterrestris</i>	Glutaraldehyde immobilization	Magnetic nanoparticles and quantum nanodots	1000 CFU/mL (90 mins)	Fluorescence	[203]
	PAE-1 DNzyme	<i>Pseudomonas aeruginosa</i>	Physical adsorption	Polystyrene	1.2 CFU/mL (10 mins)	Fluorescence	[204]
	RFD-EC1 DNzyme	<i>Escherichia coli</i>	Printing with trehalose and pullulan	Nitrocellulose paper	10,000 CFU/mL (90 mins)	Fluorescence	[206]
	DAh1T1 DNzyme	<i>Aeromonas hydrophila</i>	Printing with trehalose and pullulan	Polystyrene	36 CFU/mL (10 mins)	Fluorescence	[207]
	RFD-EC1 DNzyme	<i>Escherichia coli</i>	Epoxysilane	Polyethylene	1000 CFU/mL (Overnight)	Fluorescent	[17]
	<i>Cronobacter</i> DNzyme-aptasensor	<i>Cronobacter sakazakii</i>	Free flowing	No immobilizing substrate	1.2 CFU/mL (<1h)	Colorimetric	[214]

Antibodies	IgG Antibody	<i>Yersinia enterocolitica</i>	Thiol-mediated	Gold nanoparticles	30-130 CFU/mL (10 mins)	Colorimetric	[215]
	IgG Antibody	<i>Escherichia coli</i>	Dimyristoylphosphatidylcholine liposomes	Liposome-embedded silk microneedles	10 <sup>8</sup> CFU/mL (16h)	Colorimetric	[216]
	IgG Antibody	<i>Escherichia coli</i>	N-γ-maleimidobutyryl-oxy succinimide ester	Screen printed electrodes	15 CFU/mL (30 mins)	Electrochemical	[95]
	IgG Antibody	<i>Listeria monocytogenes</i>	Protein A, immobilized via EDC/NHS	Micro-electrodes	5.5 CFU/mL (1h)	Electrochemical impedance spectroscopy	[217]

**Table 2.4.** Food monitoring technologies in the commercial pipeline.

	Technology	Company	Year	Development Stage	Mechanism	Signal Transduction	Use Case	Ref
Food Quality and Spoilage Monitoring	BlakBear Sensor	BlakBear	2017	Incorporated, pilot testing	Carbon electrodes printed on paper, increased amine-induced impedance	Smartphone-scannable RFID chip	<i>in situ</i>	[242,243]
	CheckPack	Pack4Food	2013	Within research consortium, prototyping	Silicon photonic based detection of VOCs and CO <sub>2</sub> levels	IR signals, detectable with associated IR-reader devices	<i>in situ</i>	[244,245]
	NFC based CARDS	C2Sense	2016	Technology licensed, prototyping	Amine-binding carbon nanotube metalloporphyrins, resultant RF shifts	RF signals from NFC tags interpreted with smartphones	On-site	[246,247]
	NeOse Pro/ NeOse Advance	Aryballe	2017	Commercially available	Analysis <i>via</i> optical nose to compare food odour to database	Electronic signal readout displayed on smartphone	On-site	[248]
	Enterprise Sensor/ Preemie Sensor	Tellspec	2015	Commercially available	Portable NIR spectrometer paired with an AI engine to develop spoilage models	Electronic NIR signals uploaded to cloud-based software, paired with smartphone	On-site	[249]
Pathogen Monitoring	Sentinel Wraps	Toyota Tsusho Corporation	2020	Industry collaboration, prototyping	Fluorescently labelled DNzyme directly embedded onto packaging	Fluorescence signals detectable with handheld readers	<i>in situ</i>	[17,250]
	KRAKEN	KRAKEN SENSE	2017	Pilot testing for non-food related applications	Real time qPCR for strain-specific bacterial pathogen detection	Concentration quantification outputted onto software	On-site	[251,252]

Pathogen Monitoring	Viability Polymerase Circle Reaction (VPCIR)	VPCIR Biosciences	2018	Commercially available	Monitor activity of contaminant DNA-modifying enzymes by introducing enzyme-binding substrates	Fluorescence signals	On-site	[253]
	PIPER	Ancera	2011	Commercially available	Cell sorting platform using magnetic technology	Image analysis of microbes	On-site	[254,255]
	TrueRapid	SnapDNA	2011	Commercially available	DNA-coated beads that selectively capture live pathogens for RNA analysis	Quantitative analysis and heatmaps	On-site	[256,257]
	Food Sentinel System	SIRA Technologies Inc.	2000	Technology patented, no recent updates	Solid phase immunobead assay using pathogen-specific antibody	Bead-antigen complexes agglutinate on antibody, create a dark bar on the aptamer barcode	<i>in situ</i>	[258]
	Toxin Guard	Toxin Alert	2002	Prototyping, no recent updates	Antibodies incorporated onto packaging films	Irreversible colorimetric signal	<i>in situ</i>	[259]

## Chapter 3: DNAzyme-Based Biosensors: Immobilization Strategies, Applications and Future Prospective

### Preface

Based on prior experiments conducted in our lab, our research team has established RFDs as promising tools for food monitoring. Recognizing that in-package monitoring requires surface immobilization of sensing agents, developing a strong understanding of how RFDs can be integrated is vital towards achieving Objectives 1 and 2. Accordingly, this chapter provides a comprehensive review of immobilization strategies for DNAzyme surface functionalization. Each approach is critically evaluated, to identify their benefits, drawbacks, and reasonable use-cases. Moreover, the application of these approaches are discussed through a review of recently reported DNAzyme sensors. Alongside a discussion of food monitoring sensors, sensors designed for environmental and clinical applications are also presented. These discussions present sensor improvement approaches that have not been applied to food sensing but may prove useful. Finally, future directions in the DNAzyme-based biosensor development space are proposed.

### Authors

Shadman Khan , Brenda Burciu, Carlos D.M. Filipe, Yingfu Li, Kristen Dellinger, Tohid F. Didar

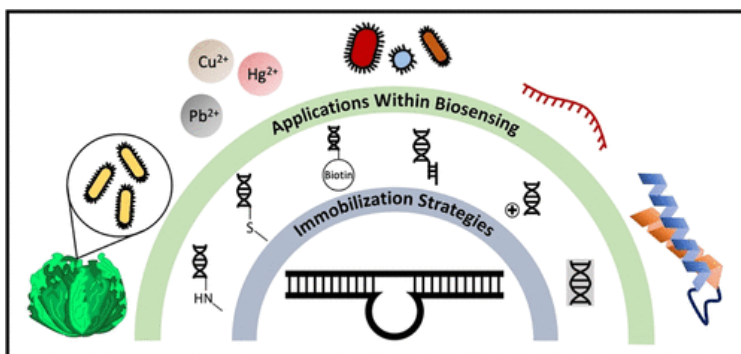
I was responsible for defining the scope of this work and carrying out initial literature review. I authored the Immobilization Strategies and Future Prospective sections entirely and contributed several sub-sections of the Applications section. I designed all figures and tables. Brenda Burciu and Kristen Dellinger authored sub-sections within the Applications section. Carlos D.M. Filipe, Yingfu Li, Kristen Dellinger and Tohid F. Didar supervised and edited this work.

### Publication

ACS Nano, 2021, 15, 9, 13943-13969

### Publication Date

September 2021





### 3.1 Abstract

Since their discovery almost three decades ago, DNAszymes have been used extensively in biosensing. Depending on the type of DNAszyme being used, these functional oligonucleotides can act as molecular recognition elements within biosensors, offering high specificity to their target analyte, or as reporters capable of transducing a detectable signal. Several parameters need to be considered when designing a DNAszyme-based biosensor. In particular, given that many of these biosensors immobilize DNAszymes onto a sensing surface, selecting an appropriate immobilization strategy is vital. Suboptimal immobilization can result in both DNAszyme detachment and poor accessibility towards the target, leading to low sensing accuracy and sensitivity. Various approaches have been employed for DNAszyme immobilization within biosensors, ranging from amine and thiol-based covalent attachment to non-covalent strategies involving biotin-streptavidin interactions, DNA hybridization, electrostatic interactions and physical entrapment. While the properties of each strategy inform its applicability within a proposed sensor, the selection of an appropriate strategy is largely dependent on the desired application. This is especially true given the diverse use of DNAszyme-based biosensors for the detection of pathogens, metal ions and clinical biomarkers. In an effort to make the development of such sensors easier to navigate, this paper provides a comprehensive review of existing immobilization strategies, with a focus on their respective advantages, drawbacks and optimal conditions for use. Next, common applications of existing DNAszyme-based biosensors are discussed. Last, emerging and future trends in the development of DNAszyme-based biosensors are discussed and gaps in existing research worthy of exploration are identified.

**Keywords:** DNAszyme, biosensor, sensing, immobilization, metal ion detection, pathogen detection, biomarker detection, cancer detection, food monitoring

### 3.2 Introduction

Deoxyribozymes (DNAszymes) have continuously intrigued the scientific community due to their potential as biosensors for various clinical and environmental applications.<sup>[260]</sup> As the name

implies, these functional oligonucleotides have enzymatic properties that allow them to mediate various chemical reactions including DNA and RNA cleavage, ligation and phosphorylation.<sup>[261]</sup> The activity of some DNazymes is dependent on the presence of specific molecules, such as metal ions and proteins.<sup>[262]</sup> Because of this property, these DNazymes can be used to engineer biosensors capable of detecting such molecules. Many DNazymes have been shown to have the capability to distinguish between similar stimuli – such as different strains of bacteria, which allows for the development of targeted biosensors with high specificity.<sup>[263,264]</sup>

DNAzyme-based biosensors offer various advantages over traditional detection strategies. Enzyme-linked immunosorbent assays (ELISAs) are one of the most common procedures used for the detection of target analytes. While a valuable tool, ELISA performance is heavily impacted by environmental conditions and they exhibit poor long-term stability due to the sensitive nature of their expensive protein components.<sup>[265]</sup> ELISAs also offer limited sensing capabilities, preventing the detection of target analytes present at concentrations below  $10^{-12}$  M. DNAzyme-based sensors offer greater stability and higher detection sensitivity at a lower cost.<sup>[265]</sup> Alternatively, when a nucleic acid target can be used for the detection of a particular entity, polymerase chain reaction (PCR) is often employed due to its strong detection capabilities. However, while significant progress has been made in the development of on-site PCR technologies, such systems remain quite complex and require a wide range of expensive components.<sup>[266]</sup> Additionally, when working with complex clinical samples, PCR platforms need to be optimized extensively based on the nature of the sample, making their widespread use as a detection platform quite cumbersome.<sup>[267]</sup> Contrarily, DNAzyme-based biosensing platforms can be easily modified for varying applications through the incorporation of the desired target-specific DNAzyme.

The process of identifying DNazymes for specific applications is well-documented within literature. In essence, it comprises an *in Vitro* selection process involving a large DNA pool consisting of as many as  $10^{16}$  distinct DNA strands.<sup>[261]</sup> These strands undergo function-based selection steps that ultimately identify the strands that engage in enzymatic activity in response to the desired target – a process commonly referred to as systemic evolution of ligands by exponential

enrichment (SELEX), which is also commonly used for the identification of other functional oligonucleotides such as aptamers.<sup>[261,268]</sup> While SELEX has historically been a very laboursome process, recent advancements have presented methods that make the procedure more efficient. Such advancements have been detailed at length elsewhere.<sup>[269,270]</sup> Once a DNAzyme sequence has been identified, large quantities can be easily produced at a low cost, given that DNA synthesis has become very inexpensive. This makes DNAzyme-based biosensors ideal for commercial use.

The subsequent process of taking an identified DNAzyme and developing a functional biosensor is much more ambiguous. That being said, many DNAzyme-based biosensors immobilize DNAzymes onto an underlying substrate, given that surface immobilization has been shown to improve detection sensitivity through a reduction in background noise.<sup>[271]</sup> This reduction is driven by the ability to wash away unreacted signalling entities, which is otherwise not possible within a solution-based sensor. Surface immobilization has also resulted in the development of reusable sensors.<sup>[271]</sup> For such surface-immobilized DNAzyme-based biosensors, various considerations – such as the nature of the underlying substrate and the signal transduction method, need to be made to optimize performance. Common substrates include various polymers,<sup>[272–274]</sup> gold<sup>[271,275,276]</sup> and graphene,<sup>[277–279]</sup> each of which possess distinct properties that make them suitable for particular sensing systems. These properties include cost, potential for mass production, the degree of background noise and the chemical groups present for surface functionalization. This last factor is key in the surface immobilization of a DNAzyme. If a surface-based sensor is prone to DNAzyme detachment, its accuracy and stability will be impaired. Thus, the selection of an appropriate immobilization strategy is critical in the development of a relevant biosensor.

DNAzyme-based biosensors have been used for widespread applications, given their strong detection capabilities and functionality within diverse environments. Namely, these biosensors have been used extensively for the detection of food contaminants,<sup>[17,280–282]</sup> pathogens,<sup>[283–285]</sup> metal ions<sup>[272,274,286]</sup> and various clinically relevant biomarkers.<sup>[287–289]</sup> Compared to traditional detection methods, DNAzyme-based biosensors have shown robust

accuracy, high detection sensitivity and resilience to non-specific entities that can often hinder sensing cascades.<sup>[290,291]</sup>

With the high degree of research activity in the field of DNAzyme-based detection, a plethora of immobilization methods have emerged. These strategies have characteristics that make them ideal for varying detection platforms. Accordingly, there has been extensive growth in the target applications of these biosensors. Herein, we provide a comprehensive review of existing immobilization methods, their respective advantages and disadvantages, as well as detection platforms for which they are most appropriate. Subsequently, we detail common applications of DNAzyme-based biosensors, with a focus on recent developments. Finally, emerging trends and future directions are discussed in relation to both DNAzyme immobilization strategies and target applications of DNAzyme-based biosensors. Discussions in this review are informed by all three DNAzyme classes – RNA-cleaving DNAzymes, DNA-cleaving DNAzymes and peroxidase-mimicking DNAzymes, to provide a comprehensive understanding of the field.

### **3.3 DNAzyme Immobilization Strategies for Biosensing**

A wide range of covalent and non-covalent immobilization strategies have been implemented in the functionalization of sensing substrates with DNAzymes. While some strategies – such as DNA hybridization and DNA-mediated electrostatic interactions, are specific to oligonucleotides, many DNAzyme immobilization strategies are non-specific to DNA entities. Rather, they are used for the immobilization of various biomolecules. However, the ways in which these strategies are selected and implemented revolve around fundamental design considerations specific to DNAzyme-based sensors. Such considerations include the nature of the target entity, the properties of the underlying substrate and the desired signal transduction method. All such considerations are discussed at length for individual immobilization methods, in the context of recent studies involving DNAzyme-based biosensors. A detailed summary of DNAzyme immobilization methods is additionally provided in Table 3.1.

### 3.3.1 Covalent immobilization

#### 3.3.1.1 Thiol-based attachment

Thiol-based attachment has presented itself as a premier strategy for DNAzyme immobilization. The resulting attachment is both robust given its covalent nature, and easy to implement as its constituent parts are often already involved in the sensing pathway. Specifically, platforms using gold (Au) can use this metal as a binding site for thiolated DNAzymes, yielding Au-S bonds.<sup>[271]</sup> The strong binding affinity associated with thiol-based immobilization has been shown to increase biosensor shelf life and has made certain sensing devices reusable.<sup>[271,292]</sup> This is especially true for DNAzyme-based biosensors, given that these functional oligonucleotides are capable of maintaining functionality in a wide range of conditions.<sup>[293,294]</sup>

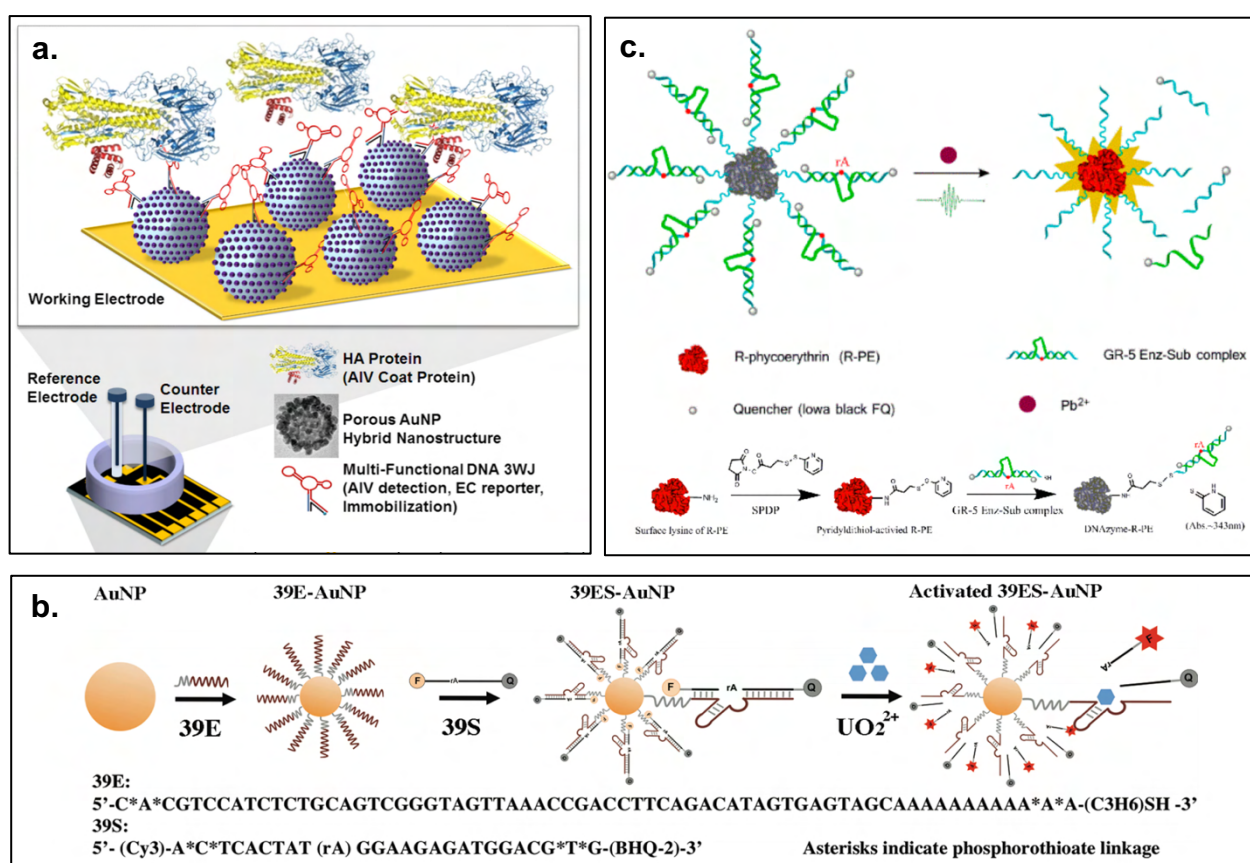
Using thiol-based immobilization, significant improvements in detection limit have been achieved. In particular, Swearingen *et al.* found that the detection limit for lead ions ( $\text{Pb}^{2+}$ ) can be reduced from 10 nM to 1 nM through immobilization onto an Au substrate, due to a reduction in background signals.<sup>[271]</sup> Their sensor involved the immobilization of a quencher-containing RNA-cleaving DNAzyme onto Au films, which would subsequently hybridize with a fluorophore-containing substrate strand. While initial fluorescence was minimal, a substantial increase was observed upon  $\text{Pb}^{2+}$ -induced cleavage of the substrate strand due to separation between the fluorophore and quencher.<sup>[271]</sup> Following a sensing cycle, replenishing the attached DNAzymes with uncleaved substrate strands was all that was needed to prepare the sensor for subsequent samples, as the immobilized DNAzyme was unaffected by the sensing cascade.<sup>[271]</sup> Electrochemical detection has also been achieved on an Au substrate by Yang *et al.*, who immobilized thiolated nickel ( $\text{Ni}^{2+}$ )-responsive RNA-cleaving DNAzymes onto an Au electrode. The DNAzymes were hybridized with substrate strands coupled with cadmium selenide quantum dots. Upon  $\text{Ni}^{2+}$ -induced cleavage, the dislocation of the quantum dots from the electrode surface was detectable through differential pulse anodic stripping voltammetry with a limit of detection of 6.67 nM.<sup>[295]</sup> Importantly, sensors aiming to immobilize biomolecules onto Au substrates are washed with mercapto-hexanol following incubation with the DNAzyme to disrupt any Au-N non-

specific interactions that may have been formed between Au substrates and oligonucleotides.<sup>[292,296]</sup> Such a treatment ensures a monolayer of Au-S bonded DNAzymes across the sensing surface.<sup>[292]</sup>

A wide range of three-dimensional form factors have been used when incorporating Au within DNAzyme-based biosensors. Specifically, Au nanoclusters (AuNCs),<sup>[292]</sup> nanoparticles (AuNPs)<sup>[275,276,283,293]</sup> and nanoflowers (AuNFs)<sup>[297]</sup> have all been used to maximize the surface area available for thiol-based attachment of biosensing components. Compared to planar sensing surfaces, these substrates can result in an improved limit of detection. Under this principle, Hu *et al.* coated glass carbon electrodes with AuNCs and subsequently used Au-S bonds to immobilize thiolated copper ( $\text{Cu}^{2+}$ )-responsive DNA-cleaving DNAzymes.<sup>[292]</sup> The DNAzymes cleaved a complementary substrate strand when exposed to  $\text{Cu}^{2+}$ , resulting in a change in the interfacial electron-transfer resistance on the surface of the electrode, which was detectable for  $\text{Cu}^{2+}$  concentrations as low as 0.07 nM.<sup>[292]</sup>

Zhang *et al.* developed a  $\text{Pb}^{2+}$  biosensor by coating magnetic AuNPs with  $\text{Pb}^{2+}$ -responsive RNA-cleaving DNAzymes, hybridized with a substrate strand. Upon exposure to  $\text{Pb}^{2+}$ , the substrate strand was cleaved, and the magnetic properties of the NPs were used to separate the particles from the cleaved oligonucleotide fragments.<sup>[276]</sup> These fragments were then subjected to a DNA extension reaction, and subsequently exposed to N, N'-bis (2-(trimethylammonium iodide) propylene) perylene-3,4,9,10-tetracarboxyldiimide ( $\text{PDA}^+$ ), to which the negatively charged DNA strands could then electrostatically interact. Upon transferring this solution to an electrode, its prior attachment interactions with DNA prohibited  $\text{PDA}^+$  from binding to the electrode. This led to a detectable electrochemical shift for concentrations above 30 pM.<sup>[276]</sup> In another recent work, Lee *et al.* used porous AuNPs to further maximize the available surface area on these particles.<sup>[283]</sup> Using thiol-based immobilization, these particles were coated with a peroxidase-mimicking DNAzyme specific to a hemagglutinin protein associated with avian influenza virus, as depicted

in **Figure 3.1a**. This sensor achieved a limit of detection in the 1 pM range. Interestingly, thiol-based immobilization has also been used to deliver DNazymes into cells for biosensing. Wu *et al.* coated AuNPs with RNA-cleaving DNazymes responsive to uranyl ions to detect the presence of these carcinogenic entities within live cells, as shown in Figure 3.1b.<sup>[275]</sup> The thiol-based attachment showed both stability in serum and resistance to the cellular environment. Cleavage within a fluorophore-quencher substrate strand allowed for uranyl ion quantification through fluorescence.



**Figure 3.1. Immobilization of DNazymes onto biosensing components using thiol-based attachment.** (a) Hemagglutinin-responsive DNazymes immobilized onto porous AuNPs, which maximize available surface area for binding. Reprinted with permission from ref <sup>[283]</sup>. Copyright 2019 Elsevier. (b) Immobilization of thiolated DNazymes hybridized with fluorophore-quencher construct onto AuNPs for uranyl ions detection. Reprinted with permission from ref <sup>[275]</sup>. Copyright 2013 American Chemical Society. (c) Pb<sup>2+</sup>-responsive DNazymes hybridized with a quencher-containing fragment immobilized onto R-phycoerythrin using N-succinimidyl 3-(2-pyridyldithio) propionate (SPDP) as a crosslinking agent. Reprinted with permission under a

Ultimately, the primary advantage of this immobilization strategy is that no crosslinker needs to be introduced into the sensing platform. For many of the sensors outlined here, Au entities play an integral role in the sensing cascade, while providing the additional benefit of immobilization. Even when Au is solely implemented for immobilization, it proves to be easier to implement compared to chemical crosslinkers, which require substantial optimization. For fluorescence-based biosensors, AuNPs provide the added benefit of acting as a quencher, providing lower background fluorescence than organic quenchers.<sup>[298]</sup> That being said, Au integration into a biosensor can increase cost substantially. To this end, thiol-based immobilization has been induced through the use of N-succinimidyl 3-(2-pyridyldithio) propionate (SPDP) as a crosslinking agent. Wu *et al.* coated R-phycoerythrin – a naturally fluorescent protein isolated from red algae, with Pb<sup>2+</sup>-responsive, thiol-modified RNA-cleaving DNazymes hybridized to substrate strands containing a quencher, as shown in Figure 3.1c.<sup>[298]</sup> SPDP bonded the thiol group of the DNzyme and the amine group of R-phycoerythrin, resulting in a disulfide and an amide bond, respectively. Sulfosuccinimidyl-4-(N-maleimidomethyl)-cyclohexane-1-carboxylate (Sulfo-SMCC) has also been used for thiol-based DNzyme immobilization. Wen *et al.* used this crosslinker to immobilize DNazymes onto aminated mesoporous silica nanoparticles as its maleimide groups were able to bind to thiolated DNazymes through thioether linkages.<sup>[286]</sup>

### 3.3.1.2 Amine-based attachment

One of the most common DNzyme immobilization strategies involves the attachment of aminated DNazymes to functionalized surfaces. The covalent nature of this approach ensures robust immobilization. A variety of crosslinkers for amine attachment have been explored in the context of DNzyme-based biosensing, typically containing an aldehyde, ester or epoxy group that can react with amine modified oligonucleotides.



Surface functionalization with aldehyde groups can be induced through a range of different pathways. For macroscale surface treatments, induction of hydroxyl groups *via* oxygen plasma or piranha incubation and subsequent treatment with aminopropyltriethoxysilane (APTES) provides an excellent platform for glutaraldehyde immobilization.<sup>[299–302]</sup> Specifically, the amine group present on APTES can react with an aldehyde group on glutaraldehyde in a condensation reaction resulting in the formation of an imine group known as a Schiff base. The second aldehyde group on glutaraldehyde can then react with aminated oligonucleotides, resulting in immobilization. Wang *et al.* recently used this approach to immobilize a peroxidase mimicking DNAzyme-containing construct for the chemiluminescence detection of thrombin on glass.<sup>[299]</sup> For biosensors using heavily hydroxylated substrates, APTES deposition can readily take place on the substrate without any prior treatment. Notably, nanoporous alumina has been directly coated with APTES and then glutaraldehyde to immobilize Pb<sup>2+</sup>-responsive RNA-cleaving DNAzymes, leading to a biosensor that achieved a limit of detection of 12 nM using interferometric reflectance spectroscopy.<sup>[303]</sup> In the case of a substrate that is rich in amine groups, glutaraldehyde has also been successfully added directly as the sole crosslinking agent for DNAzyme immobilization. Specifically, Chen *et al.* immobilized a peroxidase mimicking DNAzyme onto eggshell membranes for chemiluminescence detection of hydrogen peroxide.<sup>[304]</sup> Other studies have relied on pre-purchased reagents such as aldehyde-terminated agarose microbeads and aldehyde-coated glass slides for DNAzyme-based detection of heme and Pb<sup>2+</sup>, respectively.<sup>[305,306]</sup>

Alternatively, surface functionalization with esters provides another means by which aminated DNAzymes can be immobilized. Most prominently, this pathway involves inducing carboxyl groups onto the surface and subsequent treatment with 1-ethyl-3-(3-dimethylaminopropyl) carbodiimide (EDC) and N-hydroxysuccinimide (NHS). The resultant NHS ester can then covalently bind with primary amine groups to form amide linkages. Such a strategy has been applied for DNAzyme immobilization in both electrochemical and chemiluminescence detection platforms for Pb<sup>2+</sup> detection.<sup>[307,308]</sup> Ye *et al.* demonstrated the applicability of this strategy by treating carboxylated Fe<sub>3</sub>O<sub>4</sub> magnetic spheres with EDC-NHS to

immobilize aminated DNAzymes.<sup>[309]</sup> The resultant electrochemical biosensor was capable of detecting prostate specific antigen to a limit of detection of 0.3 fg/mL.

DNAzyme immobilization onto single-walled carbon nanotubes (SWNTs) has been an area of active research given the improvement in detection sensitivity when using these entities for biosensing.<sup>[310]</sup> In this case, 1-pyrenebutanoic acid succinimidyl ester (PBASE) is used, given that its pyrene ring can form  $\pi$ - $\pi$  interactions with the SWNT bulk material.<sup>[310]</sup> Simultaneously, its ester group can be used to immobilize aminated DNAzymes. This strategy has been used for silver, mercury and copper ion DNAzyme-based detection thus far.<sup>[310,311]</sup> Bis(sulfosuccinimidyl) suberate (BS3) has also been used as a crosslinker for DNAzyme immobilization – specifically to glucose oxidase.<sup>[312]</sup> BS3 contains two NHS esters, which are separated by an eight-carbon chain, making it ideal for linkage between two aminated entities.

Epoxy-based immobilization typically involves using (3-Glycidyloxypropyl) trimethoxysilane as a crosslinker between a hydroxylated surface and the aminated DNAzyme. Such an approach has been used for immobilization onto hydroxylated magnetic beads for the detection of  $\text{Pb}^{2+}$  at picomolar and nanomolar concentrations through electrochemical and pH detection systems, respectively.<sup>[313,314]</sup> Pre-treated epoxy surfaces have also been used for the immobilization of DNAzymes for pathogen detection in food samples. By immobilizing bacterium-specific RNA-cleaving fluorescent DNAzymes on flexible substrates and attaching them onto food wraps, Yousefi *et al.* were able to create a platform that provided strong fluorescence signals in response to pathogenic contamination.<sup>[17]</sup>

Amine-based attachment is one of the most versatile immobilization methods, given its compatibility with all common signal transduction methods. The wide range of crosslinkers available means that sensing entities do not need to undergo significant modifications for attachment to any given substrate. The primary drawback of this strategy is in that it requires the introduction of an otherwise unnecessary reagent. Given the ultrasensitive nature of DNAzyme biosensors, any additional entity has the potential to interfere with the sensing cascade, resulting in reduced detection performance.

### 3.3.2 Non-covalent immobilization

#### 3.3.2.1 Biotin-based interactions

Avidin, NeutrAvidin, and streptavidin are three biotin-binding proteins that are often paired alongside biotin to immobilize biomolecules onto surfaces. With association constants in the range of  $10^{15} \text{ M}^{-1}$  the interaction between biotin and these three proteins represent some of the strongest non-covalent interactions present in nature.<sup>[315]</sup> Of the three, avidin exhibits the highest degree of non-specific absorption. This is attributed to its glycosylated nature, which results in an overall positive charge on the protein, resulting in interactions with the various negatively-charged entities present in sensing environments.<sup>[315]</sup> Streptavidin and NeutrAvidin both lack this glycoprotein portion, making them more suitable for biosensing applications. NeutrAvidin in particular exhibits the most neutral isoelectric point, resulting in the lowest degree of non-specific absorption.<sup>[316]</sup> Nonetheless, all three proteins are widely used to immobilize biomolecules. Biotin-based immobilization allows for easy implementation and compatibility within all common signal transduction methods. Additionally, the mild nature of this immobilization strategy makes it ideal for immobilization onto delicate substrates that are prone to damage.<sup>[272]</sup> Implementation is simple, given that DNazymes can be modified with a biotin molecule at either the 3' or 5' end of the functional oligonucleotide. That biotin can then bind to binding proteins immobilized on a surface.

The use of avidin within biosensing platforms is limited due to the aforementioned prominence of non-specific adhesion. Nevertheless, its ease of use has led to its incorporation within numerous sensing platforms. Specifically, avidin graphite-epoxy composites represent one of the most common avidin-containing substrates used for biomolecule immobilization. These composites can be prepared using dry chemistry strategies, which result in the facile incorporation of avidin onto the target substrate.<sup>[317]</sup> Such composites have been most notably used for the immobilization of biotinylated  $\text{Cu}^{2+}$ -responsive DNazymes.<sup>[318]</sup> Additionally, avidin-biotin interactions were used by Song *et al.* to aid in the immobilization of biotinylated DNazymes onto mesoporous silica nanoparticles.<sup>[319]</sup> An avidin-DNAzyme complex was formed between two biotinylated enzymatic DNAzyme strands and one avidin protein. The formation of this complex

resulted in the entrapment of fluorocein within the nanoparticles, giving the binding interaction a secondary function. Upon DNAzyme-induced cleavage of the substrate strand, the biotinylated enzymatic strand was displaced resulting in the release of fluorocein, but its avidin interactions were maintained due to their high affinity.<sup>[319]</sup>

While NeutrAvidin presents itself as an excellent alternative to avidin, its use within DNAzyme-based platforms is scarce. NeutrAvidin-coated substrates have been used to immobilize DNA probes, which validate their compatibility with oligonucleotides.<sup>[320]</sup> Its minimal use may be due to the limited commercial availability of diverse NeutrAvidin-coated substrates and bioconjugates. The abundance of streptavidin-coated substrates and bioconjugates has resulted in a significant volume of literature making use of this biotin-binding protein.

Streptavidin is easily and extensively physically absorbed by various substrates – such as those composed of poly(methyl methacrylate) (PMMA) or nitrocellulose.<sup>[272,321]</sup> For sensing platforms that require particle-based immobilization, streptavidin-coated magnetic and agarose beads are both readily available and have been successfully used in the development of DNAzyme-based biosensors.<sup>[284,322]</sup> For materials that cannot readily absorb streptavidin, numerous methods of streptavidin functionalization have been developed. Such approaches are instrumental within electrochemical detection systems, as the sensitivity and stability of such sensors rely heavily on the underlying substrate. In particular, substrates composed of two-dimensional nanomaterials have gained significant attention due to their beneficial physical and chemical properties. In a recent study by Ji *et al.*, tin dioxide-functionalized reduced graphene oxide, a two-dimensional nanomaterial with high electron mobility and surface area, was functionalized with APTES and AuNPs. Streptavidin was then able to bind to the AuNPs *via* amino-Au interactions.<sup>[323]</sup>

Likewise, nanotubes have also garnered significant interest for biosensing applications. Their electrical conductance changes considerably in response to variations in electrostatic charge and the absorption of molecular entities onto their surface, which makes them ideal for detecting ongoing reactions with high sensitivity. Yim *et al.* reported a strategy for immobilizing DNAzymes onto nanotubes using biotin-streptavidin interactions.<sup>[324]</sup> In their work, multi-walled carbon

nanotubes were acid-treated to induce carboxyl groups on the surface and then functionalized with streptavidin following EDC-NHS-mediated carboxyl activation.<sup>[324]</sup> Streptavidin was thus covalently attached onto the surface and used to immobilize biotinylated DNAzymes. Notably, the Michaelis-Menten kinetics of this system indicated that immobilization onto the nanotube-streptavidin structure did not hinder enzymatic activity in any way, further supporting the use of such constructs for future studies.<sup>[324]</sup>

Given streptavidin's four binding sites, biotin-streptavidin is also compatible with complex systems that require binding between multiple molecular entities. This property has been particularly advantageous within biosensors that work *via* an enzyme-linked aptamer assay. Gong *et al.* recently developed such a biosensor for tetracycline (TC), in which a surface was coated with TC conjugated with bovine serum albumin (BSA) and subsequently exposed to a biotinylated peroxidase-mimicking DNAzyme, a biotinylated aptamer specific to TC and free TC, which competed with immobilized TC for binding to the aptamer.<sup>[325]</sup> Streptavidin used two of its binding sites to act as a crosslinker between the two biotinylated molecules. Considering that the aptamer and DNAzyme are the target detector and signaling reaction catalyzer respectively within this system, this linkage was instrumental for the sensor's functionality.

Overall, biotin-based systems are highly effective and versatile for DNAzyme immobilization. However, given that avidin, NeutrAvidin and streptavidin are proteins, their structure and binding affinity may be affected by storage under non-refrigerated conditions. Assays performed in solutions that lead to protein denaturation or in the presence of proteases also stand to deteriorate biotin-based mediated immobilization. Alongside these constraints, this approach requires sensing entities to be labelled with biotin and/or biotin-binding proteins – labels that provide no benefit to the sensing platform outside of immobilization. An attempt to incorporate immobilization entities into other aspects of the sensing system to improve performance has been a key contributor to the preference for other immobilization strategies within biosensors.

### 3.3.2.2 DNA hybridization

Studies have used the hybridization capabilities of complementary DNA sequences to immobilize DNAszymes onto target substrates for decades.<sup>[326,327]</sup> This method overcomes the need to introduce crosslinking reagents, which may interfere with the sensing cascade, resulting in reduced detection sensitivity and accuracy. The basic premise for this method is the hybridization of a DNAszyme to a complementary substrate strand already immobilized on a given entity. Such a system allows for a greater degree of creativity within the sensing cascade as the pathway through which detection occurs following cleavage can be altered in a multitude of ways to maximize detection sensitivity. In fact, three different strategies that use post-cleavage products for detection have been developed.<sup>[297,328–330]</sup> Following target-induced activation of surface-immobilized DNAszymes, sensing has been performed by: (1) detecting the presence of the cleavage product; (2) probing the presence of the residually-attached DNAszyme fragment left behind on the surface following cleavage or; (3) through the subsequent addition of a subsequent oligonucleotide that may initiate a sensing cascade depending on if cleavage has occurred.

Xu *et al.* developed a  $\text{Cu}^{2+}$  sensor by coating a metal-organic framework possessing inherent peroxidase-like activity with substrate strands capable of hybridizing to a  $\text{Cu}^{2+}$ -responsive DNA-cleaving DNAszyme.<sup>[297]</sup> Upon exposure to  $\text{Cu}^{2+}$ , the substrate strand was cleaved by the DNAszyme, resulting in detachment between the two strands. The portion of the substrate strand attached to the organic framework was then free to bind to a complementary DNA strand present on an Au-modified electrode. The peroxidase-like activity of the now immobilized organic framework onto the Au-modified electrode could then output an electrochemical signal when engaging in a catalytic reaction with 3,3',5,5'-tetramethylbenzidine (TMB) and  $\text{H}_2\text{O}_2$ . The signal amplification provided by this platform allowed for a limit of detection of 0.457 nM.<sup>[297]</sup>



beads. The portion of the substrate strand residually attached to the bead then underwent a hybridization chain reaction with other oligonucleotides present in the system to create a long strand capable of capturing HRP. The captured HRP could then catalyze the oxidation of TMB in the presence of  $\text{H}_2\text{O}_2$ .<sup>[328]</sup>

Hybridization has specifically yielded biosensors with high sensitivity *via* the fragmentation of DNAzymes for signal amplification. Wu *et al.* used this principle as described in Figure 3.2b,<sup>[329]</sup> to design a sensing platform capable of detecting  $\text{Cu}^{2+}$  ions at concentrations as low as 2 nM. In this study a  $\text{Mg}^{2+}$ -responsive DNAzyme was fragmented into four segments, named A, B, D and E. Fragment A was bonded to a magnetic bead and attached to Fragment B *via* an azide-alkyne click chemistry reaction mediated by  $\text{Cu}^{2+}$ . This reaction was supported by a complementary assistant strand named Fragment C. Upon separation from Fragment C, Fragments A and B hybridized to Fragments D and E, respectively, resulting in the formation of a functional  $\text{Mg}^{2+}$ -responsive RNA-cleaving DNAzyme. When exposed to  $\text{Mg}^{2+}$ , this construct would effectively cleave a fluorophore-quencher DNA construct, leading to fluorescence output. Given that one  $\text{Mg}^{2+}$  DNAzyme can cleave multiple fluorophore-quencher constructs, the signal from one  $\text{Cu}^{2+}$  ion in the first step can induce substantial cleavage, thus allowing for a very low limit of detection.<sup>[329]</sup> In the absence of  $\text{Cu}^{2+}$ , Fragments A and B would be unable to bind, preventing the reaction from progressing.

Target-specific DNA aptamers can be used to immobilize highly catalytic DNAzymes onto surfaces, which creates a simple system for target-dependent release of the DNAzyme from the surface to the solution.<sup>[330]</sup> In the absence of the target, the aptamer hybridizes with the DNAzyme keeping it on the surface, but in the presence of the target, the aptamer preferentially binds the target and releases the DNAzyme. After separating the liquid and solid phases, the presence of the DNAzyme in the solution can be probed by adding a reporter substrate and monitoring signal generation. This approach was explored recently by Sun *et al.*, when they hybridized a peroxidase-mimicking DNAzyme to lysozyme-binding DNA aptamers immobilized onto carbon fibre composites for the detection of lysozymes<sup>[330]</sup> – a marker for mucosal immune competence,<sup>[331]</sup>



atherosclerosis<sup>[332]</sup> and certain categories of leukemia.<sup>[333]</sup> Their sensing system is shown in Figure 3.2c. Since lysozymes bind with high specificity to lysozyme aptamers, they would kick the DNAzymes off the aptamers. The released DNAzymes then coordinated with H<sub>2</sub>O<sub>2</sub> to mediate the oxidation of luminol present in the system, giving rise to chemiluminescence.<sup>[330]</sup> This approach is especially useful for the detection of targets for which no active DNAzymes have been identified.

What these studies collectively demonstrate is the multidimensional nature of this strategy. Its advantages go beyond simple immobilization, as it also provides a means by which the sensing pathway can be mediated, and by which signals can be amplified. The primary drawback of this approach is in its need for specificity, in that it cannot be implemented into any given platform as easily as a crosslinking reagent. Whereas crosslinkers can be applied universally through the incorporation of appropriate chemical modifications, hybridization requires the use of oligonucleotides, which are specific to a given sensing system. Thus, it is not easily adaptable into existing technologies. That being said, its use alongside electrochemical, chemiluminescent, fluorescent, and colorimetric detection platforms shows its versatility within different environments.

### 3.3.2.3 *Electrostatic interactions*

Aside from hybridization, electrostatic interactions reliant on the charge and hydrophobicity of sensing components have been employed for immobilization. For these systems, reduced graphene oxide (rGO) functions as an excellent base material, especially within electrochemical detection platforms due to its high electrochemical activity.<sup>[277]</sup> Single-stranded DNA can be spontaneously absorbed onto such GO substrates through  $\pi$ - $\pi$  stacking interactions.<sup>[277]</sup> While promising, these interactions typically do not retain sufficient DNA for biosensing applications. As a result, various surface modification techniques have been developed to increase DNA retention.

Inducing amino groups onto the sensing surface is one strategy reported in literature for improved DNA retention. Under this approach, positively charged ammonium groups on the surface can interact with the negatively charged phosphate backbone of oligonucleotides. Wang *et*

*al.* used this approach to immobilize  $\text{Pb}^{2+}$  and  $\text{Hg}^{2+}$  responsive RNA-cleaving DNAzymes.<sup>[277]</sup> Nitrogen plasma enhanced chemical vapour deposition was used to introduce amino groups onto a rGO-coated gold electrode. Raman spectroscopy confirmed that nitrogen groups were uniformly distributed across the rGO surface and that the chemical structure of rGO was not significantly altered by plasma treatment. DNAzymes were pre-hybridized with single-stranded DNA probes that would more readily interact with the amine groups on the substrate. Using electrochemical impedance spectroscopy (EIS), the resulting multiplex detection system achieved ultrasensitive limits of detection of 7.8 pM and 5.4 pM for  $\text{Pb}^{2+}$  and  $\text{Hg}^{2+}$ , respectively.<sup>[277]</sup>

A structural strategy that has been used for increased DNA retention involves using 3-dimensional (3D) rGO, as opposed to the conventional layered form. This results in an increased surface area-to-volume ratio and improved in-plane conductivity in the context of electrochemical detection.<sup>[279]</sup> While 3D-rGO has not yet been applied to the immobilization of DNAzymes, Wang *et al.* used this approach to increase the retention of aptamers for lysozyme detection.<sup>[279]</sup> This study paired 3D-rGO with plasma-polymerized polypyrrole (PPy), which has been used extensively to improve DNA absorption for biosensing applications. PPy is a positively charged conductive polymer that can form electrostatic interactions with negatively charged DNA entities.<sup>[279]</sup> The primary hinderance in its use is its poor electrochemical properties, which leads to a significant deterioration in the performance of resultant electrochemical biosensors. To circumvent this issue, nanostructured PPy has been introduced as a means by which the impact of the polymer can be reduced. In the context of the aforementioned study, 3D-rGO provided a substrate for the formation of such a nanoscale layer of PPy. Nanoporous silicon has also been used as a scaffold for PPy for the same purpose.<sup>[334]</sup> As an alternative to PPy, plasma-polymerized propargylamine (PpPG) has garnered interest for use in biosensing due to its improved electrochemical properties.<sup>[278]</sup> He *et al.* paired this polymer with graphene to create nanofilms to be used in sensing platforms for DNA targets. By further inducing amino groups on the surface, they achieved a limit of detection of 1.84 nM *via* EIS.<sup>[278]</sup>

Outside of electrochemical detection, Hui *et al.* used electrostatic interactions to immobilize fluorescently labelled aptamers onto a rGO-coated nitrocellulose membrane.<sup>[335]</sup> Introduction of the target led to aptamer dissociation and a resultant fluorescence signal. Further, the released aptamer then acted as a primer for rolling circle amplification, resulting in the formation of multiple peroxidase-mimicking DNAzymes capable of providing colorimetric output in the presence of H<sub>2</sub>O<sub>2</sub> and TMB.

While a viable immobilization method, electrostatic interaction-based immobilization has thus far been largely limited to electrochemical systems, with limited studies exploring its use alongside other transduction methods. As such, its use is both restricted, and its stability is questionable given its non-covalent nature. Additionally, while a proven method for the immobilization of DNA entities, its use with DNAzymes is limited. The displacement of immobilized DNAzymes by other molecules is one potential challenge with using electrostatic interactions for immobilization. In particular, complex samples may possess molecules with the ability to bind to the sensing surface through non-specific electrostatic interactions, reducing the concentration of DNAzymes on the surface. Nonetheless, under appropriate circumstances, this approach presents itself as an ideal candidate for further exploration.

#### 3.3.2.4 Physical entrapment

While largely unexplored, physical entrapment of DNAzymes has also been reported as a means of immobilization. In particular, Liu *et al.* developed a fluorescence biosensor for the detection of ultraviolet irradiation.<sup>[273]</sup> Polysaccharidepolynucleotide coacervate microdroplets (PCMs) consisting of diethylaminoethyl dextran chloride (DEAE-dextran) and double-stranded DNA were fabricated and homogeneously immobilized within a hydrogel. PCMs located at the input site of the hydrogel were loaded with titanium dioxide and silver NPs, which reduce dioxygen into H<sub>2</sub>O<sub>2</sub> in response to ultraviolet light. H<sub>2</sub>O<sub>2</sub> molecules then migrated to the output site of the hydrogel, where the microdroplets were loaded with Amplex Red and peroxidase-mimicking DNAzymes. Peroxidation of H<sub>2</sub>O<sub>2</sub> concurrently oxidized Amplex Red into resorufin, which emits a detectable fluorescent signal.<sup>[273]</sup> Other studies that have developed fluorescence biosensors

using physical entrapment for DNAzyme immobilization have relied on pullulan and various sol-gel matrices. While pullulan entrapment has not been explored extensively, studies have found that it provides entrapped DNAzymes with a protective environment that ensures maintenance of its catalytic properties. Pullulan entrapment has been used most notable for a fluorescence biosensor for *Klebsiella pneumoniae* – a multidrug-resistant pathogen.<sup>[336]</sup> Similarly, sol-gel strategies have also been minimally applied within DNAzyme-based biosensing platforms. The use of this approach has been reviewed elsewhere.<sup>[337]</sup>

In relation to electrochemical sensing, Gao *et al.* developed a biosensor for H<sub>2</sub>O<sub>2</sub> detection that relied on the physical absorption of peroxidase-mimicking DNAzymes onto the surface of an electrode and trapped these entities using polydopamine. By oxidizing dopamine diluted in phosphate buffered saline, polydopamine was formed, resulting in the immobilization of the DNAzymes onto the electrode's surface. The resultant biosensor exhibited a limit of detection of 2.2  $\mu$ M.<sup>[338]</sup>

Ultimately, the nature of physical entrapment makes it difficult to implement in most sensing platforms and its stability over time will be a challenge. The lack of existing literature using this strategy makes it difficult to characterize its effectiveness for DNAzyme immobilization.

### **3.4 DNAzyme Applications in Biosensing**

This section provides a review of the most common immobilized DNAzyme sensing applications for efficient analyte detection. Applications were selected to highlight the potential for DNAzymes in the context of their immobilization strategies. As detailed earlier and given the variety of molecular targets, DNAzymes can be applied to a range of systems, including food safety, environmental monitoring, and clinical diagnostics. As such, this analysis will focus mainly on active research in these areas within the past 5 years. Reviews discussing earlier studies can be found in literature.<sup>[339,340]</sup> Specifically, contaminant detection in food and biological settings, as well as heavy metal detection in a variety of settings will be explored. Recent work in developing DNAzymes for biomarker analysis in the context of clinical diagnostics, with a focus on protein and nucleic acid sensing, will then be detailed. Finally, we conclude with a summary of

applications in cancer research, which has seen the most progress in recent years. Further, existing literature on food contaminant, pathogen and metal ion detection are summarized in Table 3.2, while the detection of clinical and cancer biomarkers is summarized in Table 3.3.

### 3.4.1 Detection of contaminants within food

#### 3.4.1.1 *Escherichia coli*

Foodborne illnesses have a pronounced impact on human health worldwide, with hundreds of millions being affected annually.<sup>[1]</sup> Bacterial contaminants are largely to blame, meaning that developing strategies for rapid detection is paramount. *Escherichia coli* presents itself as one of the most common food contaminants, making it a focus in ongoing research. Recent studies have developed DNzyme-based biosensors for *E. coli* detection that communicate its presence through electrochemical, fluorescence and colorimetric means.

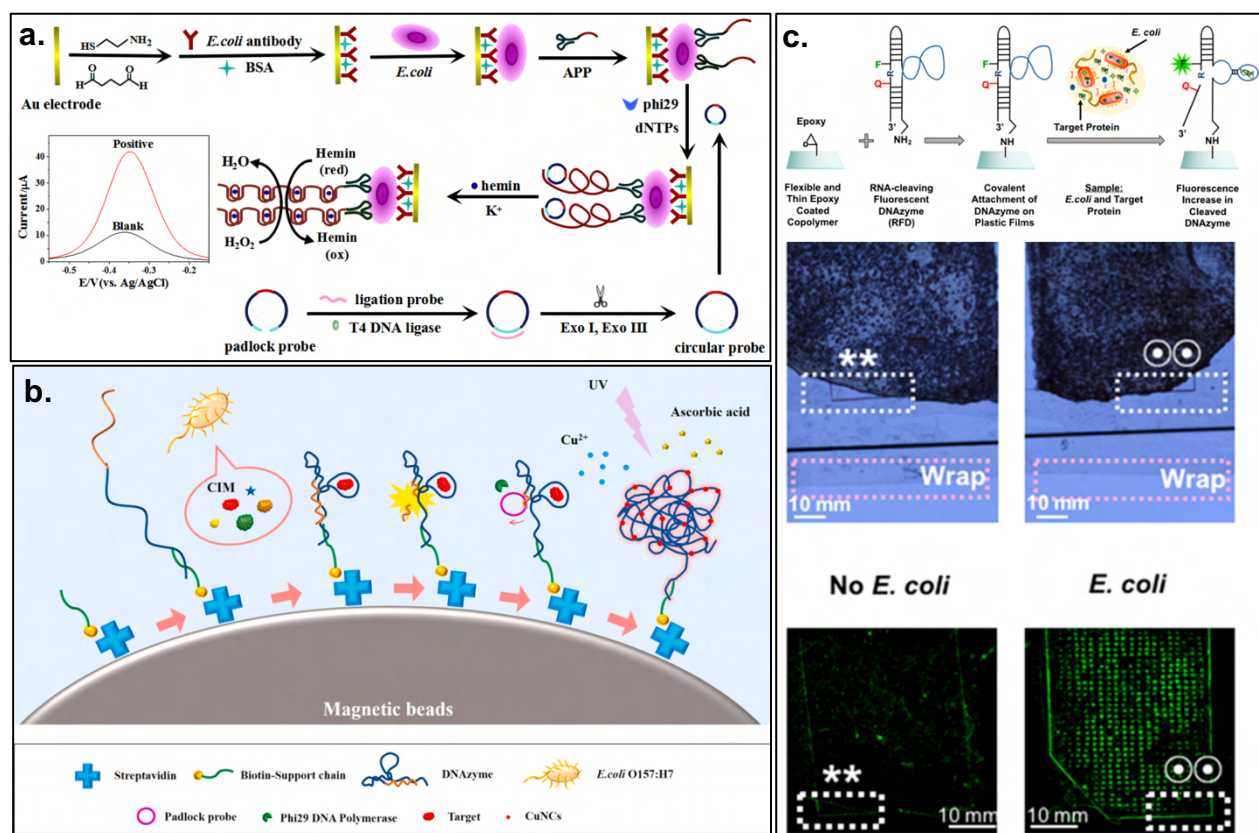


Figure 3.3. DNzyme-based sensors for the detection of *Escherichia coli*. (a) Antibody-mediated electrochemical sensing system for *E. coli* using rolling circle amplification for ultrasensitive limit of detection. Reprinted with permission from ref<sup>[341]</sup>. Copyright 2016 Elsevier.

(b) Ultrasensitive fluorescence detection system for *E. coli* O157:H7 involving rolling circle amplification . Reprinted with permission from ref. <sup>[342]</sup> Copyright 2020 Elsevier. (c) RNA-cleaving fluorescent DNAzyme sensor immobilized on flexible patch for on-package, real-time detection of *E. coli*. Associated images show sensor performance when in contact with spiked food samples. Reprinted with permission from ref <sup>[17]</sup>. Copyright 2018 American Chemical Society.

Guo *et al.* developed an electrochemical DNAzyme sensor for the detection of *E. coli* that used rolling circle amplification to achieve high sensitivity (**Figure 3.3a**).<sup>[341]</sup> Following antibody-mediated immobilization of *E. coli* onto a gold electrode, a primer-modified *E. coli*-specific aptamer was bonded to the bacterial cells. A plasmid containing a region complementary to the primer on the aptamer was then introduced. This plasmid also encoded sequences complementary to that of peroxidase-mimicking DNAzymes. The transcribed DNAzymes then became functional once complexed with hemin. The DNAzyme-mediated reduction of subsequently added H<sub>2</sub>O<sub>2</sub> gave rise to an electrochemical signal. The developed biosensor exhibited an ultrasensitive limit of detection of 8 CFU/mL, which presents strong real-world applicability when paired with its rapid test time.

In an effort to achieve such ultrasensitive detection limits within a fluorescence platform, Zhou *et al.* also used rolling circle amplification in the development of an *E. coli* biosensor, shown in Figure 3.3b.<sup>[342]</sup> *E. coli*-responsive RNA-cleaving DNAzymes were immobilized onto magnetic beads. Upon exposure to a target protein present in the crude intracellular matrix of this bacterial species, cleavage of RNA within the DNAzyme sequence freed a segment of DNA that acted as a primer for rolling circle amplification. The amplified sequence was T-rich, which resulted in the formation of copper nanoclusters in the presence of sodium ascorbate and copper sulfate. These nanoclusters have inherent fluorescence that enabled quantitative detection. This sensor showed an ultrasensitive limit of detection of 1.57 CFU/mL, and effectiveness within contaminated water and apple juice samples. That being said, the stability of this biosensor was not assessed within this study and remains the primary challenge in its incorporation onto food products. Nonetheless, both the aforementioned studies demonstrate the potential advantages rolling circle amplification

can provide. With a recent study uncovering that such amplification reactions proceed better on surface-immobilized systems compared to in-solution systems, further use of this strategy within immobilized DNAzyme biosensors is warranted for the development of alternatives to equipment-dependent lab analysis of food samples.<sup>[343]</sup> These systems however, still fail to address the need for real-time food monitoring. Widespread monitoring largely requires a greater focus on sensor stability – which the aforementioned studies did not evaluate. Contrarily, other studies have focused on developing simpler platforms that hold more potential for such widespread use.

Recognizing that package-integrated biosensors are the key to developing tangible solutions to real-time food contamination, Yousefi *et al.* used RNA-cleaving fluorescent DNAzymes for the detection of *E. coli* within food products, as depicted in Figure 3.3c.<sup>[17]</sup> *E. coli* responsive DNAzymes were covalently immobilized onto flexible polymeric surfaces that could be implemented onto food wraps. Upon bacterial exposure, cleavage within the fluorophore-quencher construct would lead to separation between the two components, resulting in a detectable fluorescence signal. This sensor showed the ability to detect the presence of *E. coli* within meat samples to a limit as low as  $10^3$  CFU/mL. While the sensitivity of this biosensor is lower than other existing platforms, the real-world applications of this system are particularly intriguing, given that its form factor as a patch on food packaging allows for individualized product screening in real-time without the need to open food samples. Tests on the developed biosensor involving variations in pH showed sustained performance irrespective of such an environmental change. However, variations in DNAzyme activity in response to temperature and fluorophore photobleaching are obstacles that need to be addressed to ensure reliable detection.

Circumventing stability issues associated with the use of traditional fluorophores, entities with inherent fluorescence properties have shown applicability within DNAzyme-based detection platforms, thus presenting an alternative. Namely, Zheng *et al.* used silver nanoclusters, which have controllable fluorescence properties and offer strong stability, fluorescence intensity and biocompatibility.<sup>[344]</sup> This study hybridized *E. coli*-responsive RNA-cleaving DNAzymes with a substrate strand containing acetylcholinesterase and immobilized this construct onto magnetic

beads. Upon target exposure, cleavage and subsequent release of acetylcholinesterase into solution allowed for its separation from the magnetic beads. Released acetylcholinesterase then mediated the hydrolysis of acetylthiocholine into thiocholine, the latter of which can enhance the fluorescence of DNA-templated silver nanoclusters added to the solution. While effective, this solution-based nature of the platform complicates its potential for on-package applications and the cost of such a system is unclear. Nonetheless, this study provides the foundation for further work involving the incorporation of silver nanoclusters within DNAzyme-based sensors for the detection of various pathogenic food contaminants.

#### 3.4.1.2 Other bacterial contaminants

The development of biosensors targeting pathogens other than *E. coli* is a very active area of research. Specifically, sensors relying on fluorescence-based detection represent a growing body of work. For example, Ma *et al.* developed a fluorescence-based biosensor for *Aeromonas hydrophila* – a highly pathogenic bacteria that is often present within food products.<sup>[345]</sup> The platform relied on a conventional RNA-cleaving fluorescent DNAzyme system in which target-induced cleavage of a fluorophore-quencher substrate by an *A. hydrophila*-responsive DNAzyme resulted in separation between the two entities, giving rise to a detectable fluorescence signal. Interestingly, the sensor provided a positive signal within ten minutes of target exposure when tested with contaminated milk and water samples, heavily supporting its potential for real-world applicability.

While undoubtedly a viable tool, fluorescence-based detection systems are limited by the need for imaging tools for food monitoring. Thus, sensors utilizing colorimetric signals for signal transduction largely occupy this space, as they allow for equipment-free monitoring at all stages of the food product pipeline. Colorimetric detection platforms for food pathogen detection largely rely on peroxidase-mimicking DNAzymes, which interact with hemin to yield defined optical changes. This design has been used in the development of sensors targeting a range of bacteria. Mondal *et al.* focused on the highly pathogenic enterotoxin B-harboring *Staphylococcus aureus*, developing a DNAzyme-based colorimetric sensor for its detection within food samples.<sup>[281]</sup> Upon



antibody-based immobilization and lysing of bacterial cells, the resulting media was exposed to a forward and reverse primers specific to the enterotoxin B gene. The forward primer was modified with a sequence complementary to the peroxidase-mimicking DNAzyme. Following PCR amplification, exposure to TMB and hemin in the presence of  $\text{H}_2\text{O}_2$  gave rise to a colorimetric change. The sensor demonstrated a limit of detection of  $10^2$  CFU/mL within spiked milk samples. Li *et al.* used a similar strategy for the detection of *Salmonella*, by integrating the sequence of a peroxidase-mimicking DNAzyme onto PCR primers.<sup>[282]</sup> While the primer initially formed a hairpin structure, DNA extension led to opening of the hairpin, allowing for interactions with hemin and TMB and subsequent colorimetric change. Lastly, Liu *et al.* used a collection of four target-specific primers that resulted in the formation of peroxidase-mimicking DNAzymes for the detection of *Listeria monocytogenes*.<sup>[346]</sup> This foodborne pathogen is known to give rise to listeriosis – a life-threatening condition associated with septicaemia and meningitis. This colorimetric sensor gave rise to an optical limit of detection of 47.5 CFU per reaction. While all three of these sensors present viable tools with strong applicability, the abundance of reagents in these systems make them unfeasible for package-integrated sensing, rather positioning their use as rapid, low cost alternatives to the laboratory testing of collected food samples.

In an attempt to achieve ultrasensitive colorimetric detection, Liu *et al.* used a split peroxidase-mimicking DNAzyme design for the detection of *Cronobacter sakazakii* – a foodborne pathogen that results in neurological or developmental disorders in 94% of infected patients.<sup>[347]</sup> In the absence of *C. sakazakii*, an aptamer specific to the bacterium combined the two halves of the split DNAzyme through complementary sequences present on the DNAzyme strands, giving rise to a functional DNAzyme. A colorimetric change was resultantly observed following the addition of hemin,  $\text{H}_2\text{O}_2$  and 2,20-azino-bis(3-ethylbenzthiazoline)-6-sulfonic acid. When the target was present, the aptamer preferentially bonded with the bacterium, meaning that the DNAzyme remained split. Thus, no colorimetric change was observed. This split system demonstrated a limit of detection of 1.2 CFU/mL. An aptamer-peroxidase-mimicking DNAzyme-pairing has also been used for the detection of *Vibrio parahaemolyticus* – a pathogen found in

seafood.<sup>[348]</sup> A *V. parahaemolyticus*-specific aptamer was used to induce competition between the bacterial target and DNazymes labelled with a sequence complementary to the aptamer. Preferential binding of the target resulted in the release of the DNzyme, leading to a colorimetric signal with a limit of detection of 10 CFU/mL. The ultrasensitive detection limits of aptamer-DNzyme paired systems indicate strong applicability within food contamination testing. The lack of aptamers available for specific bacterial targets limits the widespread use of this system, but with aptamer selection representing a rapidly growing field of work, such systems can be expected to grow in popularity.

Finally, while a resultant biosensor is yet to be developed, Rothenbrocker *et al.* recently identified and characterized an RNA-cleaving DNzyme specific to *Legionella pneumophila* – a lethal pathogen often responsible for outbreaks in water supplies.<sup>[349]</sup> The study demonstrated a limit of detection as low as 10 CFU/mL through denaturing polyacrylamide gel electrophoresis.

#### 3.4.1.3 Chemical contaminants

Alongside pathogenic contamination of food, there is growing concern regarding chemical entities, both naturally and due to human activities. Developing effective means for their detection is vital, given that many of these chemicals are known toxins, often with carcinogenic effects. Aflatoxins are of particular interest given their common presence within food samples. Naturally produced, these toxins are metabolites of *Aspergillus* fungi.<sup>[280]</sup> Aflatoxin B (AfB) is especially carcinogenic, making it a focus in research. Wang *et al.* and Setlem *et al.* both detailed strategies that involved using peroxidase-mimicking DNazymes for the colorimetric detection of AfB.<sup>[280,350]</sup> While Wang *et al.* used a split DNzyme design and competitive aptamer binding for the detection of the target, Setlem used a closed loop of blocking linker to inhibit DNzyme binding to an AfB aptamer. In this case, AfB binding to the aptamer led to the loop opening, and subsequent DNzyme attachment for colorimetric detection. Both sensors provided ultrasensitive limits of detection of 0.02 ng/mL and 22.6 parts per billion, respectively.

Similar to AfB, Ochratoxin A (OTA) is another metabolite of *Aspergillus* with significant toxic effects. Yu *et al.* used an exonuclease-mediated method for the detection of OTA, centered

upon the merging of an OTA aptamer and a peroxidase-mimicking DNAzyme sequence into one strand.<sup>[351]</sup> In the presence of OTA, its binding to the designed strand prevented exonuclease activity, allowing for subsequent hemin binding and colorimetric detection. In its absence, the strand was digested by the exonuclease, preventing any signal.

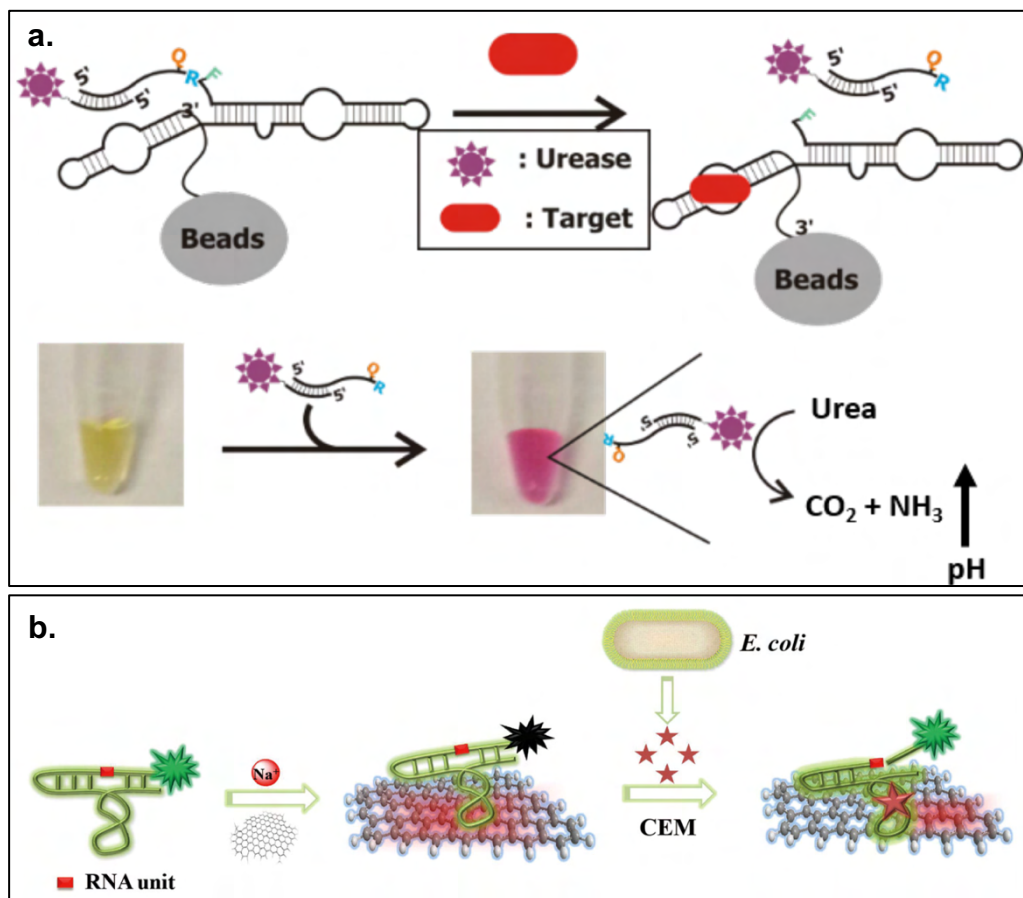
Outside of natural metabolites, human activity-related contaminants have been explored in recent years, especially with growing concerns surrounding antibiotic resistance. Tetracycline – a widely used antibiotic, has been found to be present within food products as a result of misuse.<sup>[325]</sup> Gong *et al.* developed a DNAzyme-based sensor for its detection and achieved a colorimetric limit of detection of  $8.1 \times 10^{-2}$  ng/mL in buffer.<sup>[325]</sup> Effectiveness within contaminated milk samples was also demonstrated.

### 3.4.2 Pathogen detection in biological samples

In addition to detection in food samples, and notwithstanding the recent COVID-19 pandemic, rapid, high-throughput, and sensitive detection of infectious pathogens in biological samples is critical to identify, diagnose, and isolate potential outbreaks. With the diversity of immobilization techniques previously described, it stands that the application of DNAzymes can thus be tailored to settings wherein traditional pathogenic detection tactics, such as selective enrichment and plating and polymerase chain reaction, may not be feasible. As well, in clinical settings where rapid results are often critical, such as in the diagnosis of acute sepsis, DNAzymes could provide both a rapid and precise alternative for routine detection. Within clinical detection, a variety of DNAzyme-based strategies have been proposed to overcome these challenges. In fact, DNAzymes have been employed to detect different strains of pathogenic bacteria, including *Klebsiella pneumoniae*,<sup>[336]</sup> *Clostridium difficile*,<sup>[352]</sup> and *Helicobacter pylori*.<sup>[284]</sup> In relation to *H. pylori* specifically, Ali *et al.* developed a colorimetric detection system for the pathogen (**Figure 3.4a**) and transferred the sensor onto a paper platform, providing a strong case for the use of such sensors as point-of-care systems. More recently peroxidase-mimicking DNAzymes, have been proposed as a potential mechanism for the detection of SARS-CoV-2.<sup>[353]</sup> It is certain that accurate sensing of pathogenic bacteria and viruses in clinical settings poses a particular challenge in

complex samples, such as blood, saliva, and urine, which are rife with other potentially cross-reactive biomolecules and other contaminants.<sup>[354]</sup>

While *in vitro* testing with purified samples has been met with early success, successful translation into clinical care – particularly for point-of-care detection, requires innovative strategies that can provide highly specific detection. In this regard, the robust nature of DNazymes, coupled with effective and stable immobilization approaches, make them particularly suitable for addressing these needs.



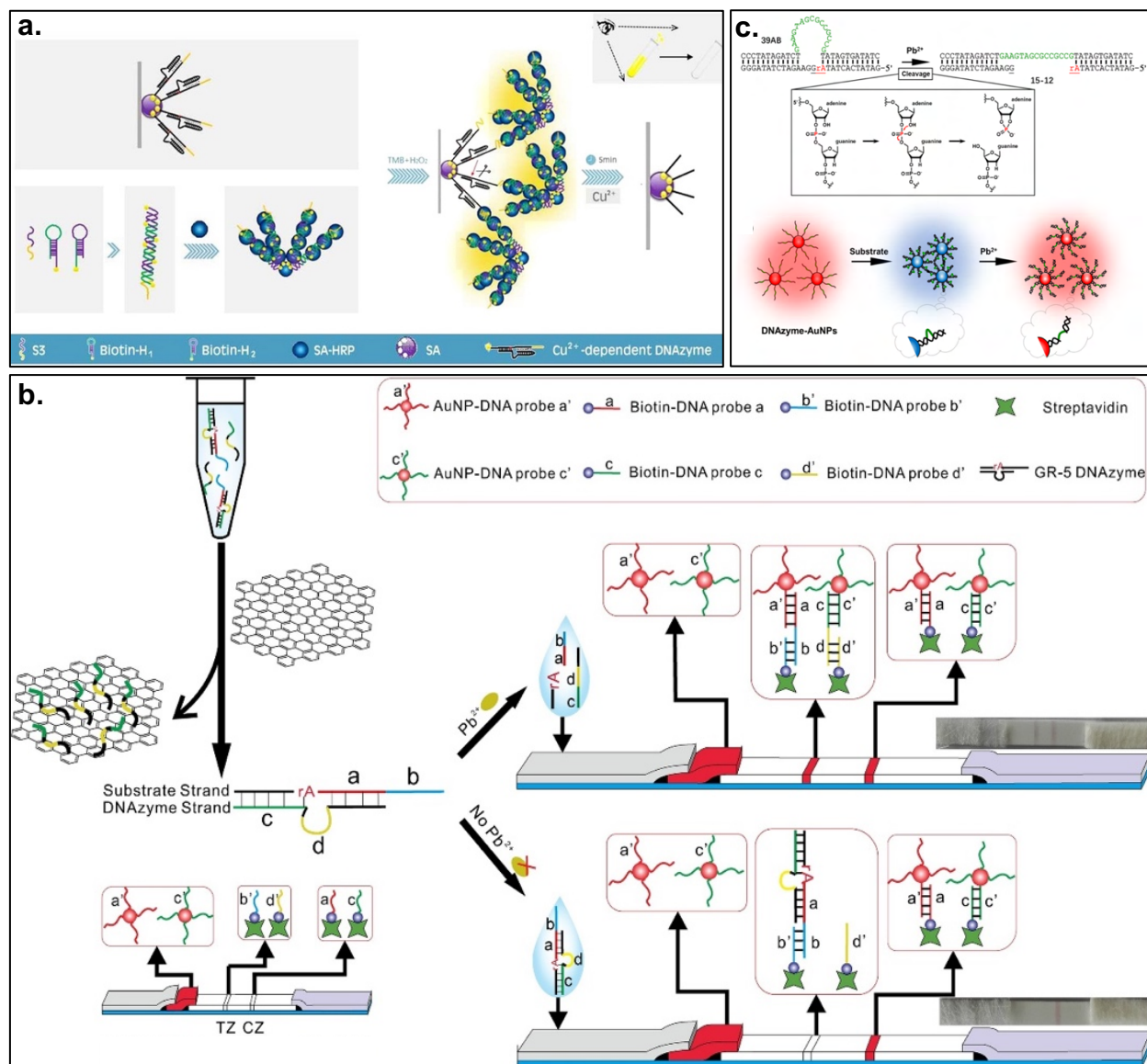
**Figure 3.4. Pathogen detection using immobilized DNazymes.** (a) Colorimetric detection of *H. pylori* through the immobilization and release of urease upon DNAzyme-induced cleavage. Reprinted with permission from ref <sup>[284]</sup>. Copyright 2019 John Wiley and Sons. (b) Fluorescence-based detection of *E. coli* using RNA-cleaving DNazymes immobilized on graphene through  $\pi$ - $\pi$  stacking interactions. Reprinted with permission from ref <sup>[224]</sup>. Copyright 2018 Springer Nature.

With the aim of detecting the avian influenza virus (H5N1), Lee *et al.* developed a sensor based on the application of a multifunctional DNA 3-way junction structure, consisting of a target recognition site, a peroxidase-mimicking DNAzyme, and thiol immobilization tether.<sup>[283]</sup> This DNA 3-way junction was then conjugated onto porous gold nanoparticles and layered onto Au electrodes *via* the thiol group. Detection of hemagglutinin protein, which makes up the viral envelope of avian influenza, was accomplished through binding and cyclic voltammetry measurements, with results demonstrating detection down to 1 pM. In another approach, Liu *et al.* applied a non-covalent immobilization technique to detect *E. coli*, as depicted in Figure 3.4b.<sup>[224]</sup> To simplify fabrication steps and avoid the need for lengthy and costly functionalization steps, immobilization of an *E. coli*-responsive RNA-cleaving DNAzyme was achieved using  $\pi$ - $\pi$  stacking interactions onto graphene. Before the introduction of *E. coli* into the system, a fluorophore-laden DNAzyme was non-covalently adsorbed onto the surface of the graphene, which quenched the signal of the fluorescent unit. However, when *E. coli* was introduced, directed cleavage occurred, which subsequently released the fluorophore from the graphene, resulting in fluorescence output. A limit of detection of 10<sup>5</sup> CFU/mL was achieved using this system, with demonstrated stability in blood indicating its potential for clinical translation. In addition to these approaches, an overview of recent studies investigating DNAzyme-based pathogen detection and their respective immobilization techniques is presented in Table 3.2.

### 3.4.3 Heavy metal detection within water and the environment

Heavy metals detection makes up a large body of DNAzyme-based biosensing research, due to the abundance of metal ion-responsive DNAzymes.<sup>[355]</sup> Equally, research demonstrating the link between heavy metals and cancer,<sup>[356]</sup> and corresponding environmental regulations<sup>[357]</sup> indicates a need for rapid and sensitive detection mechanisms. Given that detection of metal ions using DNAzymes has recently been reviewed extensively in the literature,<sup>[355,358–360]</sup> we focus this overview on immobilization strategies, innovative designs and applications for detection in environmental samples. Further, while many metal-ion-responsive DNAzymes are now available for biosensing studies, we will focus on three of the most studied analytes: copper, lead, and

mercury ions. A comprehensive list of metal detection approaches – largely in environmental settings, is presented in Table 3.2.



**Figure 3.5. Metal ion detection using DNzyme-based biosensing platforms.** (a) A hybridization chain reaction-based horseradish peroxidase concatemer sensing system for  $\text{Cu}^{2+}$  detection. Reprinted with permission under a Creative Commons CC-BY license from ref [362]. Copyright 2017 Springer Nature. (b) A nanoparticle-based lateral flow test strip for  $\text{Pb}^{2+}$  detection. Reprinted with permission from ref [363]. Copyright 2018 Elsevier. (c) Gold nanoparticles for plasmonic detection of  $\text{Pb}^{2+}$  ions. Reprinted with permission from ref [364]. Copyright 2020 American Chemical Society.

While copper is an essential nutrient with established daily recommended intake levels, acute and chronic copper exposure has resulted in changes in liver function, gastrointestinal symptoms, nausea, and even death.<sup>[361]</sup> Thus, copper (II) ion ( $\text{Cu}^{2+}$ ) detection is important to test for potential water contamination. While traditional approaches to  $\text{Cu}^{2+}$  detection, such as inductively coupled plasma mass spectrometry and atomic absorption spectroscopy, offer low detection limits and high specificity, both techniques require specialized equipment and trained personnel. The lack of portability and high cost are the driving factors for innovative approaches for rapid and on-site high throughput sensing and accurate monitoring. With this in mind, the application and versatility of DNAzymes to detect heavy metal ions, such as  $\text{Cu}^{2+}$ , has great potential to address these issues. For example, Zu *et al.* developed a “turn-off” sensing system based on the immobilization of a  $\text{Cu}^{2+}$ -dependant DNA-cleaving DNAzyme by biotin-streptavidin conjugation onto a polystyrene 96-well plate.<sup>[362]</sup> For detection, streptavidin-horseradish peroxidase was introduced, resulting in hybridization chain reactions with designer DNA hairpins and an initiator, which then complexed with the immobilized DNAzyme. Without  $\text{Cu}^{2+}$  the entire complex would remain in the well yielding a characteristic colorimetric reaction, while upon addition of  $\text{Cu}^{2+}$ , the complex was cleaved and washed away, as shown in **Figure 3.5a**.

In another approach, presented in Figure 3.2b, Wu *et al.* presented a  $\text{Cu}^{2+}$  sensing strategy developed around the concept of combining click chemistry with fluorescence.<sup>[329]</sup> Briefly, immobilization of a DNAzyme subunit was achieved using EDC to link -COOH magnetic beads with an  $\text{NH}_2$ -oligomer. This was followed by the hybridization of specific sequences to form a double-stranded oligomer complex. These sequences were tailored in such a way that in the presence of  $\text{Cu}^{2+}$  and sodium ascorbate, a cycloaddition reaction resulted in the formation of a triazole ring ligated complex. Upon temperature cycling, the two strands were separated and then  $\text{Mg}^{2+}$  reactive RNA-cleaving DNAzyme assembly was initiated using the triazole ring strand. Detection was carried out in the presence of  $\text{Mg}^{2+}$  by the formed DNAzyme, which catalyzed the cleavage of a reporter substrate molecule tethered to a fluorescent probe. In this way, fluorescence intensity could be related to the presence of  $\text{Cu}^{2+}$ , with a detection limit of 2 nM.

Concurrently, lead pollution is one of the most widespread and concerning forms of environmental contamination, with severe effects demonstrated on multiple organ systems.<sup>[365]</sup> Most sources of lead poisoning originate from petroleum, batteries, and other chemical industries, commonly leaching into waterways and soil to subsequently be introduced into the food chain. While many robust  $\text{Pb}^{2+}$  detection approaches have been in use for decades, most techniques still suffer from a lack of portability and sensitivity for rapid detection. The application of DNAzymes offers high specificity, with the potential for ultra-sensitive detection given that  $\text{Pb}^{2+}$  can serve as a powerful co-factor for enzymatic catalysis.

While DNAzyme/ $\text{Pb}^{2+}$  specificity itself is well established,<sup>[366]</sup> as with all DNAzyme platforms, the critical components for robust detection is the selection of a signal amplifier, immobilization strategy, and sample handling platform. With this in mind, Wang *et al.* demonstrated the application of GR-5 (a  $\text{Pb}^{2+}$ -dependent RNA-cleaving DNAzyme), coupled with a lateral flow test system and graphene oxide as a mechanism to remove unhybridized DNA from the test solution.<sup>[363]</sup> As shown in Figure 3.5b, the lateral flow test strip was prepared by immobilizing two gold nanoparticle-DNA probes with specificity toward cleaved and un-cleaved DNA strands. Ultimately, in the presence of  $\text{Pb}^{2+}$  and successful hybridization to the appropriate gold nanoparticle-DNA probes, the test strip would yield colorimetric detection in both the test and control strips, with reported  $\text{Pb}^{2+}$  recognition down to 0.05 nM. While this scheme employs a graphene oxide-based pre-treatment step with the need for a centrifuge, through the development of strategic sorting, DNAzyme-based lateral flow detection platforms could be a particular area of expansion given that they typically require little in the way of instrumentation, trained labor, and can be conducted on-site.

In another approach, Diao *et al.* developed a highly sensitive DNAzyme-based mechanism for  $\text{Pb}^{2+}$  detection using a “turn-on” strategy, as depicted in Figure 3.5c.<sup>[364]</sup> Briefly, the system consisted of a thiolated  $\text{Pb}^{2+}$ -dependent DNAzyme bonded to gold nanoparticles, which were subjected to hybridization of the substrate strand. Thus, when hybridization occurred, base stacking caused the nanoparticles to aggregate, which in turn decreased their localized surface



plasmon resonance (LSPR). However, when  $\text{Pb}^{2+}$  was introduced into the system, the substrate was cleaved, disassembling the stacking and increasing LSPR. Overall, these two systems demonstrate the potential for  $\text{Pb}^{2+}$  detection using DNAzyme-centered strategies with flexibility in terms of design and system optimization.

In another vein, mercuric ions ( $\text{Hg}^{2+}$ ) are another environmentally pervasive heavy metal contaminant, with well-characterized toxicity at both the acute and chronic exposure levels.<sup>[367]</sup> While  $\text{Hg}^{2+}$  detection *via* DNAzymes is notably less common than  $\text{Pb}^{2+}$ , several nanomaterial, chemical, and hydrogen bonding techniques are described in the literature,<sup>[368]</sup> with approaches ranging from peroxidase-mimicking DNAzymes,<sup>[369]</sup> to strategies coordinating with graphene oxide,<sup>[370]</sup> and incorporation into hydrogel systems.<sup>[274]</sup> The system developed by Yun *et al.* is particularly notable given that the strategy is based on an RNA-cleaving DNAzyme motor.<sup>[371]</sup> Specifically,  $\text{Hg}^{2+}$  sensing was achieved by integrating thiolated DNA probes onto the surface of AuNPs. With this tethered system, quenching of the fluorophore was achieved, while the introduction of  $\text{Hg}^{2+}$  resulted in cleavage and fluorescent detection down to 30 pM.

#### **3.4.4 Detection of clinically relevant biomarkers**

Applications in the field of medical diagnostics and monitoring is a major area of DNAzyme research and advancement.<sup>[358,372]</sup> The potential for miniaturization in point-of-care devices, rapid results, and high sensitivity and target selectivity enable the translation of technologies from the bench to the bedside. While nearly any illness or disease state with defined biomarkers, be they nucleic acids, proteins, or other small molecules, has the potential for DNAzyme-based diagnostics, this section presents recent advances in protein-based biomolecule detection, followed by a discussion of DNA and microRNA detection, with a brief overview of cardiovascular marker sensing. Applications specifically in cancer detection are presented subsequently. Generally, two types of DNAzymes are widely applied in biomarker detection: RNA-cleaving DNAzymes, which are primarily used as the recognition elements, and peroxidase-mimicking DNAzymes, which function exclusively as reporter molecules because of their ability

to coordinate with hemin to oxidize particular substrates, yielding a colorimetric or chemiluminescent signal in the presence of  $\text{H}_2\text{O}_2$ .

As detailed in Table 3.3, several protein-based biomarkers have been investigated for detection *via* DNazymes, including alpha-fetoprotein,<sup>[373]</sup> lysozyme,<sup>[330]</sup> and prions.<sup>[374]</sup> In most of these systems, peroxidase-mimicking DNazymes are exploited in an analogous method to how horseradish peroxidase is utilized as an enzyme label in ELISAs. In other words, peroxidase-mimicking DNazymes confer catalytic conversion of a particular substrate, such as TMB, 2,2'-azino-bis(3-ethylbenzothiazoline-6-sulfonic acid) (ABTS) or luminol in the presence of a metal ion ( $\text{Pb}^{2+}$ ,  $\text{NH}_4^+$ ,  $\text{K}^+$ ) and  $\text{H}_2\text{O}_2$ , which then generates a signal for detection and subsequent quantification.<sup>[375]</sup>

By and large, these peroxidase-mimicking DNazymes exhibit lower activity compared to their protein counterparts.<sup>[376]</sup> However, these oligonucleotides offer several advantages that justify their use in such applications. Specifically, the structural stability of these enzymes in a wide range of chemical and thermal environments is enhanced compared to protein-based enzymes. The ease of manufacturing through chemical synthesis and polymerase chain reaction is generally preferred over more complicated protein synthesis techniques – a particular advantage in biosensing applications that could involve several complex fabrication steps.

A system developed by Chen *et al.* for the detection of thrombin is a prime example of the peroxidase-mimicking DNzyme approach.<sup>[377]</sup> Briefly, Au-coated octahedral  $\text{Cu}_2\text{O}$  nanocrystals were functionalized with aminated thrombin binding aptamers (TBAs). These nanocrystals functioned primarily as signal amplifiers. A gold-coated electrode was similarly functionalized with TBAs. When present, thrombin acted as a binding agent between the nanocrystals and the electrode *via* interactions with TBA. Interestingly, thrombin binding triggered a conformational change within TBA, resulting in the adaptation of a G-quadruplex structure. Subsequent attachment of hemin gave rise to a peroxidase-mimicking DNzyme, which, in this case, was used for the electrochemical detection of the target to an ultrasensitive limit of detection of 23 fM.

Detection of nucleic acids is also widely applicable to various fields: environment, agricultural, forensic, and as detailed in this section, markers for clinical diagnostics. In this regard, recent drives towards personalized medicine and pharmacogenetics mean that rapid detection of, for example, genetic variants, could result in rapid assessment of a patient's potential response to a particular treatment based on their genotype. While next-generation sequencing has made significant strides towards this reality, costs, time and labor associated with even the simplest of sequencing procedures make such activities challenging to execute in many clinical settings. DNAzymes are thus poised to offer a rapid alternative with high specificity when incorporated into point-of-care devices.

For example, Azuake-Hualde *et al.* demonstrated the application of a paper-based device for the detection of single-stranded DNA using physical entrapment within wax-printed circles.<sup>[287]</sup> Specifically, they demonstrated DNAzyme-based detection of a synthetic fragment of the Y amelogenin gene – a model for the detection of genetic variations. The system achieved precise colorimetric detection, showcased through its ability to distinguish between the target and a control that only differed by six base pairs. Interestingly, this methodology allowed for a visual detection limit of 143 ng. With a mobile phone camera, the limit of detection was reduced to 37 ng. The ultrasensitive capabilities of this sensing platform indicate great potential for use within real-world enabled sensors.

In another approach, a fluorescence-based system was devised for microRNA detection with potential for the detection of single nucleotide polymorphisms in clinical and biomedical research.<sup>[378]</sup> In this work, miRNA let-7, a potential marker for stroke,<sup>[379]</sup> cardiomyopathy,<sup>[380]</sup> traumatic brain injury,<sup>[381]</sup> and various cancers,<sup>[382,383]</sup> was used as an analyte in a system that combined a peroxidase-mimicking DNAzyme with an RNA-cleaving DNAzyme. In this method, thiolated DNA probes, with a recognition site for a  $Mg^{2+}$ -dependant RNA-cleaving DNAzyme and a region capable of complexing with  $K^+$  and hemin to form the peroxidase-mimicking DNAzyme, were immobilized onto a Au-coated electrode. In the presence of the target miRNA, a suite of non-immobilized hairpin structures would assemble to produce the RNA-cleaving DNAzyme, which

could then cleave the immobilized probe at the recognition site, thus releasing a portion of the probe to form the peroxidase-mimicking DNAzyme required for electrochemical sensing. The limit of detection was 0.46 fM in pure buffer and 10 pM in diluted human serum.

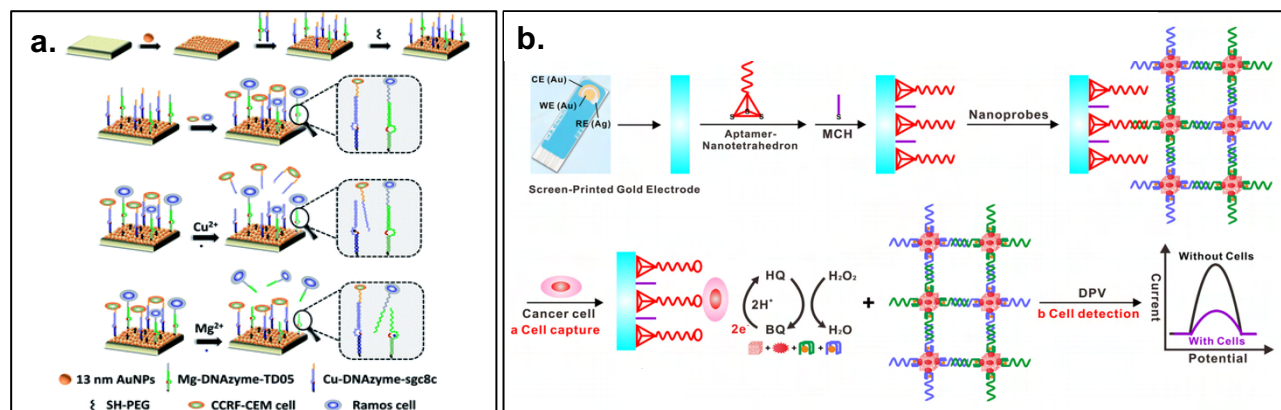
Cardiovascular biomarkers similarly play a significant role in diagnostics and patient monitoring in both acute and chronic vascular diseases. One such marker, cardiac troponin I, validated as a marker for myocardial tissue damage, has been studied extensively with a variety of immobilization strategies.<sup>[288,384,385]</sup> For example, an oligonucleotide aptamer-based sensor was developed based on a sandwich-type assay, wherein a DNA nanotetrahedron structure with a cardiac troponin aptamer serving as the capture molecule, was thiolated to a gold electrode.<sup>[384]</sup> This was coupled with the application of multifunctional nanoparticles complexed with a peroxidase-mimicking DNAzyme and horseradish peroxidase. This electrochemical sensing system demonstrated a limit of detection of 7.5 pg/mL, which was on the order of clinically relevant values for damaged myocardium. Another vascular-related biomarker is thrombin, a serine protease that engages in various, typically pro-inflammatory, activities and is used clinically to diagnose thrombosis and other clot-related disorders. The application of peroxidase-mimicking DNAzymes in biosensing systems has also shown significant potential in the pursuit of ultrasensitive and rapid thrombin detection.<sup>[377,386–389]</sup> Recently, a magnetic composite based on the application of a  $\text{Pb}^{2+}$ -dependant RNA-cleaving DNAzyme showed detection of thrombin at 1.8 pM.<sup>[386]</sup> This system was based on the immobilization of a DNA substrate onto  $\text{Fe}_3\text{O}_4@\text{Au}$  nanoparticles. The substrate contained a cleavage site-specific to  $\text{Pb}^{2+}$ -dependant RNA-cleaving DNAzymes, while also exhibiting complementarity to a thrombin-specific aptamer. In the absence of thrombin, the aptamer would be bonded to the immobilized substrate strand, preventing DNAzyme-mediated cleavage. However, in the presence of thrombin, the aptamer would preferentially bind to thrombin, leaving the immobilized substrate exposed, allowing for its cleavage. The subsequent addition of methylene blue – which binds to DNA molecules, quantified the presence of thrombin, given that the amount of methylene blue directly correlated to the length of DNA present.

### 3.4.5 Detection of cancer markers

To successfully improve cancer survival rates, better diagnostic tools capable of early stage detection are necessary. Traditional approaches for cancer detection – such as tumor biopsies, are limiting and their effectiveness is influenced by tumor size and location. Alternative approaches such as liquid biopsies may provide a solution.<sup>[390]</sup> To this end, DNazymes have been proposed as valuable tools to analyze tumor biomarkers in liquid biopsies for the detection of clinically relevant targets, including exosomes,<sup>[391]</sup> circulating tumor cells (CTCs),<sup>[392]</sup> circulating tumor DNA,<sup>[393]</sup> and microRNA (miRNA).<sup>[394]</sup> For the purpose of this review, we focus on three target categories most widely studied in DNzyme systems: CTCs, intracellular markers, and miRNA. A list of DNzyme-based cancer detection strategies is presented in Table 3.3 to complement this discussion.

CTCs are shed from primary or metastatic tumors and circulate in the blood.<sup>[395]</sup> They carry proteins, DNA, and RNA associated with the tumor of origin and can be used as biomarkers in liquid biopsies. However, given that their concentrations typically remain low relative to other cells, there is a pressing need for the development of technologies capable of highly specific capture and detection of CTCs. DNzyme-based platforms can be engineered with various isolation strategies to overcome these limitations.

Although not yet incorporated into a detection strategy, Zhang *et al.* designed a platform to capture and selectively release multiple CTCs using DNazymes, as shown in **Figure 3.6a**.<sup>[392]</sup> This design utilized two aptamers coupled with  $Mg^{2+}$  and  $Cu^{2+}$ -dependent RNA-cleaving DNazymes to select for two distinct cell types (CCRF-CEM and Ramos). The thiolated DNazymes were immobilized onto a substrate covered with AuNPs. Upon capture, cellular release was initiated *via* the introduction of  $Mg^{2+}$  or  $Cu^{2+}$  for selective CTC enrichment. Results using blood samples from lung cancer patients indicated that the platform could be adapted for clinical use. Sun *et al.* also developed a CTC capture and release platform, with their sensor capable of detecting HepG2 cells associated with liver cancer (Figure 3.6b).<sup>[396]</sup>



**Figure 3.6. Detection of circulating tumor cells using immobilized DNazymes.** (a) DNAzyme-based platform for the capture and release of circulating tumor cells. Reprinted with permission under a Creative Commons Attribution 3.0 unported license from ref <sup>[392]</sup>. Copyright 2020 Royal Society of Chemistry. (b) Target cancer cells compete with nanocages to bind to nanotetrahedron-aptamer probes, triggering release from screen-printed gold electrodes. Reprinted with permission from ref <sup>[396]</sup>. Copyright 2018 Elsevier.

This method relied on the immobilization of DNA nanotetrahedron structures containing HepG2-specific aptamers onto the surface of screen-printed gold electrodes *via* thiol-based chemistry. Palladium-platinum nanocage-based structures incorporating horseradish peroxidase and peroxidase-mimicking DNazymes were then hybridized onto the nanotetrahedrons. When present, target cancer cells outcompeted the nanocage structures for nanotetrahedron binding. This led to their release from the surface, allowing them to engage in an oxidation reaction that transduced signals *via* differential pulse voltammetry. The system demonstrated a detection limit of 5 cells/mL. Cellular release was also demonstrated by breaking Au-S bonds through the application of negative potential, with minor losses in cellular viability.

In another vein, telomeres have garnered significant interest as cancer cells exhibit increased telomerase activity relative to healthy cells,<sup>[397]</sup> which has led to the development of platforms that use this property for diagnostic purposes.<sup>[398,399]</sup> While there are many approaches to telomerase detection, DNAzyme-based strategies provide avenues for both ultrasensitive and *in situ* detection.<sup>[400]</sup> For example, Xu *et al.* developed a sensor capable of imaging telomerase

activity through a DNAzyme motor consisting of gold nanoparticles functionalized with thiolated  $Mn^{2+}$ -dependent, RNA-cleaving DNAzymes.<sup>[401]</sup> Using a locking strand method, fluorescence signals were quenched owing to their proximity to gold. However, in the presence of telomerase, DNAzyme activity was initiated, yielding cleavage of the fluorescent tag, which could be detected *via* confocal imaging. This sensor was successfully translated to use within live cells. Notably, this approach utilized the inherent function of telomerase, incorporating a telomerase substrate (TS) onto the gold surface to yield a functional DNAzyme in the presence of telomerase.

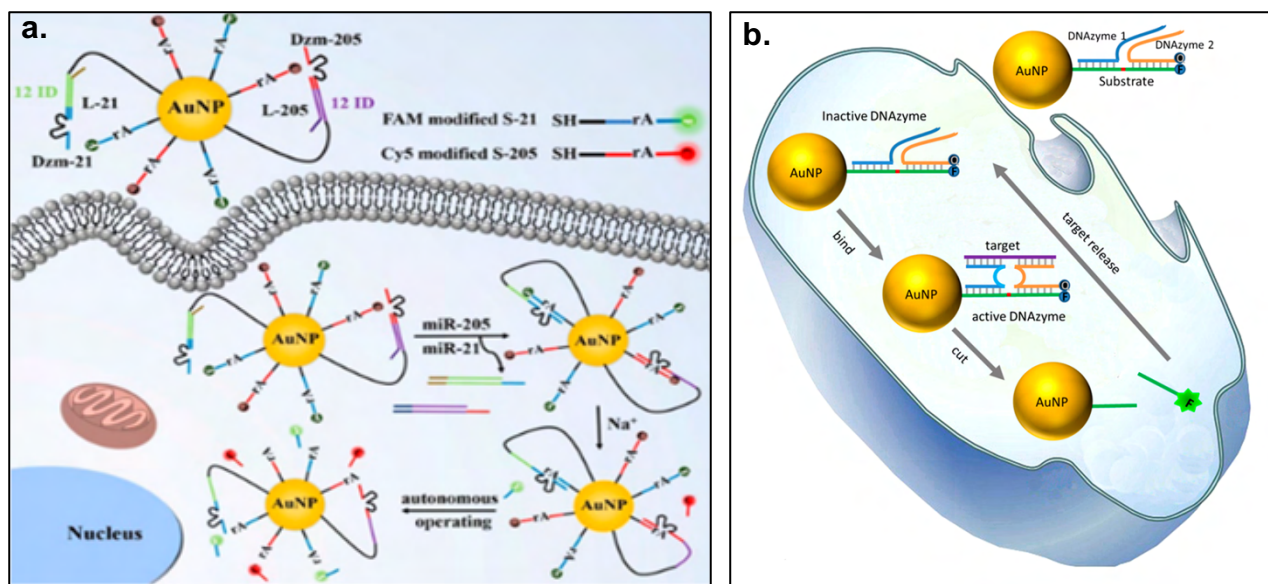
Wang *et al.* similarly exploited the innate function of telomerase using magnetic beads with a TS.<sup>[402]</sup> An amine-aldehyde reaction achieved immobilization of TS onto the magnetic beads. In the presence of telomerase, the strategic addition of TTAGGG resulted in G-rich sequences that could form peroxidase-mimicking DNAzymes in the presence of  $K^+$  and hemin. Telomerase activity in HeLa cells could be detected down to a concentration of 0.5 cells/ $\mu$ L using a UV-vis spectrometer and 1 cell/ $\mu$ L with the naked eye. As evidenced by these strategies, the nature of DNAzymes paired with telomerase activity are suited for the screening of cancerous cells.

Finally, given recent developments in the use of miRNAs as clinical biomarkers, it follows that methods for their detection, particularly in cancer, are needed.<sup>[403]</sup> An investigation of several DNAzyme-based approaches for miRNA-driven cancer detection has been recently been conducted.<sup>[404]</sup> For an in-depth analysis of DNAzyme approaches for miRNA detection overall, the reader is directed to a recent review by Mahdiannasser *et al.*<sup>[405]</sup> However, we highlight a few cancer-based applications herein.

Chen *et al.* developed a system for the intracellular detection of miRNA-21 and miRNA-205 in A549 and H520 lung cancer cells.<sup>[406]</sup> As depicted in **Figure 3.7a**, their system was based on a DNAzyme motor, which consisted of AuNPs coated with both  $Na^{2+}$ -dependant RNA-cleaving DNAzymes hybridized to locking strands preventing their activity and fluorophore-conjugated substrate strands specific to each DNAzyme. In the presence of target miRNA, the locking strands preferentially hybridized to the target strand, allowing the DNAzymes to interact with their corresponding substrate strands. Cleavage of the substrate strands would then result in the release

of the fluorophores off the AuNPs. The dependence of DNAzyme activity on a  $\text{Na}^{2+}$  cofactor is of particular note given the ubiquity of  $\text{Na}^{2+}$  in cells, which enabled the system to progress *in Vitro* without any additional components. In addition, miRNA-21 is tied to many other cancers, including gastric, prostate, breast, and neuroblastoma, further expanding applications beyond lung cancer.<sup>[407]</sup>

In another approach to miRNA-21 detection, Wu *et al.* engineered a thiolated split-DNAzyme probe, which was conjugated to AuNPs (Figure 3.7b).<sup>[408]</sup> This split probe formed active RNA-cleaving DNAzymes in the presence of the target miRNA, which resulted in cleavage from the AuNP and activation of the fluorophore. Without the target miRNA, the DNAzyme would remain in an inactive form, leaving the fluorophore in a quenched state. Results showed promising evidence for accurate miRNA imaging in live cells, with applications in fundamental research and cancer diagnostics.



**Figure 3.7. MicroRNA detection using immobilized DNAzyme-based platforms.** (a) A platform of miRNA-initiated and intracellular sodium fueled DNAzyme-probes to differentiate lung cancer cell subtypes. Reprinted with permissions from ref. <sup>[406]</sup>. Copyright 2020 American Chemical Society. (b) DNAzymes conjugated to gold nanoparticles for intracellular miRNA detection. Reprinted with permissions from ref. <sup>[408]</sup>. Copyright 2017 American Chemical Society.



### 3.5 Future Directions

This review aimed to provide an overview of current immobilization techniques and biosensing applications of DNazymes, with an emphasis on recent developments in the detection of food contamination, pathogens, metal ions, and clinical biomarkers. Given the magnitude of research in this space, rapid advancements can be anticipated in the sensitivity, specificity, and feasibility of DNzyme-based biosensors for real-world applications. These developments can be expected to coincide with improvements in functionalization and immobilization strategies. Given the advantages of DNazymes, including stability across a variety of environmental conditions and ease of synthesis, particularly compared to protein enzymes, we anticipate that the diversity and translational capabilities of these technologies will continue into the future. [375]

While many of the discussed immobilization strategies have been well established for quite some time, recent studies have aimed to compare their effectiveness in immobilizing DNA under various conditions.[201] Such studies will continue to better our understanding of the compatibility of different strategies for particular sensing systems. Contrarily, strategies such as physical entrapment and graphene-mediated electrostatic interactions have gained traction only recently. Given the advantages these methods present compared to more traditional immobilization strategies, further research into their use can be anticipated. Further, many of the discussed strategies have only been applied in the detection of a handful of targets. With a growing body of literature supporting their viability in diverse detection environments, more widespread application of the discussed strategies is expected. Considerations moving forward should include surface stability, the shelf life of immobilized substrates, compatibility within target environments (*e.g.* water, serum or food) and the minimization of non-specific binding, which is a challenge in achieving the very low limits of detection needed within many applications. Ultimately, the performance of DNzyme-based biosensors depends on immobilization, activity after immobilization, and adequate transduction of signals, which supports the need for advances in robust and stable immobilization techniques. In addition, fabrication costs should be considered to allow for potential implementation within large-scale applications.

Recent developments involving the structural modification of DNAzymes into a three-dimensional form can be expected to continue. These DNA structures provide numerous benefits, including the ability to physically adsorb onto substrates such as paper without the need for any chemical modifications, resistance to nuclease activity, high signal-to-noise ratios and suppression of non-specific protein adsorption.<sup>[409]</sup> In terms of modifications to the sensing surface, lubricant infusion has garnered interest as a scalable modification that can improve biosensor performance through the omniphobicity it induces on sensing surfaces.<sup>[209,410,411]</sup> In particular, lubricant infused surfaces have demonstrated excellent blood repellency, making them ideal for use within clinical biosensors seeking to detect biomarkers within blood samples.<sup>[210,412–417]</sup> Furthermore, through the attachment of capture ligands onto such lubricated surfaces, selective cell adhesion has been achieved.<sup>[210,413,418]</sup> This presents a promising avenue towards cell-specific intracellular detection of biomarkers with increased precision. Hierarchical structuring has also been identified as a means through which omniphobicity can be induced and used for improvements in biosensing, presenting itself as another possible surface modification for future works.<sup>[69]</sup> The incorporation of such surface modifications stands to provide sensors with improved accuracy and lower limits of detection.

Perhaps one of the most intriguing applications for DNAzyme-based biosensors is in the detection of food contaminants. Given the global implications of foodborne illnesses and food waste, there is a defined need for the development of in-package sensors capable of providing easy-to-detect signals of contamination and spoilage without the need to open packaging. By relying on such dynamic indicators of safety and freshness, societal reliance on generic expiry dates may be eliminated. Fluorescence and colorimetric transduction platforms are of particular interest given the ease with which signals could be detected along the food production pipeline. Similarly, regarding pathogen, metal ion, and biomarker detection in both environmental and clinical settings, the application of DNAzymes might be able to address the selectivity and sensitivity needed to advance point-of-care and on-site testing. Within the context of reducing lengthy waiting periods and labor costs associated with most clinical and heavy metal testing,

DNAzyme-integrated sensors may challenge traditional approaches, offering an alternative that is both time and cost-effective. With that said, careful consideration regarding the efficacy, reproducibility, and scale-up, particularly at the immobilization level, will be critical to achieving this reality. While the robust nature of covalent linkages is in widespread use, during initial design and conception non-covalent, as well as physical entrapments, should be considered to consolidate fabrication steps and potentially decrease costs.

In a similar vein, DNAzyme-based platforms may overcome the hurdle of low biomarkers concentrations that characterize early-stage cancer. Additionally, the potential to multiplex various targets – such as CTCs and miRNAs, could further assist in clinical characterization and staging. Combined with improved specificity and sensitivity, the versatility to integrate such DNAzyme-based strategies into point-of-care devices may lead to these platforms leading the next generation of clinical tests in cancer detection.

DNAzymes also have the potential to play a substantial role in increasing our chances of success in our fight against infectious diseases. The COVID-19 pandemic has highlighted the need to have methods that enable rapid, simple and equipment-free detection of infectious agents, such as SARS-CoV-2. We expect soon to see the identification of DNAzymes that are able to detect and report the presence of specific proteins in viruses surfaces (such as the spike protein), as well as the identification of DNAzymes that can be activated by the presence of specific genomic sequences, such as the presence of the RNA sequence that encodes for the production of the spike protein in SARS-CoV-2. This second approach would avoid the need to use RT-PCR for nucleic acid-based detection of the virus. As highlighted in this review, DNAzymes are tools that are ideally suited to serve as the backbone for highly specific and simple tests, including paper-based sensors.

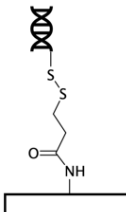
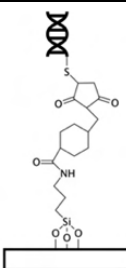
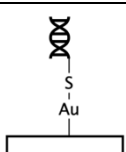
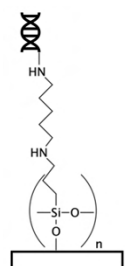
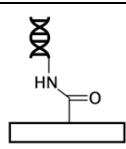
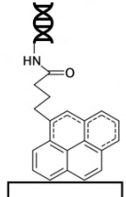
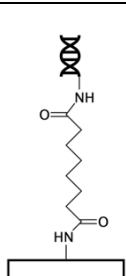
### **3.6 Acknowledgements**

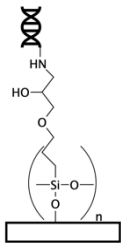
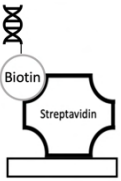
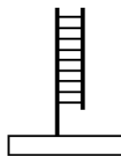
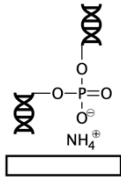
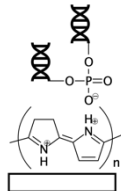

SK is supported by a Vanier Canada Graduate Scholarship awarded by the Natural Sciences and Engineering Research Council. KD is supported by the North Carolina A&T State University KL2 Scholar Award from the National Center for Advancing Translational Sciences, National

Institutes of Health, through Grant KL2TR002490 and start-up funds from the Joint School of Nanoscience and Nanoengineering, North Carolina A&T State University. The content is solely the responsibility of the authors and does not necessarily represent the official views of the NIH. TFD is supported by NSERC Discovery and CRD grants, Ontario Early Researcher Award grant and McMaster start-up funds.

### 3.7 Tables

**Table 3.1.** Comprehensive overview of existing DNAzyme immobilization techniques for biosensing.

Immobilization Strategy	Surface Functionalization	DNAzyme Functionalization	Detection Targets	Transduction Methods	Considerations	Schematic	Ref
Thiol-mediated	N-succinimidyl 3-(2-pyridyldithio) propionate-treated	Thiolated	Lead ions	Fluorescence	<i>Advantages</i> 1. Robust covalent immobilization 2. Easy implementation 3. Crosslinker not needed if using Au 4. Inherent quenching properties if using Au  <i>Disadvantages</i> 1. Increased cost 2. Limited to certain transduction methods		[298]
	Sulfosuccinimidyl-4-(N-maleimidomethyl) - cyclohexane-1-carboxylate		Uranyl ions	Electrochemical			[286]
	Gold ( <i>via</i> electro-deposition or treatment with cysteamine, Fe3O4 or chromium)		Lead, copper, nickel, uranyl ions	Fluorescence, electrochemical			[271,275,276, 283,292,295,296]
			Avian influenza virus	Electrochemical			
			L-histidine				
Aldehyde-mediated	Aldehyde (hydroxyl + APTES + glutaraldehyde or pre-purchased)		Lead	IR spectroscopy	<i>Advantages</i> 1. Robust covalent immobilization 2. Wide selection of available chemistries 3. Compatibility with all transduction methods 4. Well established immobilization technique with extensive supporting literature 5. Limited cost  <i>Disadvantages</i> 1. Introduction of a crosslinker		[299,303–306]
			H2O2	Colorimetric			
			Thrombin				
Ester-mediated	NHS-ester (COOH + EDC/NHS)		Lead	Electrochemical			[307–309]
	1-pyrenebutanoic acid succinimidyl ester		Prostate specific antigen	Colorimetric			
	Bis(sulfosuccinimidyl) suberate		Silver, mercury, copper ions	Electrochemical			[310,311]
			Glucose	Colorimetric			[312]

Epoxy-mediated	Epoxy (GPTMS or pre-purchased)		Lead	Electrochemical, pH			[17,313,314]
			Food pathogen detection	Fluorescence			
Biotin-streptavidin interaction	Streptavidin (via spotting, bonding with AuNPs, EDC-NHS mediation, or pre-purchased)	Biotinylated	Lead	Fluorescence, electrochemical, colorimetric	<b>Advantages</b> 1. Very stable interaction 2. Compatibility with all transduction methods  <b>Disadvantages</b> 1. Need to label sensing entities with protein		[272,284,321–325,419]
			Tetracycline	Colorimetric			
			Bacteria ( <i>Helicobacter pylori</i> , <i>Vibrio anguillarum</i> )	Fluorescence, colorimetric			
DNA hybridization	Coated with DNA complimentary to DNzyme	N/A	Copper ions	Fluorescence, electrochemical	<b>Advantages</b> 1. Provides mediation of sensing cascade 2. Compatibility with all transduction methods  <b>Disadvantages</b> 3. Requires very specific sensor design		[297,328–330]
			Uranyl ions				
			Lysozymes	Colorimetric			
Electrostatic interactions	Ammonium	N/A	Lead, mercury ions	EIS	<b>Advantages</b> 1. High efficacy with reduced graphene oxide  <b>Disadvantages</b> 1. Relatively weak interactions 2. Limited to electrochemical systems 3. Existing work with DNzymes is limited		[277]
	Plasma-polymerized propargylamine		DNA fragments				
	Plasma-polymerized polypyrrole		Lysozymes, <i>Salmonella</i>	Electrochemical			[278]
Physical entrapment	Polysaccharide-polynucleotide coacervate microdroplets	N/A	Ultraviolet irradiation	Fluorescence	<b>Advantages</b> 1. Unmodified DNzymes can be used 2. Pullulan provides strong long-term stability 3. Increased DNzyme activity upon sol-gel matrix optimization		[273,284,336–338,420]
	Polydopamine		H <sub>2</sub> O <sub>2</sub>	Electrochemical			

	Pullulan		Klebsiella pneumoniae, Helicobacter pylori	Fluorescence, colorimetric	<i>Disadvantages</i> 1. Not compatible with many existing platforms 2. Requires significant sensor-specific optimization 3. Stability of non-pullulan approaches are unknown 4. Limited studies		
	Sol-gel-derived matrices		Metal ions mixture (multiplex detection)	Fluorescence			

**Table 3.2.** Overview of existing literature involving the use of DNAzymes for environmental detection. Studies segregated into subsections pertaining to food contaminant, pathogen, and metal ion detection.

	Detection Method	DNAzyme Name	Immobilization Strategy	Target	Sample Type	LOD	Ref
Food Contaminant Detection	Electrochemical	G-quadruplex-hemin DNAzyme	Aptamer-mediated binding	<i>Escherichia coli</i>	Buffer and milk samples	8 CFU/mL	[341]
	Fluorescence	<i>E. coli</i> specific RNA-cleaving DNAzyme	Hybridization	<i>E. coli</i> O157: H7	Drinking water and apple juice	1.57 CFU/mL	[342]
	Fluorescence	<i>E. coli</i> specific DNAzyme	Biotin-streptavidin	<i>E. coli</i>	Buffer , tap water and milk	60 CFU/mL	[344]
	Fluorescence	RNA-cleaving DNAzyme – <i>E. coli</i>	$\pi$ - $\pi$ stacking interactions	<i>E. coli</i>	Buffer	10 <sup>4</sup> CFU/mL	[224]
	Fluorescence	DAh1T1	Physical entrapment	<i>Aeromonas hydrophila</i>	Buffer, drinking water and milk	36 CFU/mL	[345]
	Fluorescence	RNA-cleaving DNAzyme – <i>E. coli</i>	Epoxy-mediated	<i>E. coli</i>	Buffer, apple juice and meat	10 <sup>3</sup> CFU/mL	[17]
	Colorimetric	G-quadruplex-hemin DNAzyme	Hybridization	<i>Vibrio parahaemolyticus</i>	Buffer and salmon	10 CFU/mL	[348]
Pathogen Detection	Electrochemical	HRP mimicked	Thiol-gold	Avian influenza virus	Chicken serum	Undisclosed	[283]
	Colorimetric	G-quadruplex-hemin DNAzyme	Thiol-silver	Hepatitis B virus	Human serum samples	0.2 nM	[421]
	Fluorescence	RNA-cleaving fluorogenic DNAzyme	Non-covalent functionalization; $\pi$ - $\pi$ stacking interactions	<i>E. coli</i>	Blood samples and <i>E. coli</i> K12 culture	10 <sup>5</sup> CFU/mL	[224]
	Electrochemical	Hemin/G-quadruplex HRP-mimicking DNAzyme	Thiol-gold	Hepatitis B virus surface antigen	Serum samples	0.19 pg/mL	[285]
	Fluorescence	RNA-cleaving fluorogenic DNAzyme	Not specified	<i>E. coli</i> – lysozyme	Drinking water, milk, apple juice	100 cells/ml	[206]
	Colorimetric – smartphone readout	RNA-cleaving DNAzyme	Hybridization	<i>E. coli</i> K12	Juice, milk or complex samples	10 <sup>3</sup> CFU/mL	[422]
	Fluorescence	DNAzyme-based fluorescent paper sensor	Covalent	<i>Klebsiella pneumoniae</i>	Buffer and bacterial isolates	10 <sup>5</sup> CFU/mL	[336]



Pathogen Detection	Fluorescence	RFD-CD1	Not specified	<i>Clostridioides difficile</i>	Buffer CEM	Not specified	[352]
	Electrochemical	VAE-1 and VAE-2 RNA cleaving DNazymes	Biotin-streptavidin	<i>Vibrio anguillarum</i>	Water samples and fish tissue	4000 CFU/mL	[322]
	Colorimetric	RNA-cleaving DNzyme	Biotin-streptavidin	<i>Helicobacter pylori</i>	Human stool samples	10 <sup>4</sup> CFU/mL	[284]
	Fluorescence	Cis (hairpin) and trans DNzyme	Amide-agar media	<i>E. coli</i>	Buffer and wastewater treatment plant	10 <sup>4</sup> –10 <sup>5</sup> cells per mL	[423]
Metal Ion Detection	Plasmonic (UV-vis spectroscopy)	15-12 DNzyme	Thiol-gold	Lead ions	Tap water	8.0 nM	[364]
	Electrochemical	Custom Pb <sup>2+</sup> DNzyme	Poly adenine binding to AuNPs; thiol-gold; hybridization	Lead ions	Tap water	96 pM	[424]
	Colorimetric	GR-5 DNzyme	Thiol-gold; biotin-streptavidin	Lead ions	Soil	0.05 nM	[363]
	Electrochemical	8-17 DNzyme	Hybridization	Lead ions	Lake and tap water	0.07 pM	[425]
	Surface plasmon resonance	GR-5 DNzyme	Thiol-gold; hybridization	Lead ions	HEPES and NaCl buffer	80 pM	[426]
	Colorimetric (interferometric reflectance spectroscopy)	K <sup>+</sup> -stabilized hemin G-quadruplex; Pb <sup>2+</sup> -stabilized quadruplex	Aldehyde-mediated	Lead ions	Buffer and seawater	12 nM	[303]
	Fluorescence	Pb <sup>2+</sup> DNzyme	$\pi$ - $\pi$ stacking and non-covalent hydrophobic interactions	Lead ions	Tap and lake water	6.7 pM	[427]
	Electrochemical	8–17 DNzyme	Biotin-streptavidin	Lead ions	Tap, lake and pool water	38 fg/mL	[323]
	Electrochemical	8-17 DNzyme	NHS-ester	Lead ions	Tap and river water	17.4 fM	[308]

Metal Ion Detection	Colorimetric	GR-5 DNAzyme	Biotin-streptavidin	Lead ions	Soil	0.05 nM	[363]
	Electrochemiluminescence	Hemin/G-quadruplex DNAzyme	NHS-ester	Lead ions	River water	0.98 fM	[428]
	Electrochemical	8-17 DNAzyme	Thiol-gold	Lead ions	Drinking water, serum	0.29 pM	[429]
	Fluorescence	Mg <sup>2+</sup> dependent DNAzyme	Thiol-gold	Mercury ions	Herbs	30 pM	[371]
	Digital drop PCR	GR-5 DNAzyme	Biotin-streptavidin	Lead ions	Lake water	500 pM	[430]
	Colorimetric	Cu <sup>2+</sup> dependent DNAzyme	Biotin-streptavidin	Copper ions	Bottled, lake and domestic sewage water	8 nM	[362]
	Fluorescence	GR-5 DNAzyme	$\pi$ - $\pi$ stacking; hydrogen bonding	Lead and magnesium ions	Tap and lake water	96 pM (Pb <sup>2+</sup> ) 356 pM (Hg <sup>2+</sup> )	[370]
	Electrochemical	UO <sub>2</sub> <sup>2+</sup> specific DNAzyme	Thiol-gold	Uranyl ions	River water	20 pM	[431]
	Electrochemical	Pb <sup>2+</sup> specific DNAzyme	Thiol-gold	Lead and magnesium ions	Tap and lake water	0.034 pM	[432]
	Raman scattering	Pb <sup>2+</sup> specific DNAzyme	Thiol-gold	Lead ions	Lake, tap and industrial water	8.9 pM	[433]

**Table 3.3.** Overview of existing literature on the use of DNAzymes for clinical applications. Studies segregated into sub-sections pertaining to nucleic acid, protein, and cancer detection.

	Detection Method	DNAzyme Name	Immobilization Strategy	Target	Sample Type	LOD	Ref
Nucleic Acid Detection	Colorimetric	Hemin/G-quadruplex DNAzyme	Physical entrapment	Y human amelogenin fragment	Buffer	45.7 ng	[287]
	Electrochemical	Trivalent DNAzymes	Thiol-gold	microRNA let-7a	Dilute human serum	0.46 fM	[378]
	Electrochemiluminescent	Hemin/G-quadruplex DNAzyme	NHS-ester	miRNA-155	Cell lysate	0.3 fM	[434]
Protein Detection	Chemiluminescence	Hemin/G-quadruplex DNAzyme	Hybridization	Lysozyme	Human urine	$1.25 \times 10^{-11}$ g/L	[330]
	Electrochemical	Hemin/G-quadruplex DNAzyme	Metal-thiol interactions	Cardiac troponin I	PBS spiked with human serum	7.5 pg/mL	[384]
	Electrochemical	Pb <sup>2+</sup> -dependent DNAzymes	Thiol-gold	Prostate specific antigen	Clinical serum samples	0.1 pg/mL	[435]
	Electrochemical	Pb <sup>2+</sup> -dependent DNAzymes	Thiol-gold	Thrombin	PBS and dilute serum	1.8 pM (in PBS)	[386]
	Electrochemical	Hemin/G-quadruplex DNAzyme	Hybridization	Thrombin	Spiked serum	0.3 fM	[387]
	Chemiluminescence	Hemin/G-quadruplex DNAzyme	Hybridization	Thrombin	Spiked serum	$6.3 \times 10^{-15}$ mol/L	[388]
	Fluorescence	8-17 DNAzyme	Thiol-gold	Thrombin	Serum samples	4.5 pM	[436]
	Colorimetric	8-17 DNAzyme	Hybridization	Platelet-derived growth factor BB	Buffer	0.11 fM	[437]
	Electrochemical	Hemin/G-quadruplex DNAzyme	Thiol-gold	Prion protein	Diluted serum samples	0.38 pg/mL	[374]
	Electrochemical	Pb <sup>2+</sup> -dependent DNAzymes	Thiol-gold	Alpha-fetoprotein	Clinical serum samples	0.8 pg/mL	[438]
	Photoelectrochemical	Hemin/G-quadruplex DNAzyme	Thiol-gold	Alpha-fetoprotein	Diluted serum samples	14.7 pg/mL	[373]

Cancer Detection	Fluorescence	3D DNA motor	Thiol-gold	Telomerase	Living cells of MCF7, A549 and HeLa	46 cells/ml	[401]
	Colorimetric	Hemin/G-quadruplex DNAzyme	Aldehyde-based	Telomerase	Telomerase activity in HeLa cells	0.5 HeLa/ $\mu$ L	[402]
	Fluorescence	DZM-21 and DZM 205 – Na <sup>2+</sup> DNAzymes	Thiol-gold	miRNA-21; miRNA-205	A549 and H520 cells	97 fM; 137 fM	[406]
	Fluorescence	Cu <sup>2+</sup> -DNAzyme-sgc8c and Mg <sup>2+</sup> -DNAzyme-TD05 Cy5	Thiol-gold	CTC	Whole blood sample	10 <sup>2</sup> -10 <sup>3</sup> cells/mL	[392]
	Electrochemical	Pd-Pt nanocage–HRP–cDNA/hemin/ G-quadruplex hybrid nanoprobe	Hybridization/Thiol-gold	CTC	HepG2 tumor cells	5 cell/ml	[396]

## **Chapter 4: Comprehensive Fluorescence Profiles of Contamination-prone Foods Applied to the Design of Microcontact-printed *in situ* Functional Oligonucleotide Sensors**

### **Preface**

While RFDs stand to be exceptional sensing tools for in-package food-monitoring – owing to their all-in-one sensing and transduction capabilities, considerations towards their effective implementation need to be made. This chapter details such a consideration, through the comprehensive fluorescence assessment of target food products. This directly addresses Objective 1, wherein improving our understanding of the fluorescence background of target foods allows us to make better sensor design choices – specifically with regards to the optimal fluorophore to be used in a given system. Specifically, employing a sensing wavelength in which a target food product exhibits low inherent fluorescence will yield an imaging interface with low background interference. Produce and meat products that are susceptible to pathogenic contamination were selected for evaluation. Different types and/or form factors of each food product were tested to identify variations. While baseline fluorescence profiles were gathered under sensing-relevant imaging parameters as an initial benchmark, changes in these profiles were also studied over time. This ensured that wavelengths noted to be optimal for sensing exhibit low sensing interference through a given product's life span. To contextualize these findings to sensing, contact-printed fluorescent oligonucleotide probes were deposited onto food packaging films and overlaid onto the products of interest. Effective visualization was obtained across several fluorescence wavelengths for each food, acting as a guide for future on-food fluorescence sensing studies. To validate visibility from a sensing perspective, RFDs were contact printed, and their cleavage-induced fluorescence increase was visualized with overlaid food backgrounds. Importantly, this was the first time RFD contact printing has been reported in literature, adding an additional tool to our sensor development arsenal. Ultimately, while many studies have proposed on-food fluorescence sensing, the approaches used for proof-of-concept testing are often unrealistic. This ranges from removing the smart packaging film from the food product during imaging to using thin food samples that offer reduced background. Our visualization of sensing agents positioned adjacent to dense food matrices confirms the viability of strong fluorescence sensing systems for hands-free monitoring of sealed food products.

### **Authors**

Shadman Khan, Amid Shakeri, Jonathan K. Monteiro, Simrun Tariq, Akansha Prasad, Jimmy Gu, Carlos D.M. Filipe, Yingfu Li, Tohid F. Didar

In this work, contamination-prone food products were comprehensively assessed with regards to their sensing-relevant properties. Fluorescence was assessed at excitation/emission wavelengths corresponding to diamidino-2-phenylindole (DAPI), fluorescein isothiocyanate (FITC), tetramethylrhodamine (TRITC), and Cyanine5 (Cy5)-range fluorophores. Lettuce, spinach, chicken and beef were selected for analysis. Four types of high-risk lettuce were evaluated to

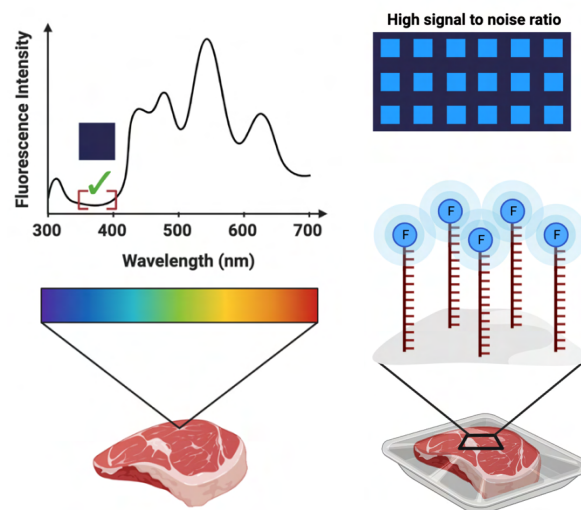
identify variations that may exist between their fluorescence profiles. On the other hand, meat products were studied in both whole and ground form factors to identify variations induced by product processing procedures, with insignificant differences observed amongst the product forms. Studies evaluating fluorescence output over the course of product lifespans were performed to identify changes over time. Next, a direct understanding of how these background intensities pertain to sensing was sought. Contact-printed, fluorescently-labelled oligonucleotide microarrays were used to determine signal-to-noise ratio (SNR) and coefficient of variation (CV) values for every fluorophore-food product pairing. Finally, microcontact-printing of a TRITC-range, 5-Carboxytetramethylrhodamine (TAMRA) fluorophore-labelled functional nucleic acid probe (fNAP) was used to validate sensing visibility on food backgrounds.

## Publication

Scientific Reports, 2024, 14, 8277

## Publication Date

April 2024



## 4.1 Abstract

With both foodborne illness and food spoilage detrimentally impacting human health and the economy, there is growing interest in the development of *in situ* sensors that offer real-time monitoring of food quality within enclosed food packages. While oligonucleotide-based fluorescent sensors have illustrated significant promise, the development of such on-food sensors requires consideration towards sensing-relevant fluorescence properties of target food products – information that has not yet been reported. To address this need, comprehensive fluorescence profiles for various contamination-prone food products are established in this study across several wavelengths and timepoints. The intensity of these food backgrounds is further contextualized to biomolecule-mediated sensing using overlaid fluorescent oligonucleotide arrays, which offer perspective towards the viability of distinct wavelengths and fluorophores for *in situ* food monitoring. Results show that biosensing in the Cyanine3 range is optimal for all tested foods, with the Cyanine5 range offering comparable performance with meat products specifically. Moreover, recognizing that mass fabrication of on-food sensors requires rapid and simple deposition of sensing agents onto packaging substrates, RNA-cleaving fluorescent nucleic acid probes are successfully deposited *via* microcontact printing for the first time. Direct incorporation onto food packaging yields cost-effective sensors with performance comparable to ones produced using conventional deposition strategies.

**Keywords:** food fluorescence, *in situ* monitoring, fluorescence sensing, smart packaging, on-food sensing, functional DNA probe

## 4.2 Introduction

Despite extensive commercial and legislative efforts, foodborne illness caused by pathogenic contamination represents a growing global health concern, with an estimated annual

caseload exceeding 600 million and over 420,000 associated deaths.<sup>[439]</sup> The associated cost of such illnesses continues to weigh heavily on healthcare systems, to the order of billions of dollars each year.<sup>[3]</sup> The economic effects of food contamination are further exaggerated by the associated food waste and the cost of retroactive food recalls, which are implemented once a contamination event is identified.<sup>[440,441]</sup> Alongside pathogenic contamination, food spoilage represents a concurrent concern. While illnesses caused by the consumption of spoiled food products offer significantly better prognoses, the predicted expiry dates used to prevent such events yield significant food waste due to their limited accuracy.<sup>[442]</sup> With several studies estimating that approximately a third of edible food products are wasted each year, continued societal reliance on static expiry dates has become a significant economic and environmental concern.<sup>[443,444]</sup>

Fueled by this crisis, the intersection between food science and biosensing has garnered significant interest. Efforts have been made towards the development of real-time, on-package contamination and spoilage detection platforms, which provide a comprehensive solution that would significantly improve food safety.<sup>[9,25,200,445]</sup> While various detection strategies have been applied in the development of on-package detection platforms, considerations toward commercial viability and ease-of-use have brought focus towards colorimetric and fluorescence transduction systems.<sup>[200,446,447]</sup> Colorimetric systems are optimal from an ease-of-use perspective, but the incorporation of colorimetric systems *in situ* has proven difficult. Specifically, most colorimetric signaling mechanisms require intricate reaction cascades that rely on numerous reagents.<sup>[200]</sup> The incorporation of such complex reaction mixes onto food packaging is largely impractical. While a few commercially feasible platforms have been proposed,<sup>[21,25]</sup> their real-world applicability is limited by their poor sensitivity and specificity.

Comparatively, fluorescence transduction platforms present a much more viable strategy, given the ease with which fluorophores can be integrated onto biorecognition molecules – such as protein and oligonucleotide probes, yielding singular entities with both recognition and reporting capabilities.<sup>[448,449]</sup> Antibodies have been somewhat explored within this space, however,



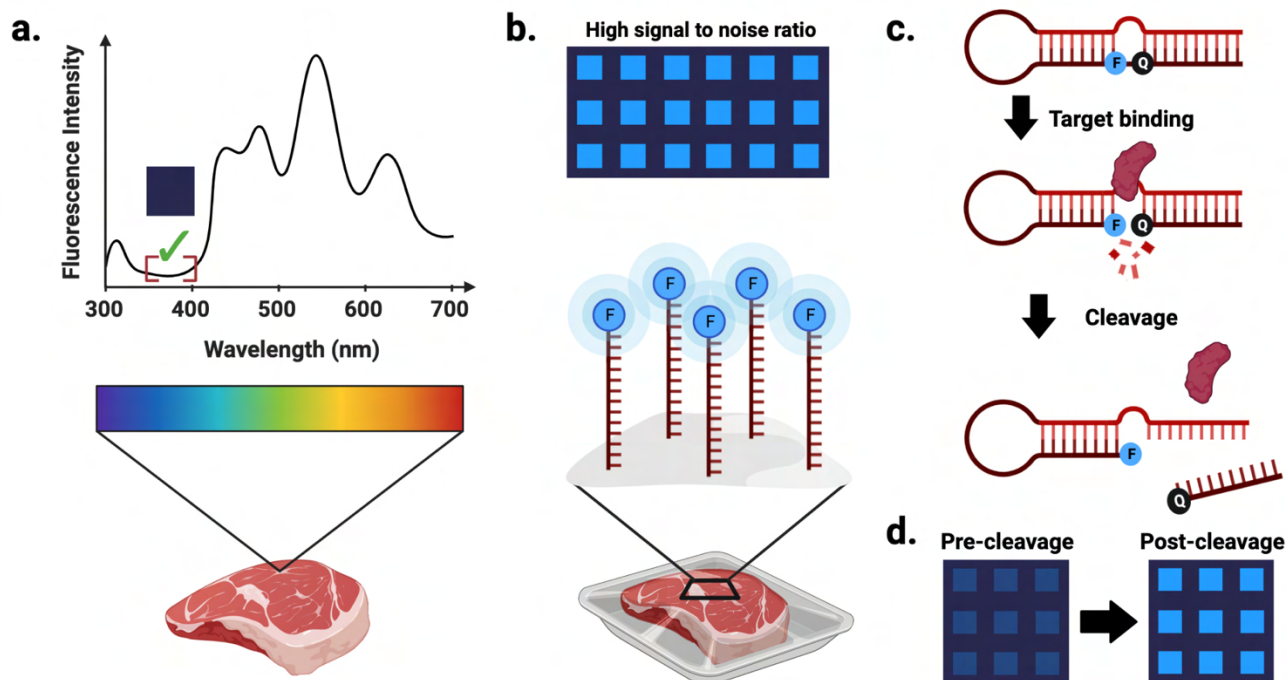
oligonucleotide probes in particular, represent some of the most applied biorecognition probes, given their stability under varying conditions. These oligonucleotides have been labelled with fluorophores such as Pacific Blue, FITC, FAM, Cy3, and Cy5 to illicit fluorescent signals upon the identification of target molecules such as bacterial pathogens and chemical contaminants within food.<sup>[450–452]</sup> Yet, these oligonucleotides lack the functional properties required for food testing, making RNA-cleaving fluorescent nucleic acid probes (fNAPs) the most extensively explored platform in the food sensing space owing to their ease of functionalization, high stability, low cost, and simple detection cascade.<sup>[8,16,17,24,453]</sup> Composed of a probe strand joined to a substrate strand, their design usually involves the incorporation of a fluorophore-quencher pair within the substrate strand, flanking the ribonucleotide cleavage site. In the event of target exposure, cleavage induces the release of the quencher, resulting in fluorescence recovery.<sup>[200]</sup> With regards to contamination, several highly specific, pathogen-responsive fNAPs have been reported in recent years, some of which have shown efficacy within food-based applications.<sup>[17,24]</sup> Contrarily, fNAP-based approaches to spoilage detection have not been explored yet, but fluorescent aptamer-based systems targeting histamine – a spoilage marker for fish products such as tuna, have been reported.<sup>[454]</sup>

The development of *in situ* food sensors is expected to be a growing area of research, especially with the continued discovery of new probes that detect targets of interest with high sensitivity. However, with consideration towards subsequent sensor development, there is a lack of research aimed at determining relevant baseline properties of target food products – work that would better educate the design of future platforms. With regards to fluorescent sensors specifically, optimal transduction fluorophores for target food products are yet to be identified. Existing studies exploring the fluorescence spectra of food products have largely collected fluorescence profiles for compositional analysis and quality assessment.<sup>[455]</sup> While valuable, such works cannot inform the design of probe-based food sensors, as arbitrary quantifications of fluorescence cannot be readily compared to the intensity of fluorophore-labelled probes. Given the

lack of data available regarding fluorophore visibility on food backgrounds, food sensing studies have employed a range of different fluorophores with no consideration towards the label best suited for their system, possibly limiting the resultant platforms' sensitivity and reliability.<sup>[456]</sup>

Concurrently, growing interest in *in situ* food sensors also brings focus towards the ease with which sensing platforms can be integrated onto food packaging. While biomolecular microarrays are most often produced *via* non-contact piezoelectric deposition owing to significant commercial optimization, such systems remain slow.<sup>[457]</sup> As such, they are unsuitable for applications that require deposition over large surface areas, as would be required in the mass production of biofunctionalized food packaging.<sup>[458]</sup> Comparatively, contact printing can deposit target bio-inks over large substrates rapidly *via* roll-to-roll printing.<sup>[458]</sup> Further, the physical nature of contact deposition eliminates bio-ink evaporation post-deposition, inducing high lateral resolution within printed arrays.<sup>[459]</sup> Importantly, while the contact printing of antibodies has been successfully demonstrated in previous works,<sup>[209,210,300]</sup> the contact-based deposition of fNAPs has not yet been reported. Considering that contact printing offers limited control over biomolecule orientation – a necessary condition to permit signal-inducing fluorophore-quencher separation within fNAPs, developing functional arrays using such an approach can be considered difficult.

The presented work aimed to provide: (1) a comprehensive assessment of the inherent fluorescence background of several target food products across several wavelengths, (2) an evaluation of fluorophore-labelled oligonucleotide visibility when positioned alongside target food backgrounds, and (3) the first report of fNAP contact printing. Collectively, objectives 1 and 2 sought to deliver a holistic evaluation of the suitability of specific wavelengths and their associated fluorophores for *in situ* food monitoring – results that have high applicability towards the future design of sensors in this space. They also informed the design of probes used in objective 3, where contact-printed sensors directly embedded onto food packaging offered performance comparable to conventional array fabrication strategies, substantiating the presented approach.



**Figure 4.1. Schematic illustration of experimental approach.** (a) Establishing inherent fluorescence profiles of target food products. (b) Evaluation of array visibility using fluorophore-conjugated oligonucleotides to identify labels that offer high signal to noise ratios. (c) Mechanism of action of RNA-cleaving fluorescent nucleic acid probes. (d) Fluorescence shift in fNAP microarrays following target-mediated fNAP cleavage. Created using BioRender.

### 4.3 Results and Discussion

Our experimental approach is summarized in **Figure 4.1**. Briefly, fluorescence profiles were derived for lettuce, spinach, chicken, and beef products through evaluation at four wavelengths commonly employed within fluorescence biosensing (Figure 4.1a). Fluorescence was also assessed over time to account for changes that occurred over the food products' lifespans. Fluorophore visibility against target food backgrounds was evaluated using contact-printed oligonucleotides labelled with fluorophores corresponding to each of the four selected wavelengths (Figure 4.1b). Contact printed fNAPs were similarly immobilized onto food packaging, where they demonstrated both functionality and visibility with underlying food samples (Figure 4.1c-d).

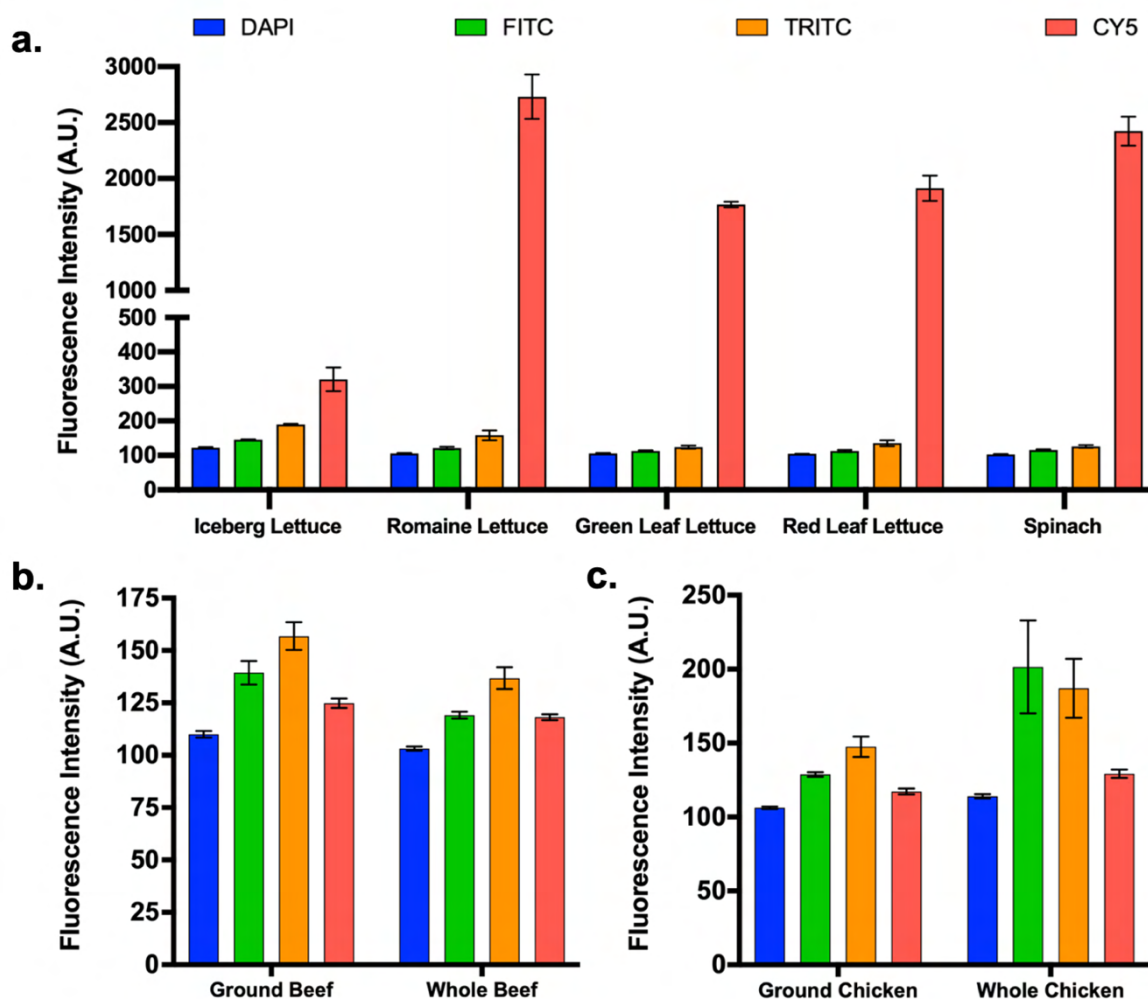
### 4.3.1 Establishing the fluorescence profiles of target food products

The inherent fluorescence of target food products was assessed using four channels with excitation/emission wavelengths of 350 nm/470 nm, 490 nm/525 nm, 557 nm/576 nm, and 649 nm/666 nm. Given that this collection of wavelengths extends throughout the entire visible light spectrum, the collected data comprehensively established the fluorescence profiles of the selected products. Further, these wavelengths roughly correspond with diamidino-2-phenylindole (DAPI), fluorescein isothiocyanate (FITC), tetramethylrhodamine (TRITC), and Cy5 fluorescence dyes, which yield blue, green, orange, and red emission, respectively.<sup>[460–462]</sup> Given that all commercially available fluorophores exhibit excitation/emission wavelengths comparable to one of these four dyes, the study was also comprehensive from a fluorescence biosensing perspective.

The five produce products selected for assessment were iceberg lettuce, romaine lettuce, green leaf lettuce, red leaf lettuce, and spinach (**Figure 4.2a**). Across DAPI, FITC, and TRITC fluorescence channels, the five products showed similar profiles. Specifically, sample fluorescence was low across all three channels, but increased gradually at higher wavelengths. Mean intensity values ranged from 102 – 122 arbitrary units (A.U.) in the DAPI channel, 113 – 146 A.U. in the FITC channel, and 124 – 190 A.U. in the TRITC channel. Comparatively, the Cy5 channel yielded significantly higher fluorescence. Here, iceberg lettuce samples exhibited a mean fluorescence intensity of 321 A.U. This was still much lower than the four other tested products, which exhibited mean intensity values in the range of 1768 – 2762 A.U. High Cy5 fluorescence was attributed to chlorophyll molecules, which are highly abundant within produce and emit red light.<sup>[463]</sup> Importantly, chlorophyll is significantly less prominent within iceberg lettuce, explaining its lower fluorescence intensity in the Cy5 channel.<sup>[464]</sup>

Next, recognizing that chlorophyll exhibits poor photostability,<sup>[465]</sup> we sought to assess whether the Cy5 fluorescence intensity of lettuce samples could be decreased *via* concentrated light exposure. Romaine lettuce samples were imaged over the course of four minutes, during which a significant reduction in fluorescence intensity was observed (Figure S4.1). This reduction

was characterized by a sharp initial decrease in fluorescence, followed by a more gradual downward slope, that collectively induced a reduction in mean intensity from 2454 A.U. to 1148 A.U. Yet, despite this significant reduction, fluorescence intensity in the Cy5 channel remained significantly higher than what was observed in the DAPI, FITC, and TRITC channels. As such, Cy5 labelling was noted as unsuitable for produce-targeting biosensing applications.



**Figure 4.2. Baseline fluorescence properties of target food products.** (a) Mean fluorescence intensities of produce products. (b and c) Mean fluorescence intensities of beef and chicken samples, respectively. All values consist of at least four data points. Error bars and dashed lines represent standard deviation.

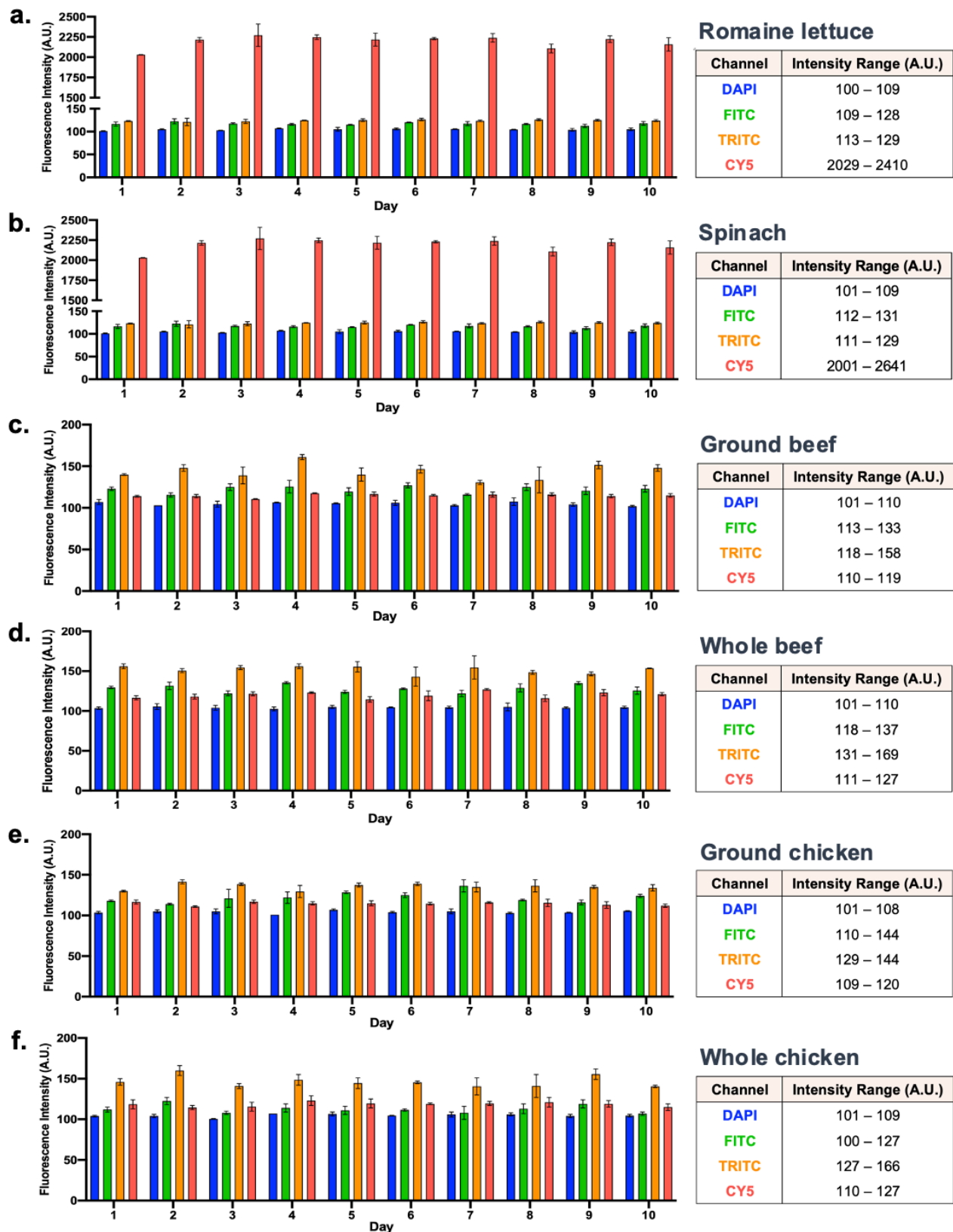
With regards to meat products, beef and chicken samples were assessed (Figure 4.2b-c). Both ground and whole meat samples were evaluated to account for changes in fluorescence

induced by post-slaughter processing. With ground beef samples, mean intensities of 110 A.U., 139 A.U., 157 A.U., and 125 A.U. were observed in DAPI, FITC, TRITC, and Cy5 channels, respectively. Comparatively, whole beef samples exhibited slightly lower mean fluorescence intensities, with values of 103 A.U., 119 A.U., 137 A.U., and 118 A.U. for each of the four channels, respectively. Ground chicken exhibited very similar mean intensities of 106 A.U., 129 A.U., 148 A.U., and 117 A.U. for DAPI, FITC, TRITC, and CY5, respectively. Whole chicken showed slightly higher mean fluorescence intensities of 114 A.U., 202 A.U., 187 A.U., and 129 A.U. for each of the four channels, respectively. Overarchingly, the relatively low intensities observed with meat samples across all evaluated channels yielded confidence towards broad applicability for biosensing.

#### **4.3.2 Monitoring changes in fluorescence profiles over product lifespans**

Given that the visibility of signals from fluorescence sensors embedded within food packaging needs to be maintained throughout the course of a given food product's lifespan, we then sought to evaluate changes in fluorescence over time. An optimal fluorescence channel would exhibit minimal changes over time, as such increases or decreases in background would make the calibration of signal-to-noise sensing thresholds unfeasible. Fluorescence consistency was quantified by the range of intensity values observed over the course of a 10-day test period.

With regards to produce, romaine lettuce and spinach samples were assessed, with limited variations in fluorescence intensity being observed in the DAPI, FITC, and TRITC channels (**Figure 4.3a-b**). Specifically, the range between the minimum and maximum fluorescence intensity values obtained for romaine lettuce were 9 A.U., 19 A.U., and 16 A.U. in the three channels, respectively. Similarly, spinach samples exhibited limited fluorescence variations, equating to ranges of 8 A.U., 19 A.U., and 18 A.U., respectively. Such high fluorescence consistency maintained the viability of these three channels for biosensing applications. Large variations were observed in the Cy5 channel, with romaine lettuce and spinach exhibiting ranges of 381 A.U. and 640 A.U., respectively. This further highlighted Cy5 as unsuitable for produce.



**Figure 4.3. Changes in mean fluorescence intensity of target food products.** Graphical depiction paired with intensity ranges for each evaluated wavelength provided for (a) romaine

lettuce, (b) spinach, (c) ground beef, (d) whole beef, (e) ground chicken, and (f) whole chicken. All values consist of at least four data points. Error bars represent standard deviation.

Ground beef exhibited fluorescence ranges of 9 A.U., 20 A.U., 40 A.U., and 9 A.U. in the DAPI, FITC, TRITC, and Cy5 channels, respectively, while whole beef displayed ranges of 9 A.U., 19 A.U., 38 A.U., and 16 A.U (Figure 4.3c-d). Here, the higher variation observed within the TRITC channel was noted as a potential hinderance. Comparatively, ground chicken offered ranges of 7 A.U., 34 A.U., 15 A.U., and 11 A.U. in the four respective channels, while whole chicken exhibited ranges of 8 A.U., 27 A.U., 39 A.U., and 17 A.U (Figure 4.3e-f). Accordingly, the FITC and TRITC channels were identified as wavelengths at which higher variation is present.

Collectively, DAPI offered limited fluorescence variation with each target food product, yielding confidence towards its applicability within sensing. Cy5 offered similarly low variation with meat products. While moderate variation was observed within TRITC and FITC channels, contextualizing the effect such variation would have on biosensing proved difficult given that the presented fluorescence intensities were quantified as arbitrary units. Thus, their value was limited to relative comparisons between channels and over time. To better understand how these background food intensities compare to what is emitted by fluorescently labelled biomolecules, we sought to assess the visibility of such agents when imaged against these products.

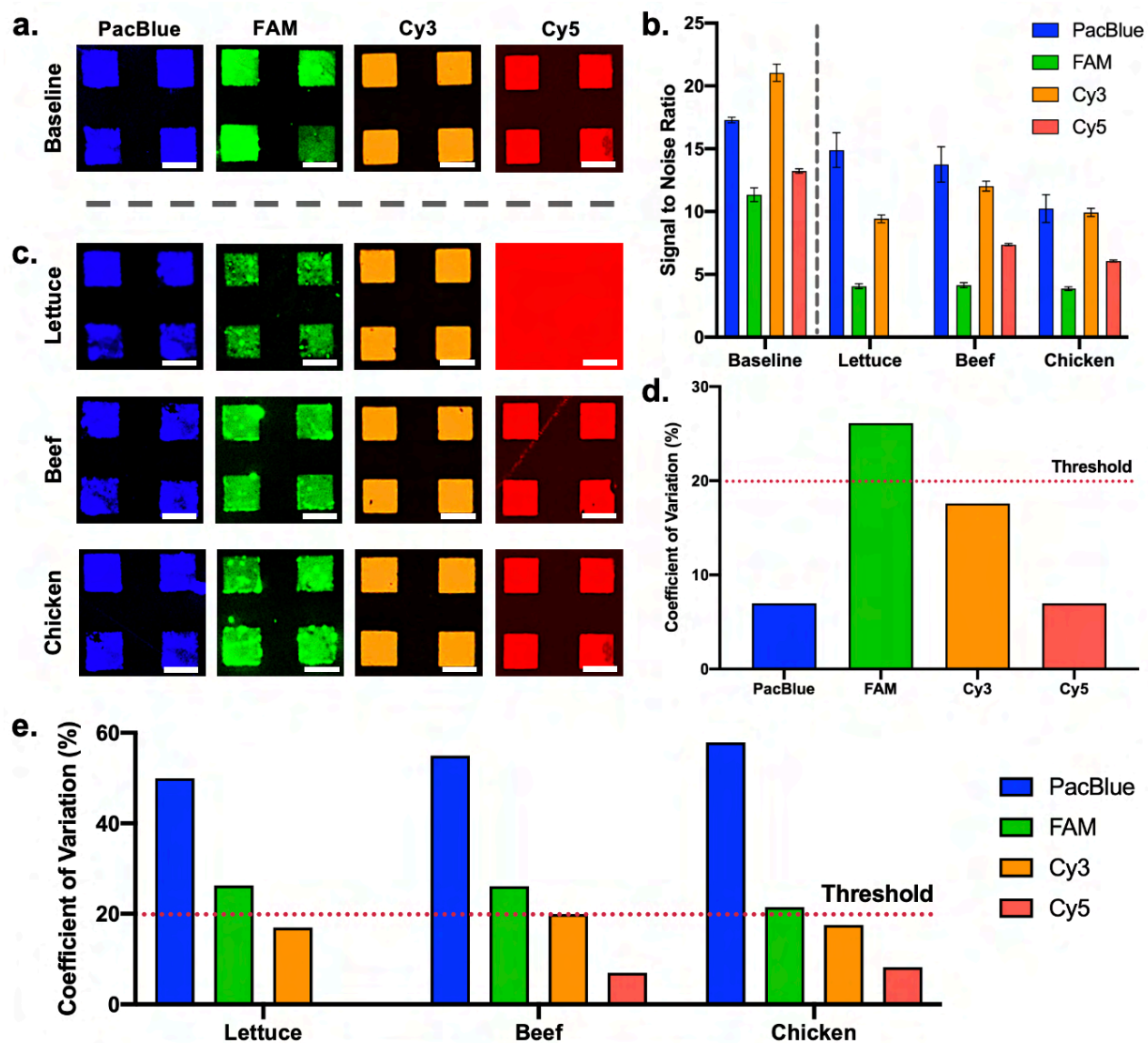
#### **4.3.3 Assessing fluorophore-biomolecule conjugate visibility on food backgrounds**

Recognizing that many food monitoring systems employ oligonucleotide probes, we immobilized fluorophore-labelled, single-stranded DNA oligonucleotides onto transparent polyethylene food wraps, which were then imaged with target food products.<sup>[16,466–468]</sup> To this end, DNA oligonucleotides labelled with Pacific Blue, FAM, Cy3, and Cy5 fluorophores – compatible with DAPI, FITC, TRITC, and Cy5 channels, respectively, were deposited onto the polymer substrate *via* microcontact printing. Immobilization *via* physical adsorption was employed to eliminate the possibility of confounding fluorescence induced by crosslinking reagents.



Each of the fluorophore-labelled DNA oligonucleotides formed high-resolution arrays (**Figure 4.4a**). As expected, differences in intensity were observed between the different fluorophores, which was attributed to the varying properties of each fluorescent label and their compatibility with contact printing. With consideration towards the baseline fluorescence noise produced by the polyethylene substrate, signal-to-noise ratios (SNR) were used to quantify the intensity of each array (Figure 4.4b). SNRs of 17.3, 11.3, 21.0, and 13.2 were derived for the Pacific Blue, FAM, Cy3, and Cy5 arrays, respectively. Subsequent visualization with overlaid food products employed romaine lettuce, ground beef, and whole chicken, given that all evaluated products showed fluorescence profiles comparable to one of these three products (Figure 4.4c). SNR values were used to quantify reductions in array visibility induced by food (Figure 4.4b).

Microcontact-printed arrays fabricated using the four respective fluorescence labels produced SNR values of 14.9, 4.1, 9.4, and 0, respectively when overlaid with romaine lettuce. This corresponded with 13.9%, 63.7%, 55.2%, and 100% reductions in SNR, respectively, relative to baseline SNR values. Accordingly, Pacific Blue was identified as an excellent candidate label, due to both its high baseline SNR and limited SNR reduction with romaine lettuce. Opposingly, the FAM-labelled oligonucleotide lost significant visibility – an outcome driven by both a low baseline SNR and significant romaine lettuce-induced fluorescence impedance. While the Cy3-labelled microarray also experienced significant fluorescence interference from overlaid romaine lettuce, high visibility was still retained, owing to a very high baseline SNR. Lastly, the Cy5 microarray was completely unobservable given the high fluorescence background produce exhibits at this wavelength.



**Figure 4. 4. Visibility of contact-printed microarrays composed of fluorophore-labelled DNA oligonucleotides.** (a) Fluorescence images of DNA microarrays deposited onto polyethylene food packaging. (b) SNR values of fluorescent DNA microarrays at baseline and with overlaid products. Each value consists of 30 data points. Error bars represent standard deviation. (c) Fluorescence images of DNA microarrays once overlaid with target food products. (d) Coefficient of variation of baseline DNA microarrays. Performance threshold identified with a dashed line. (e) Coefficient of variation of DNA microarrays overlaid on target food products. All scale bars depict 50  $\mu\text{m}$ .

Pacific Blue, FAM, Cy3, and Cy5 DNA microarrays imaged with underlying ground beef exhibited SNR values of 13.7, 4.2, 12.0, and 7.4, respectively. SNR was resultantly noted to have decreased by 20.8%, 62.8%, 42.9%, and 43.3% with the respective labels. Similar to romaine

lettuce samples, the presence of a ground beef background slightly reduced the SNR of the Pacific Blue-labelled microarray, but to a comparatively limited degree. The reduction in the visibility of the FAM-labelled DNA microarray when imaged with a beef background was identical to what was observed with produce – a finding substantiated by the similar fluorescence profiles both foods exhibit at this wavelength. Cy3-labelled microarrays also behaved similarly between the two products, with a high SNR being maintained despite fluorescence interference from the overlaid food sample. The most notable difference with beef samples was observed with the Cy5-labelled microarray, as the significantly lower background fluorescence of meat at this wavelength allowed for successful visualization of the printed arrays. Nonetheless, the Pacific Blue and Cy3-labelled DNA microarrays offered higher visibility, owing to the lower baseline SNR of the Cy5-labelled microarray. Finally, the four respective microarrays exhibited SNR values of 10.2, 3.9, 9.9, and 6.1, respectively, when overlaid with chicken samples. This correlated with SNR reductions of 41.0%, 65.5%, 52.9%, and 53.8% relative to the baseline arrays. Again, Pacific Blue and Cy3-labelled microarrays offered the highest SNR values, despite significant fluorescence interference from overlaid food samples. Similar to what was observed with beef, the FAM-labelled microarray offered considerably low visibility and the Cy5-labelled microarray offered moderate visibility.

As a secondary measure of performance, the variation observed within printed arrays was also considered. Coefficient of variation (CV) values were calculated from fluorescence images, with a performance threshold of <20% being implemented. Pacific Blue, Cy3, and Cy5-labelled baseline microarrays exhibited CV values of 7.0, 17.6, and 7.0, respectively – all within the acceptable range (Figure 4.4d). Comparatively, the CV value of FAM-labelled baseline microarrays was 26.1. Higher variation here was attributed to unintended transfer of PDMS residue onto the polyethylene substrate during micro-contact printing, which causes non-specific fluorescence at this wavelength.<sup>[469]</sup> Various approaches to minimize this transfer have been previously explored in literature, including plasma functionalization and sonication.<sup>[470,471]</sup>

When overlaid with foods, significant changes in CV values were observed (Figure 4.4e). Specifically, Pacific Blue-labelled microarrays exhibited very high CV values of 50.0, 55.0, and 57.9 with overlaid romaine lettuce, beef, and chicken, respectively. Thus, while these microarrays retained high SNR values when imaged with target foods – owing to their high baseline fluorescence intensity, their high variability limits their suitability for biosensing. Recognizing that Pacific Blue offers comparatively low stability,<sup>[472]</sup> it is likely that interactions with complex food matrices induced variable degradation of the label. FAM-labelled microarrays offered better consistency, but still surpassed the <20% performance threshold, with CV values of 26.3, 26.1, and 21.5 with the three respective food products. Oppositely, Cy3 and Cy5 offered values consistently below the set threshold, with Cy3 offering CV values of 16.9, 19.9, and 17.6 for the three respective products, and Cy5 exhibiting values of 7.0 and 8.2 for beef and chicken, respectively.

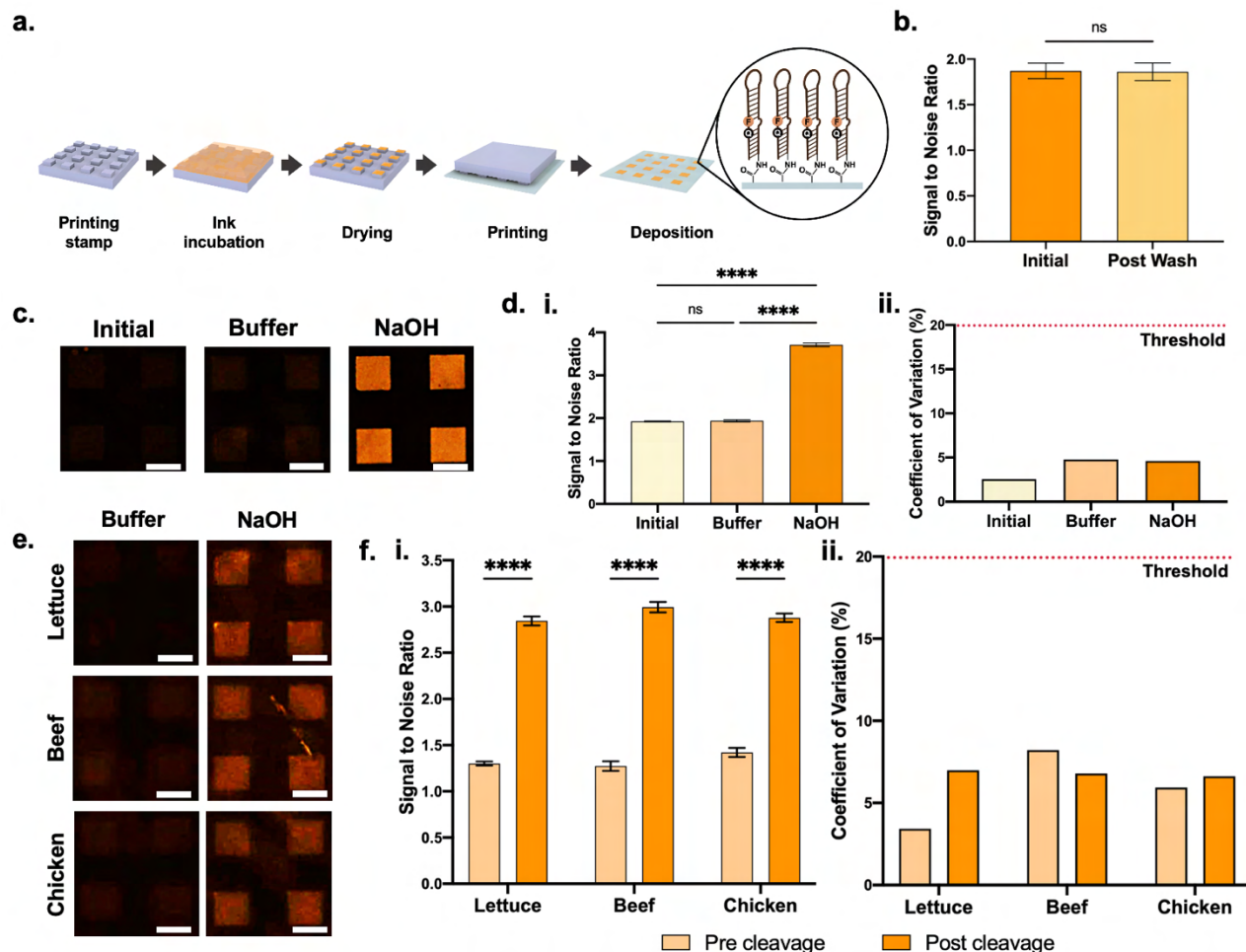
Based on all the presented data, Cy3 range fluorophores appears to offer the highest compatibility with the tested food products, based on the inherent fluorescence profiles of target products and the concurrent visibility of Cy3 arrays. While Pacific Blue-labelled microarrays offer high SNR values, poor CV values bring into question its stability, which limits its applicability for lengthy incubations with food. Cy5 range fluorophores exhibit excellent performance but are compatible only with meat products since the emission wavelength of chlorophyll is within the range of these fluorophores, rendering it incompatible with produce products.<sup>[463–465]</sup> Finally, FITC range fluorophores offered comparatively poor performance. While a SNR of about 4 was observed with overlaid food samples, substantiating its potential use within food monitoring, better alternatives are available.

#### **4.3.4 Stability and functionality of microcontact printed fNAPs**

Recognizing that Cy3 range fluorophores appear best suited for *in situ* sensing applications targeting the selected food products, we aimed to investigate the visibility of fNAPs conjugated with such labels. To this end, an aminated 5-Carboxytetramethylrhodamine (TAMRA)-labelled

fNAP construct was employed. While fluorescently labelled, single-stranded oligonucleotides can be visualized with relative ease given the abundance of fluorophores, fNAP visualization is complicated by the presence of associated quenchers. Confirming that such functional molecules can be visualized when exposed to food backgrounds is key in oligonucleotide-mediated sensing. Functionality was assessed using sodium hydroxide (NaOH), given its ability to hydrolyze the ribonucleotide cleavage site efficiently, thus inducing maximal fNAP signal generation.

A bio-ink composed of 3  $\mu$ M fNAP solution and N-ethyl-N'-(3-(dimethylamino)propyl) carbodiimide/N-hydroxysuccinimide (EDC/NHS) crosslinker solution was used to induce covalent immobilization onto carbon dioxide plasma-treated polyethylene substrates. Yet, owing to the limited control previously reported protocols for microcontact printing offer over biomolecule orientation,<sup>[209]</sup> insignificant changes in fluorescence intensity were observed following NaOH exposure. Thus, to better mediate fNAP orientation we introduced two modifications to our protocol (**Figure 4.5a**). First, the volume of residual solution present on stamps prior to deposition was increased. While this reduced print quality at times, it increased bio-ink transfer onto the target substrate. Second, printing was performed under 65% humidity. Both these measures increased moisture in the printing environment, yielding increased moisture on the target substrate. We hypothesize that this moisture allowed for some degree of fNAP and crosslinker mobility post-deposition, thus facilitating proper crosslinking and fNAP orientation.



**Figure 4.5. Stability and functionality of fNAP arrays deposited *via* microcontact printing.** (a) Schematic illustration of fNAP microcontact printing. (b) SNRs of fNAP arrays before and after wash cycle. (c) Fluorescence images of fNAP arrays before and after testing. (d) (i) SNRs and (ii) CVs of fNAP arrays before and after testing. (e) Fluorescence images of fNAP arrays overlaid with target food products. (f) (i) SNRs and (ii) CVs of positive and negative state fNAP arrays when overlaid with target food. Error bars show standard deviation. Significance is indicated via ns/\*\*\*\* markers, corresponding to no significance and  $P < 0.0001$ , respectively. Scale bars show 50  $\mu\text{m}$ .

Following deposition, fNAP microarrays were exposed to a vigorous wash cycle to evaluate the stability of fNAP attachment (Figure 4.5b). Quantitative measurements demonstrated an insignificant degree of detachment, with the SNR remaining at 1.8. With microarray stability established, functionality tests using NaOH were conducted, where a magnesium chloride-rich buffer solution acted as the negative control. Resultant images are provided in Figure 4.5c. While the baseline fNAP microarray exhibited a SNR of 1.9, NaOH exposure yielded a significant

increase as depicted by a SNR of 3.7 (Figure 4.5d.i). This corresponded with a fold change of 2 respective to the baseline fNAP array. Importantly, the buffer control exhibited no evident change, retaining a SNR of 1.9. The three conditions offered CV values of 2.6%, 4.8%, and 4.6%, respectively, confirming high array consistency (Figure 4.5d.ii).

Next, the visibility of buffer and NaOH-exposed fNAP microarrays was evaluated against target food backgrounds. The resultant fluorescence images are presented in Figure 4.5e. While the presence of overlaid food products expectedly interfered with the visibility of fNAP microarrays, both pre and post-cleavage states remained distinguishable. Of course, pre-cleavage microarrays offered minimal visibility, with SNRs of 1.3, 1.3, and 1.4 for romaine lettuce, beef, and chicken, respectively (Figure 4.5f.i). Comparatively, post-cleavage microarrays exhibited SNRs of 2.8, 3.0, and 2.9 with the three respective food products. With optimization of fNAP concentration and incubation conditions, the SNR of such systems can be expected to improve. More definitively, image processing would significantly increase the SNR of the presented platform, as the reported values were all derived from unprocessed images to provide a baseline evaluation of sensor signal intensity. All conditions offered CV values below 10%, confirming minimal food-mediated disruption of the arrays (Figure 4.5f.ii).

Finally, to substantiate the microcontact printing of fNAPs against conventional approaches, its performance was compared to that of inkjet-printed fNAP arrays. Baseline inkjet arrays offered a SNR of 1.6, while the buffer and NaOH conditions yielded SNRs of 1.8 and 3.8, respectively (Figure S4.2). CV values were found to be well below the established 20% threshold as well. Here, the performance of the contact and non-contact printing strategies was similar. When overlaid with food, pre-cleavage inkjet arrays offered SNRs of 1.0, 0.8, and 0.8 with romaine lettuce, beef, and chicken, respectively (Figure S4.3). Comparatively, post-cleavage SNR with the three respective overlaid food products were 2.1, 1.7, and 1.8. This was considerably lower than what was observed with microcontact-printed fNAP arrays overlaid with food, suggesting that inkjet-printed fNAP arrays suffered more signal interference from food backgrounds. This can be

attributed to the comparatively low deposition homogeneity exhibited within singular inkjet-printed dots, which was likely induced by oligonucleotide aggregation within deposited droplets as a result of unintended evaporation. Nonetheless, the CV values were below the set threshold.

#### 4.4 Conclusion

With growing interest towards *in situ* food sensing platforms, establishing relevant baseline properties of target food products is of utmost importance. Optical sensing offers significant promise due to the ease with which such systems can be assessed in real-time throughout the entire food production pipeline, substantiating the need for optical evaluation of target foods. Accordingly, the comprehensive fluorescence profiles presented here for romaine lettuce, spinach, chicken, and beef and the adjacent visualization of these foods with fluorophore-labelled biomolecular arrays provides a foundation for future works in this space. With consideration towards all the presented data, Cy3 range fluorophores are best suited for platforms targeting the aforementioned food products, owing to the low inherent backgrounds of the products at this wavelength, paired with the high SNR and low CV of Cy3-labelled DNA microarrays. DAPI and FITC range fluorophores offer strong and moderate degrees of viability, respectively, while Cy5 range fluorophores are only applicable with livestock products.

Importantly, commercial manufacturing of *in situ* platforms requires rapid fabrication of sensors that are easily integrated onto food packaging materials. To this end, we demonstrate the functionalization of polyethylene food packaging films with fNAPs *via* contact printing. We are the first to report the contact deposition of functional DNA oligonucleotides – an approach that offers significant commercial potential, specifically with recent developments in roll-to-roll printing. Further, it overcomes the limited lateral resolution and bio-ink evaporation issues often associated with non-contact printing. Through the deposition of a range of bio-responsive oligonucleotides – appropriately labelled with suitable fluorophores, multiplex platforms can be easily produced using the strategies detailed in this study. Future studies based on this work may explore automating this contact printing process with fNAPs at an industrial scale to enable



offering cost efficient, individualized product contamination monitoring.<sup>[473]</sup> Additionally, signal amplification strategies or methods to minimize noise may also be explored.<sup>[24,37,38]</sup>

#### **4.5 Materials and Methods**

*Inherent fluorescence imaging of target food products.* All evaluated food products used in this study were sourced from three different local grocery stores to increase generalizability (Walmart, Fortino's, Food Basics; Hamilton, Canada). Iceberg lettuce, romaine lettuce, green leaf lettuce, and red leaf lettuce samples were layered to a thickness of 10mm and placed onto glass slides. Whole chicken and whole beef samples cut to a thickness of 10mm were similarly placed onto glass slides. 10mm thick ground chicken and ground beef samples were prepared using a doctor's blade deposition strategy to ensure homogenous thickness. Samples were imaged using a Nikon Ti-2 inverted microscope (New York, United States) at excitation and emission wavelength pairings of 350 nm/470 nm, 490 nm/525 nm, 557 nm/576 nm, and 649 nm/666 nm. The selected wavelengths cover the majority of the electromagnetic spectrum which spans from around 300 nm to 700 nm, enabling comprehensive fluorescence profiling for the variety of food products examined in this work. All images were taken at an exposure time of 300ms. Mean intensity was calculated for each collected image, and a minimum of ten images were taken for each sample. Average intensities for each food product were derived.

*Photobleaching analysis.* Romaine lettuce samples with a thickness of 10 mm were imaged using a Nikon Ti-2 inverted microscope under the Cy5 fluorescence channel (649 nm/666 nm) for four minutes. Images were automatically taken every 300 ms at an exposure time of 1s and the mean fluorescence intensity of the collected images were quantified. This procedure was repeated three times.

*Fluorescence imaging of target food products over time.* On Day 1, the target food products – romaine lettuce, spinach, ground beef, whole beef, ground chicken and whole chicken, were aliquoted into 10 g portions, which were stored within sealed bags at 4 °C. Each day, three samples were deposited as 10 mm slices onto glass slides as previously described. Samples were imaged

under the same parameters as the baseline studies – at excitation and emission wavelength pairings of 350 nm/470 nm, 490 nm/525 nm, 557 nm/576 nm, and 649 nm/666 nm using a Nikon Ti-2 inverted microscope set to an exposure time of 300 ms. Mean intensity was calculated for each collected image, and a minimum of ten images were taken for each sample. This process was repeated five times using food products from different grocers to ensure reproducibility in the reported trends.

*Contact printing stamp preparation.* Polydimethylsiloxane SYLGARD 184 (Dow Corning, Michigan, United States) was prepared using a 10:1 weight ratio of base resin to curing agent. This mixture was stirred for 10 min and subsequently desiccated for 20 min. The uncured mixture was then poured onto a micro-patterned silicon wafer to a thickness of 1 cm. The polydimethylsiloxane was then heat cured at 145 °C over 15 mins, mediating pattern transfer from the wafer to the polymer.<sup>[209]</sup> The cured polymer was then cut into 1 cm × 1 cm × 1 cm cubes, which were used as stamps for microcontact printing.

*Oligonucleotide contact printing.* 10 µL oligonucleotide solutions (Integrated DNA Technologies, Iowa, United States; Millipore Sigma, Texas, United States) containing 3 µM DNA diluted in DNase-free water (ThermoFisher Scientific, Ontario, Canada) were deposited onto micro-patterned polydimethylsiloxane stamps and incubated for 8 min. Concurrently, glass slides wrapped with the target polyethylene substrate (Thomas Scientific, New Jersey, United States) were oxygen plasma-treated for 3 mins (PlasmaEtch, Nevada, United States). Subsequently, the stamps were briefly rinsed in phosphate buffered saline (Bioshop Canada, Ontario, Canada). and deionized water. Following momentary drying under nitrogen flow, the stamps were placed onto the oxygen plasma-treated polyethylene substrates and weighed down with 500 g of mass. After 2 mins, the stamps were removed.

*Fluorescence imaging of patterned fluorescently labelled oligonucleotides.* Baseline imaging of printed arrays was conducted at an exposure time of 1s using a Nikon Ti-2 inverted microscope. Images were captured at 4× and 10× magnifications. Stability testing involved imaging under the

same parameters after 30 mins of immersed water wash at 220 RPM using a shaking incubator (VWR, Ontario, Canada). Food overlay imaging using romaine lettuce, ground beef, and whole chicken was done under the same parameters, but with 10 mm thick samples placed on the arrays.

*fnAP synthesis.* A substrate strand possessing a fluorophore-quencher separated by a riboadenosine base (Keck Oligonucleotide Synthesis Facility, Yale University, Connecticut, United States) was enzymatically ligated to the 5' terminal of a probe fragment with a 3' amino modification (Integrated DNA Technologies, Iowa, United States). This was templated by a splint strand. In preparation for ligation, 4 nmol of the probe strand was first phosphorylated using excess adenosine triphosphate, 1× T4 polynucleotide kinase buffer A and 40 U T4 polynucleotide kinase in a 50 µL reaction at 37 °C for 30 minutes (Thermofisher Scientific, Ontario, Canada). Following phosphorylation, 4 nmol of the substrate strand and 4 nmol of the split strand were added to the reaction, then heated at 90 °C for 1 minute and cooled at room temperature for 5 minutes to anneal the fragments. The cooled ligation reaction was then diluted to 400 µl by addition of T4 DNA ligase buffer to 1×, 20 U T4 DNA ligase, and water (Thermofisher Scientific, Ontario, Canada). The ligation reaction was then incubated at room temperature for 1 hour and ethanol precipitated using 2.5 volumes of chilled ethanol, followed by centrifugation at 4 °C, 20000 × g for 20 minutes. The ligated product was purified on a 10%, 8 M urea polyacrylamide gel. The band corresponding to the ligated product was excised from the gel, crushed, and eluted in buffer (200 mM NaCl, 10 mM Tris pH 7.5, 1 mM EDTA; Thermofisher Scientific, Ontario, Canada). The elution supernatant containing the nucleic acid probe was then ethanol precipitated, followed by a final wash with 70% ethanol. The pellet was then air dried and resuspended in water.

*Inkjet-printed fnAP arrays.* A print solution containing 3 µM nucleic acid probe, EDC, and NHS was prepared in MES buffer at a pH of 4.5 (Millipore Sigma, Ontario, Canada).<sup>[201]</sup> A GeSIM Nanoplotter 2.0 (Radeberg, Germany) was used to deposit 12 nL droplets onto carbon dioxide plasma-treated polyethylene substrates. Each array was composed of 36 spots arranged in a 6 × 6 configuration. Each slide contained four arrays, ensuring replicates with all subsequent assays.

Printed arrays were incubated at 70% humidity for 2 h to mediate covalent attachment. The sensors were then washed in deionized water for 30 mins at 220 RPM using a shaker set to 40 °C.

*Contact-printed fNAP arrays.* A print solution containing 3  $\mu$ M nucleic acid probe, EDC, and NHS was prepared in MES buffer at a pH of 4.5.<sup>[201]</sup> 10  $\mu$ L of the solution was deposited onto polydimethylsiloxane stamps and incubated for 8 mins. Concurrently, glass slides wrapped with the target polyethylene substrate were carbon dioxide plasma-treated for three minutes. The solution was subsequently pipetted off, to permit control over residual volume present on the stamps. The stamps were then momentarily exposed to nitrogen flow, and then placed onto carbon dioxide plasma-treated substrates and weighed down with 500g of mass under 65% humidity. After two minutes, stamps were removed. The substrates were left under humidity for 30 mins before testing, to permit covalent attachment.

*fNAP functionality testing.* Inkjet and contact printed arrays were incubated with 0.5 M sodium hydroxide (Millipore Sigma, Texas, United States) as a positive test condition and deionized water as a negative test condition.<sup>[17]</sup> Arrays were imaged prior to incubation to establish baseline intensities. Arrays were then incubated with 200  $\mu$ L of test solution for 2 h and subsequently imaged again. All imaging occurred at 1 s exposure using a Nikon Ti-2 inverted microscope. The visibility of positive state fNAPs when overlaid with food involved imaging with 10 mm samples of romaine lettuce, ground beef, and whole chicken placed on top of the arrays.

*Fluorescence quantification.* Mean fluorescence intensities for the determination of the inherent fluorescence of target food products were calculated by the NIS Elements imaging software. SNR and CV values of oligonucleotide arrays both with and without overlaid romaine lettuce, ground beef, and whole chicken food backgrounds were calculated using ImageJ.

*Statistical analysis.* All data in this work are presented as the mean across a minimum of triplicate measurements with all error bars representing the standard deviation across all measurements. A paired, 2-tailed t-test, CI 95% was used to analyze the SNRs of fNAP before and after the wash

cycle (Figure 4.5b). One way ANOVA tests, CI 95%, were used to analyze the SNRs of the fNAP arrays before and after testing with buffer and NaOH (Figure 4.5d.i) and the positive and negative state fNAP arrays when overlaid with romaine lettuce, ground beef, and whole chicken samples (Figure 4.5f.i). *P* values greater than 0.05 were considered insignificant indicated by *ns* and *P* < 0.0001 was indicated by \*\*\*\*. All graphs and associated statistical analysis were completed using GraphPad Prism.

#### **4.6 Acknowledgements**

S.K. is a recipient of the Vanier Canada Graduate Scholarship awarded by the Natural Sciences and Engineering Research Council of Canada. J.K.M. and S.T. are recipients of Undergraduate Student Research Awards from the Natural Sciences and Engineering Research Council of Canada. T.F.D. is a Tier II Canada Research Chair in Nanobiomaterials. This work was funded by Toyota Tsusho Canada Incorporated and Mitacs.

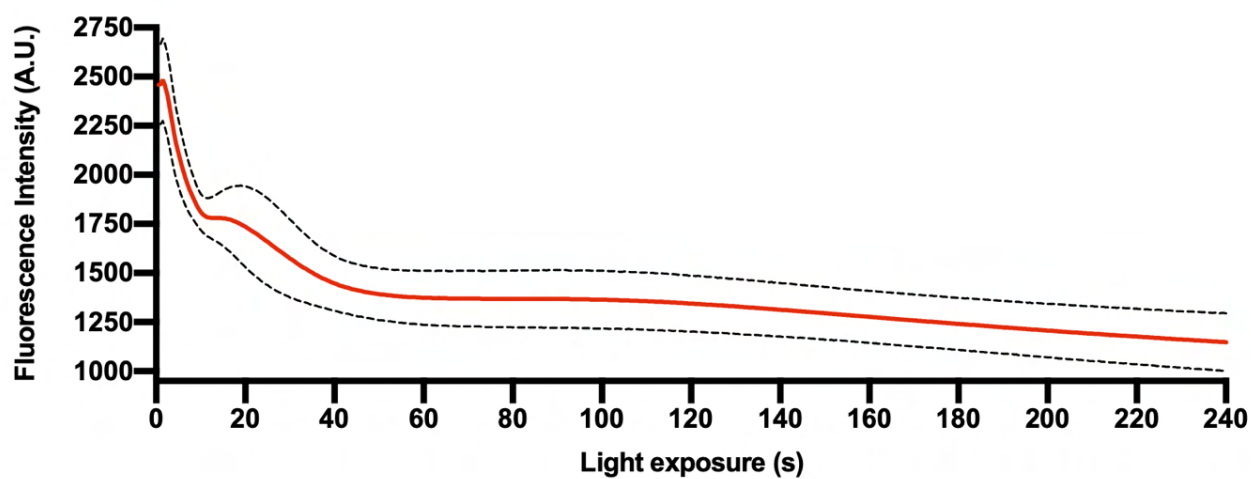
#### **Competing Interests**

The author(s) declare no competing interests.

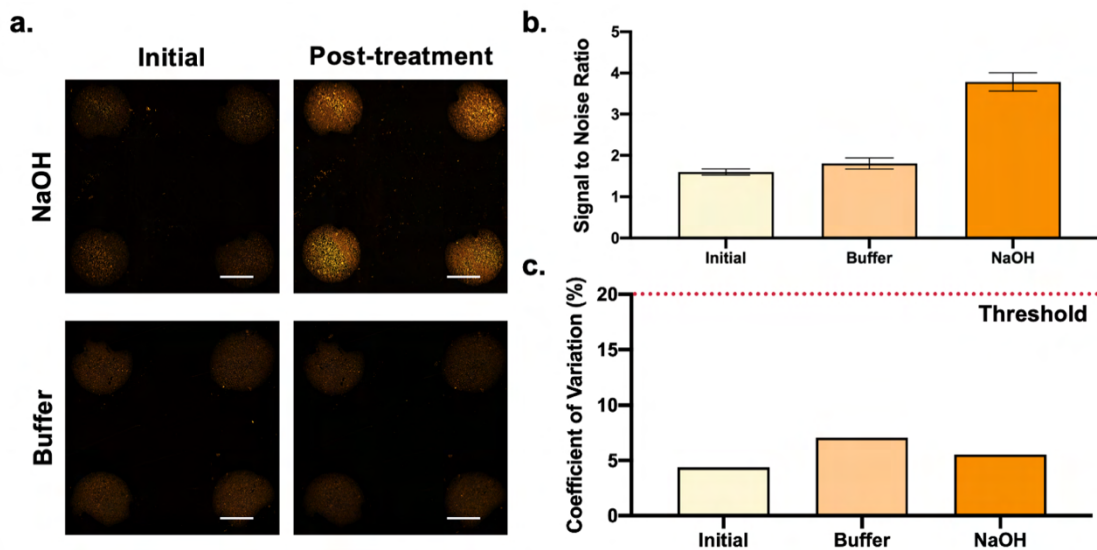
## 4.7 Supplementary Information

**Table S4.1.** Fluorescently labelled single stranded oligonucleotides used in the study.

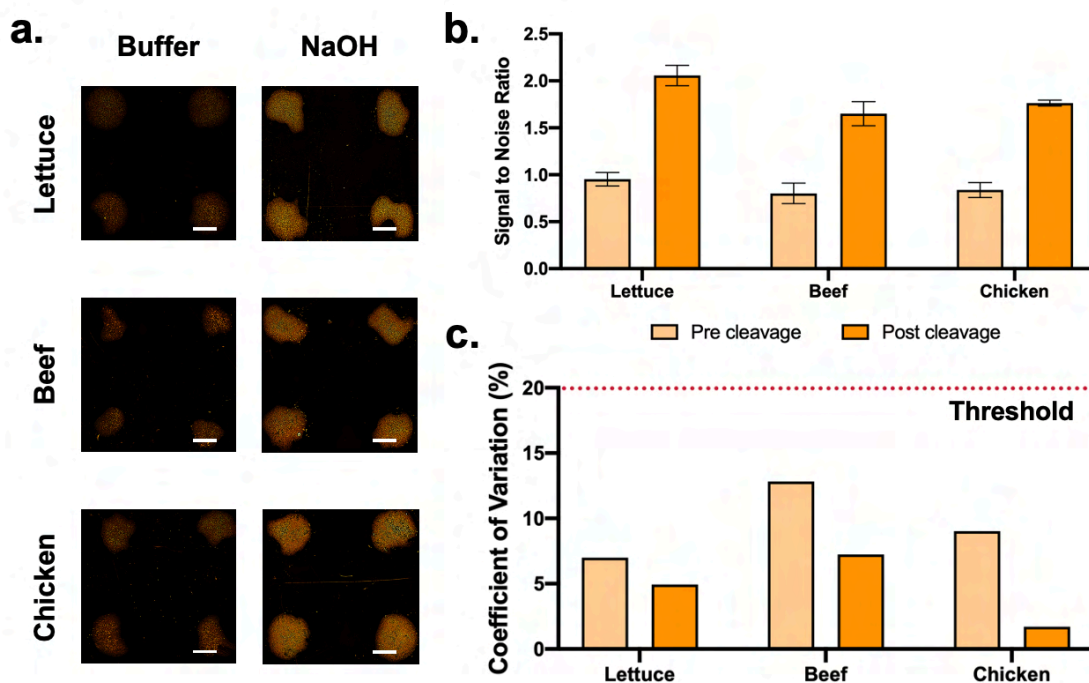
Probe	Sequence
PacBlue	ACCAGTGCTCAGACA/PacBlue
FAM	AmC6/ACCAGTGCTCAGACA/36-FAM
Cy3	AmC6/ACCAGTGCTCAGACA/Cy3
Cy5	AmC6/ACCAGTGCTCAGACA/Cy5



**Figure S4.1.** Photobleaching of romaine lettuce under the Cy5 channel over four minutes.



**Figure S4.2.** Inkjet-printed RNA-cleaving fluorescent nucleic acid probe arrays. (a) Fluorescence images before and after positive and negative control treatments. Scale bars indicate 200μm. (b-c) SNR and CV values of resultant arrays, respectively. Error bars represent standard deviation.



**Figure S4.3.** Inkjet-printed RNA-cleaving fluorescent nucleic acid probe arrays overlaid with food products. (a) Fluorescence images of positive and negative control-treated arrays with overlaid food samples. Scale bars indicate 200μm. (b-c) SNR and CV values of resultant arrays, respectively. Error bars represent standard deviation.

## Chapter 5: Advancing in situ Food Monitoring Through a Smart Lab-in-a-Package System Demonstrated by the Detection of Salmonella in Whole Chicken

### Preface

Now armed with a better understanding of the fluorescence sensing-relevant properties of target foods, we sought to develop impactful food monitoring systems with better design considerations. This chapter details such a design measure, through the employment of a novel Salmonella-responsive fNAP that is labelled with a TAMRA fluorophore for optimal visibility on the chicken food matrix used in this study. Concurrently, this chapter details the development of an in-package test sample collection and reagent integration mechanism, in accordance with Objective 2. Coined Lab-in-a-Package, the platform employs an inclined packaging tray that concentrates purge released from chicken to a central testing site. This site has a cut-out for the integration of a transparent optical sensor, to ensure that products can be monitored without any disruption of the closed package. Optimization of the packaging tray involved fluid dynamic analysis of different tray designs. Overlaying the embedded sensor is a membrane that localizes food-safe reagents that are necessary for RFD sensor functionality. The membrane being located adjacent to the sensing interface ensures high reagent availability. Optimization of the membrane centered upon material selection based on platform-relevant properties. Subsequent combination of the Salmonella fNAP sensor and redesigned food packaging tray enabled effective monitoring of contaminated ready-to-eat (RTE) whole chicken – even when contamination was sourced from indirect modes of contamination. The sensitivity, specificity, and stability of the fNAP sensor, with considerations made towards long-term storage and diverse food storage temperatures. Finally, the system was employed for actualized hands-free, non-disruptive monitoring of a sealed chicken product contaminated with *Salmonella* using a handheld fluorescence reader and smartphone. Accordingly, this platform presented a comprehensive in-package sensing platform that accounted for real-world variables that were often overlooked in prior literature.

### Authors

Akansha Prasad<sup>†</sup>, Shadman Khan<sup>†</sup>, Jonathan K. Monteiro, Jiuxing Li, Fatima Arshad, Liane Ladouceur, Lei Tian, Amid Shakeri, Carlos D. M. Filipe, Yingfu Li, Tohid F. Didar

<sup>†</sup> These authors contributed equally.

In this work, the design of the 3D-printed packaging tray involved consideration towards incline angles of 45°, 60°, and 90°. The fluid transfer capabilities of the trays were assessed to determine the best form factor for test sample localization. Concurrent membrane selection involved considerations towards factors such as background fluorescence, porosity, fluid capacity, fluid retention, fluid diffusivity and microbial diffusivity. Cotton, cotton-cellulose, cellulose, cellulose-polyester and polyester membranes were considered. With regards to fNAP surface sensor development, the amine-modified oligonucleotide was covalently bonded onto packaging film



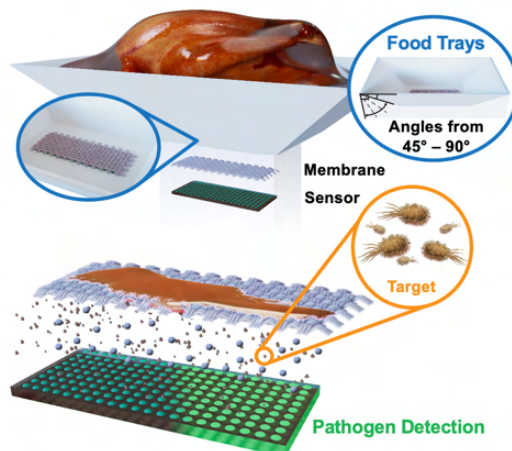
using N-(3-Dimethylaminopropyl)-N'-ethylcarbodiimide (EDC)/ N-Hydroxysuccinimide (NHS) crosslinking. The LOD of the fNAP sensor was evaluated using bacterial dilutions ranging from  $10^3$  to  $10^8$  CFU/mL, alongside its stability and specificity. After optimizing the magnesium ion buffer concentration necessary for in-package fNAP functionality, contaminated ready-to-eat (RTE) chicken with bacterial loads ranging from  $10^2$  to  $10^6$  CFU/g were evaluated. Chicken products that were indirectly contaminated *via* gloves, surfaces and utensils were also evaluated, to determine if the contamination mechanism impacted sensor performance. Finally, closed package imaging using a handheld fluorescence reader and smartphone was performed on RTE chicken, to demonstrate actualized real-time, hands-free contamination monitoring.

## Publication

Advanced Materials, 2023, 35, 2302641

## Publication Date

June 2023



## 5.1 Abstract

With food production shifting away from traditional farm-to-table approaches to efficient multi-step supply chains, the incidence of food contamination has increased. Consequently, pathogen testing *via* inefficient culture-based methods has increased, despite its lack of real-time capabilities and need for centralized facilities. While *in situ* pathogen detection would address these limitations and enable individual product monitoring, accurate detection within unprocessed, packaged food products without user manipulation has proven elusive. Herein, we present Lab-in-a-Package, a platform capable of sampling, concentrating, and detecting target pathogens within closed food packaging, without intervention. This system consists of a newly designed packaging tray and reagent-infused membrane, that can be paired universally with diverse pathogen sensors. The inclined food packaging tray maximizes fluid localization onto the sensing interface, while the membrane acts as a reagent-immobilizing matrix and an antifouling barrier for the sensor. The platform is substantiated using a newly discovered *Salmonella enterica* serovar Typhimurium-responsive nucleic acid probe, which enables hands-free detection of  $10^3$  CFU/g target pathogen in a packaged whole chicken. The platform remains effective when contamination is introduced with culinary tools, gloves, and surfaces, ensuring widespread efficacy. Its real-world use for *in situ* contamination detection is simulated using a handheld fluorescence scanner with smartphone connectivity.

**Keywords:** food contamination, pathogen detection, *in situ* monitoring, *Salmonella* detection, smart packaging, food sensing, functional DNA probe

## 5.2 Introduction

Foodborne illness represents a growing crisis, with an estimated annual caseload surpassing 600 million globally – largely attributed to the consumption of pathogen-contaminated food products.<sup>[474]</sup> In the United States alone, there are an average of 37 million annual incidences of foodborne illness, with associated treatment costs exceeding \$14 billion.<sup>[475,476]</sup> Concerningly,

the growing demand for food and climate change-induced shifts in the prevalence of pathogens such as *Escherichia coli* and *Salmonella enterica* serovar Typhimurium are expected to intensify this crisis in the coming years.<sup>[477–479]</sup> While various procedural and regulatory interventions have been introduced to reduce the incidence of food contamination, testing all foods as they transition through the food production pipeline remains instrumental in illness prevention. That being said, ready-to-eat (RTE) food products are of particular concern, given the lack of a cooking step prior to consumption.<sup>[480]</sup> Unfortunately, culturing protocols remain the industry standard for such testing, despite their costly, laborious, and time-consuming nature.

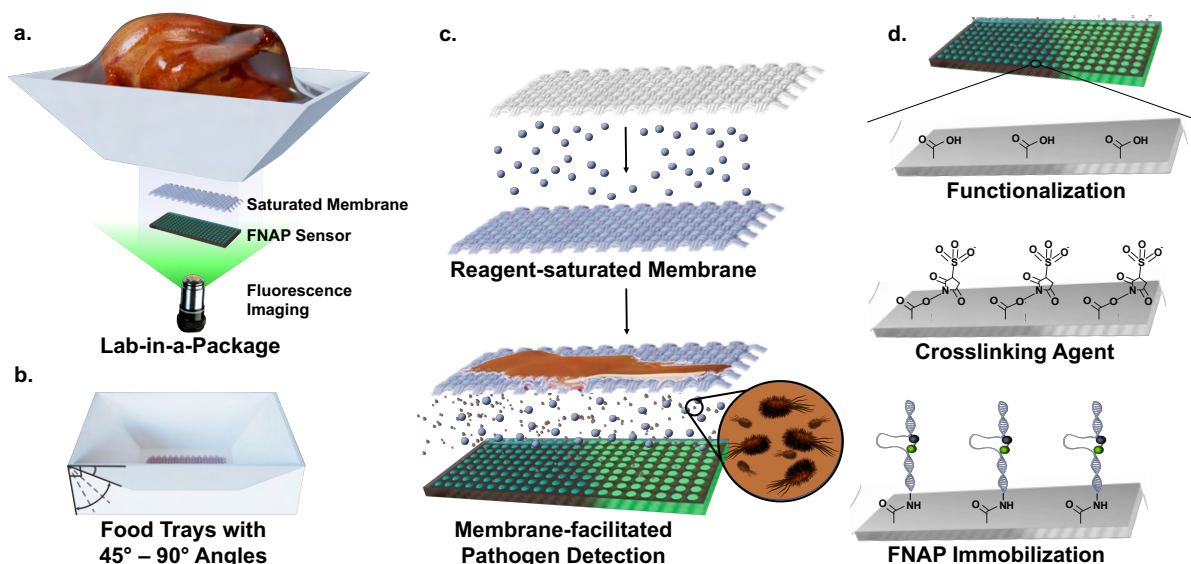
In an effort to address these limitations, several on-site detection platforms have been developed.<sup>[195,202,203,214,468,481]</sup> However, such systems yield significant food waste and operate under the assumption that the food products selected and opened for testing are representative of all products within a given batch. To advance individual product monitoring, in-package incorporation of pathogen sensors is required – a premise that has been explored using various sensing modalities.<sup>[8,25,96,192,204,208,482]</sup> Specifically, functional bacteriophages, oligonucleotides, and antibodies have all been used *in situ* as highly specific biorecognition probes for the detection of pathogens within complex food matrices. While promising proof-of-concepts have been reported, the means by which these systems have been validated are not commercially feasible.<sup>[17,197,206]</sup> Namely, these probes all rely on complementary reagents such as buffers and metal ions for functionality, meaning that food samples must be extensively treated with these agents prior to testing – a measure that severely alters their organoleptic properties. Further, reported tests largely involve the contamination and testing of small food samples, wherein target bacteria is localized to the test site. In reality, contamination can occur at any given site on bulk food products with large surface areas. Given that placing sensors across an entire food surface is commercially unfeasible, testing in a manner that provides results representative of the entire food sample is difficult. Lastly, these sensors largely detect target pathogens within liquid test media, which is not easily isolated within closed packaging systems. Consequently, there exists a critical

gap between the myriad of sensing platforms discovered in recent works and their real-world implementation into food packaging for real-time food monitoring, necessitating the innovation of traditional packaging.

While food packaging has been reengineered significantly in recent years to create intelligent packaging materials that are more sustainable, delay food spoilage, and have innate antibacterial capabilities, redesign aimed at improved *in situ* sensing has not been proposed.<sup>[37,483–487]</sup> Under this premise and based on the aforementioned limitations, we propose that an ideal food monitoring packaging system should: (1) enable sensor visualization without disrupting the closed package, (2) localize all sample solution released by the food matrix onto the sensor, (3) retain necessary reagents within the food packaging in a manner that minimizes organoleptic alternations to the adjacent food, and (4) facilitate analyte diffusion from the food matrix onto the sensor surface. Achieving these four objectives would then enable (5) the *in situ* integration of novel biorecognition elements, to advance complete hands-free, real-time monitoring of packaged foods – the primary objective of this work. Importantly, the proposed system must employ food safe materials to ensure regulatory and commercial viability.

Consequently, we have developed a three-pronged food-safe packaging system consisting of a newly designed food packaging tray to meet objectives (1) and (2) and a membrane interface to meet objectives (3) and (4). The developed Lab-in-a-Package platform is completed through the incorporation of pathogen sensors, which act to facilitate sensing within individual packages. Importantly, the generalized nature of the developed packaging tray and membrane interface enable the universal incorporation of various pathogen sensing platforms. For this study, a new synthetic fluorescent nucleic acid probe (FNAP) highly specific to *S. Typhimurium* was developed to meet objective (5). The probe functions as a highly specific substrate for cleavage by the RNase H2 protein of *S. Typhimurium* – a reaction that can be monitored through the integration of a fluorophore-quencher pairing into the FNAP construct. Incorporation of the newly discovered probe with the tray and membrane, yielded the complete Lab-in-a-Package platform. Artificially contaminated bulk, RTE chicken products were subsequently stored within this sensor-embedded

packaging system, wherein high detection performance was observed. Next, recognizing that different avenues of contamination localize pathogens on food products in different ways, bulk, RTE chicken products were exposed to *S. Typhimurium*-contaminated culinary instruments, gloves, and surfaces and subsequently monitored using Lab-in-a-Package. The platform's high detection performance was maintained. Finally, the platform's real-world use was fully simulated using a handheld fluorescence scanner with smartphone connectivity, wherein successful target detection was observed without any disruption to the closed package.



**Figure 5.1. Schematic illustration of the Lab-in-a-Package platform.** (a) Complete Lab-in-a-Package in situ detection platform with inclined packaging tray, reagent-saturated membrane, and sensor incorporation shown for RTE chicken products. Imaging procedure involving fluorescence scanning also shown. (b) Inclined food packaging trays with angles ranging from 45° to 90° to optimize test sample localization. (c) Depiction of membrane saturation with reagent components, diffusion of buffer components and target analyte to sensor surface, and fouling prevention. (d) FNAP sensor development with corresponding material surface and biochemical modifications.

## 5.3 Results and Discussion

### 5.3.1 Lab-in-a-Package platform design

Overarchingly, we sought to develop Lab-in-a-Package to facilitate test sample localization, *in situ* reagent incorporation, target diffusion, and fouling prevention on the sensing interface. Collectively, these efforts contribute to pathogen detection – all while eliminating the

need to open food packaging or manipulate food products. The integration of the aforementioned universally applicable novel food packaging tray design, membrane interface, and pathogen sensor are shown in **Figure 5.1**. Importantly, all materials considered in this study were selected from the Indirect Food Substances provisions, ensuring regulatory viability in accordance with the Generally Recognized As Safe (GRAS) designation from the Food and Drug Administration (FDA).<sup>[488]</sup>

### 5.3.2 Test sample localization optimization

A dramatic shift in packaging design compared to traditional packaging was performed to facilitate sensor visualization and localization of sample fluids. A sensing window was first introduced to enable the integration of fluorescent sensing interfaces that can be monitored without opening packaged foods. Optimization of fluid localization from target food matrices was then explored through three packaging trays with varying levels of incline – 45°, 60°, and the traditional 90°, which were fabricated using 3D printing (**Figure 5.2a**, S5.1, S5.2). Here, the angle refers to the incline at the fluid-package interface. The 60° model was developed as an intermediary model to substantiate any trends observed with changes in incline angle.

Fluid transfer efficiency of the models was first assessed, where the 90° model significantly outperformed the other models ( $P < 0.01$ ). This was attributed to its steeper angle, inducing the strongest forces of downward acceleration (Figure 5.2b). Accordingly, the 60° model also outperformed the 45° model. Yet, while fluid transfer efficiency offers an important preliminary understanding of the models' fluid transport capabilities on a droplet scale, macroscale fluid accumulation at a central collection site better defines suitability for the desired application. As such, subsequent tests focused on characterizing the localization efficiency of each model. This was first accomplished by measuring fluid localization over time (Figure 5.2c). Here, the 45° model significantly outperformed the 60° ( $P < 0.001$ ) and 90° models ( $P < 0.0001$ ). This improved performance was attributed to the 45° model offering a consistent decline directly into the sensor window for the milliliter-scale test volumes. Fluid localization was then evaluated based on the volume localized onto the sensing window within a fixed period of time with both phosphate

buffered saline (PBS) (Figure 5.2d) and chicken purge (Figure 5.2e). Specifically, this was represented as the percentage of volume localized and was calculated according to Equation (1) below.

$$\% \text{ volume localized} = \frac{V_f}{V_i} \times 100\% \quad \text{Equation (1)}$$

Here,  $V_f$  represents the final volume collected from the base of the packaging tray after a constant timepoint, and  $V_i$  is the initial volume of fluid applied to the trays at the start of the study. In both studies, the 45° model exhibited significantly higher fluid localization compared to both the 60° ( $P < 0.001$ , 0.01) and 90° models ( $P < 0.0001$ , 0.001). However, overall localization with chicken purge was lower due to a combination of a viscosity-induced reduction in fluid transfer rate and a longer incubation time. Together, these factors led to purge drying along the fluid-package interface prior to reaching the sensor window, decreasing the fluid volume available for localization. A timepoint analysis of this study was also briefly conducted (Figure S5.3). Ultimately, the 45° model was selected for use within the final Lab-in-a-Package platform given its superior localization when compared to the collective properties exhibited by the other models as quantitatively summarized in Table S5.1.

### 5.3.3 Absorption and diffusion-focused materials characterization

With regards to the membrane interface, the buffer absorption, macromolecular filtration, and target diffusion properties of five candidate materials were evaluated (Figure 5.1c). Namely, cotton, cotton-cellulose, cellulose, cellulose-polyester, and polyester materials were considered, owing to their inherent biocompatibility, filtering potential, and permeability. The candidate membranes were imaged *via* optical microscopy (Figure S5.4) and scanning electron microscopy (SEM) (Figure 5.2f) to visualize their fibrous structures. Cotton exhibited the most unique structure due to its convoluted fibril arrangement, with comparatively larger pores.<sup>[489]</sup> All materials exhibited low fluorescence across the visible light spectrum, substantiating further characterization given their potential applicability to fluorescent systems (Figure 5.2g).

After optical characterization, the absorption capacity of candidate membranes was assessed by volume (Figure 5.2h) and over time (Figure S5.5). Here, cotton-cellulose significantly outperformed all other candidate membranes ( $P < 0.0001$ ). This was attributed to the abundance of cellulose hydroxyl groups present within the matrix, giving the material high hydrophilicity and affinity for moisture.<sup>[490]</sup> While pure cellulose offers a larger number of hydroxyl groups, cotton-cellulose has comparatively higher crystallinity, resulting in the formation of complex hydrogen bonds that further elevate hydrophilicity and in turn, buffer absorption.<sup>[491]</sup> As polyester fibres are densely packed and lack polar groups, they are intrinsically hydrophobic and thus had the lowest absorption.<sup>[492]</sup> Buffer retention was subsequently evaluated within a closed package environment, wherein all of the candidate materials exhibited limited changes in buffer volume after 120 hours (Figure S5.6).

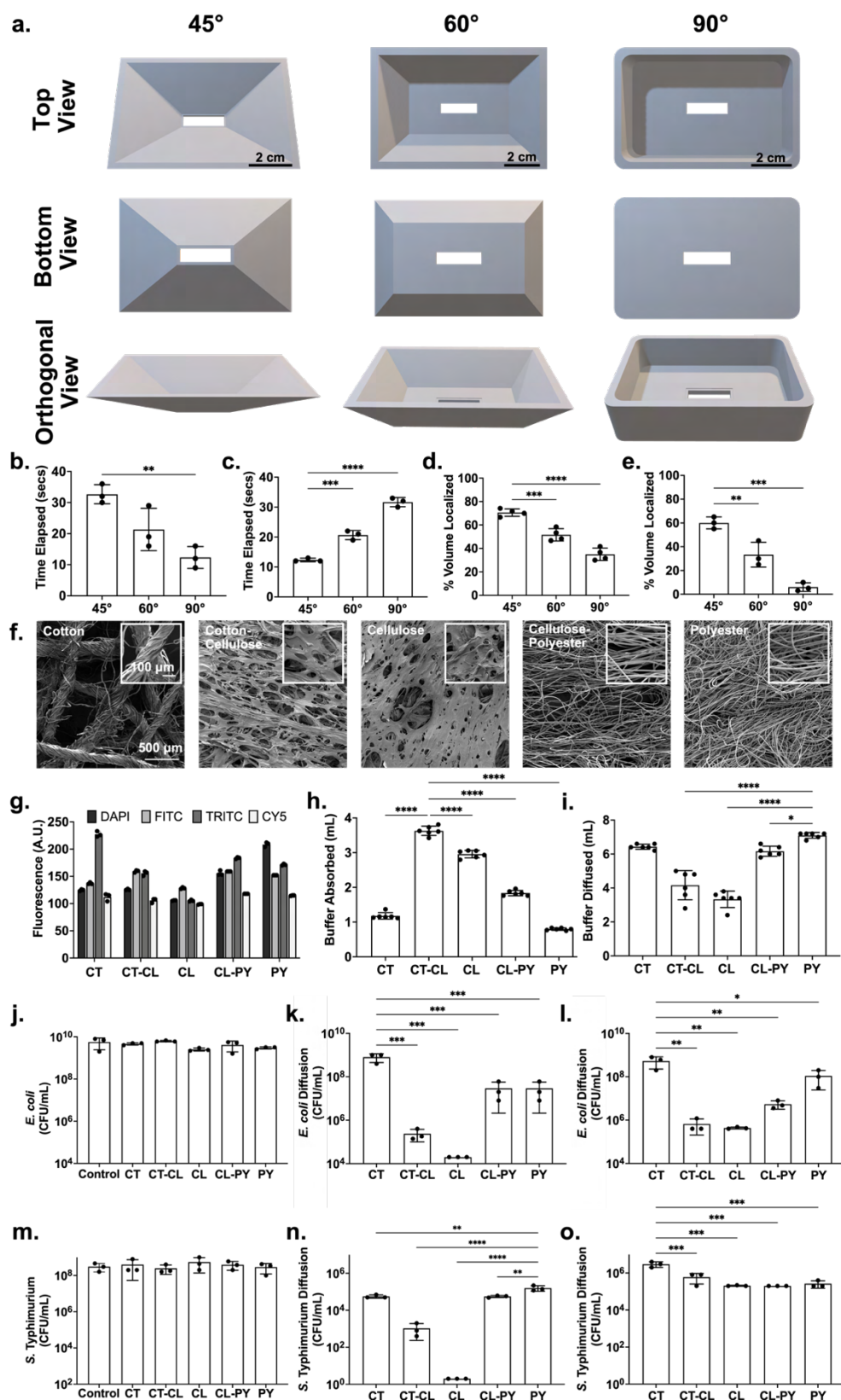
Next, diffusion testing was performed to ensure that agents of interest can permeate through the membrane matrix onto the sensing interface. Polyester, cellulose-polyester, and cotton membranes performed best in preliminary buffer diffusion studies (Figure 5.2i). Bacterial diffusion was subsequently evaluated using *E. coli*. A preliminary control study confirmed that the candidate materials did not influence bacterial proliferation or survival (Figure 5.2j). Two bacterial diffusion studies were then performed with both unsaturated and buffer-saturated membranes to evaluate the effects of hydration on bacterial diffusion (Figure 5.2k-l). In both studies, cotton significantly outperformed all other candidate materials, facilitating the diffusion of *E. coli* at a concentration of  $10^9$  CFU/mL in both unsaturated ( $P < 0.001$ ) and saturated states ( $P < 0.01$ ), given its unique fibrous arrangement. Membrane performance was also tested with *S. Typhimurium* (Figure 5.2m-o). Again, no effect on bacterial proliferation or survival was observed. Similar trends were observed with the five membrane candidates with regards to bacterial diffusion, except that the magnitude of diffusion was much lower in the unsaturated state with *S. Typhimurium*. This is attributed to its larger size, requiring saturation-mediated pore expansion for substantial diffusion opportunities.<sup>[493,494]</sup>



Finally, porosity was also directly quantified as the percentage of the total top surface covered by pores within previously collected SEM images (Figure S5.7). Here, the cotton membrane had the best combination of surface porosity and low fiber density, making its pores better suited for the facilitation of buffer and bacterial diffusion. Consequently, cotton membranes were selected given their high buffer retention, diffusion, and porosity when compared to the other materials, as summarized in Table S5.2. While the material offered comparatively lower absorption capacity, we hypothesized that this drawback could be overcome through the use of a more concentrated reagent mix.

Lastly, the benefits of a cotton membrane as a physical barrier between a food sample and the sensing substrate were explored. Specifically, recognizing that food represents a very complex matrix, fouling of the sensing interface is a major concern. The optical density of crude chicken purge and chicken purge processed through cotton membranes was measured for each sample (Figure S5.8a). The collected values showed that the cotton membrane significantly decreased the presence of macroscale entities present within the chicken purge test samples ( $P < 0.0001$ ). This effect can be expected to be amplified with the saturation of the cotton membrane, as wet cotton fibres offer a larger physical footprint and higher mechanical strength.<sup>[489]</sup>

To visualize anti-diffusive effects towards macroscale entities, buffer-saturated cotton membranes were visualized *via* SEM after chicken purge processing (Figure S5.8b). These images indicated lipid deposition onto the cotton fibres at a macroscale, while retaining sufficient porosity to permit analyte and buffer diffusion at the microscale, further substantiating the use of this membrane within the proposed platform.



**Figure 5.2. Characterization of packaging models and membrane candidates based on application-relevant properties.** (a) CAD models for all packaging models with top, bottom, and

orthogonal views shown. (b) Time required for water a droplet to fall down packaging edge. (c) Time required for 5 mL of buffer to reach sensing window when dispensed at a rate of 0.5 mL/s. (d) Percentage of original PBS volume localized on sensing window after 1 minute when dispensed at a rate of 0.2 mL/s. (e) Percentage of original chicken purge volume localized after 24h at 37°C. (f) SEM images of candidate membranes at 100X with overlays at 500X. (g) Mean background fluorescence of candidate membranes. (h) Absorption capacity of candidate membranes. (i) Volume of buffer diffused through candidate membranes after 2 minutes. (j) Membrane effects on bacterial growth following a 6h incubation with *E. coli*. (k-l) Bacterial diffusion through (k) unsaturated and (l) buffer-saturated membranes onto underlying substrates following a 6h incubation at 37°C with *E. coli*. (m) Membrane effects on bacterial growth following a 6h incubation with *S. Typhimurium*. (n-o) Bacterial diffusion through (n) unsaturated and (o) buffer-saturated membranes onto underlying substrates following a 6h incubation at 37°C with *S. Typhimurium*. All reported values represent the mean of all samples with error bars representing sample standard deviation. All asterisks represent significant differences at corresponding significance levels.

#### 5.3.4 *S. Typhimurium* sensor development

With packaging and membrane optimization complete, we next sought to incorporate a compatible sensor into the developed platform. While we have previously reported *E. coli*-responsive, real-time fluorescence sensors for potential *in situ* incorporation, growing concerns surrounding *S. Typhimurium* contamination led us to develop a new sensor altogether.<sup>[17,208]</sup> Using systematic evolution of ligands by exponential enrichment (SELEX), a highly sensitive nucleic acid probe that cleaves in the presence of RNase H2 from *S. Typhimurium* was identified. This probe was hybridized with a substrate strand embedded with a fluorophore-quencher pairing. *S. Typhimurium*-induced cleavage induced quencher separation, yielding an increase in fluorescence (**Figure 5.3a**). The complete sequence for this construct is provided in Table S5.3.

The surface-immobilized sensor was developed through the covalent attachment of an aminated, FITC-labelled version of the *S. Typhimurium*-responsive probe to polyethylene food packaging substrates. To ensure an adequate sensor signal, probe surface density was optimized and subsequently quantified to be  $1.3 \times 10^{-5}$  nmol per array spot (Figure S5.9). The sensitivity, stability, and specificity of this surface sensor was then evaluated. Given that chicken food matrices are most commonly contaminated by *S. Typhimurium*, and RTE foods offer the highest risk of illness, RTE chicken products were selected as the target matrix for our studies. Sensitivity testing

was thus performed using contaminated chicken purge samples. The effects of chicken purge on bacterial proliferation and survival were first assessed, to ensure consistency between reported and experimental bacterial concentrations. Chicken purge spiked with bacteria, bacteria resuspended in buffer, and chicken purge alone were all selectively plated (Figure S5.10). No significant changes in bacterial count were observed within any of the tested conditions.

**Figure 5.3. *S. Typhimurium* sensor development and testing.** (a) Schematic illustration of *S. Typhimurium*-responsive nucleic acid probe cleavage activity within food matrices, with associated pre-cleavage, cleavage, and quencher separation states. (b) Sensitivity testing of nucleic acid probe using bacterial dilutions in chicken purge, with associated images with 100  $\mu\text{m}$  scale bars. (c) Temperature profile of nucleic acid probe with bacterial species of  $10^7$  and  $10^5$  CFU/mL at 4°C, 25°C, 37°C, and 45°C. (d) Covalent attachment confirmation of nucleic acid probe on substrate surface. (e) Stability testing of developed sensor tested with  $10^6$  to  $10^3$  CFU/mL of bacteria after storage for three months at 4°C. (f) Specificity testing of nucleic acid probe using

various bacterial species at  $10^6$  CFU/mL, with associated images with 100  $\mu\text{m}$  scale bars. All reported values represent the mean of all samples with error bars representing standard error of the mean. All asterisks represent significant differences at corresponding significance levels.

Subsequent sensitivity testing was performed using spiked chicken purge, wherein sensors were incubated with the bacterial test solutions for eight hours at  $37^\circ\text{C}$  – environmental conditions in line with RTE chicken storage within grocery stores (Figure 5.3b). The limit of detection of the developed sensor was confirmed to be  $10^3$  CFU/mL of *S. Typhimurium*, where a distinct 2.34-mean fold change was observed following incubation – significantly higher than the non-specific 1.50-mean fold change of the control condition ( $P < 0.05$ ). Chicken purge samples contaminated with *S. Typhimurium* concentrations ranging from  $10^8$  to  $10^4$  CFU/mL were also tested, showing a linear relationship between bacterial concentration and mean fluorescence fold change, with the  $10^8$  CFU/mL showing the highest significant mean fold change at 4.36 ( $P < 0.0001$ ). The developed sensor exhibited a significant linear operating range based on linear regression analysis ( $R^2 = 0.98$ ,  $P < 0.001$ ), further validating its detection efficacy (Figure S5.11). The detection range of this sensor is summarized by Equation (2) below, where  $y$  represents the fluorescence signal fold change and  $x$  is the logarithmic *S. Typhimurium* concentration in CFU/mL.

$$y = 0.3952x + 1.113 \quad \text{Equation (2)}$$

Importantly, higher variations in fluorescence signals were observed at high bacterial concentrations. This is of limited real-world concern however, as industry guidelines for *S. Typhimurium* monitoring seek positive versus negative detection results. Variations at these high concentrations do not affect the accuracy of such Yes/No test results. The functionality of the sensors was then further evaluated at  $4^\circ\text{C}$ ,  $25^\circ\text{C}$ , and  $45^\circ\text{C}$  (Figure 5.3c). Sensing performance was maintained at  $45^\circ\text{C}$ , whereas reduced activity was observed at  $25^\circ\text{C}$ . Unfortunately, sensing activity was not observed at  $4^\circ\text{C}$ . These results are in line with the temperature-dependent properties of the probe, wherein its activity is limited at low temperatures and peaks around  $37^\circ\text{C}$ .

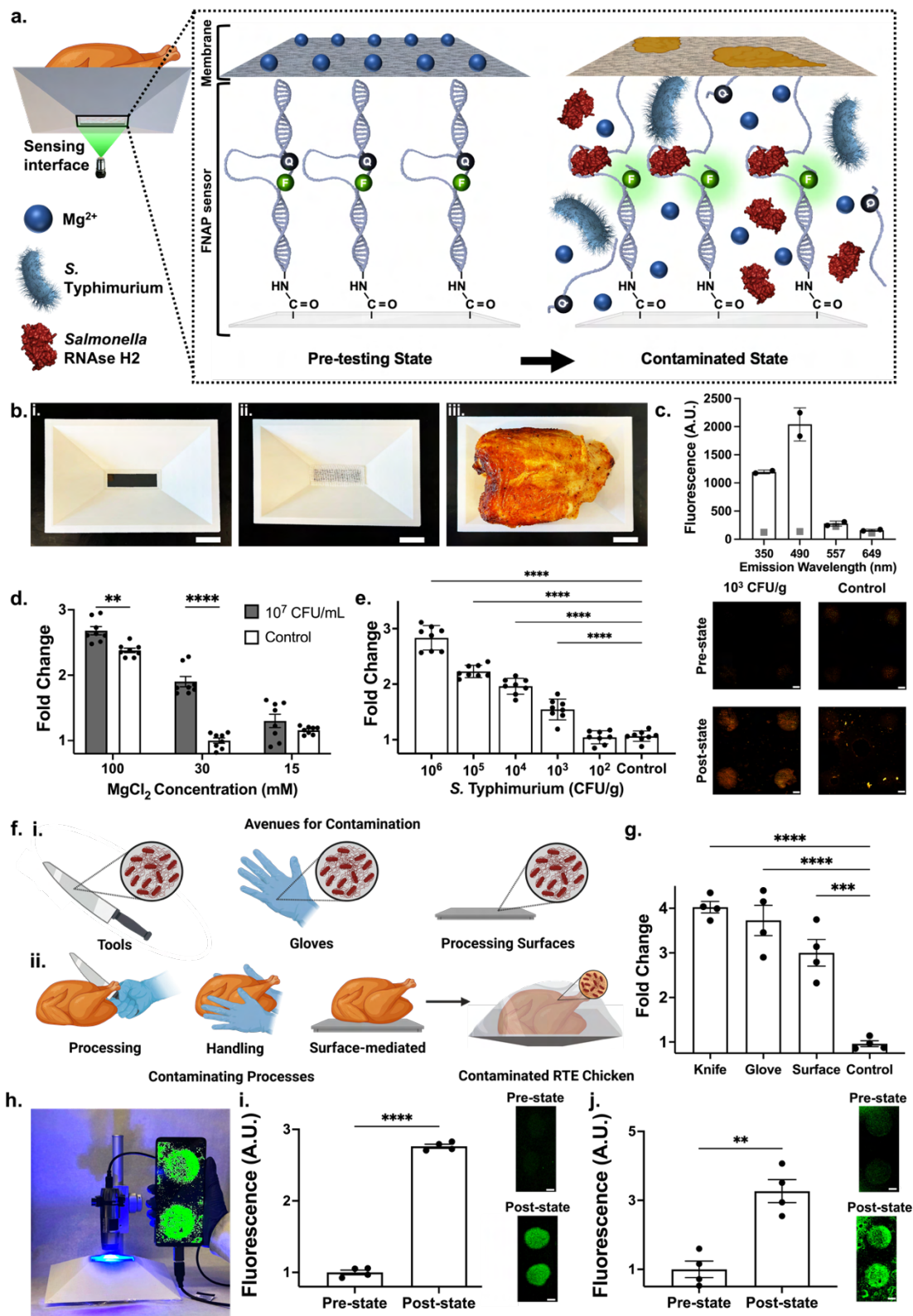
Next, the stability of these sensors was further established to ensure long-term storage viability. First, covalent attachment of the nucleic acid probe onto the polyethylene substrate was

confirmed to ensure the sensors could withstand induced shear stresses (Figure 5.3d). Here, probes that were covalently attached with crosslinker retained 85% of their original fluorescence signal, significantly higher ( $P < 0.0001$ ) than the 14% retention of the probes that were not covalently attached. To evaluate sensing performance after prolonged storage, sensors were tested three months after fabrication (Figure 5.3e). Sensors tested with  $10^6$  CFU/mL *S. Typhimurium* exhibited a slight increase in signal, which can be attributed to the variation that is observed at higher target concentrations. With all other concentrations, sensing performance deteriorated to a degree, but a limit of detection of  $10^4$  CFU/mL was obtained ( $P < 0.0001$ ), confirming sensor resilience.

Specificity testing then involved incubating the sensors with *S. Typhimurium* and other common foodborne pathogens – namely, *Klebsiella pneumoniae*, *E. coli* O157:H7, *Pseudomonas aeruginosa*, *Listeria monocytogenes*, and *Bacillus subtilis* (Figure 5.3f). The developed sensors exhibited a significantly higher 2.59-mean fold ( $P < 0.0001$ ) change in fluorescence when incubated with *S. Typhimurium*, compared to the less than 1.10-mean fold change observed with other bacterial species. Accordingly, after sensitivity, stability, and specificity were confirmed, the sensors were then applied for proof-of-concept testing of the developed packaging platform using commercial-scale, solid food products.

### 5.3.5 Proof-of-concept testing of sensor-embedded packaging platform

The complete Lab-in-a-Package platform was then tested by integrating the newly developed FNAP sensor into the aforementioned packaging and membrane system (**Figure 5.4a**). The final *in situ* detection platform consisted of a concave packing tray with a  $45^\circ$  incline and a sensing window, a *S. Typhimurium*-responsive real-time fluorescence sensor embedded within this window, and an adjacent buffer-infused cotton membrane (Figure 5.4b). Recognizing that chicken exhibits significant fluorescence noise at the FITC emission/excitation wavelengths of 490nm/525nm, we transitioned to a TAMRA fluorophore-labelled version of the probe with excitation and emission wavelengths of 557nm/576nm (Figure 5.4c).<sup>[495]</sup>



**Figure 5.4. Lab-in-a-Package platform development and testing.** (a) Schematic illustration of in situ sensing interface with FNAP-based *S. Typhimurium* detection. (b) Images of packaging

platform assembly, involving (i) sensor implantation within sensing window, (ii) membrane incorporation, and (iii) food addition into the package. Scale bars represent 3 cm on printed packaging tray. (c) Inherent fluorescence of chicken purge at four fluorescence wavelengths. Mean fluorescent values of overlayed cotton membranes shown with grey boxes. (d)  $\text{MgCl}_2$  concentration optimization for membrane absorption and diffusion. (e) Sensitivity testing following in situ full platform testing of contaminated whole chicken sample, with associated images with 100  $\mu\text{m}$  scale bars. (f) Contamination of food products from (i) various avenues of contamination, introduced during (ii) stages of the production process. (g) Induced real-world contamination detection in situ with Lab-in-a-Package platform. (h) Optical image of experimental set-up for handheld fluorescence scanner with associated smartphone readout. (i) *S. Typhimurium* detection using FNAP sensor as visualized using a handheld scanner, and associated images with 3.33 mm scale bars. (j) Handheld fluorescence detection of *S. Typhimurium* in Lab-in-a-Package, with associated sensor images with 3.33 mm scale bars. All reported values represent the mean of all samples with error bars representing standard error of the mean. All asterisks represent significance differences at corresponding significant levels. (a) and (f) created using BioRender.

Importantly, the activity of enzymatic oligonucleotide probes largely relies on the presence of divalent metal ions, substantiating the need for a buffer immobilizing membrane within this *in situ* monitoring platform. The developed *S. Typhimurium*-responsive probe in particular, offers excellent performance with  $\text{Mg}^{2+}$  ions – a metal safe for consumption, which made the leaching of buffer from the membrane onto adjacent foods of limited concern. The concentration of the  $\text{MgCl}_2$  ions used within the Lab-in-a-Package platform was optimized for surface-based sensing, to a value of 30 mM (Figure 5.4d).

RTE rotisserie chicken products were weighed and placed within inclined packaging trays, which already contained FNAP sensors and  $\text{MgCl}_2$  saturated membranes (Figure S5.13, S5.14). Collected chicken purge was spiked with *S. Typhimurium*, and this contaminated purge was then applied to the test products to perform a sensitivity analysis of the complete system, with concentrations ranging from  $10^6$  to  $10^2$  CFU/g. Concurrently, uncontaminated chicken purge was applied onto control chicken samples. The samples were then incubated at 37°C for eight hours to simulate grocery store RTE chicken storage environments. After eight hours, sufficient localization was visually confirmed through the accumulation of significant chicken purge on the cotton membrane and adjacent sensing interface. Specifically, the top surface of the membrane was coated with macroscale fouling agents such as lipids, confirming the membrane's anti-fouling capabilities



within an *in situ* environment. With regards to sensitivity, sensors incubated with contaminated chicken samples exhibited a significantly higher ( $P < 0.0001$ ) mean fold change of up to 2.83 at  $10^6$  CFU/g compared to the 1.09 mean fold change of the control samples (Figure 5.4e). The limit of detection of Lab-in-a-Package was determined to be  $10^3$  CFU/g, which exhibited a significant mean fold change of 1.54 ( $P < 0.0001$ ) compared to the control. The operating range of the complete system was significant ( $R^2 = 0.98$ ,  $P < 0.05$ ) based on linear regression analysis (Figure S5.12). The linear operating range of Lab-in-a-Package is summarized by Equation (3). In this model,  $y$  represents the fluorescence signal fold change and  $x$  is the logarithmic *S. Typhimurium* concentration in CFU/g.

$$y = 0.4135x + 0.2820 \quad \text{Equation (3)}$$

Further, a bacterial growth study was conducted to assess opportunities for improved sensitivity using this platform. It was determined that  $10^2$  CFU/mL of *S. Typhimurium* suspended in chicken purge grows to  $10^4$  CFU/mL within 4 hours. This suggests that extended incubation periods may offer improved detection limits (Figure S5.15).

The specificity of Lab-in-a-Package was also studied through sensor incubation with a mixture of common food contaminants. Specifically, FNAP sensors were placed at the base of the packaging and then incubated with control chicken samples contaminated with a  $10^6$  CFU/g mixture of *E. coli* O157:H7 and *Listeria monocytogenes*. Test samples also contained *S. Typhimurium* (Figure S5.16). Here, the test samples which contained *S. Typhimurium* exhibited a significantly higher mean fold change of 2.70 compared to the 1.25 mean fold change of the control samples ( $P < 0.0001$ ). To further confirm the specificity of the system, a target verification study was also performed (Figure S5.17). Here, spiked purge and purge localized on the sensing window after 8 hours of incubation were selectively plated. Insignificant differences were observed between the two samples. These results confirmed that the developed packaging platform successfully mediates the localization of representative test solution onto the sensing interface for detection, alongside buffers required for biomolecular functionality with a degree of sensitivity and specificity.

Next, to further simulate real-world food contamination, the platform was used to detect contamination within samples that were spiked *via* means of handling and processing. Specifically, the test chicken samples were contaminated through contact with a contaminated knife, glove, and surface (Figure 5.4f) spiked with a solution corresponding to  $10^7$  CFU/g of the corresponding chicken sample. The contaminated chicken samples exhibited high mean fold changes of 4.03 ( $P < 0.0001$ ), 3.73 ( $P < 0.0001$ ), and 3.00 ( $P < 0.001$ ) following contamination induced from the knife, glove, and surface, respectively, further validating the presented platform as a means of *in situ* contamination detection in real-world settings (Figure 5.4g).

To further evaluate the generalizability of the presented platform, contamination detection was performed in spiked lettuce samples at 25°C (Figure S5.18). Test samples that were spiked with  $10^6$  contaminated wash water exhibited significant mean fold changes of 1.51 ( $P < 0.001$ ) compared to the 1.15 fold change of the control samples. These results suggest the potential use of this system for other food products including produce and consumer goods.

Finally, we sought to simulate real-world use of the developed platform to evaluate its full *in situ* sensing capabilities using a portable handheld fluorescence scanner that visualizes images onto a smartphone (Figure 5.4h). The capabilities of the handheld scanner were first evaluated with the sensor alone, wherein a significant mean fold change of 2.76 ( $P < 0.0001$ ) was observed following incubation with a  $10^8$  CFU/mL solution of *S. Typhimurium* (Figure 5.4i). When used to monitor a sealed Lab-in-a-Package set-up containing  $10^6$  CFU/g contaminated RTE rotisserie chicken, a significant fold change of 3.27 ( $P < 0.01$ ) was observed without any disruption to the closed food package (Figure 5.4j). Using such a portable system over a laboratory-scale microscope makes sensor monitoring possible across the entire food production pipeline on an individual product level, emulating real-time, hands-free, *in situ* detection.

## 5.4 Conclusion

We have developed Lab-in-a-Package, a revolutionary solution to advance *in situ*, real-time food contamination detection – bridging the gap between the myriad of developed food sensors and their adoption into food products at the retail and consumer levels. The platform

combines a newly designed food packaging tray and a buffer-infused membrane to address the complete lack of an *in situ* monitoring-compatible packaging platform. This combinatory approach meets the key objectives required to facilitate real-time, hands-free detection as it: (1) enables sensor imaging within a closed package format, (2) localizes sample solution onto the sensing interface, (3) retains all necessary buffers inside the food packaging, (4) facilitates sample diffusion from the food matrix to the sensor, and (5) enables the *in situ* incorporation of novel biorecognition elements. The redesigned 45° inclined packaging model displayed the highest levels of fluid localization and fluid transfer when compared to a traditional food packaging tray and an intermediately inclined one. Moreover, the selected cotton membrane was rigorously tested through a variety of experiments to insure adequate diffusivity and buffer retention. Complete proof-of-concept testing with a newly-developed *S. Typhimurium* sensor demonstrated the successful *in situ* detection of this target pathogen within food products, with high sensitivity and specificity. The efficacy of the developed solution was also confirmed *via* application-specific testing that involved contaminating food samples with a *S. Typhimurium*-contaminated glove, surface, and knife, to better simulate real-world conditions. Finally, real-world use was simulated using a handheld fluorescence scanner attached to a smartphone for sensor visualization. This solution has immense application for a variety of food samples beyond RTE chicken, including the packaging trays used for other meats and seafood products, as well as for the plastic containers used for produce. Its generalized design, cost-effectiveness, and food-safe nature positions it well to forward commercial implementation of *in situ* food sensors. Overarchingly, Lab-in-a-Package represents a paradigm shift, as the first packaging technology designed for *in situ* monitoring. Whereas existing traditional food testing protocols only test select products at central laboratories *via* time-consuming and laborious procedures, this system offers: (1) continuous monitoring of packaged foods, (2) with results available on an hour-scale, (3) without the need for any product processing, (4) in a manner that does not destroy tested foods. Collectively, these traits define the system's delivery of (5) individual product monitoring *in situ*.

## 5.5 Materials and Methods

*Materials.* 3D printing filament was obtained from Creality 3D Technology (Shenzhen, China). Membrane materials were acquired from TNG Worldwide (Michigan, United States), Superscandi (London, United Kingdom), EcoJeannie (New Jersey, United States), Shoppers Drug Mart (Ontario, Canada), and Walmart Canada (Ontario, Canada). Polyethylene wraps were sourced from Thomas Scientific (New Jersey, United States). N-(3-Dimethylaminopropyl)-N'-ethylcarbodiimide (EDC), N-Hydroxysuccinimide (NHS), 2-(N-morpholino)ethanesulfonic acid (MES) buffer, and  $\text{MgCl}_2$  were purchased from Millipore Sigma (Ontario, Canada). Oligonucleotide sequences were ordered from Integrated DNA Technologies (Iowa, United States). Adenosine triphosphate (ATP), polynucleotide kinase buffer A, polynucleotide kinase, T4 DNA ligase buffer, and T4 DNA ligase were purchased from Thermofisher Scientific (Ontario, Canada). Fluorophore-quencher substrate sequences were acquired from the Keck Oligonucleotide Synthesis Facility at Yale University (Connecticut, United States). Ready-to-eat chicken products were sourced from local grocery stores.

*Packaging Tray Fabrication.* All three packaging trays and their associated 2D drawings were developed using 3D computer assisted design (CAD) software (Autodesk Fusion) and then 3D printed using PLA filament (Ender 3 V2, Shenzhen Creality 3D Technology Co., Ltd., China). These packages were then smoothened using acetone to lower the coefficient of friction on the fluid-interface. All packages were printed at a 50% scaled down rendering to improve characterization efficiency.

*Fluid Transfer and Localization Efficacy.* The fluid transfer efficiency involved recording the time it took for a droplet to transport down the edge of each packaging model, when dispensed at a rate of  $16.54 \mu\text{L/s}$  using an automated syringe (DSA30, Krüss Scientific, Hamburg, Germany). This study was video tapped using the Krüss Advance software and then viewed in slow motion to accurately quantify time measurements. The time required to localize 5 mL of deionized water into the sensing window was quantified through the time required for 5 g of water to collect within a weigh boat positioned directly below the sensing window, as PBS was dispensed onto the trays'

edges from above. Here, PBS was dispensed at a rate of 0.5 mL/s. All studies had at least triplicate measurements. Fluid localization based on volume was characterized as the percent of solution that reached a weigh boat collection basin that was attached to the bottom of each packaging model, relative to the total applied volume. PBS studies involved dispensing the buffer over 1 minute at a rate of 0.2 mL/s. Chicken purge studies involved applying 4 mL of chicken purge onto 62 g samples of RTE chicken and assessing the percent volume collected within an attached collection basin after 24 hours storage at 37°C. Timepoint readings were also done to develop trends for volume localization across a 60 second timespan. Here, 5 mL of solution were applied for 10 seconds and 20 seconds on each packaging model and 10 mL of solution were applied for timepoints from 30 to 60 seconds and the total volume of fluid collected in collection basins after each time period was recorded. All values were considered relative to the initial volume applied.

*Preliminary Membrane Characterization.* All membrane candidates were first cut to the same size of 4 cm x 2.5 cm. Their thicknesses were then matched to the same general thickness of approximately 1.1 mm. The samples were then microscopically imaged using an inverted microscope (Nikon Eclipse Ti2, Nikon Instruments Inc.) at 4X and 10X magnifications. Fluorescence analysis was done on the same samples using the same imaging system, with at least three samples imaged for each membrane. Samples were imaged across DAPI, FITC, TRITC, and Cy5 fluorescence wavelengths. Membrane samples were also cut to approximately 1 x 1 cm sizes and then mounted using carbon tape and nickel paste. A sputter coater (Polaron model E1500, Polaron Equipment Ltd., Watford, Hertfordshire) was then used to coat the samples with 10 nm of gold, which were then imaged using the TESCAN VEGA-II LSU SEM.

*Membrane Absorption Quantification.* The absorption capacity of each candidate membrane was assessed using 3.5 cm x 2.0 cm x 1.1 mm samples, wherein samples were weighed when dry, submerged in PBS for 1 minute, and then reweighed. The density of PBS was then used to convert the weight readings into volumetric measurements, which yielded the total absorption capacity of each membrane. To prevent measurement error, the hydrated samples were briefly shaken to remove residual, unabsorbed PBS. Additionally, a timepoint study was also created to confirm that

the membranes were saturated in 1 minute. This involved repeating the above protocol for different submersion times spanning 5 seconds to 30 minutes.

*Membrane Retention Analysis.* Membranes were submerged in PBS for 1 minute, shaken to remove unabsorbed solution, and then weighed as the initial starting weight. Membrane weight was measured and then converted to volumetric values using the density of PBS. These samples were then stored within packaging. Membranes were reweighed at 24h and 120h to quantify the volume of buffer retained within the membranes over time.

*Membrane Diffusion Analysis.* Buffer diffusion was assessed by quantifying the volume of PBS that diffused through 5 cm x 2.5 cm pre-saturated membrane samples over 2 minutes of continuous flow at a rate of 0.1 mL/s. Samples were supported by a plastic scaffold and placed on top of a collection basin. PBS was then pipetted onto the top surface of the membrane and the amount of buffer which diffused through each membrane into the basin below was collected and quantified. Triplicate measurements were obtained to reduce experimental error.

*Membrane Bacterial Studies.* To assess membrane effects on bacterial proliferation and survival, 1 cm x 1 cm membrane samples were incubated with  $10^8$  CFU/mL of bacteria for 6 hours. The contaminated membranes were then vortexed for 1 minute to extract bacteria from the membrane into solution. This solution was then serially diluted and plated onto Gram-negative selective MacConkey agar (MilliporeSigma) plates. A control (no membrane) condition consisting of  $10^8$  CFU/mL of bacteria was maintained for the same incubation period and concurrently plated. The bacterial plates were incubated overnight at 37°C. Following incubation, the total number of colony-forming units were counted for each membrane and compared to that of the control. Bacterial diffusion through the membranes was assessed across both unsaturated and saturated membranes, where the latter had 1 mL of PBS buffer added on the surface. Both groups of membranes were then placed on top of glass substrates and  $10^6$  CFU/mL of bacteria was distributed on top of each membrane candidate. After 6 hours, any solution which diffused through the membrane onto the glass substrate below was collected, serially diluted, and plated onto the same

selective plates. Once again, the total number of colony-forming units formed after the overnight incubation was used to determine the overall bacterial diffusion through each membrane.

*Bacteria Preparation.* *S. Typhimurium*, *E. coli* K12 and O157:H7, *Klebsiella pneumoniae*, *Pseudomonas aeruginosa*, *Listeria monocytogenes* 1/2a, and *Bacillus subtilis* were cultured in appropriate media for 18 hours at 37 °C under constant agitation at 180 RPM from glycerol stock solutions. The bacteria from these overnight incubations were then centrifuged at 7000 RPM for 15 minutes to form a bacterial pellet. This pellet was then resuspended in PBS buffer solution for use in all bacterial studies.

*Membrane Antifouling Assessment.* Chicken purge was extracted from chicken samples and heated in a water bath at 60°C to melt any solidified lipid molecules. The filtered chicken purge was then pipetted through a cotton membrane and then collected. Both the filtered and unfiltered membrane samples were pipetted into a well plate and had their optical density measured using a Synergy Neo2 plate reader (Aligent Technologies). Samples were measured across an absorbance spectrum ranging from 400 nm to 700 nm in increments of 10 nm. Deionized (DI) water was also assessed for baseline readings. Quadruplicate readings were obtained. SEM images of cotton membranes saturated in chicken purge were obtained to visualize antifouling properties. 1 x 1 cm<sup>2</sup> cotton membrane samples were saturated with chicken purge and then dried in ambient conditions for 24 hours. These samples were then mounted, coated, and imaged in a method identical to the SEM procedures outlined in *Preliminary Membrane Characterization*.

*FNAP Synthesis.* All relevant sequences are listed in Table S5.3. 3' amino-modified probe fragments were phosphorylated using ATP, T4 polynucleotide kinase buffer A, and T4 polynucleotide kinase in-solution, over 30 minutes at 37°C. Substrate fragments (FQ30, TB30) and ligation template fragments were then added, heated for 1 minute at 90 °C, and cooled at ambient temperature, to mediate the annealing of the three fragments. T4 DNA ligase buffer, T4 DNA ligase, and water were then added and incubated at ambient temperature for 1 hour to mediate ligation of the probe and substrate fragments. The sample was then ethanol precipitated and

centrifuged for 20 minutes at 4°C,  $20000 \times g$ . A polyacrylamide gel was used to purify the ligated product. The final nucleic acid probe product was resuspended in water.

*Sensor Development and Preliminary Characterization.* Nucleic acid probe was first mixed with EDC-NHS crosslinker in MES buffer to facilitate covalent attachment to polyethylene substrates. A GeSiM Nano-Plotter piezoelectric printer was used to deposit nucleic acid probe onto the sensor surface. The sensors were then incubated in a 75% humidity environment for 2 hours and then washed in a water bath at 220 RPM for 30 minutes on a platform shaker (VWR International) to remove any unbound probe molecules. They were then dried and imaged using an inverted fluorescent microscope. Covalent attachment was confirmed by comparing the fluorescence of nucleic acid probes both with and without the EDC-NHS covalent crosslinker before and after the aforementioned water washing step. Next, a calibration curve was developed to confirm the density of nucleic acid probe added to the sensor surface. This curve was created using intensity measurements of arrays composed of known concentrations of fluorescent, single-stranded TRITC DNA molecules. Maximal fluorescence intensity of the nucleic acid probe was obtained using 1M NaOH, at which point probe density was quantified using the curve.

*Sensor Sensitivity and Specificity Testing.* The effects of chicken purge on bacterial proliferation and survival were assessed through the resuspension of  $10^6$  CFU/mL *E. coli* in chicken purge and in PBS. These solutions were then plated on selective MacConkey agar plates, alongside chicken purge alone. These plates were incubated overnight at 37°C and then the colony-forming units were quantified. Sensor sensitivity was tested by incubating printed, pre-imaged sensors with *S. Typhimurium* concentrations ranging from  $10^7$  to  $10^3$  CFU/mL, where all dilutions were performed using chicken purge. 100 mM  $MgCl_2$  was also added into the incubation solution. Control samples were composed of chicken purge and  $MgCl_2$  alone. After an 8 hour incubation at 37°C, all test solution was removed from the sensor surface. The sensors were then briefly washed in DI water and re-imaged to assess their fluorescence fold change. Sensor selectivity was tested in a similar manner except this time a constant bacterial concentration of  $10^6$  CFU/mL was tested using *S.*



*Typhimurium*, *Klebsiella pneumoniae*, *Escherichia coli* O157:H7, *Pseudomonas aeruginosa*, *Listeria monocytogenes* 1/2a, and *Bacillus subtilis*, while the control solution remained the same.

*Sensor Stability and Temperature Profile Development.* Printed sensors were washed, imaged, and then stored at 4°C. After three months of storage, the sensors were incubated with *S. Typhimurium* in concentrations ranging from  $10^6$  to  $10^3$  CFU/mL and were then re-imaged to confirm sensor viability. A temperature profile of sensor performance was also developed to confirm their functionality in a variety of food storage conditions. To this end, sensors were incubated with  $10^7$  and  $10^5$  CFU/mL contaminated chicken purge and incubated for 24 hours at 4°C, 25°C, 37°C, and 45°C and then reimaged.

*Proof-of-Concept Testing.* Full-scale models of the 45° packaging tray were 3D printed for the proof of concept testing. A printed sensor was placed in the window at the base of the packaging and an MgCl<sub>2</sub> buffer-saturated membrane of the same size as the sensor was placed directly on top. Cooked RTE rotisserie chicken purchased from local grocery stores was cut into 250 g samples and placed on the packaging trays. These chicken samples were contaminated with 10 mL volumes of *S. Typhimurium* chicken purge suspensions to yield the desired CFU/g concentrations. Control samples were treated with 10 mL of uncontaminated chicken purge. The samples were incubated at 37°C for 8 hours. After 8 hours, the packaging was opened, the membrane was removed, and the extracted sensor was fluorescently imaged. Application-based testing followed the exact same protocol, except introduction of the bacteria onto food samples was done *via* a contaminated surface, glove, and knife, rather than through contaminated chicken purge.

*S. Typhimurium Growth Study.* An original concentration of  $10^2$  CFU/mL of *S. Typhimurium* suspended in chicken purge was selectively plated at a timepoint of 0 hours. It was then incubated at 37°C, with selective plating repeated at 2 hour and 4 hours timepoints. The total number of colony-forming units formed after an overnight incubation at 37°C was used to quantify the growth of the original  $10^2$  CFU/mL of *S. Typhimurium*.

*Full System Specificity Testing.* Full system specificity was tested in a similar manner to sensor selectivity testing. Equal amounts of  $10^6$  CFU/mL of *Escherichia coli* O157:H7, *Listeria*

*monocytogenes* 1/2a, and *S. Typhimurium* were resuspended in chicken purge and applied onto chicken samples within sensor and membrane containing packaging trays for an 8 hour incubation at 37°C. After this incubation, sensors were fluorescently imaged as previously described.

*Target Verification Study.* Chicken samples were contaminated with 10<sup>6</sup> CFU/g *S. Typhimurium*. The final target that reached the sensor interface was collected after the 8 hour incubation period and selectively plated along with some of the original contaminated chicken purge that was applied. After the plates were stored for a standard overnight incubation at 37°C, the total number of colony-forming units formed for both the initial and post-incubation samples were compared to both assess that the collected target contained *S. Typhimurium* and that there was no significant change in the overall bacterial concentration.

*S. Typhimurium Detection in Lettuce Samples.* Bagged lettuce was obtained from a local grocery store and washed thoroughly. Water used to wash the lettuce was collected as the wash fluid, which was then spiked with 10<sup>6</sup> CFU/mL of *S. Typhimurium* to simulate contaminated lettuce. Lettuce leaves were placed within the Lab-in-a-Package system and 10 mL of the contaminated wash fluid was readministered onto the samples. The sensors were reimaged after a 24 hour incubation at 25°C to assess contamination detection.

*Handheld Fluorescence Detection.* A handheld fluorescence scanner (Dino-Lite Edge, Dino-Lite US, Dunwell Tech., Inc.) was used to image *S. Typhimurium* contamination in sensor samples and Lab-in-a-Package. Initial characterization was performed with 10<sup>8</sup> CFU/mL contaminated FNAP sensor samples. *In situ* detection was performed with chicken samples that were contaminated with 10<sup>6</sup> CFU/g chicken purge. In this case, the handheld microscope was used to image the sensor window on the base of the packaging, without opening the package or extracting the sensor. The scanner can be connected to either an associated computer software or smartphone application for sensor visualization and final signal readout, through which all images were obtained.

## **5.6 Acknowledgements**

A.P. is a recipient of the Canada Graduate Scholarship – Master’s from the Natural Sciences and Engineering Research Council of Canada. S.K. is a recipient of the Vanier Canada Graduate

Scholarship awarded by the Natural Sciences and Engineering Research Council of Canada. J.K.M. and F.A. are recipients of Undergraduate Student Research Awards from the Natural Sciences and Engineering Research Council of Canada. This work was supported by the Ontario Early Researcher Award, Mitacs and Toyota Tsusho Canada Inc. grants to TFD. T.F.D. is a Tier II Canada Research Chair in Nanobiomaterials.

### **Conflict of Interest**

The authors declare no conflict of interest.

## 5.7 Supplementary Information

**Table S5.1.** Summary of packaging tray model characterization.

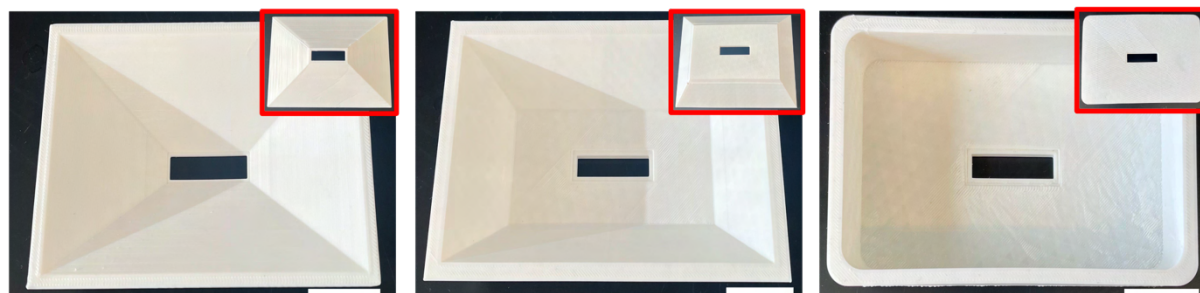
Model	Fluid Transfer Efficiency (s)		Fluid Localization over Time (s)		Fluid Localization by Volume (% volume PBS localized)		Fluid Localization by Volume (% volume chicken purge localized)	
45°	32.7	↑	12.3	↑↑↑	71	↑↑↑	60	↑↑↑
60°	21.3	↑↑	20.6	↑↑	52	↑↑	33	↑↑
90°	12.3	↑↑↑	31.6	↑	35	↑	6	↑

**Table S5.2.** Summary of membrane materials characterization.

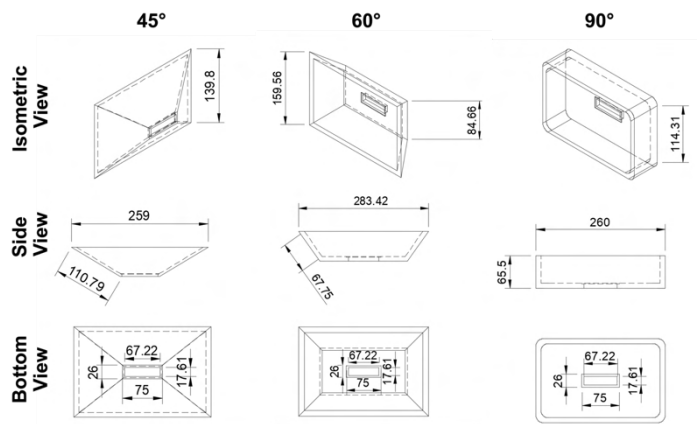
Material	Absorption (mL)	Retention (% ret. in 120 hrs)	Buffer Diffusion (mL)	Unsaturated Bacterial Diffusion (CFU/mL)	Saturated Bacterial Diffusion (CFU/mL)	Porosity (%)
Cotton	1.18	92.33	6.43	$8.00 \times 10^8$	$5.33 \times 10^8$	28.58
Cotton-Cellulose	3.63	95.00	4.17	$2.40 \times 10^5$	$6.67 \times 10^5$	35.79
Cellulose	2.96	94.00	3.33	$2.00 \times 10^4$	$4.33 \times 10^5$	20.47
Cellulose-Polyester	1.84	93.33	6.17	$2.93 \times 10^7$	$5.47 \times 10^6$	28.70
Polyester	0.80	90.00	7.10	$2.93 \times 10^7$	$1.10 \times 10^8$	9.73

**Table S5.3.** Oligonucleotide sequences used for *S. enterica* serovar Typhimurium sensor.

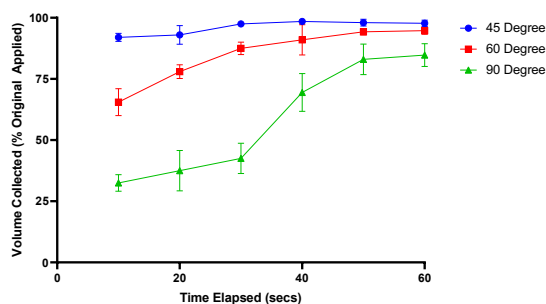
Oligo	Sequence (5' to 3')
Probe	GCAGTCGAGTTAGTGATGGTGCATAGTCCTCCGATTTTTTTTTTT-NH <sub>2</sub>
Ligation template	GATTTCACTAGACTCGACTGCCTTGGTAGTGAGGTC
FQ30	CTATGAACTGACFrAQGACCTCACTACCAAG F = dT-Fluorescein; rA = riboA; Q = dT-DABCYL
TB30	CTATGAACTGACQrAMGACCTCACTACCAAG Q = dT-BHQ2; rA = riboA; M = dT-TAMRA
FNAP-FITC	CTATGAACTGACFrAQGACCTCACTACCAAGGCAGTCGAGTTAGTGA TGGTGCATAGTCCTCCGATTTTTTTTTTT-NH <sub>2</sub>
FNAP-TAMRA	CTATGAACTGACQrAMGACCTCACTACCAAGGCAGTCGAGTTAGTG ATGGTGCATAGTCCTCCGATTTTTTTTTTT-NH <sub>2</sub>



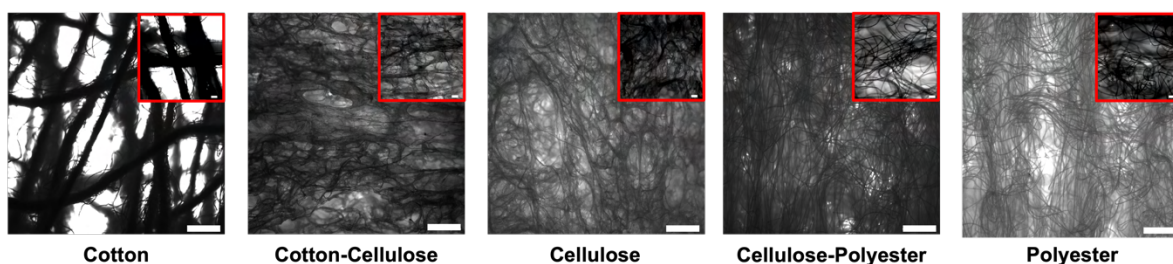
**Figure S5.1.** Top views of 45, 60, and 90 degree 3D-printed packaging models (left to right) with bottom view images overlaid. Scale bars represent 2.5 cm on printed packaging trays. Printed trays were smoothed according to previously reported acetone-based approaches.



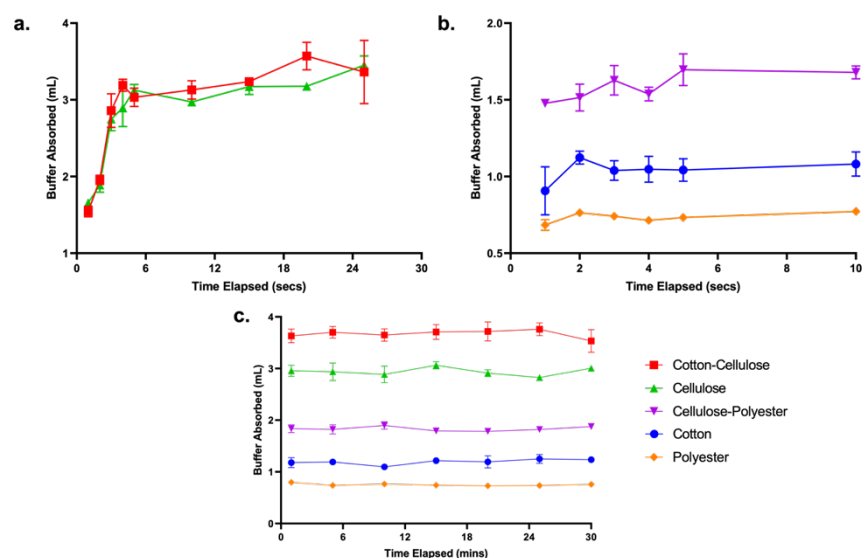
**Figure S5.2.** 2D drawings of packaging trays with key dimensions shown in mm in isometric, side and bottom views. Sensor window dimensions are highlighted in the bottom view along with dimensions for the inner edges used to secure sensors in place.



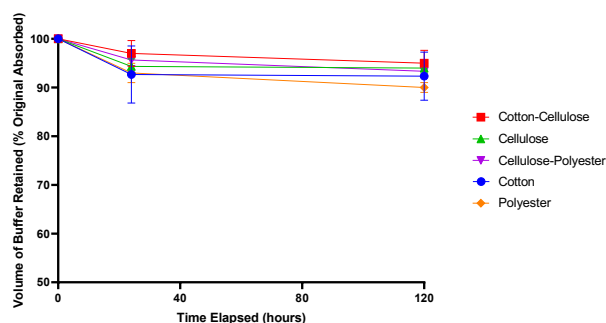
**Figure S5.3.** Volume localization over time for all packaging models based on an original applied volume of 5 mL across 10 and 20 seconds and 10 mL across 30 to 60 seconds. Reported values represent mean of all samples with error bars representing sample standard deviation.



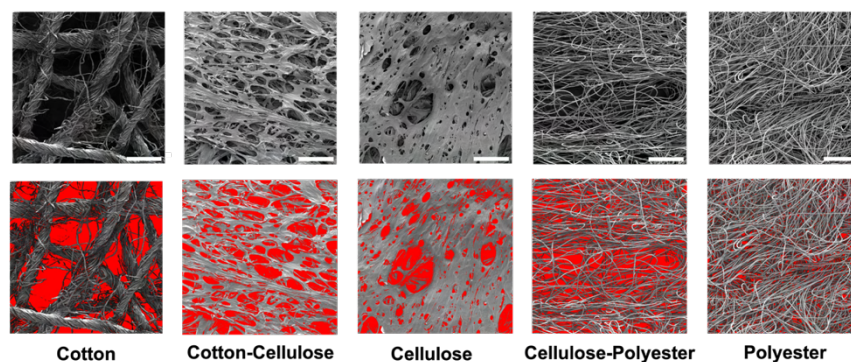
**Figure S5.4.** Microscopic images of tested membrane materials at 4X with overlays of 10X images. Scale bars represent 500  $\mu$ m at 4X and 100  $\mu$ m at 10X.



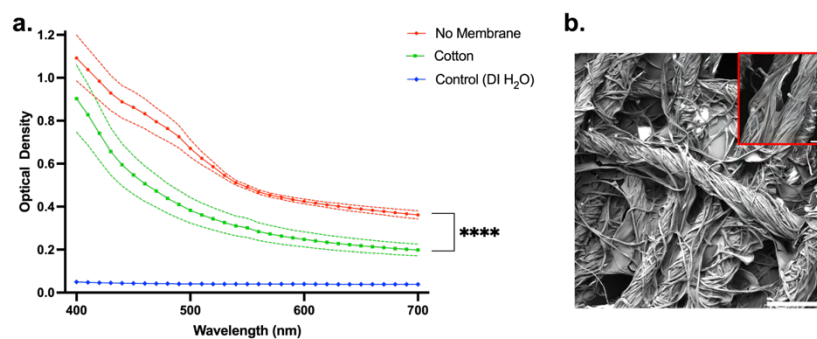
**Figure S5.5.** Membrane absorption capacity over time based on volume of buffer absorbed. (a) Carrying capacity of cotton-cellulose and cellulose membranes over 30 seconds. (b) Carrying capacity of cellulose-polyester, cotton, and polyester membranes over 10 seconds. (c) Carrying capacity of all five membrane materials over 30 minutes. Reported values represent the mean of all samples with error bars representing sample standard deviation. Graphs with different axes ranges were used based on the higher absorption capacities of cellulose and cotton-cellulose materials compared to cotton, polyester, and cellulose polyester.



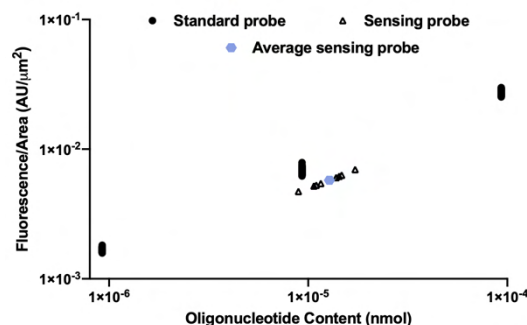
**Figure S5.6.** Membrane buffer retention over 120 hours as a percent of the original volume of buffer applied for all five membrane materials. Membranes were submerged in excess PBS buffer for 1 minute and stored for 120 hours. Reported values represent the mean of all samples with error bars representing sample standard deviation.



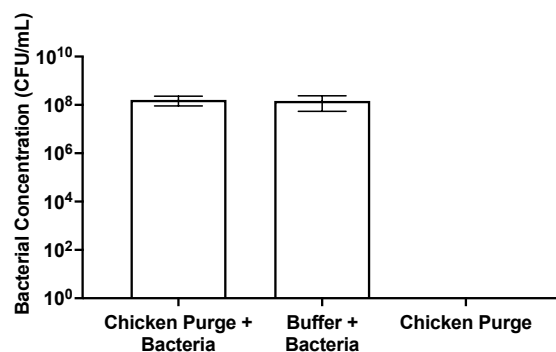
**Figure S5.7.** Membrane porosity characterization based on percent area covered by pores compared to total sample area. Unmodified membrane SEM images (top) and analyzed SEM images with pores shown in red (below). Scale bars represent 500  $\mu\text{m}$ .



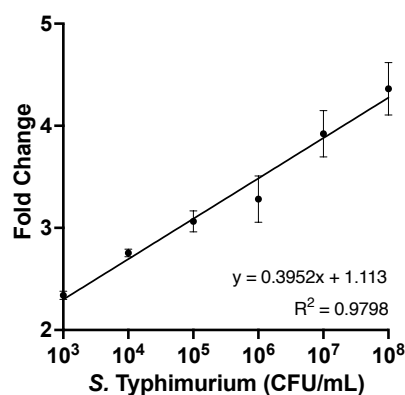
**Figure S5.8.** Characterization of membrane antifouling capabilities. (a) Optical density measurement of chicken purge, chicken purge filtered through a cotton membrane, and water (control). Asterisks represent a significant difference between OD of membrane-filtered chicken purge and unfiltered chicken purge at the corresponding significance level. (b) SEM image of cotton membrane saturated in chicken juice at 100X with 500X overlay. Scale bars represent 500  $\mu\text{m}$  at 100X and 100  $\mu\text{m}$  at 500X.



**Figure S5.9.** Calibration curve for the determination of probe density on sensing interface. TRITC-labelled single-stranded DNA molecules were used to establish calibration curve correlating fluorescence per unit area and oligonucleotide content. The resultant linear relationship was used to quantify immobilized sensing probe density based on NaOH-induced maximal fluorescence per unit area. Average of sensing probe values denoted as a unique data point. The calibration curve was developed using a previously described protocol.

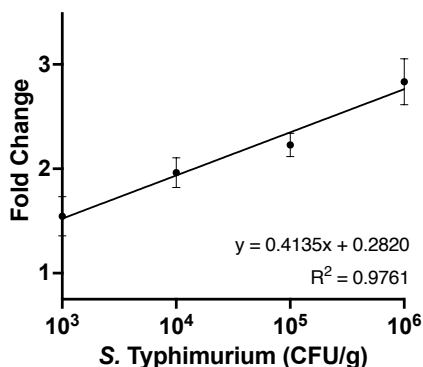


**Figure S5.10.** Effect of chicken purge on bacterial growth. Comparison of bacterial concentration present in chicken purge contaminated with bacteria, bacteria resuspended in PBS buffer, and chicken purge. Reported values represent the mean of all samples with error bars representing sample standard deviation. MacConkey agar was used based on its selectivity for gram-negative bacteria.

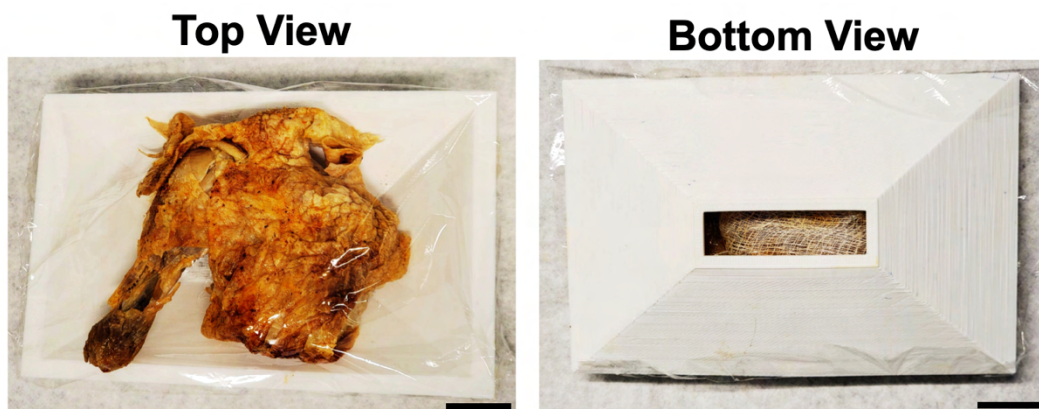


**Figure S5.11.** Linear regression analysis on FNAP sensor sensitivity data (Figure 5.3b) with regression coefficient and model equation shown. Model significance was evaluated based on slope coefficient value ( $P < 0.001$ ).

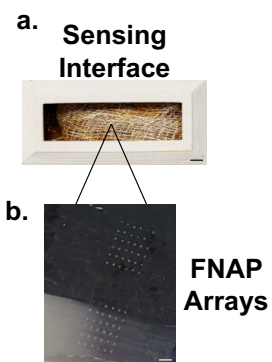




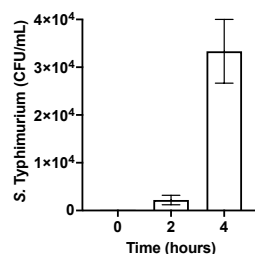
**Figure S5.12.** Linear regression analysis on Lab-in-a-Package sensitivity (Figure 5.4e) with regression coefficient and model equation shown. Model significance was evaluated based on slope coefficient value ( $P < 0.05$ ).



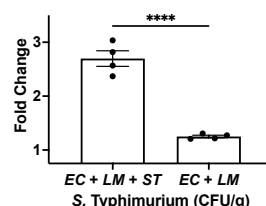
**Figure S5.13.** Optical images of complete Lab-in-a-Package set-up. Whole, unprocessed RTE chicken product sample and polyolefin food wrap shown in top view. Saturated membrane, FNAP sensor, and inclined tray shown in bottom view. Scale bars represent 4 cm.



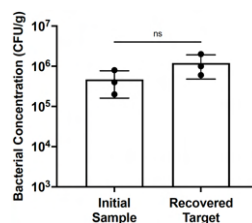
**Figure S5.14.** Overview of Lab-in-a-Package sensing window. (a) Optical image of sensing interface with membrane and FNAP sensor shown within the sensing window of the redesigned packaging tray. Scale bars represent 0.6 cm. (b) Zoomed-in optical image of FNAP sensor arrays with 2.5 cm scale bars.



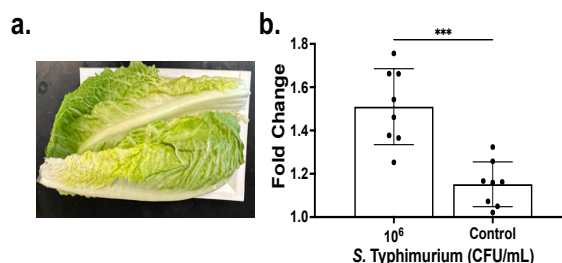
**Figure S5.15.** *S. enterica* serovar Typhimurium growth study demonstrating exponential growth of an original  $10^2$  CFU/mL sample over a 4 hour timespan. Reported values represent the mean of all samples with error bars representing standard error of the mean.



**Figure S5.16.** Full system specificity testing where samples were contaminated with a mixture of common food contaminants including *E. coli* O157:H7 (EC), *Listeria monocytogenes* (LM), and *S. enterica* serovar Typhimurium (ST). Reported values represent the mean of all samples with error bars representing standard error of the mean. Asterisks represent a significant difference at corresponding significance level.



**Figure S5.17.** Target verification study comparing the concentration of *S. enterica* serovar Typhimurium recovered from the sensor surface after an 8-hour incubation period compared to the initial contaminated purge sample. Reported values represent the mean of all samples with error bars representing standard deviation.



**Figure S5.18.** Full system testing with *S. enterica* serovar Typhimurium contaminated lettuce samples. (a) Optical image of experimental set-up. (b) Quantification of sensor signals from lettuce samples contaminated with  $10^6$  CFU/mL of spiked produced washing water. Reported values represent the mean of all samples with error bars representing standard deviation. Asterisks represent a significant difference at corresponding significance level.

## **Chapter 6: Food-Activated, Spoilage Sensing Microneedles For Real-Time, Consumer-Directed Monitoring of Packaged Fish**

### **Preface**

While Chapter 5 details a platform that advances real-time, in-package contamination monitoring, this chapter shifts the focus to real-time spoilage monitoring. While industry-directed efforts powerful in their ability to drive widespread adoption, the industry-level value-add of spoilage monitoring is not commercially enticing. This is because the burden of food waste falls largely on consumers, who proceed to purchase excessive food products to replace the edible food products that they pre-emptively disposed – a profitable cycle for industry. This is in addition to the added packaging cost that such sensors would enact, where the risk of failure comes with possible legal ramification. Thus, in accordance with Objective 3, this chapter details the development of an inexpensive real-time fish spoilage sensor to be purchased and used directly by consumers. The sensor employs microneedles that are composed of dehydrated gelatin – a material produced through a gelling, freezing, and dehydrating three-step protocol. The resultant microneedles exhibit excellent mechanical integrity, to a point where they can repeatedly penetration through food packaging films with limited deterioration in performance. However, when introduced into fluid-rich environments, the microneedles return to their native gelatin hydrogel state. Dehydrated gelatin microneedles embedded with non-toxic, food-derived red cabbage anthocyanin were then developed. Anthocyanins offers dramatic pH responsive colour change, allowing them to signal spoilage-induced pH changes in food. The microneedle spoilage sensors were applied to fish products, due to the extensive literature that details the relationship between their spoilage and pH. Here, the dehydrated microneedle sensors penetrated through sealed food packages in a non-destructive fashion and rehydrated once positioned within the underlying fish. This enabled effective real-time monitoring of spoilage within these sealed products over the course of their lifespan. Additionally, the microneedle sensor was applied to opened food products for rapid spoilage testing, wherein the large sensing surface interface afforded by microneedles yielded colour change within 45 minutes.

### **Authors**

Shadman Khan<sup>†</sup>, Akansha Prasad<sup>†</sup>, Mahum Javed, Roderick Maclachlan, Carlos D. M. Filipe, Tohid F. Didar

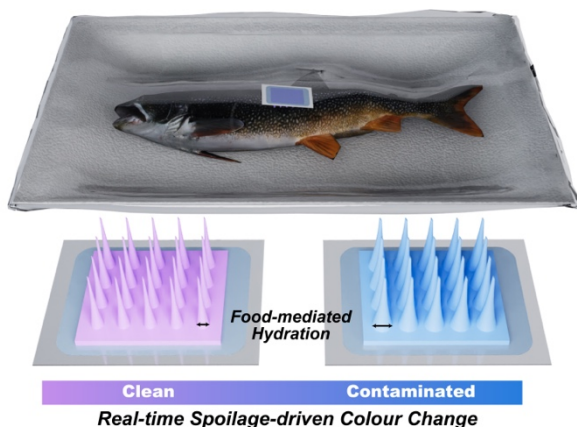
<sup>†</sup> These authors contributed equally.

In this work, dehydrated microneedles were developed through the simple casting of gelatin solution only negative microneedle molds, followed by freezing and dehydration. Microneedle properties were optimized to maximize mechanical integrity, with various gelatin concentration and dehydration times being assessed. Mechanical force testing was employed for assessment, while SEM was used for microneedle visualization. The penetration rate of the developed microneedles through polyethylene packaging films was then assessed. Reusability was also

quantified through the number of intact needles at the end of each trial across ten successive penetration events. The relationship between red cabbage anthocyanin and fish spoilage was then assessed, to ensure good sensing compatibility. Next, anthocyanin-embedded microneedles were developed through the addition of the agent into the gelatin casting solution. Anthocyanin concentration was optimized in accordance with pH responsiveness and mechanical integrity, with resultant needles subjected to SEM. The final anthocyanin-embedded, microneedle spoilage sensor, was employed through food packaging for the day-scale assessment of sealed fish products. The sensors were also employed towards the rapid testing of spoiled fish products. In both cases, colour change was quantified through the loss of red colour intensity. Finally, the pH responsiveness and mechanical stability of the developed sensors was assessed following long-term storage, as well as after 5-day incubation at varying food-relevant temperatures.

## Publication

*Pending*



## 6.1 Abstract

Unnecessary food waste is largely enacted by ongoing societal reliance on ultraconservative static expiry dates. While the need for real-time spoilage sensing is pronounced, the added cost of in-package sensors is difficult for food manufacturers to justify from a commercial standpoint. This is especially true given the profit they earn from excess consumer purchasing induced by the disposal of edible foods. Directly providing consumers with an inexpensive, accessible tool for the monitoring of food spoilage thus presents the most effective means of reducing waste. To this end, we present an inexpensive, colorimetric spoilage sensor that offers both real-time spoilage monitoring of sealed fish products and rapid spoilage testing of opened fish products. The sensor is composed of dehydrated gelatin microneedles, which are fabricated through a gelling, freezing, and dehydrating three-step approach. This yields microneedles with high mechanical integrity in their base state, that exhibit reversion to their hydrogel state when exposed to fluid-rich environments. pH-responsive anthocyanins are embedded within these dehydrated microneedles and subsequently used for fish spoilage monitoring. When applied to sealed fish products, the dehydrated microneedles non-destructively penetrate through packaging films and are rehydrated once positioned within the underlying fish matrix. As spoilage occurs, a defined colour shift from purple to blue is observed in correlation with established spoilage-indicative pH changes. When applied to unpackaged fish products for rapid testing, the high sensing interface offered by the microneedles yield the aforementioned colour change within 45 minutes. Both use cases empower consumers to perform real-time spoilage monitoring for the first time.

**Keywords:** food spoilage, spoilage sensing, smart food monitoring, pH monitoring, anthocyanins, microneedle sensors

## 6.2 Introduction

With food insecurity at record levels, the effects of foodborne illness and unnecessary food waste have become increasingly pronounced worldwide.<sup>[1,496]</sup> While various legislative and operational measures have been enacted across the food production and distribution pipeline, little

improvement has been observed. The United States continues to experience approximately 48 million cases of foodborne illness per year, with over 128,000 hospitalizations and 3000 deaths.<sup>[497]</sup> Many of these cases originate from the consumption of spoiled food products. Food spoilage is characterized by the breakdown of macromolecular textures, the overgrowth of native and contaminating microbes, and the accumulation of toxins.<sup>[498,499]</sup> The complex network of molecular changes that define food spoilage makes single entity monitoring questionable. To this end, accurate spoilage tracking efforts in literature has been largely enabled through pH monitoring. Specifically, food texture degradation, microbial growth, and toxin accumulation all induce changes in pH, positioning this metric acts as a comprehensive measure of food quality.<sup>[500,501]</sup>

While food-specific pH meters are sometimes used by industry stakeholders to assess food quality, spoilage monitoring stands to offer the greatest benefits at the consumer level, as this is when most products reach spoilage. Given that the use of such complex devices is not feasible on a mass market scale, developing simple, cost-effective pH sensors has been a very active area of research.<sup>[502]</sup> Here, anthocyanins, which are pH-responsive flavonoids derived from fruits and vegetables, have garnered significant interest.<sup>[21]</sup> As these agents are native to food, they are completely food-safe and offer dramatic shifts in colour in response to single logarithmic unit changes in pH. Anthocyanins have most broadly been employed within soft, food-safe polymer films that act as entrapping matrices, without hindering the molecules' ability to interact with fluids present in food.<sup>[21,90,500]</sup> Cellulose, chitosan, and polyvinyl alcohol have been most commonly used within such systems. The non-toxic, biodegradable nature of these films ensures that they can be safely used to package foods for real-time, consumer-level monitoring. As spoilage is transduced *via* a visible colour change, consumers can assess food state without using any equipment.<sup>[9,153]</sup>

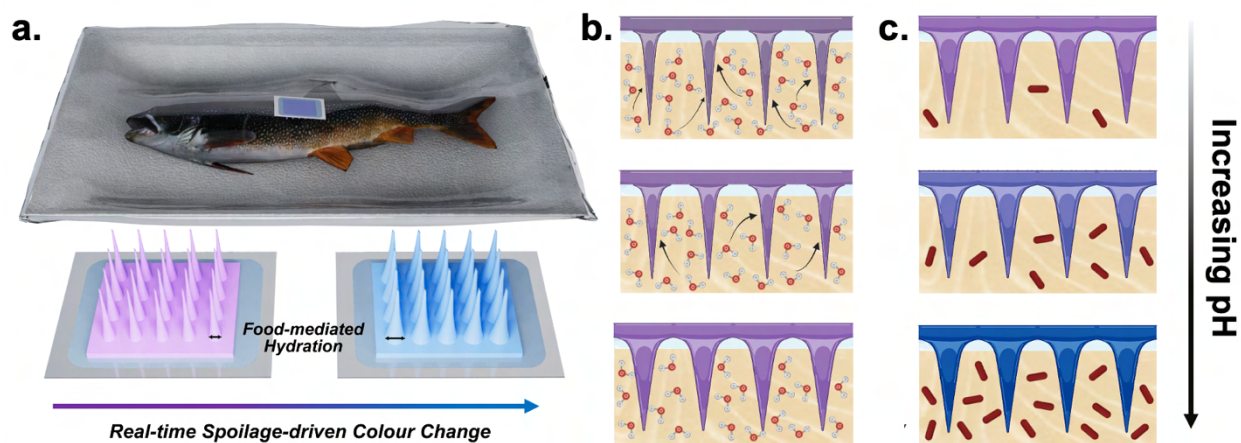
Yet, while intriguing, such anthocyanin-embedded spoilage sensing films offer limited real-world viability. Most notably, these films generally exhibit poor mechanical integrity.<sup>[87,155]</sup> The retention of anthocyanin functionality requires such films to be highly permeable to fluids, meaning that they must be composed of porous, hydrophilic matrices. Such a composition does

not act as a sufficient environmental barrier for packaged food, preventing the use of such films as standalone packaging.<sup>[500]</sup> An alternative approach involves the integration of a small anthocyanin film substrate onto the interior surface of traditional polyethylene films. While this ensures effective food protection, in-package integration subjects such films to significant moisture exposure, wherein the films stand to lose all structural integrity over the course of a product's lifespan. Furthermore, from a commercial standpoint, food product distributors are extremely resistant towards increases in food packaging costs, making the adaptation of either approach unlikely. Ultimately, developing a platform that offers anthocyanin-mediated spoilage at the consumer level is necessary.

To address this, we have developed inexpensive, food-activated microneedle spoilage sensors, to be used by consumers at home (**Figure 6.1**). Our first objective was to develop a material that acted like a hard plastic initially, before transitioning into a hydrogel once localized in food. This objective was met using gelatin as the material of choice, owing to its food-safe nature, material versatility, and demonstrated applications in food sensing films.<sup>[503–505]</sup> The developed microneedles were fabricated using a three step approach that involved casting, freezing, and dehydration. The microneedles were optimized with regards to their gelatin concentration and dehydration time, to be extremely dense and mechanically robust. Accordingly, they demonstrated effective penetration of food packaging plastics, even when subjected to repeated use. Still, they offered reversible rehydration when exposed to a fluid-rich environment. These spoilage-sensing microneedles were employed towards fish product monitoring. Fish provided a strong proof-of-concept platform as a perishable food that is often implicated in foodborne illness.<sup>[506]</sup> Moreover, the relationship between its spoilage and associated shifts in pH have been well-characterized.<sup>[10,507]</sup>

These dehydrated gelatin microneedles were then embedded with red cabbage anthocyanin at varying concentrations, wherein limited changes in mechanical integrity were observed. While the colour shifts offered by 0.1% w/v anthocyanin microneedles were suboptimal, 0.5% and 0.9%

w/v microneedles demonstrated similar preliminary performance. The primary use case proposed for these microneedles involved the at-home, real-time spoilage monitoring of packaged fish. Here, the needles were first non-destructively inserted through overlaid packaging. To prevent unwanted air exposure at the penetration site, a transparent film was secured above the microneedle patch and sealed to the surrounding packaging. Successful penetration was succeeded by the microneedles absorbing fluids from the packaged haddock fish, resulting in a gradual return to a hydrated state. Hydration induced significant contact between the embedded anthocyanins and fluids from within the fish matrix, facilitating spoilage monitoring. As the packaging product spoiled over several days, 0.5% w/v anthocyanin-embedded sensors exhibited a gradual transition in colour from purple to blue, correlating well with changes in pH. A second proposed use case involved the employment of the microneedle spoilage sensors for the rapid assessment of opened products, immediately before consumption. While the penetration of packaging films was no longer required, the microneedles acted to induce a significant increase in surface contact area between the sensing patch and fish, accelerating spoilage detection. Here, 45 minutes was sufficient for 0.5% w/v anthocyanin-embedded sensors to exhibit a pronounced blue signal when incubated with spoiled fish. Lastly, storage and temperature stability studies confirmed that microneedle spoilage sensors maintained their pH responsiveness and mechanical integrity, despite exposure to diverse environmental condition.



**Figure 6.1. Overview of gelatin-anthocyanin fish spoilage sensor.** (a) Schematic illustration of developed sensor applied to sealed fish product for real-time monitoring. (b) Food-activated



hydration of gelatin-anthocyanin microneedles, inducing increase in microneedle diameter. (c) pH-induced colour change from purple to blue within microneedles as food product spoils. Some components produced using BioRender.

## 6.3 Results and Discussion

### 6.3.1 Dehydrated gelatin microneedle fabrication and characterization

Polydimethylsiloxane (PDMS) negative molds were first casted from a positive master mold with the desired dimensions, printed *via* stereolithography. Preliminary gelatin microneedles were fabricated through a simple casting approach (**Figure 6.2a**). Briefly, 5–20% w/v gelatin was added to deionized water, incubated at room temperature for 20 minutes to enable blooming, and then heated until completely transparent. This solution was then deposited onto the PDMS mold and stored under vacuum for 30 minutes to draw out entrapped air pockets. This procedure was performed at 80°C to prevent premature gelatin solidification. Upon subsequent removal from heat, the casted gelatin fully solidified within 10 minutes.

Reversible dehydration was enacted through treatments that succeeded gelatin gelation. Specifically, the casted gelatin microneedles were first stored at –20°C overnight to induce freezing. The needles were then incubated at 30°C overnight, yielding the final dehydrated microneedle patch (Figure 6.2b). This freeze-thaw approach is necessary to induce microstructural changes that increase microneedle strength, fluid absorption capacity, and dehydration efficacy. Specifically, as the water within the gelatin matrix freezes, it forms large, disorganized ice grains.<sup>[508]</sup> These grains condense surrounding polymer chains, facilitating physical crosslinking and the formation of inter-macromolecular bonds. This in turn, increases the microneedles' mechanical integrity. Moreover, the cavities produced by these large ice grains do not dissipate following thawing of the ice grains,<sup>[508]</sup> resulting in increased liquid absorption capacity relative to non-frozen gelatin microneedles. Finally, water molecules that are entrapped within the core of individual ice grains are unable to form hydrogen bonds with surrounding gelatin chains.<sup>[508]</sup> These water molecules are thus largely unstable within the polymer matrix, making them prone to

dehydration. Importantly, the microneedle patches were only removed from the PDMS negative mold following dehydration, wherein the mold acted as a structural scaffold for the microneedles during the freezing and dehydration steps.

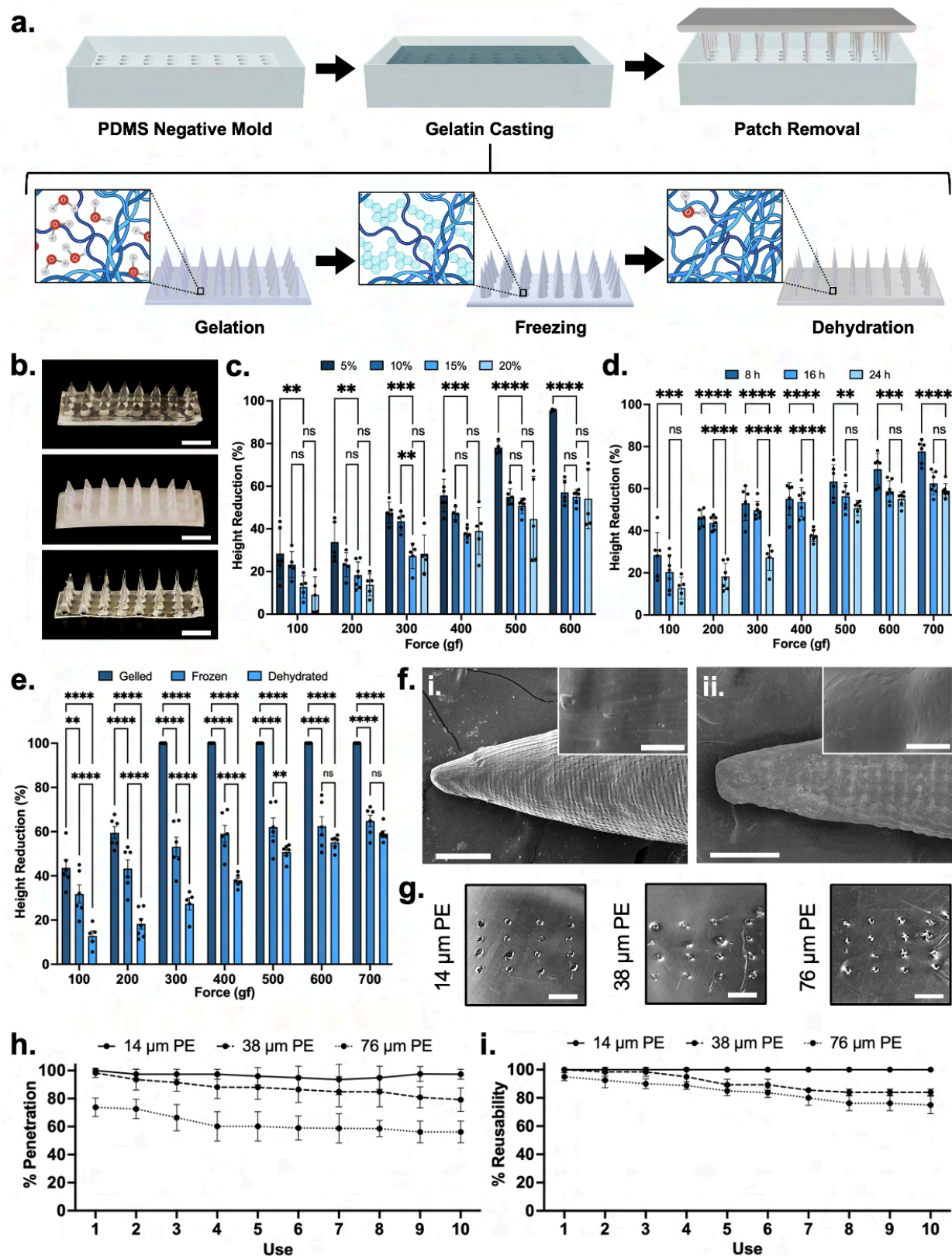
Mechanical optimization of the dehydrated microneedles involved considerations towards gelatin concentration in the precursor solution and the dehydration time. Sample conditions assessed through the microneedle height reduction observed following the application of perpendicular mechanical force, wherein a lower height reduction signals higher mechanical integrity. Gelatin w/v concentrations of 5%, 10%, 15%, and 20% were evaluated at forces ranging from 100 to 600 gram-force (gf) (Figure 6.2c). Dehydrated 5% gelatin microneedles exhibited significantly reduced mechanical integrity across all tested force conditions ( $P < 0.01, 0.01, 0.001, 0.001, 0.0001, 0.0001$ ) compared to dehydrated 15% microneedles. Between the dehydrated 10%, 15% and 20% microneedles, a slight decrease in mean height reduction was observed as concentration was increased. While these differences were generally not statistically significant, 10% dehydrated microneedles were noted to be slightly inferior to 15% and 20% dehydrated microneedles due to their higher height reduction mean values. While 15% and 20% dehydrated microneedles were largely similar with regards to their mean values, the latter exhibited higher variance in the degree of height reduction. It was noted that 20% gelatin concentrations yielded increasingly brittle properties, making the needles prone to snapping upon force application. As such, the 15% gelatin concentration was selected, wherein a height reduction of  $12.77\% \pm 5.20$  was observed at 100 gf and a height reduction of  $55.10\% \pm 3.33$  was observed at 600 gf.

To assess the effect of dehydration time on mechanical strength, samples dehydrated for 8 hours, 16 hours, and 24 hours were evaluated at forces between 100 and 700 gf (Figure 6.2d). Compared to the 24 hour samples, 8 hour samples exhibited significantly higher height reduction at all tested forces ( $P < 0.001, 0.0001, 0.0001, 0.0001, 0.01, 0.001, 0.0001$ ). Samples dehydrated for 16 hours demonstrated a significant improvement in mechanical strength relative to the 8 hour samples but were still significantly weaker than 24 hour samples at forces between 200 and 400

gf ( $P < 0.0001, 0.0001, 0.0001$ ). While differences were not significant at the other tested forces, the 24 hour samples consistently exhibited a mean height reduction lower than the 16 hour samples. Improvements in strength were not observed when dehydration was performed for longer than 24 hours. As such, 24 hours was noted to be the optimal dehydration time, wherein height reductions of  $12.77\% \pm 5.20$  and  $59.06\% \pm 3.05$  were observed at 100 gf and 700 gf, respectively.

With optimized fabrication parameters selected, an assessment of microneedle integrity was performed as each stage of post-gelation processing to understand the impact of freezing and dehydration (Figure 6.2e). Gelled microneedles offered very low mechanical strength, with height reductions of  $43.64\% \pm 9.03$  and  $55.55\% \pm 6.65$  at forces of 100 gf and 200 gf, respectively. This was significantly higher than both their frozen ( $31.80\% \pm 10.05, P < 0.01$ ;  $43.28\% \pm 9.61, P < 0.0001$ ) and dehydrated counterparts ( $12.77\% \pm 5.20, P < 0.0001$ ;  $18.25\% \pm 6.24, P < 0.0001$ ). Complete height reduction was observed at forces of 300 gf and above.

With regards to frozen microneedles, it is important to note that their mechanical integrity was temporary, as they mirrored the performance of gelled microneedles soon after removal from the  $-20^{\circ}\text{C}$  environment. Specifically, the exterior surface of the microneedle thawed almost immediately, while the inner core thawed within two minutes. Accordingly, frozen microneedles exhibited significantly higher height reductions at forces between 100 and 500 gf compared to dehydrated microneedles ( $P < 0.0001, 0.0001, 0.0001, 0.0001, 0.01$ ), as the thawed exterior offered little structural resistance to applied forces. At forces of 600 and 700 gf, the difference between the two conditions was not significant, owing to the temporarily intact ice core. Still, the mean height reduction values exhibited by dehydrated microneedles at these forces were lower than that of frozen microneedles. The dehydrated microneedles presented a breakthrough material that offered mechanical integrity superior to that of frozen microneedles, in a format that remains stable at room temperature.



**Figure 6.2.** Fabrication and characterization of dehydrated gelatin microneedles. (a) Schematic illustration of fabrication protocol. (b) Optical images of gelled, frozen and

dehydrated gelatin microneedles. Scale bar depicts 4 mm. (c) Optimization of gelatin concentration based on the mechanical strength of resultant microneedles. (d) Optimization of dehydration time based on the mechanical strength of resultant microneedles. (e) Baseline mechanical characterization of optimized gelled, frozen, and dehydrated microneedles. (f) Scanning electron microscopy images of (i) gelled and (ii) dehydrated microneedles. Main image scale bar depicts 150  $\mu\text{m}$ , while inset image scale bar depicts 10  $\mu\text{m}$ . (g) Optical images of food packaging films penetrated by dehydrated gelatin microneedles. Scale bar depicts 3 mm. (h) Percent penetration of dehydrated gelatin microneedles through food packaging films through ten uses. (i) Percent reusability of dehydrated gelatin microneedles through food packaging films through ten uses. All error bars depict standard deviation. All asterisks represent corresponding significance levels.

The gelled and dehydrated microneedles were subjected to scanning electron microscopy (SEM) (Figure 6.2f). Dehydration was signified by a significant reduction in microneedle diameter, alongside microscale textures that was attributed to gelatin crystallization. The dehydrated microneedles exhibited excellent penetration of fish – as a representative food matrix, and polyethylene food packaging films with thicknesses of 14 $\mu\text{m}$ , 38 $\mu\text{m}$  and 76 $\mu\text{m}$  (Figure 6.2g). To quantify the packaging penetration capabilities of the dehydrated microneedles, the percent of applied microneedles that effectively penetrated through the three polyethylene films was determined (Figure 6.2h). Single patches were tested over ten times to simultaneously assess the microneedles' resilience, with the number of reusable needles – total needles minus broken needles, noted after each trial (Figure 6.2i). With 14 $\mu\text{m}$  thick polyethylene, the penetration rate was consistently above 93% and reusability was noted to be 100.0% following ten trials. 38 $\mu\text{m}$  thick polyethylene films offered slightly more resistance, yielding 79.3% penetration by the tenth trial, and an 83.7% reusability rate.

Finally, testing with 76 $\mu\text{m}$  films resulted in a 56.2% penetration rate and a 75% reusability rate. Importantly, the reusability rate consistently references the number of intact microneedles at the start of the first use. When adjusted to the number of intact needles at the start of the tenth use, the penetration rates for 38 $\mu\text{m}$  and 76 $\mu\text{m}$  films are 94.7% and 74.9%, respectively. While the use of these microneedles for real-time spoilage sensing would only require a single penetration event, these studies demonstrate the mechanical robustness of the needles.

### 6.3.2 Anthocyanin integration and optimization

The integration of anthocyanin within the dehydrated gelatin microneedle matrix represented the next objective. Red cabbage anthocyanin was suitable due to its defined colour shift from purple to blue at pH 7.0, which corresponds with the fish spoilage threshold reported in prior literature.<sup>[31,509]</sup> Anthocyanin powder was first dissolved within deionized water to create a 1% w/v stock solution. This solution was then further diluted to 0.1%, 0.5%, and 0.9% in deionized water. Here, it was hypothesized that too low of a concentration would offer a suboptimal colour shift, which too high of a concentration would buffer the colour shift beyond the desired spoilage threshold. The change in absorbance exhibited by these three anthocyanin concentrations when exposed to fresh versus spoiled fish was quantified (**Figure 6.3a**).

Measurements were taken at several wavelengths to identify the optimal parameters for colour shift monitoring, wherein absorbance measured at 300 nm and 350 nm exhibited the most dramatic changes. While the differences between conditions were statistically insignificant, increased anthocyanin concentrations yielded slightly higher mean shifts in absorbance at 300 nm and 350 nm. Next, we sought to assess how shifts in absorbance correlated with pH on a day-to-day basis throughout the products' lifespan. Regression analyses were performed between the absorbance of anthocyanin solutions incubated with fish for 30 minutes and fish pH, over the course of 6 days (Figure 6.3b). Here, 0.1% anthocyanin solutions exhibited the lowest correlation with fish pH, with *r*-values of 0.8557 and 0.8424 at wavelengths of 300 nm and 350 nm, respectively ( $P < 0.05, 0.05$ ). On the other hand, the changes in absorbance exhibited by 0.5% and 0.9% anthocyanin solutions demonstrated strong correlation with fish pH, with *r*-values all above 0.95 ( $P < 0.01, 0.01, 0.01$ ). Importantly, 0.9% anthocyanin solutions were only quantified at 350 nm, as overflow was noted at 300 nm.

Recognizing that the dehydrated gelatin matrix may alter the colour-responsive properties of embedded anthocyanin, subsequent studies employed dehydrated gelatin microneedles embedded with the pH-responsive agent. In its initial state, the patch exhibits a faint purple hue (Figure 6.3c).

However, upon incubation within solutions with pH values of 6.0, 8.0, and 10.0, expected shifts to dark purple, blue, and green were observed in under five minutes. Importantly, this was the first indication that anthocyanin embedded within dehydrated gelatin remained fully functional and accessible for pH sensing. In fact, it was observed that the microneedles returned to a largely rehydrated state, similar to their initial gelled state to freezing and dehydration. To quantify the pH responsive behaviour of anthocyanins embedded within dehydrated gelatin matrices, the percent colour shift was then calculated between samples incubated at pH values of 4.0, 6.0, 8.0, and 10.0 (Figure 6.3d). When pH increased from 4 to 6 and 8 to 10, the shifts exhibited by the 0.5% dehydrated anthocyanin patches were significantly more dramatic than that of 0.1% ( $P < 0.0001$ , 0.0001) and 0.9% patches ( $P < 0.0001$ , 0.0001). While intriguing, applications towards fish spoilage were more accurately depicted by the pH 6.0 to 8.0 transition, wherein the 0.5% dehydrated anthocyanin patches demonstrated a much more substantial  $8.8\% \pm 1.7$  mean shift in colour compared to the  $2.6\% \pm 1.3$  mean shift exhibited by 0.1% patches ( $P < 0.0001$ ). The  $10.2\% \pm 1.3$  mean shift in colour exhibited by the 0.9% patches was not significantly different from the 0.5% patches, making both candidates relevant for application-specific testing.

### **6.3.3 Analysis and testing of spoilage-sensing microneedles**

To ensure that the introduction of anthocyanin at high concentrations does not yield significant alterations to the mechanical integrity of dehydrated gelatin microneedles, force testing was performed on dehydrated microneedles embedded with 0.1%, 0.5%, and 0.9% anthocyanin (Figure 6.3e). While samples embedded with higher anthocyanin concentrations exhibited slightly higher microneedle height reductions in response to the application of a perpendicular force, the changes were small in magnitude. Specifically, 0.1% and 0.9% dehydrated anthocyanin microneedles differed by less than 14% across all tested conditions.

Interestingly, 0.1% dehydrated anthocyanin microneedles generally exhibited less height reduction than dehydrated anthocyanin-free microneedles. This improvement in mechanical integrity is attributed to increased structural stability afforded by hydrogen bonding between free

anthocyanins and the polymeric microneedle matrix. While this would suggest that 0.5% and 0.9% dehydrated anthocyanin microneedles would exhibit even greater mechanical integrity, the aforementioned results depict the opposite effect. It is likely that the abundant free anthocyanins present within these samples engage in interactions with water molecules present within the gelled and frozen microneedle states. Bonded water molecules are resistant to extraction *via* dehydration, yielding a dehydrated material with slightly higher moisture content. Owing to these counteracting effects, there is little difference in the mechanical integrity of dehydrated anthocyanin-free and dehydrated 0.9% anthocyanin microneedles. Specifically, the two respective microneedle conditions demonstrate height reductions of  $12.77\% \pm 5.20$  and  $14.51\% \pm 6.94$  at 100 gf, alongside reductions of  $59.06\% \pm 3.05$  and  $60.87\% \pm 3.13$  at 700 gf. The hypothesized increase in anthocyanin-driven intermolecular interactions is supported by SEM images of anthocyanin-embedded microneedles (Figure 6.3f). Dehydrated microneedles with embedded with anthocyanins exhibit a significant increase in surface textures attributed to gelatin crystallization.

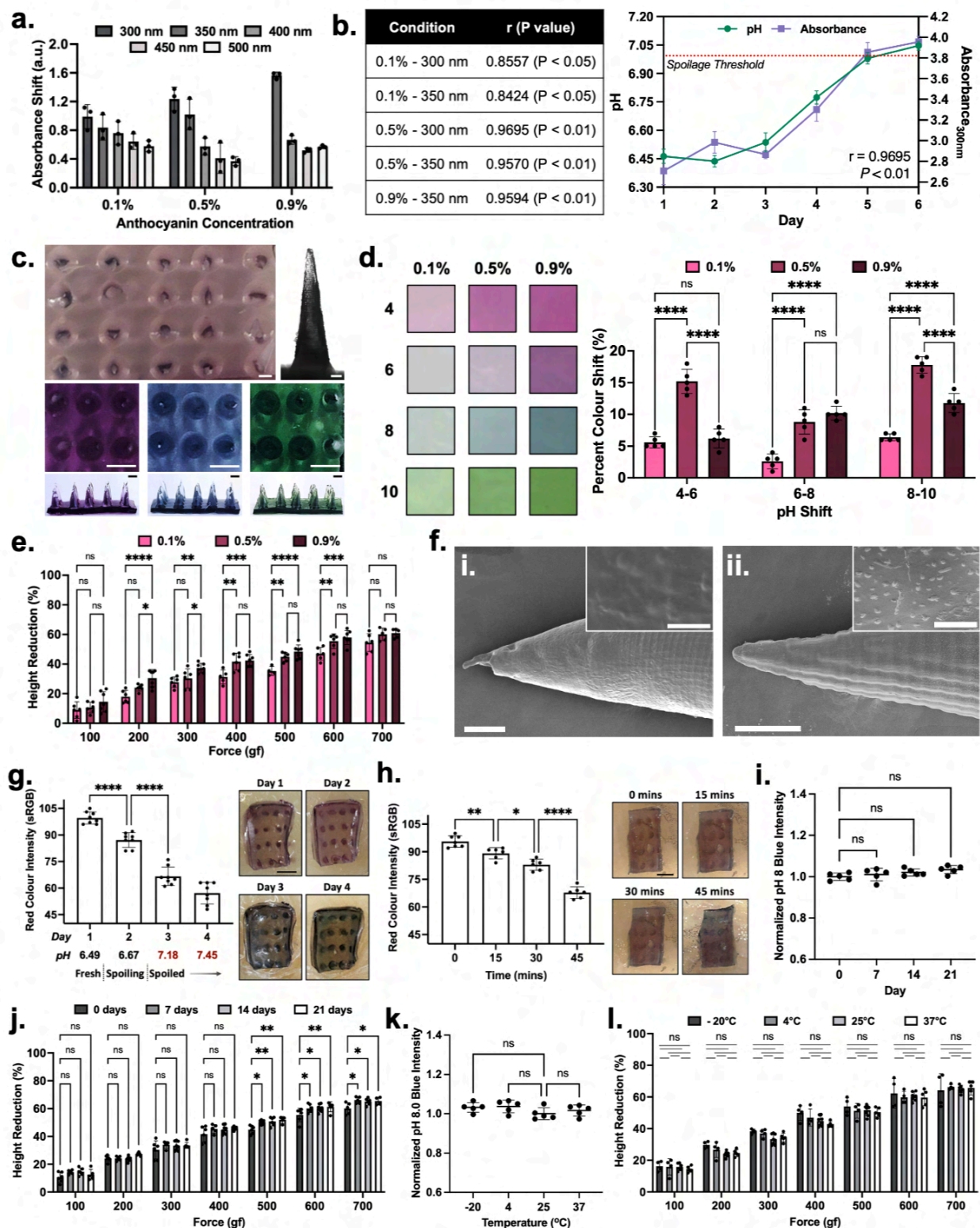
Next, we sought to investigate the real-time spoilage sensing properties of the developed microneedles, wherein the two aforementioned consumer-centric use cases were considered. With regards to non-destructive penetration of sealed food packaging for at-home, real-time spoilage monitoring, the 0.5% anthocyanin-embedded spoilage sensing patches behaved as predicted (Figure 6.3g). When packaged fish samples remained edible (Days 1 and 2), optical images collected using a smartphone depict patches with a defined purple hue. However, once the spoilage threshold of 7.0 was passed on Day 3, a dramatic shift to blue was observed, that became increasingly pronounced on Day 4.

A standard RGB scale was employed to quantify the loss of red colour intensity, as a function of the overall spoiled-induced colour shift exhibited by the microneedle spoilage sensors. Red colour intensity averaged arbitrary unit values of  $99.6 \pm 3.4$ ,  $87.1 \pm 4.2$ ,  $66.6 \pm 4.9$ , and  $57.1 \pm 6.0$  on Days 1 through 4, respectively. The significant decrease in red colour intensity that occurred between Days 1 and 2 ( $P < 0.0001$ ) as the fish approached spoilage was particularly



intriguing, as it presented the possibility of fresh, spoiling, and spoiled three classifications for automated sensing patch assessment. Contrarily, 0.9% anthocyanin-embedded spoilage sensing patches did not offer effective performance. This is attributed to the fluid content available within the fish matrix being insufficient for the induction of colour change within the highly concentrated anthocyanin environment present within these samples.

With regards to an at-home rapid test for opened products prior to consumption, spoiled fish samples were penetrated with the spoilage sensors and imaged with a smartphone every 15 minutes (Figure 6.3h). Again, a pronounced shift from purple to blue was observed. The mean red colour intensity was quantified according to a standard RGB scale, yielding arbitrary unit values of  $96.0 \pm 3.1$ ,  $89.2 \pm 3.1$ , ,  $84.8 \pm 3.2$ , and  $67.8 \pm 3.2$  at 0, 15, 30, and 45 minutes, respectively. Significant shifts were observed between each respective timepoint ( $P < 0.01$ , 0.05, 0.0001). Recognizing that passing the spoilage threshold in the day-scale monitoring study corresponded with a red colour intensity of  $66.6 \pm 4.9$ , 45 minutes was noted to be the required time for rapid test sensing. That being said, the significant downward trend exhibited at the 15 and 30 minute marks suggests that an automated sensing patch assessment platform may confirm spoilage within a shorter time span. Again, 0.9% anthocyanin-embedded spoilage sensing patches did not offer effective performance, which is attributed to the same reasoning detailed above.



**Figure 6.3. Anthocyanin incorporation into dehydrated gelatin microneedles and corresponding performance testing.** (a) Absorbance shifts observed through fish spoilage using various anthocyanin concentrations and measurement wavelengths. (b) Correlation analysis of anthocyanin concentration-absorbance wavelength combinations. (c) Optical images of an

anthocyanin-embedded dehydrated gelatin microneedle sensor, a single needle, and rehydrated patches following exposure to pH. 6.0, 8.0, and 10.0, from left to right. Coloured images have scale bars depicting 1 mm, while Brightfield image scale bar depicts 200  $\mu\text{m}$ . (d) Percent colour shift exhibited by sensors prepared using varying anthocyanin concentrations at different pH ranges. (e) Mechanical assessment of anthocyanin-embedded microneedle sensor. (f) Scanning electron microscopy images of (i) gelled and (ii) dehydrated anthocyanin-embedded microneedles. Main image scale bar depicts 150  $\mu\text{m}$ , while inset image scale bar depicts 10  $\mu\text{m}$ . (g) Quantification and associated images of real-time monitoring of sealed fish throughout its product lifespan. (h) Quantification and associated images of spoiled fish rapid test. (i) pH responsiveness of sensors after long-term storage. (j) Mechanical integrity of sensors after long-term storage. (k) pH responsiveness of sensors after storage at diverse temperature for 5 days. (l) Mechanical integrity of sensors after storage at diverse temperature for 5 days. All error bars depict standard deviation. All asterisks represent significant differences at corresponding significance levels.

Next, the impact of long-term storage on the pH responsiveness and mechanical integrity of dehydrated, anthocyanin-embedded microneedles was assessed. 0.5% anthocyanin-embedded sensing patches were stored for 7, 14, and 21 days in ambient conditions. These samples were subsequently incubated in pH 8.0 standard solution for 30 minutes, with the resultant blue colour intensity quantified (Figure 6.3i). No significant differences in the blue colour output was observed, confirming that the dehydrated gelatin environment did not influence anthocyanin functionality. Mechanical integrity also remained largely unchanged, with no significant differences observed amongst all storage samples below 400 gf (Figure 6.3j). While slight increases in mean height reduction were observed with long-term storage between forces of 500 and 700 gf ( $P < 0.01\text{--}0.05$ ), these differences did not exceed 8% under any tested conditions. With regards to on-package application, such a difference would induce negligible changes in penetration and reusability rates.

Finally, impact of temperature on the pH responsiveness and mechanical integrity of dehydrated, anthocyanin-embedded microneedles was evaluated. 0.5% anthocyanin-embedded sensing patches were stored at  $-20^{\circ}\text{C}$ ,  $4^{\circ}\text{C}$ ,  $25^{\circ}\text{C}$ , and  $37^{\circ}\text{C}$  for 7 days and subsequently tested using the same approaches used to assess the long-term storage samples. No significant changes in blue

colour output were observed, and mechanical stability did not significantly differ across any of the tested conditions (Figure 6.3k-l).

#### **6.4 Conclusion**

In this work, we introduce pure gelatin microneedles that offer shifts in their mechanical properties in response to environmental stimuli. The microneedles are produced through a three step process that involves gelation, freezing, and dehydration. In their initial state, the microneedles exhibit robust mechanical integrity – similar to that of frozen needles, in a stable form. Their excellent physical properties allow them to effectively penetrate through food packaging in a largely non-destructive fashion. Only when they come into contact with fluids, do these dehydrated gelatin microneedles return to a hydrogel state more typical of gelatin. When embedded with pH-responsive, colour-changing anthocyanins, this rehydration event makes anthocyanins accessible to the hydrating fluid, permitting colorimetric sensing. Recognizing that fish exhibits a defined pH change as it spoils and offer a fluid-rich sensing environment, it acted as an optimal testing matrix for a gelatin-anthocyanin microneedle spoilage sensor. When applied towards real-time monitoring of packaged fish, our spoilage sensor exhibits good correlation with spoilage events, offering dramatic shifts from purple to blue. In another vein, when applied directly onto spoiled fish as a rapid test to be used prior to consumption, a complete shift to blue is observed within 45 minutes. Moreover, while not obvious to the naked eye, subtle shifts in colour occur prior a full transition to blue. This introduces the possibility of improved performance using artificial intelligence. In the case of real-time packaged food monitoring, this could enact a “spoiling” classification to convey to the consumer that a product is approaching spoilage. With regards to rapid testing, such efforts stand to reduce detection time. Long-term storage and food-relevant temperature exposure both yielded limited changes to both the mechanical integrity and pH responsiveness of the developed sensor. Owing to its inexpensive, food-safe nature, this high performance sensor stands to offer consumers with the power to effectively assess the quality of purchased foods for the first time.

## 6.5 Materials and Methods

*Materials.* Polydimethylsiloxane (SYLGARD 184) was purchased from Dow Corning (Michigan, United States). Gelatin was purchased from Fortino's (Ontario, Canada). Polyethylene wraps were sourced from Thomas Scientific (New Jersey, United States) and Walmart Canada (Ontario, Canada). pH standard solutions were sourced from Millipore Sigma (Ontario, Canada). Red cabbage anthocyanin was purchased from Universe of Science (United States). Haddock fillet samples were purchased from Food Basics (Ontario, Canada).

*Resin master mold fabrication.* A CAD model of a microneedle mold was designed in Autodesk Inventor, ensuring precise dimensions and features. The 3D model file was then converted into an STL file, recognized by the stereolithography (SLA) 3D printer. Black resin was used as the printing material, and the printer created the mold layer by layer, resulting in a detailed and accurate microneedle mold. Once the print was complete, it was rinsed with 100% isopropyl alcohol to remove excess resin on the surface and then dried. Post-curing of the molds involved placing the printed parts in a water bath and exposing them to UV light on both sides for 10 minutes, followed by overnight drying at 30°C. This post-curing process maximized the mechanical strength and ensured stability of the molds.

*PDMS negative mold fabrication.* PDMS Sylgard 184 was prepared at a 10:1 ratio of base resin to curing agent, stirred for 10 mins, and then desiccated for 30 mins. This mixture was then casted onto the resin master molds and desiccated again for 30 mins. The casted PDMS were then cured at 60°C overnight and then detached from the master mold to obtain the PDMS negative mold.

*Gelled microneedle fabrication, freezing, and dehydration.* Gelatin powder was added to deionized water at 5%, 10%, 15%, and 20% w/v concentrations. The mixtures were then stirred and left to bloom for 10 mins and then heated until transparent using a conventional microwave. The resultant solution was casted onto pre-heated PDMS negative molds and placed under vacuum at  $-0.08$  MPa for 5 mins at 80°C. Any entrapped air pockets visible after desiccation were physically agitated with a needle and removed. The casted solutions were left to gel for 10 minutes before proceeding

to post-fabrication treatment steps. At this point, the gelled microneedles were left adhered to the negative mold and placed into a conventional freezer set to  $-20^{\circ}\text{C}$  for 24 h. The microneedles-mold pairing was then subsequently placed onto a hot plate set to  $30^{\circ}\text{C}$  for 8 h, 16 h, or 24 h dehydration times. Microneedles were separated from the mold only after dehydration. Anthocyanin-embedded microneedle fabrication followed the same protocol, but used 0.1%, 0.5%, and 0.9% anthocyanin solutions instead of deionized water.

*Microneedle imaging.* Colour optical images of the microneedle patches were taken using a Samsung Galaxy S21 Ultra smartphone. Brightfield imaging of a single needle was performed using a Nikon Eclipse Ti2 inverted microscope.

*Mechanical testing.* In preparation for mechanical testing, each microneedle patch was precisely cut into rows of four needles. To evaluate mechanical integrity, the force was normalized to range from 100 gf to 700 gf per individual needle. High-resolution images of the needles were taken before any force application to document the baseline structure. A Biomomentum Mach 1 mechanical tester was used to apply perpendicular incremental forces, ranging from 100 gf to 700 gf, to the microneedles. After each subsequent increase in force, additional images were captured to analyze any deformations or structural failures. Using these images, the height reduction of the individual microneedles was then measured to assess mechanical strength. Lower height reductions indicated higher mechanical integrity. Data from different force levels were compared to evaluate the mechanical properties of the microneedles under varying stress conditions. This standardized method ensured consistent evaluation of microneedle mechanical properties across multiple samples with varying conditions.

*Scanning electron microscopy.* Single microneedles were isolated from their base to induce a two-dimensional form factor that was better suited for top-down perspective imaging. Samples were mounted using carbon tape and nickel paste. A sputter coater (Polaron E1500, Polaron Equipment Ltd., Watford, Hertfordshire) was subsequently used to coat the samples with 5 nm of platinum. Samples were imaged using the JEOL JSM-7000F.

*Penetration and reusability studies.* Polyethylene films of varying thickness were secured across the top of a cylindrical support. Microneedle patches were then placed on top of the films with the needles facing down. A mechanical tester was used to apply a consistent force of 500 gf. The patches were then removed, and the number of penetration sites was quantified to determine the penetration rate. This number of undamaged individual microneedles in a patch was also quantified to determine the patch reusability rate. Both rates were calculated as a function of the initial needle count. Patches were subjected to 10 successive trials each.

*Anthocyanin absorbance versus pH studies.* Haddock fish fillets purchased from a local grocery store were divided into 5 g samples and individually stored in sealed bags. Three samples were subjected to pH assessment each day using a Mettler Toledo SevenExcellence pH meter. Next, 0.5 g portions were isolated from each sample for anthocyanin colour change assessment. These portions were added to 1 mL aliquots of anthocyanin solutions with concentrations of 0.1%, 0.5%, and 0.9% and incubated for 30 mins. 100 $\mu$ L samples of the tested solutions were then added to a well plate for absorbance measurements at various wavelengths. Absorbance readings were taken using a Synergy Neo2 plate reader.

*Colour shift studies on dehydrated anthocyanin-embedded patches.* Dehydrated anthocyanin-embedded patches were subjected to 4.0, 6.0, 8.0, and 10.0 pH standard solutions. After 15 mins of incubation, the samples were imaged using an Epson Perfection V850 Pro Scanner. Quantification of colour shifts involved viewing each colour as a three-dimensional coordinate on an RGB colour map. From here, the distance between two colours was quantified as:

$$d = \sqrt{[(R_1 - R_2)^2 + (G_1 - G_2)^2 + (B_1 - B_2)^2]}$$

The distance was then referenced as a percent of the maximum distance between two colours:

$$\text{Percent colour shift (\%)} = d/\sqrt{[255^2 + 255^2 + 255^2]}$$

*Day-scale monitoring of sealed fish products.* Haddock fish fillets purchased from a local grocery store were divided into 5 g samples and individually wrapped with polyethylene packaging film.

Microneedle spoilage sensors were inserted through the packaging film, into the underlying fish matrix. A secondary film was secured overtop the sensor to prevent unwanted air exposure. The samples were stored in the fridge and imaged using a smartphone every day, until spoilage was well-established. Quantification of colour involved assessing the intensity of red colour at the microneedle dots observable through the patch. As fish spoiled, a loss in red colour was observed.

*Minute-scale monitoring of opened fish products.* Haddock fish fillets purchased from a local grocery store were divided into 5 g samples and stored until spoiled. The samples were then penetrated with microneedle spoilage sensors and imaged every 15 minutes. Again, quantification of colour change involved assessing the intensity of red colour at the microneedle dots observable through the patch, wherein a loss in intensity was observed as the microneedle patches rehydrated.

*Storage and temperature stability studies.* Microneedle spoilage sensors were stored under ambient conditions for 7, 14, and 21 days. They were then subjected to mechanical testing, as described above. Their pH responsiveness was assessed through 20 mins incubation in pH 8.0 standard solution, wherein the samples were scanned using an Epson Perfection V850 Pro Scanner. Quantification involved assessing the blue colour intensity outputted at the microneedle dot sites observable through underside of the patch.

## **6.6 Acknowledgements**

S.K. and A.P. are recipients of the Vanier Canada Graduate Scholarship awarded by the Natural Sciences and Engineering Research Council of Canada. S.K. is also a recipient of the Banting Postdoctoral Fellowship awarded by the Natural Sciences and Engineering Research Council of Canada. This work was supported by the Ontario Early Researcher Award, Mitacs and Toyota Tsusho Canada Inc. grants to TFD. T.F.D. is a Tier II Canada Research Chair in Nanobiomaterials.

## **Conflict of Interest**

The authors declare no conflict of interest.



## **Chapter 7: Antimicrobial Bacteriophage-loaded Microneedle Patches that Counteract Bacterial Pathogen Contamination to Prevent Foodborne Illness**

### **Preface**

As discussed in Chapter 1, a second approach towards improving food safety involves efforts to decontaminate foods harbouring pathogenic agents. Given their cost-effective and food-safe nature, bacteriophages represent one of the most effective tools towards such enacting such measures. In fact, there is an extensive body of literature the details the potent antibacterial activity afforded by bacteriophage-incorporating materials towards the decontamination of food surfaces. However, recognizing that pathogen contamination extends beyond the accessible surface of food products, effective delivery of these agents into interior matrices is needed. Under this premise, and in accordance with Objective 4, this chapter details the development of a microneedle-based bacteriophage delivery platform for food. The system is designed for use on fluid-rich food products with difficult-to-permeate external layers. This includes peel-encased fruits and vegetables, as well as meat products with oil-rich skins. When employed against contaminated products with such properties, microneedles offer a cost-effective, easy-to-use mechanism for bacteriophage delivery into the underlying fluid-rich environment, wherein the agents can autonomously distribute themselves. Given the lack of literature detailing the use of microneedles for on-food applications, this work first assesses five well-established, food-safe microneedle materials with regards to their material properties and how they can be employed towards food-centric applications. Subsequent analysis of the microneedle candidates involves subjecting them to food-specific environmental stimuli to evaluate their resilience. Identification of the optimal material for the proposed platform is succeeded by the spray-based loading of *E.coli*-specific bacteriophages onto these microneedles. These microneedles were evaluated with regards to their antibacterial activity within whole chicken breast products. When compared with flat material patches loaded with the same concentration of bacteriophage, a near 99.9% reduction in target bacterial load is observed. When employed against products soon after a contamination event – when the bacterial load is still relatively low, the bacteriophage-loaded microneedles effectively return contaminated products to a food-safe state, where their pathogen load is below regulatory thresholds.

### **Authors**

Akansha Prasad<sup>†</sup>, Shadman Khan<sup>†</sup>, Hareet Sidhu, Fatima Arshad, Kyle Jackson, Roderick MacLachlan, Zeinab Hosseinidoust, Carlos D. M. Filipe, Tohid F. Didar

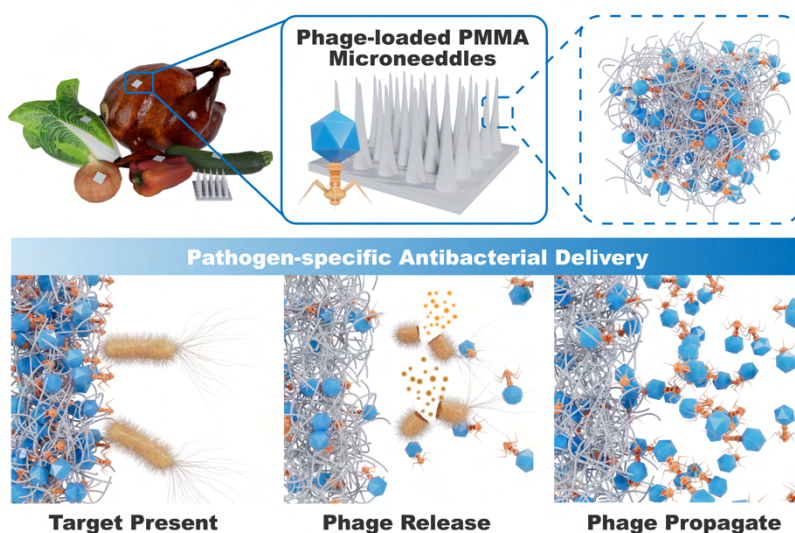
<sup>†</sup> These authors contributed equally.

In this work, five food-safe microneedle material candidates were selected for assessment towards on-food applications. Criteria for assessment included background fluorescence, force testing, material swelling, reusability, and resiliency testing following exposure to diverse storage time, mechanical strain, temperature, and pH conditions as indicated by mechanical force testing.

Baseline penetration studies were also performed using agarose as a sample matrix. Penetrative ability was then more comprehensively assessed using a diverse range of target foods, where force application was mediated by a force tester. The resilience of the microneedle materials was then assessed in the face of various food-specific conditions, as quantified by subsequent penetrative ability and reusability. These included produce tumbling, chicken and fish microenvironment exposure, and vacuum packaging. Finally, the selected microneedle material was loaded with an *E. coli*-specific bacteriophage. The baseline food-relevant properties of the bacteriophage and its associated delivery mechanism were assessed via plaque assays. Bacterial reduction in contaminated food involved pulverizing food products after incubation and subjecting the collected solution to selective plating.

## Publication

*Pending*



## 7.1 Abstract

Foodborne illness continues to persist as a major global crisis, only exasperated by retroactive food recalls that are often placed after contaminated food has been consumed. Consequently, various antibacterial food additives have become increasingly popular, despite hesitancy surrounding their specificity, stability, and food safety. Bacteriophages represent extremely promising antibacterial agents for food treatment, offering targeted bacterial lysis while being food-safe. However, successful commercial viability of bacteriophage-platforms requires delivery into the 3D food matrix without any organoleptic property disruption – a design requirement which has proven elusive. Herein, we present bacteriophage-loaded PMMA microneedle patches that are capable of providing effective bacteriophage delivery into food in a minimally disruptive manner, yielding significant reductions in pathogen load. Various microneedle materials are first comparatively assessed to determine the optimal substrate for this platform. For the first time, microneedle performance is also evaluated for food-specific application through penetration, reusability and stability studies performed with a diverse range of food products as well as through the use of food-centric experimental conditions. The platform is finally substantiated by comparing its bacterial reduction efficacy against flat patches. Here, a near 3-log bacterial reduction improvement was enacted by the microneedle platform, rendering the treated product food-safe under certain circumstances.

**Keywords:** food safety, antibacterial food additives, bacteriophages, microneedle arrays

## 7.2 Introduction

Despite recent technological advancements and more stringent regulatory measures, foodborne illness persists as a major global crisis, resulting in over 600 million annual cases and causing 7.5% of all annual deaths.<sup>[510,511]</sup> The presence of pathogenic contaminants such as *Escherichia coli* O157:H7, *Salmonella typhi*, and *Listeria monocytogenes* will only rise as our reliance on intricate, multi-faceted global supply chains continues to grow.<sup>[512]</sup> Current industry standards for mitigating this crisis involves pathogen detection through inefficient food analysis procedures,

which trigger retroactive and expensive food recalls.<sup>[513]</sup> Almost 50% of these recalls are attributed to the presence of microbiological contamination, making the removal of pathogenic entities from our food supply imperative. Ready to eat (RTE), produce and poultry products are amongst the most recalled items, making them of particular interest.<sup>[514]</sup>

Given the gravity of this crisis, the introduction of various antibacterial agents directly into food products has garnered significant interest.<sup>[515]</sup> Metal additives including silver and zinc oxide nanoparticles as well as chemical compounds such as vanillin derivatives and phenols are popular choices as they are scalable, food-safe, and have high bactericidal activity.<sup>[516–519]</sup> However, these agents are all limited in their poor specificity to pathogenic bacteria, often also eliminating naturally occurring microbes within the food matrix and in turn disrupting the organoleptic properties of the food product.<sup>[520,521]</sup> The addition of essential oils has also been considerably explored given their strong antibacterial activity and improved specificity.<sup>[522]</sup> However, their real-world use is also unfeasible given their poor stability and effect on organoleptic food properties.<sup>[523]</sup>

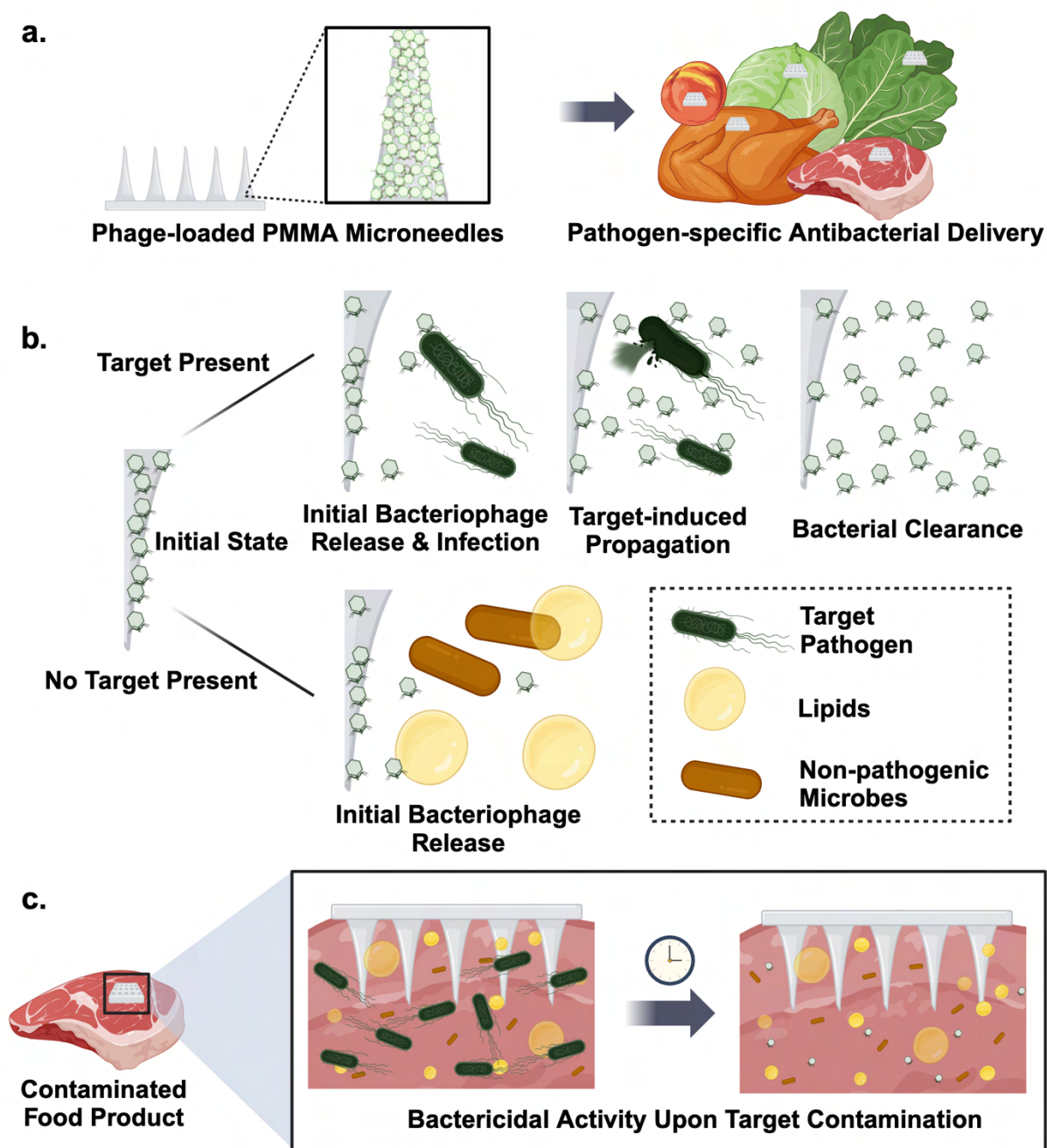
Another organic additive, lytic bacteriophages, or viruses that infect and lyse bacteria with strain-level specificity, have now emerged as one of the most promising antibacterial food additives.<sup>[524–526]</sup> These agents are abundant in nature, diverse, and FDA-approved for use in food, making them especially advantageous for widespread use.<sup>[527,528]</sup> Notably, they also offer target-induced antibacterial amplification – a property that sets it apart from every other antibacterial agent. Specifically, upon infecting a host bacterium infection, a single bacteriophage effectively hijacks the host's machinery to exponentially produce progeny copies of itself. Once bacterial lysis occurs, a burst of progeny bacteriophage is released, yielding a higher free bacteriophage concentration for subsequent antibacterial activity. Known as autodosing, this phenomenon is largely responsible for the potent antibacterial activity exhibited by these agents.<sup>[524]</sup>

Bacteriophage-centric efforts for food have largely sought to develop liquid suspensions that are specific to the aforementioned high-risk pathogens, with many suspensions now commercially available.<sup>[526,529]</sup> While these platforms have immense promise given that they are safe and cost-effective, their efficacy is questionable against solid food matrices, as they are only

applied on the exterior surface of treated foods.<sup>[530,531]</sup> While such immersion and spray-based deposition onto food surfaces has offered effective pathogen eradication of surface-borne pathogens, very limited antibacterial activity is observed within the contaminated food matrix.<sup>[531]</sup> This ineffective performance driven by an inability to both penetrate through protective exterior layers of food, and disseminate throughout the dense, interior matrix. While recent developments towards sprayable bacteriophage microgels and bacteriophage-incorporated packaging films have presented intriguing benefits, neither offer the in-food antibacterial activity that is needed.<sup>[532,533]</sup>

Bacteriophage dissemination through dry food matrices would require an external propulsion mechanism – a premise that would prove difficult to enact in a food-safe, cost-effective manner. However, fluid-rich foods that are protected by external layers with low permeability offer an environment in which the enactment of initial bacteriophage delivery would offer significant benefit. Here, bacteriophage penetration through the outer layer would be followed by autonomous agent distribution. Such penetration may be most easily enacted through the use of microneedles. While these structures have been extensively explored for clinical applications, they have rarely been used for on-food applications.<sup>[25]</sup> Microneedles represent a robust tool for the delivery of desirable agents into food, as they offer penetrative ability through dense matrices, in a low-cost form factor that is easily applied by hand.

Under this premise, we have developed food-safe, bacteriophage-loaded microneedles, which enable bacteriophage delivery into food high-risk, fluid-rich matrices, for effective antibacterial activity. To ensure widespread applicability to a diverse range of food products, we first compared the performance of various polymeric materials through various mechanical and stability characterization as well as through food-specific validation studies to determine the ideal candidate material. While microneedle arrays pose immense promise within the food monitoring industry, the lack of research towards this application limits their use in the space. Such food-centric testing represents the only extensive characterization of microneedles for food-based application and stands to provide a foundation for future works.



**Figure 7.1. Schematic overview of bacteriophage-loaded microneedles.** (a) PMMA polymeric chains with bacteriophage incorporation applied to assorted food items as antibacterial additives. (b) Selective bacteriophage delivery only upon target presence to provide contaminant lysis and resultant bacterial clearance and bacteriophage propagation. Bacteriophage remain loaded in the presence of other food constituents including lipid molecules and non-pathogenic microbes to prevent nonspecific delivery. (c) Bacterial clearance and decontamination in food products to prevent foodborne illness and food waste.

Once an optimal material for bacteriophage delivery was identified, T7 bacteriophages specific to *Escherichia coli* were incorporated onto their surface *via* spray deposition. Here, effective delivery of bacteriophages into produce and meat products was demonstrated. Finally, to assess their antibacterial activity, these bacteriophage-loaded microneedles were applied to *E. coli*-contaminated whole chicken breasts. Contamination was induced deep within the bulk food matrices, to ensure that autonomous bacteriophage movement was viability in such environments. High bacterial reduction was demonstrated, exceeding the performance offered by a bacteriophage spray-coated flat patch by over three-logs. Under some test conditions, the degree of pathogen reduction was sufficient to render the product safe to consume, in accordance with established regulatory guidelines.

## **7.3 Results and Discussion**

### **7.3.1 Bacteriophage-loaded microneedles overview**

Overarchingly, we aimed to design the bacteriophage-loaded microneedle platform to provide pathogen-specific antibacterial activity within fluid-rich food products *via* penetration through dense external layers. This effectively decontaminates food products, making them safe for consumption. A full overview of our developed platform is shown in **Figure 1**. Notably, all materials used in this work are approved for on-food use by the Food and Drug Administration (FDA), designated as Generally Recognized As Safe (GRAS).<sup>[512,534]</sup>

### **7.3.2 Baseline microneedle material performance assessment**

A detailed comparison of various microneedle material candidates was first performed to better understand the affect material choice has on microneedle properties and in turn, possible on-food applications. The biocompatible polymers polymethyl methacrylate (PMMA), polyvinyl alcohol (PVA), polydimethylsiloxane (PDMS), and gelatin were selected as potential candidates. A micromolding-based fabrication approach was employed for all four materials using a stereolithography (SLA)-printed custom mold, a tuneable and scalable method commonly used for microneedle fabrication (**Figure 2a**). Microneedle patches of the candidate materials (**Figure 2b**) were then imaged *via* scanning electron microscopy (SEM) (**Figure 2c**) to better visualize their

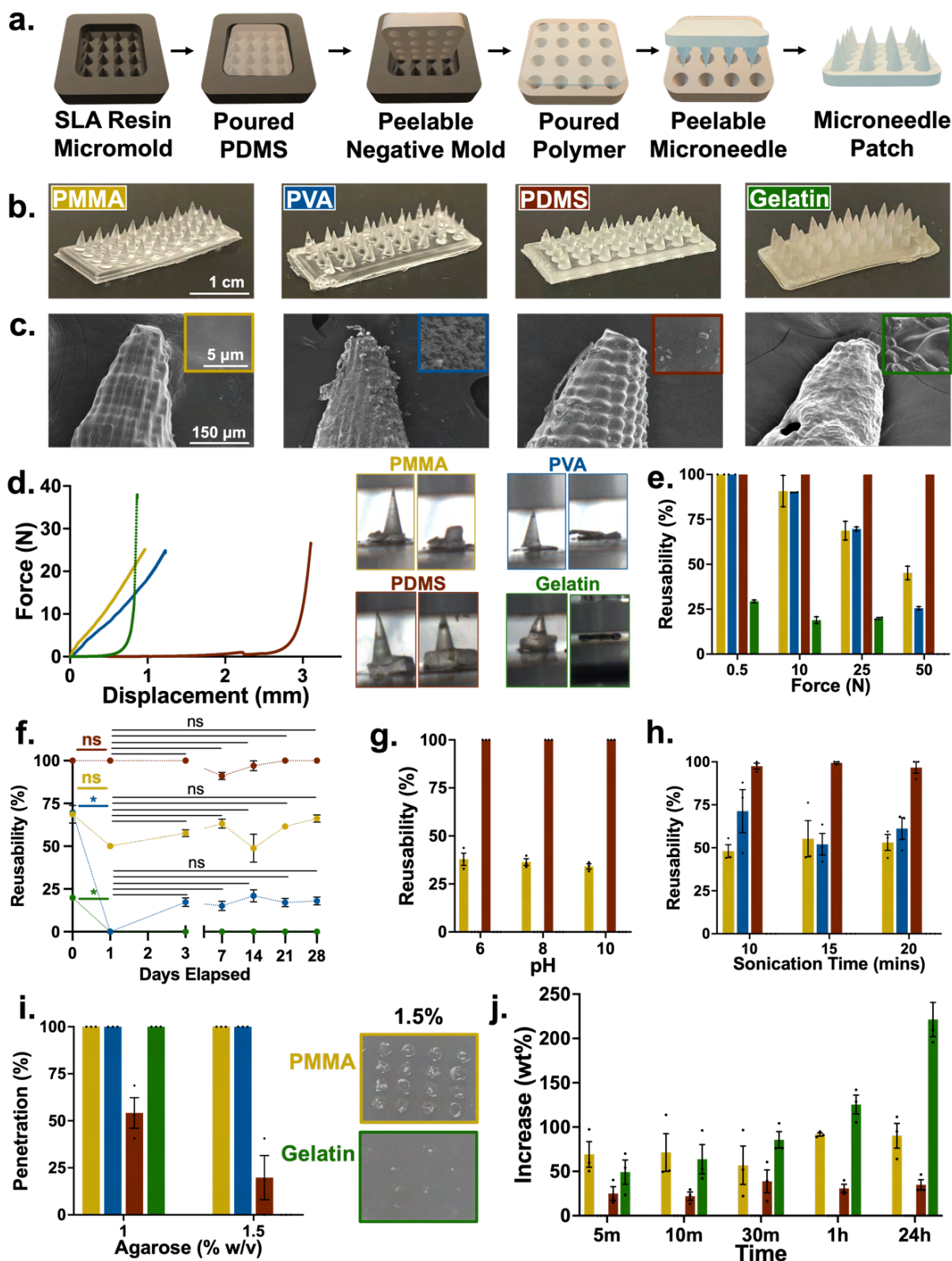
resolution and structure. While PMMA, PVA, and PDMS appeared relatively similar in structure, gelatin exhibited a highly textured surface both in 350X and 10000X images due to the amorphous nature of its polymeric chains.<sup>[535]</sup> The fluorescence profiles of all materials were also assessed, where all materials exhibited low fluorescence across the visible light spectrum, suggesting potential use for fluorescent-based monitoring.

Extensive stability and penetration characterization of the microneedle arrays was then performed. Preliminary assessments were conducted using compression testing, with deformation curves shown on force versus displacement graphs (Figure 2d). Owing to its relatively brittle nature, PMMA is more fracture-prone but boasts high tensile strength, resulting in a steep linear curve with a sudden drop.<sup>[536]</sup> PVA exhibited a similar curve, also indicative of its high elastic modulus and in turn stiffness when under compression until its compressive stress is reached.<sup>[537]</sup> Opposingly, both PDMS and gelatin demonstrated elastic behaviour, demonstrated by the gradual increase in slope until a failure point is reached.<sup>[538,539]</sup> PDMS, in particular, demonstrated high abilities to recover original shape given its low elastic modulus.<sup>[538]</sup> The reusability of the needles was then assessed under compressive loads, quantified as the percentage of microneedles that remained undamaged – and thus could be reused after compression at forces of 0.5, 10, 25, and 50 N (Figure 2e). As expected, both PMMA and PVA demonstrated linear decreases in recovery as force increased, in line with their linear deformation curves. Both PDMS and PMMA had relatively consistent reusability, however the PDMS microneedles remained undamaged even at the highest forces given their high elasticity. Since only 25% of gelatin needles remained intact after only 0.5 N of force, their use as penetrative microneedles remained uncertain. Subsequent stability testing involved storing the microneedle samples for short-term (24h, 48h, 72h) and long-term (1wk, 2wk, 3wk, and 4wk) periods and subsequently repeating 25 N compression testing (Figure 2f). Overall, these tests displayed similar trends, with PDMS exhibiting the highest reusability across all timespans and conditions and PVA and gelatin both exhibiting minimal reusability. Both PDMS and PMMA had no significant deficits in their strength compared to their baseline value throughout the 1 month period ( $P > 0.05$ ). However, both PVA and gelatin exhibited significant depletion in



their mechanical strength over the initial 24 hour period ( $P < 0.05$ ), after which performance stabilized. The poor stability of the latter polymers is attributed to their aqueous hydrogel nature, which deteriorates with long-term storage, yielding a depletion in mechanical strength.<sup>[540]</sup> A similar test was performed after 24 hour storage in environments with pH levels of 6.0, 8.0, and 10.0 to assess resiliency in acidic and basic environments (Figure 2g). Again, PDMS had no deterioration in performance, while PMMA saw about a 50% reduction in reusability. Both PVA and gelatin microneedle were completely degraded by aqueous storage. Resilience against mechanical stress *via* exposure to sonication was also explored after 10, 15, and 20 minutes (Figure 2h). As expected, PDMS and PMMA both had similar reusability compared to their baseline value. Intriguingly, the PVA microneedles were also able to retain their original performance despite the mechanical stress, which is attributed to the strong hydrogen bonds innately present within the hydrogel. The gelatin microneedles were fully degraded, given their poor mechanical strength.

After stability was characterized, broad application-specific properties were explored. The general penetrative strength of the different microneedle materials was first considered by exploring the penetration of these patches into agarose discs of varying strength (Figure 2i). Given their high tensile strength, both PMMA and PVA microneedles outperformed the other candidates and exhibited 100% penetration. The gelatin microneedles were also able to provide complete penetration of the softer 1% agarose disk but were destroyed when attempting to penetrate through a 1.5% disk. Despite their high reusability, the PDMS microneedles had extremely poor penetration due to their extremely elastic nature, which provided insufficient penetrative strength, yielding a maximum penetrative strength of only 50%. The absorption capacity of the various microneedle candidates was also briefly explored, where the gelatin microneedles absorbed significantly higher amounts of water based on its natural swellability (Figure 2j).<sup>[535]</sup>



**Figure 7.2. General microneedle characterization and material comparison.** (a) Overview of microneedle fabrication via micromolding process. (b) Optical images of microneedle array patches. (c) SEM images of microneedles at 350X with 10000X overlays. (d) Compression testing

force-displacement curves of all material candidates with associated pre- and post-compression microneedle images. (e) Microneedle reusability across increasing forces for all candidate materials. (f) Short and long-term stability of all microneedle with asterisk representing significant differences at corresponding significant levels. (g-h) Continued microneedle stability testing through exposure to (g) pH levels and (h) sonication-based stressors. (i) Preliminary penetration assessment of all microneedle material candidates based on penetrative performance in agarose pucks of varying density with pictures showing penetration in 1.5% agarose. (j) Water absorbance of PMMA, PDMS, and gelatin overtime. All reported values represent the mean of all samples with error bars representing standard error of the mean.

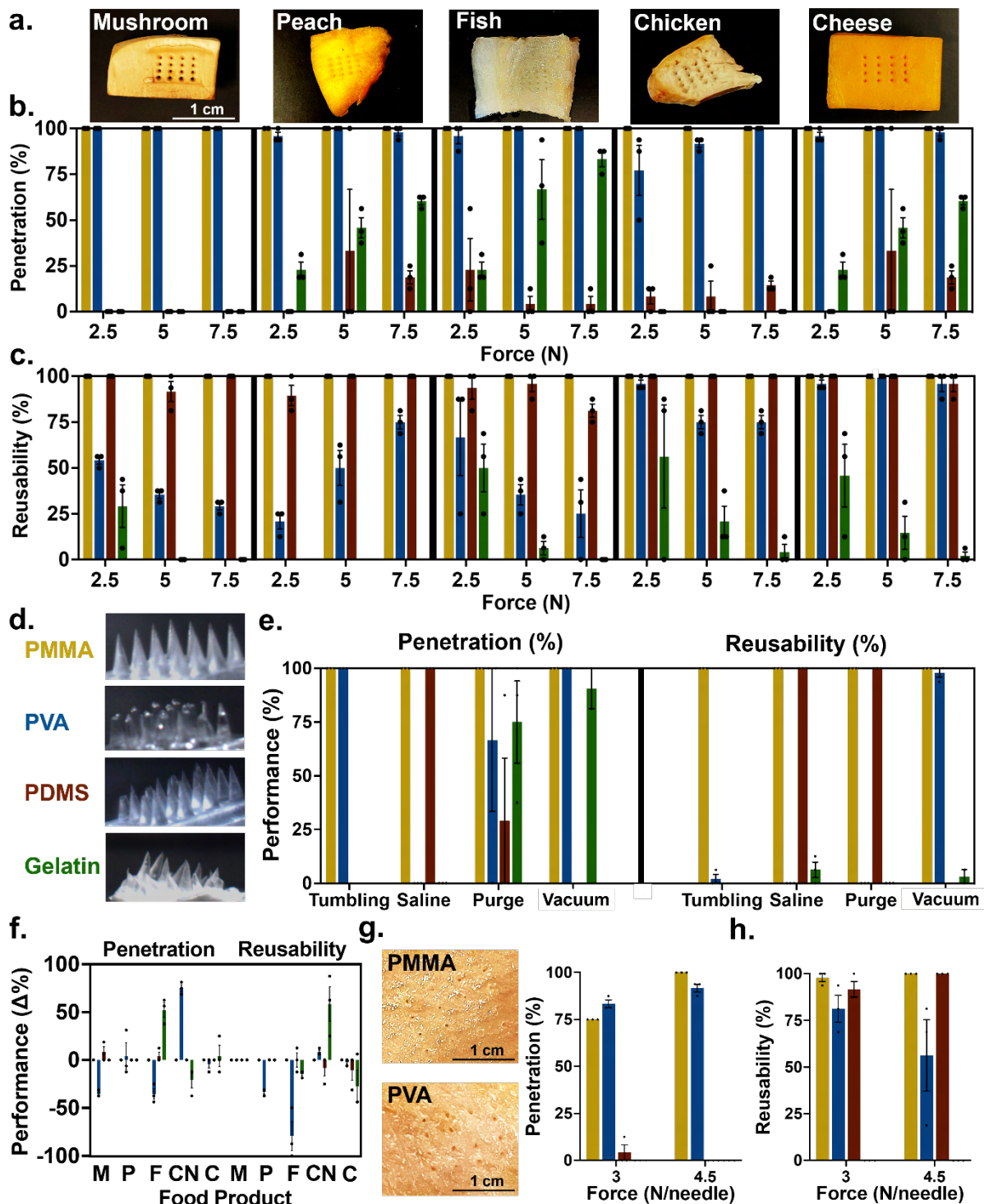
The PVA microneedles were omitted from this study as they readily dissolve in water.<sup>[541]</sup> Overall, the PMMA microneedles demonstrated the best balance between stability as well as mechanical and penetrative strength. While extremely stable, the elastic PDMS microneedles lacked penetrative abilities. Finally, while gelatin microneedles offer very low penetrative ability, PVA microneedles could be employed towards rapid agent delivery given their dissolvable nature. They are, however, not suitable for prolonged on-food applications. Nonetheless, all materials were still characterized for their potential application within food products, especially considering that various additives and fabrication techniques may be employed to tune material properties.

### **7.3.3 Comparison of microneedle materials for food-specific applications**

The different microneedle materials first underwent extensive penetration and reusability characterization to assess their on-food viability with diverse food products. Reusability is of particular concern when creating products for use within the food industry to ensure cost efficiency. Importantly, the ideal material candidate for bacteriophage delivery will offer both high penetration and reusability. The assorted food products selected for testing included produce (mushrooms and peaches), fish, poultry (ready-to-eat chicken), and cheese (**Figure 3a**). Undoubtedly, microneedle patches cannot be used with every food product. However, the selected range of products exhibited diverse textures, fluid compositions, temperatures, and densities to ensure the robust characterization of the microneedle materials. Penetration and reusability studies (**Figure 3b-c**) were conducted at insertion forces of 2.5, 5, and 7.5 N, a range in line with those used in clinical studies to consistently approximate user-applied penetrative force. PMMA

demonstrated regularly higher 100% penetration and reusability for all food items, making it a strong candidate. PVA also demonstrated high penetration across almost all food items except for chicken, while displaying mixed reusability. Similar to the previous characterization studies, PDMS exhibited high reusability, but poor and inconsistent penetration performance due to its elasticity. Interestingly, gelatin had improved penetration in fluid-rich foods such as peach and fish samples as well as softer foods like cheese. However, it had relatively low and very inconsistent reusability. To further elaborate on reusability, the PMMA microneedle patches remained perfectly intact, only the microneedle tips were damaged in PVA and PDMS needles, and the gelatin microneedle patches were completely destroyed across most food items (Figure 3d).

The validity of these platforms was then substantiated through more food-centric studies, wherein microneedles were inserted into food items and then subjected to various food-relevant stressors (Figure 3e). First, microneedle-containing mushrooms and peaches were subjected to mechanical tumbling at similar speeds to those utilized in automated produce processing, where both PMMA and PVA had high penetration but only the former exhibited any reusability. Both the PDMS and gelatin patches failed to stay within the food products during tumbling, given their elastic nature. Next, the microneedle samples were exposed to food matrix fluids in the form of fish saline fluid and chicken purge. With respect to immersion in fish saline, both PMMA and PDMS demonstrated high resiliency. However, both PVA and gelatin had poor performance despite their previously high penetration in fish. This drastic decrease in performance is attributed to the significantly higher volume of salt they were exposed to in this incubation. The hygroscopic nature of the salt-rich exterior environment is credited to the exasperated hydrogel breakdown and in turn poor mechanical performance.<sup>[542]</sup> PMMA outperformed the other candidates in chicken purge, with all other materials exhibiting moderate to low penetration and mixed reusability.



**Figure 7.3. Food-specific microneedle characterization.** (a) Optical images of various food items post penetration from PMMA microneedle arrays. (b-c) Microneedle material assessment through (b) penetration and (c) reusability assessment at 2.5, 5, and 7.5 N of force. (d) Associated optical images of microneedle reusability after insertion into peach samples at 5 N. (e) Comparison of penetration and reusability through food-centric applications and tests. (f) Change in microneedle performance after 24h incubation in mushrooms (M), peaches (P), fish (F), RTE

chicken (CN), and cheese (C). (g-h) Performance assessment with porcine skin through (g) penetration and (h) reusability analysis with associated images of PMMA and PVA penetration.

Finally, the microneedles were inserted into cheese samples and placed under vacuum conditions repeatedly to simulate the vacuum sealing process commonly used in food packaging processes by both producers and consumers. Interestingly, both PMMA and PVA demonstrated excellent performance and gelatin had high penetration, but poor reusability. PDMS patches were unable to remain penetrated throughout the vacuuming process. A brief stability study was also performed where the microneedles were stored within respective food products for 24h and then assessed through the same penetration and reusability studies (Figure 3f). Importantly, both PMMA and PDMS saw no changes to their performance. Owing to their hydrogel composition, both PVA and gelatin typically demonstrated decreases in their overall performance. Finally, the microneedle performance was also assessed with porcine skin, an extremely dense product that is often used to characterize clinical microneedles (Figure 3g-h). Similar trends were observed such that both PMMA and PVA had high penetration and reusability, PDMS had poor penetration but high reusability, and gelatin had poor performance throughout.

On the whole, PMMA demonstrated the most consistently high performance across all material candidates and was consequently selected as the base material for the bacteriophage-loaded microneedle platform.

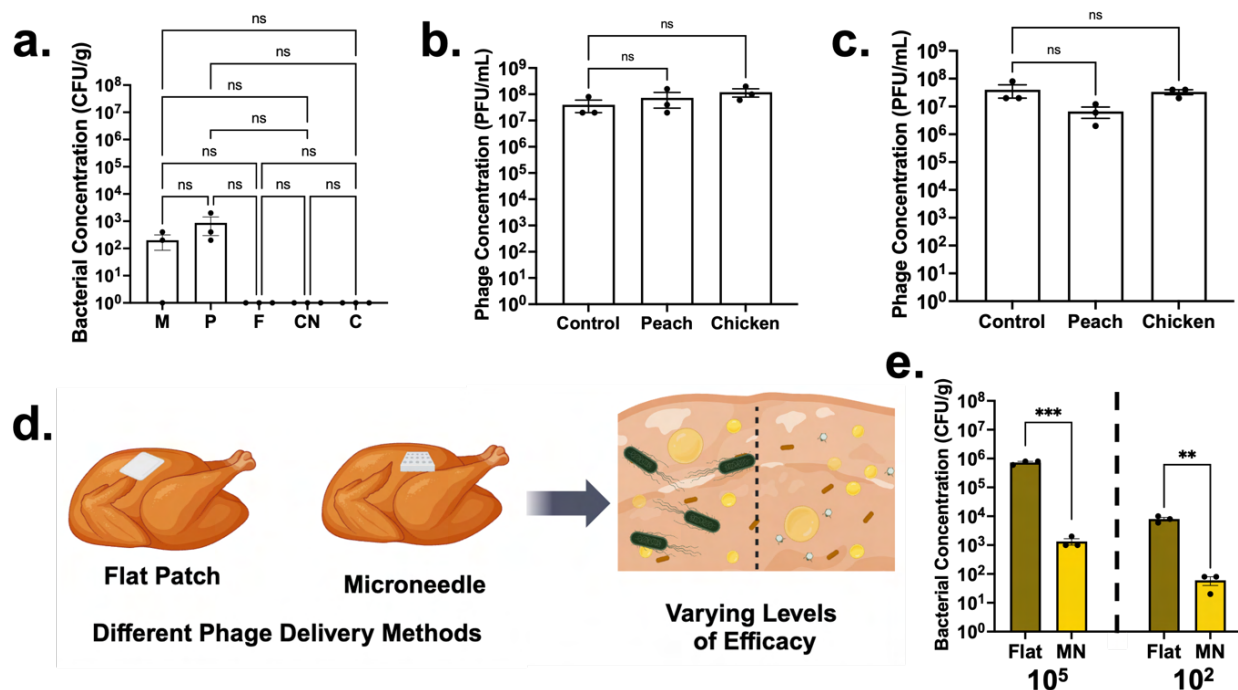
#### **7.3.4 Bacteriophage integration onto PMMA microneedles and system characterization**

Once PMMA was identified as the ideal microneedle material for agent delivery into food, bacteria and bacteriophage-based quantification studies were performed to assess the proposed food decontamination system. Prior to full-system assessment, innate bacterial loads capable of growing on McConkey agar were quantified for each food product. (**Figure 4a**). As such selective plating was to be enacted as our bacterial quantification mechanism, the proof-of-concept food product had to exhibit a 0 CFU/g baseline. To this end, mushroom and peach products were noted have some interfering bacterial species. From the remaining three food products, RTE chicken was

selected as the best medium for on-food testing, given the high contamination risk posed by chicken products. That being said, subsequent baseline studies still employed peach alongside RTE chicken, to offer insights into the impact of acidic fruit matrices on bacteriophage viability.

Specifically, to confirm that food matrix fluids had no adverse effects towards bacteriophage infectivity, we individually mixed peach pulp and chicken purge with liquid bacteriophage suspensions (Figure 4b). These food fluids had no significant effect on bacteriophage infectivity when compared to pure bacteriophage suspensions, as quantified *via* plaque assays. A final baseline test involved spray coating microneedle arrays with T7 bacteriophage and assessing the quantity of bacteriophage delivered into peach and RTE chicken (Figure 4c). These value were compared to buffer solutions mixed with the same volume of bacteriophage used for spray-based loading. Overall, no significant depletion in bacteriophage concentration was observed, indicating that the microneedles offer very efficient delivery. Final system testing involved comparing the antibacterial activity of bacteriophage-loaded flat patches to the bacteriophage-loaded microneedles when applied to *E.coli*-contaminated RTE chicken (Figure 4d). High and low levels of *E.coli* contamination to the order of  $10^5$  CFU/g and  $10^2$  CFU/g were induced within whole chicken breasts. In both respective cases, the microneedle patches resulted in significantly lower ( $P < 0.001, 0.01$ ) levels of bacterial concentration relative to the flat patches, following an 18 hour incubation. Specifically, with a  $10^5$  CFU/g initial load, microneedles offered a 99.8% mean improvement in bacterial reduction over flat patches, while a  $10^3$  CFU/g initial load yielded a 99.3% mean improvement. Importantly, the post-reduction *E. coli* load present in chicken that was contaminated at a  $10^2$  CFU/g initial dose was below the regulatory threshold for the pathogen, making the product theoretically safe for consumption.





**Figure 7.4. Full-system assessment of bacteriophage-loaded PMMA microneedles.** (a) Baseline bacterial counts in mushrooms (M), peaches (P), fish (F), RTE chicken (CN), and cheese (C). (b) Effect of peach juice and chicken purge on bacteriophage populations compared to pure bacteriophage suspensions. (c) Bacteriophage delivery into peach and chicken pieces compared to control bacteriophage suspensions. (d) Bacteriophage delivery via flat and microneedle array patches to provide varying levels of bacterial clearance. (e) Quantification of bacterial reduction post bacteriophage delivery from flat and microneedle patches with high (left) and low (right) levels of contamination.

## 7.4 Conclusion

We have developed bacteriophage-loaded microneedles that offer potent antibacterial activity without disrupting the organoleptic properties of the treated food product. Recognizing that microneedles have not been characterized for on-food applications, this work first assessed a variety of polymeric microneedle materials with regards to their mechanical properties and how they relate to food-centric applications. PMMA microneedles best balanced penetrative performance with high reusability and resiliency, making them well suited for widespread on-food applications. While PDMS microneedles offered high stability, their poor penetrative performance made them suboptimal as a microneedle material. Both PVA and gelatin microneedles offered



poorer penetration and stability than their counterparts but posed advantages – such as rapid dissolution and high loading capacity, respectively, which stand to make them valuable within specific use-cases.

The microneedle patches were then subjected to various food-specific activities including tumbling, incubation in fish saline and chicken purge, and vacuum packaging, with their performance assessed through post-testing mechanical resilience. PMMA microneedle arrays were noted to be optimal for the proposed bacteriophage delivery system, enacting the spray-deposition of *E. coli*-specific bacteriophages onto their surface. Here, these patches demonstrated significantly higher bacterial reduction compared to flat bacteriophage-loaded PMMA patches, when applied to contaminated RTE chicken breast products. This demonstrated the advantages of a three-dimensional, surface-penetrating delivery approach. The developed platform stands to revolutionize current food safety efforts, as a new approach towards pathogenic decontamination. Its customizability, food-safe nature, and cost-effectiveness makes it well-suited for applications within the food industry. Future works on this platform involve exploring other bacteriophage-incorporation methods which can provide improved bacterial reduction, as well as assessing performance against other food products contaminated with a variety of harmful pathogens.

## **7.5 Materials and Methods**

*Materials.* 3D printing filament was obtained from Creality 3D Technology (Shenzhen, China). Polydimethylsiloxane (SYLGARD 184) was purchased from Dow Corning (Michigan, United States). Polyvinyl alcohol, polymethyl methacrylate, ethyl lactate, agarose, and pH standard solutions were purchased from Millipore Sigma (Ontario, Canada). Phosphate buffered saline (pH 7.4) was purchased from Bioshop Canada (Ontario, Canada). Gelatin and all employed food products were purchased from Food Basics (Ontario, Canada).

*Microneedle fabrication.* Microneedles (MNs) were manufactured using a replica-moulding process in which a PDMS positive mold is first produced using a Creality 3D printer. Positive PDMS molds were then used to form the corresponding negative (master) molds which were then

cast with 10:1 PDMS polymer to curing agent solution. The PDMS master mold then was used as a template for the PDMS MNs where a surfactant chemical treatment was applied to the mold to facilitate release. The PDMS polymer solution of 7.5:1 ratio of PDMS and curing agent was poured into the PDMS master molds. This was followed by desiccation of the samples for 60 minutes and a heating procedure at 145°C for 20 minutes to cure the needles. The MNs were then left to cool and peeled to reveal the final PDMS MN patch. To prepare a 12% PVA solution, 6 grams of PVA was added into 50 ml of deionized (DI) water, using a serological pipette. The mixture was heated to 85°C while employing magnetic stirring at a rate of 250 rpm for 1 hour. Subsequently, the solution was allowed to cool before it was transferred to a Falcon tube. For the fabrication of PVA microneedles, 250 µl of a 10% mold release agent was pipetted onto the negative molds and desiccated for 10 minutes. The desiccation process was repeated twice. The prepared molds were placed onto a hot plate set at 145°C for 30 minutes to facilitate the evaporation of the mold release solution. The PVA solution was thoroughly vortexed and centrifuged at 2000 rpm for 30 seconds to move all the bubbles from the top of the Falcon tube. Using a pipette, these bubbles were carefully removed. 250 µl of PVA was pipetted onto each negative mold. The molds were desiccated for an hour, then any bubbles which surfaced were removed using a pipette. This was followed by adding another 200 µl of PVA onto each mold. A thumb tack was used, gently going in circular motions within each microneedle hole, to effectively expel any residual bubbles from the bottom. Ensuring the absence of bubbles at this stage, the molds were desiccated for an additional 45 minutes, and the thumbtack technique was repeated to remove any bubbles. Subsequently, the PVA needles were allowed to solidify over a period of 2 days. After 2 days, the PVA microneedles were removed from the mold. To prepare 15% Gelatin Microneedles, 1.5 grams of halal gelatin powder was slowly added into 10 ml of DI water, using a serological pipette. The gelatin was allowed to bloom in the water for 10 minutes. Then, the solution was heated in a microwave for 30 seconds, with 10-second increments, until a clear solution formed. Meanwhile, the oven desiccator was heated to approximately 100°C. Using a pipette, 300 µl of the gelatin solution was dispensed onto PDMS negative molds, and they were placed into the oven desiccator.

The molds were desiccated at 0.8 pressure for 2 minutes to ensure bubbles rose to the top. Any bubbles on the surface were carefully removed using a pipette. A thumb tack was used, gently going in circular motions within each microneedle hole, to effectively expel any residual bubbles from the bottom. Another 150  $\mu$ l of the gelatin solution was added, then the gelatin was allowed to set at room temperature for 15 minutes before freezing overnight. The following day, the microneedles were removed from the mold. PMMA powder was dissolved in 30% w/v ethyl lactate. The 30% w/v PMMA solution was vortexed and cast on PDMS negative molds. 250 mL of the 30% w/v solution was required for casting of 1 PMMA MN. After casting, the PMMA MNs were desiccated to ensure the solution was properly integrated into the molds and remove bubbles. After the desiccation treatment, the ethyl lactate was evaporated from the solution overnight through a heating procedure in the oven desiccator at 50°C. The PMMA microneedle array was then peeled from the mold.

*Optical microneedle visualization.* An iPhone 12 was used to image each microneedle material patch, with pictures taken at about a 45° angle at a magnification of 2.8 on a black surface.

*Background fluorescence.* Flat patches of all the materials used in the experiment, including PVA and Gelatin were prepared using a flat patch negative mold. It was ensured that these patches were uniform and free from any irregularities. A high-quality Nikon Inverted microscope with fluorescence filters for DAPI, FITC, TRITC, and CY5 channels was utilized to capture images of the materials at magnifications of 4X and 10X. The region of interest (ROI) tool available in the microscope software was used to record background fluorescence values for each channel to establish baseline measurements.

*Single-needle force testing experiments on different MN materials.* MN patches were cut into single needles and tested for individual needle strength using the Biomomentum micromechanical tester. The individual MNs were subjected to differing forces (250, 500 and 750 gf) at a velocity of 0.75 mm/s. Height reduction rates were measured using Image J software.

*Initial penetration testing using agarose pucks.* To obtain baseline penetration testing results, both 1% and 1.5% agarose pucks were made using a well plate. The pucks were allowed to cool. A

mechanical tester with 500 gf force at a speed of 0.75 was used to penetrate each needle into an agarose puck. For each agarose percentage (both 1 and 1.5%), 3 samples of both gelatin and PVA were penetrated. The number of penetration holes, the number of microneedles broken, and the number of microneedles

*Sonication stability studies.* Half patches (4 by 4 microneedle patches) were prepared for both PVA and gelatin. Three patches were added into a falcon tube and sonicated for 20 minutes. Then, another three patches were added and sonicated for 40 minutes, followed by the addition of three more patches and sonication for 60 minutes. This process was repeated for the other material. After sonication, 1% agarose pucks were made and used to test penetration. The number of penetration holes, the number of microneedles broken, and the number of microneedles deformed were recorded for each patch.

*pH testing for individual microneedles.* Individual MNs were exposed to differing pH conditions, pH 4, 6, 8, and 10, for 24 hours. The individual MNs were placed on the testing platform of the Biomomentum micromechanical tester and subjected to differing forces (250, 500 and 750 gf) at a velocity of 0.75 mm/s. Height reduction rates were measured using Image J software.

*Long term storage for single needles.* Individual microneedles were cut from each material. Three needles from each material were stored at -20°C, 4°C, and 25°C for 1, 2, 3, and 4 weeks. After the incubation period, each needle was subjected to a force of 2500 gf with a speed of 0.1 on a mechanical tester. ImageJ software was utilized to record the height of the needles before and after applying the force. The percentage decrease in height for each material at every pH level was calculated.

*Short term storage for single needles.* Individual microneedles were cut from each material (PVA and gelatin). Three needles from each material were stored at -20°C, 4°C, and 25°C for 24, 48, and 72 hours. After the incubation period, each needle was subjected to a force of 2500 gf with a speed of 0.1 on a mechanical tester. ImageJ software was utilized to record the height of the needles before and after applying the force. The percentage decrease in height for each material at every pH level was calculated.

*Baseline food testing for MNs.* MN patches were inserted into 5 food products (peach, mushroom, cheese, chicken, fish) using the biomechanical tester and strength was tested using constant force application of 250, 500 and 750 gf at 0.75mm/s. Penetration and breakage rates were measured.

*24-hour patch storage in food.* MN patches were inserted into 5 food products (peach, mushroom, cheese, chicken, fish) using the Biomomentum micromechanical tester at 500 gf at 0.75 mm/s. They were stored overnight, and breakage/penetration rates were measured.

*Mushroom and peach tumbling test.* MN patches were inserted into food products (peach and mushroom) using the Biomomentum micromechanical tester at a constant force application of 500 gf at 0.75 m/s. The food products were then subjected to tumbling force at 500 rpm for 2 hours. The samples were stored at 4°C for 24 hours, after which penetration and breakage were measured.

*Cheese vacuum test.* MN patches were inserted into 5cm by 5 cm cheese pieces using the biomechanical tester at a constant force application of 500 gf at 0.75 m/s. MN patches were subject to pressurized conditions using a desiccator. 5 desiccation periods were conducted, and the samples were stored at 4°C for an overnight incubation of 24 hours. Following the 24-hour incubation period, penetration and breakage rates were measured.

*Chicken purge test.* 5 cm by 5 cm pieces of rotisserie chicken were prepared. Using a mechanical tester exerting a force of 500gf at a speed of 0.75, each microneedle material (PVA and Gelatin) comprising 4 by 4 microneedles were inserted onto each chicken segment (n=3 for each material). Following the insertion of all microneedle patches, 1000uL of chicken purge solution was dispensed onto each chicken piece, focusing primarily on the needle insertion sites. Subsequently, the samples were stored at 4°C for a duration of 24 hours. Following 24-hours, the count of penetration holes and the instances of broken or deformed microneedles were documented.

*Fish saline solution test.* 5 cm by 5 cm pieces of haddock were prepared. Using a mechanical tester exerting a force of 500gf at a speed of 0.75, each microneedle material (PVA and Gelatin) comprising 4 by 4 microneedles were inserted onto each chicken segment (n=3 for each material). Following the insertion of all microneedle patches, 1000uL of fish saline solution was dispensed onto each fish piece, focusing primarily on the needle insertion sites. Subsequently, the samples

were stored at 4°C for a duration of 24 hours. After 24-hours, the count of penetration holes, as well as the instances of broken or deformed microneedles for each patch, were documented.

*Bacteriophage studies.* Baseline bacterial studies were performed using selective plating on MacConkey agar plates (SigmaAldrich) with *E. coli* K12 that was cultured overnight from glycerol stocks. All bacteriophage quantification was performed on soft agar plates with *E. coli* K12 bacterial lawns to assess bacteriophage clearance *via* plaque assays. The effect of food fluids on bacteriophage was explored using peach juice and chicken purge that was extracted by pulverizing each food product. Baseline bacteriophage delivery quantification was performed by cutting each food product into microneedle-array sized pieces. Bacteriophage-loaded microneedles were then penetrated into the respective samples and incubated for 18h. The individual food products were then vortexed in phosphate buffered saline solution post-incubation and the resulting solution was plated on soft agar plates through plaque assays. Full system testing involved using full 200 g pieces of RTE chicken and applying either bacteriophage-loaded flat or microneedle patches onto the samples. The food was then pulverized to extract remaining bacteria, following an 18h incubation. Collected samples were assessed *via* selective plating. Bacterial counts were quantified from the selective plates following an overnight incubation at 37°C.

*Statistical analysis.* Where required, statistical analyses of the results were performed with GraphPad Prism 10 (GraphPad software Inc., San Diego, California, USA). In all cases, >0.05 p-value was taken to represent statically significant difference. Analysis was conducted on Image J.

## **7.6 Acknowledgements**

A.P. and S.K. are the recipients of the Vanier Canada Graduate Scholarship awarded by the Natural Sciences and Engineering Research Council of Canada. This work was supported by the Ontario Early Researcher Award, Mitacs and Toyota Tsusho Canada Inc. grants to TFD. T.F.D. is a Tier II Canada Research Chair in Nanobiomaterials.

## **Conflict of Interest**

The authors declare no conflict of interest.

## Chapter 8: Smart Food Packaging Commercialization

# Preface

This chapter provides a comprehensive overview of the smart food packaging space through a commercial lens. Barriers that continue to hinder real-world translation are discussed, with considerations made towards technical, industry-level, and consumer-level challenges. Opportunities for high impact progress are then presented. Concurrently, the value-add of food technologies developed by our research consortium are highlighted. This work acts to guide future efforts in this space towards technologies and strategies that stand to have real-world impact.

## Authors

Shadman Khan, Zeinab Hosseinidoust, Yingfu Li, Carlos D.M. Filipe, Tohid F. Didar

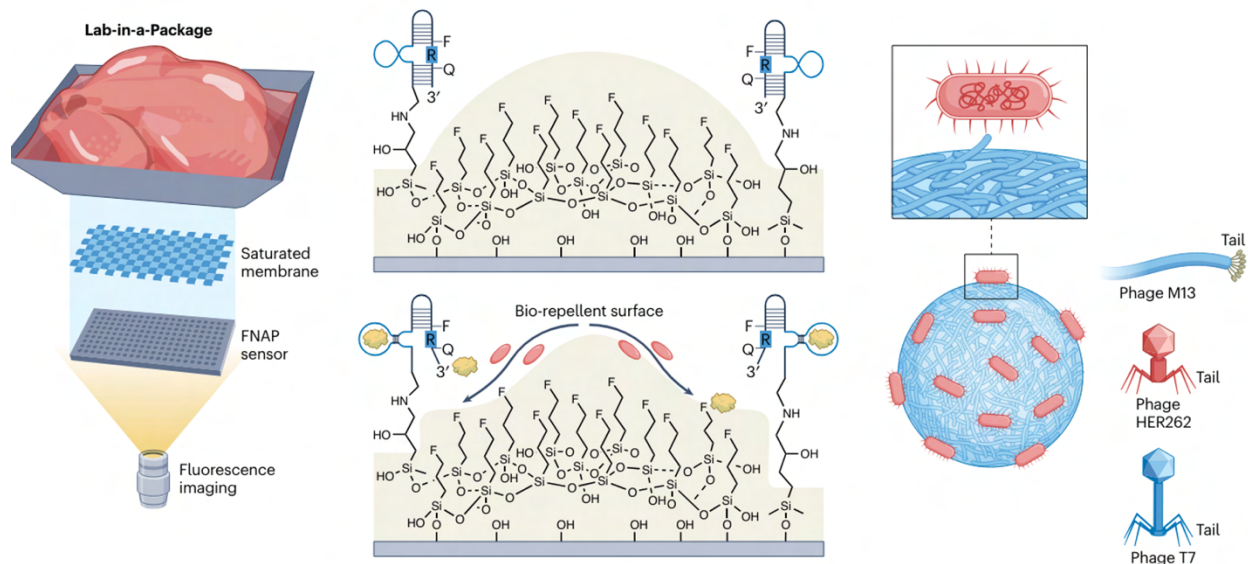
I was responsible for defining the scope of this article and performing literature review towards identifying topics of discussion. I authored all sections. Zeinab Hosseinidoust reviewed the work. Yingfu Li, Carlos D.M. Filipe, and Tohid F. Didar supervised and reviewed the work.

## Publication

Nature Reviews Bioengineering, 2024

## Publication Date

April 2024



## **8.1 Standfirst**

Smart food packaging technologies can actualize real-time, in situ food quality monitoring, increasing food safety and decreasing food waste. Here, we detail challenges that hinder the commercialization of such smart packaging systems and identify opportunities to facilitate their translation from prototype to product.

## **8.2 Introduction**

Ineffective food product monitoring has enabled foodborne illness to remain rampant, with over 600 million annual global cases and an associated death toll exceeding 420 000.<sup>[543]</sup> Concurrently, over 40% of the food produced in the United States is wasted, with similar values reported globally.<sup>[543]</sup> Much of this waste is attributed to widespread reliance on ultraconservative, static expiry dates. Smart food packaging systems – consisting of food-safe biorecognition elements embedded directly into existing packaging materials, can monitor and report the quality of individual products in real-time throughout their lifespan. However, the commercialization of these innovative technologies remains scarce. Understanding the challenges that hinder translation and identifying opportunities for impact can guide future developments.

## **8.3 Technical Challenges**

Quantitative thresholds of food spoilage are not clearly defined by regulators. Nevertheless, several metrics, such as pH, biogenic amine concentration and total bacterial count are correlated with food spoilage, with innovators employing variable thresholds to validate proposed sensing platforms.<sup>[8]</sup> Such inconsistent performance standards has made the value-add of individual platforms difficult to determine. Regulatory bodies such as the Food and Drug Administration need to define quantitative spoilage marker thresholds in relation to the physical and chemical changes of distinct food products as they transition to inedibility.

Although pathogen thresholds are well-established, proof-of-concept contamination sensing protocols often lack real-world consideration. Firstly, simulated pathogen detection studies largely employ small food samples that are contaminated at a localized site. A smart packaging sensing



interface, measuring a few square centimeters, is applied directly to this site. This offers a best case scenario, as the real-world likelihood of a smart sensing interface being situated at the exact site of contamination on a large food product is small. Second, reagents required for sensor functionality (such as buffers) are often broadly dispensed onto tested products, altering the organoleptic properties of the food product and raising safety concerns. To overcome this issue, the Sentinel Wraps Group has developed the *Lab-in-a-Package* technology (Fig. 1a).<sup>[16]</sup> The system employs a redesigned packaging tray that localizes fluids naturally released by food products to a central testing site, yielding a test sample representative of the entire product. The testing site features a cutout that can be embedded with any transparent optical sensor. This tray is paired with a reagent-immobilizing membrane that is placed adjacent to the embedded sensor, ensuring high reagent availability at the sensing interface. Pairing the system with a *Salmonella* sensor enables hands-free, in-package detection of the pathogen at concentrations as low as  $10^3$  colony-forming unit (CFU) per gram on whole chicken.<sup>[16,468]</sup> Similar technologies that help actualize real-world application are critically needed.

#### 8.4 Commercial Challenges

Various smart packaging systems employ complex detection and transduction techniques to achieve high performance. Namely, antibody-mediated detection cascades, multiagent amplification strategies, and ultrasensitive electrochemical signal readouts have all been employed.<sup>[8]</sup> While effective, increased sensor complexity generally yields higher cost. Corporate tolerance towards increases in packaging cost is in the range of \$0.01 to \$0.05 USD per product, making such high performance systems commercially unfeasible.<sup>[544]</sup> In order to develop cost-effective systems, we employ low-cost RNA-cleaving fluorescent deoxyribozymes (RFDs) as highly specific biorecognition molecules with built-in optical transduction capabilities.<sup>[17]</sup>

Concurrently, we have identified two mechanisms for increasing cost tolerance. The first mechanism involves developing clearer profitability arguments for private industry stakeholders. Although hundreds of billions of dollars in global annual losses are associated with food

contamination and waste, such numbers cannot be contextualized to the operations of individual industry stakeholders.<sup>[545]</sup> If corporations quantify the potential savings to their business through smart food packaging integration, they may be able to justify increased costs. Importantly, these assessments should also account for legal liability in the case of smart packaging failure and social return on investment. There is growing industry interest towards such assessments, yielding optimism. The second mechanism for increasing cost tolerance involves creating a stronger commercial need for smart food packaging employment. Currently, conservative food testing regulations fail to motivate corporations to explore new technologies. Although increased testing frequency requirements would improve food safety, a bottleneck exists because producers may raise food prices to circumvent the added costs. This would not be acceptable for consumers at a time of heightened food insecurity. However, given that low-cost smart food packaging has progressed, reconsideration of current regulations is warranted. This may encourage policymakers to impose stringent, yet economically reasonable testing regulations that motivate corporations to explore smart packaging as an alternative to the expensive, laborious testing protocols used today.

Finally, despite using food-safe reagents in smart packaging, consumers remain hesitant consuming products that are in contact with agents not native to food. Much of this hesitancy may stem from the scientific terminology used to describe smart platforms to consumers <sup>[546]</sup> and the unclear real-world accuracy of these systems. By increasing the reliability of smart packaging systems, increased interest from consumers is expected. Still, this will be weighed against the slightly elevated prices at which smart packaged foods are expected to be sold. Accordingly, consumers' willingness to pay for smart packaging remains a key focus within various public inquiries.<sup>[546]</sup>

## **8.5 Opportunities for Impact**

*Developing platform technologies:* Smart food packaging is often developed with very specific use-cases in mind (for example, apple monitoring), wherein the high degrees of system customization aid in performance optimization. Consequently, certain universal in-package

monitoring issues remain unaddressed, hampering real-world translation. Thus, developing platform technologies applicable to a wide range of food products may advance real-world smart food monitoring – a premise that inspired the *Lab-in-a-Package* platform.<sup>[16]</sup> As the technology is not specific to the *Salmonella* sensor used for its validation, it can act as a plug-and-play platform, which can be employed for the in-package integration of other food sensors.

*Employing proven technologies from other industries:* Technical barriers in smart food packaging mirror issues in biomedical material development, drug delivery and environmental biosensing. Accordingly, sourcing established technologies from these spaces may yield low-risk, high-reward opportunities. For example, coating RFD sensors with food-safe lubricant-infused coatings can reduce food-induced fouling (Fig. 1b)<sup>[24]</sup>, increasing sensor sensitivity by 75% within complex food environments. In another example, food-safe microneedles have been employed within smart food packaging to enable monitoring below a product's surface. Finally, machine learning algorithms can eliminate user bias by automating the signal readout process. Algorithms with a robust training set can differentiate between a negative and positive result with high accuracy. Moreover, variations arising in sensor signal intensity through inconsistent food storage conditions – that currently yield a high rate of false results, can be addressed. By employing data derived from sensors stored under diverse conditions, machine learning algorithms can adjust positive result thresholds for a product based on its storage conditions. Accordingly, our group is currently developing both sensor output image classification algorithms and robust RFD image libraries.

*Developing multifunctional technologies:* The value-add of smart food packaging systems can be increased by combining functions, such as preservation, quality enhancement, sensing and pathogen eradication into singular platforms. For example, we are currently developing kill-and-detect packaging that aims to eliminate pathogens and report their presence simultaneously. Our kill function employs sprayable bacteriophage microgels that eliminate up to  $10^6$  CFU g<sup>-1</sup> of *Escherichia coli* O157:H7 from food products within nine hours (Fig. 1c).<sup>[37,38]</sup> This technology complements our pathogen sensing platform, as RFDs rely on a protein target for detection.

Therefore, cell eradication does not deteriorate sensing activity. By combining these two low-cost systems, we expect to deliver a multifunctional platform of increased value proposition.

*Concentrating efforts towards priority issues:* It is important to concentrate smart food packaging efforts towards a couple of objectives at a time. This approach has been employed by the US Food and Drug Administration to address Shiga toxin-producing *Escherichia coli* outbreaks, developing the Leafy Greens STEC Action Plan.<sup>[547]</sup> This plan seeks to confront prevention, response and knowledge gaps through collaboration between regulators, innovators and corporations. Such synchronization in the smart food packaging space will accelerate commercialization.

## Chapter 9: Conclusion

### 9.1 Thesis Summary

With both foodborne illness and food waste imposing massive ramifications on human health and the economy, there is a defined need for engineering solutions that offer mechanisms for alleviation. While various measures have been proposed to address these crises, efforts that have dominated literature seek to enable effective monitoring of contamination and spoilage in food, as well as introduce effective strategies for pathogen decontamination. In this dissertation, all of these approaches were explored, yielding systems that stand to offer real-world impact.

With regards to food monitoring, optical sensing in the form of fluorescence and colorimetric signal transduction was sought, due to the more accessible means by which signal readout can be enacted. To support such efforts, the inherent fluorescence properties of contamination-prone food products were first comprehensively evaluated. This provided subsequent works with the data necessary to make optimal sensor design choices. It was recognized that the most significant value-add a food contamination detection system could provide would be in the form of an in-package, real-time food monitoring platform. Such a set-up enables contamination assessments throughout food production and distribution. To facilitate such a platform, RFDs and fNAPs were employed. These fluorescently-labelled sensing molecules offer all-in-one sensing and signal transduction, yielding a form factor that can be easily integrated onto existing packaging at low cost. While fluorescence readout would not be accessible to consumers, effective monitoring on the grocer-level scale was sought through the employment of a handheld fluorescence reader. To actualize in-package monitoring, mechanisms for in-package test sample collection and sensing reagent integration were developed. The resultant platform was paired with a novel *Salmonella*-responsive fNAP sensor, to demonstrate hands-free, real-time pathogen monitoring within packaged foods.

Recognizing that spoilage sensing would be most impactful on a consumer-level, a colorimetric sensor was developed for at-home use. The microneedle sensor was composed entirely of gelatin and food-derived anthocyanins, making it extremely inexpensive. The sensor

was fabricated through a gelling, freezing, and dehydrating three-step protocol. This yielded environment-responsive microneedles that exhibited high mechanical integrity in their initial dehydrated state but would return to a hydrogel state upon fluid exposure. The sensing platform was validated through application onto fish products, because of the defined pH changes they exhibit as they spoil. The sensing patch was designed to offer benefits as both a real-time monitoring platform applied non-destructively to sealed food products, and a rapid test for opened products, wherein spoilage can be reported within 45 minutes prior to product consumption. For real-time monitoring, the dehydrated microneedles enabled packaging film penetration, after which rehydration and sensing was activated by fluids present in the packaged fish. For rapid test applications, the microneedles significantly increased the sensor-fish sensing interface surface area. In both cases, the sensor exhibited a defined shift in colour when exposed to spoiled fish.

To induce improvements in food decontamination, pathogen-targeting bacteriophages were employed. Here, microneedles were hypothesized to be an effective means of delivering such agents through the surface of fluid-rich foods and into interior matrices, where they would act to reduce pathogen loads. The mechanical integrity, stability, and food-penetrating abilities of various microneedle materials were assessed, from which PMMA microneedles were found to be best suited for the target application. When employed against contaminated foods, the phage-loaded PMMA microneedles offered effective pathogen reduction, suggesting viability as a food decontamination tool.

Finally, with a pronounced understanding of the food technology space gathered through these works, a summary of the operational landscape was produced to guide future works.

## **9.2 Thesis Conclusions**

- I. In line with Objective 1, comprehensive understanding of the sensing-relevant fluorescence profiles of target food products was gathered. Lettuce, spinach, chicken, and beef products were evaluated at excitation/emission wavelengths of 350 nm/470 nm, 490 nm/525 nm, 557 nm/576 nm, and 649 nm/666 nm, which correspond with DAPI, FITC, TRITC, and Cy5 range

fluorophores. Fluorescence was evaluated throughout product lifespans, wherein limited shifts were observed as products transitioned to a spoiled state. Oligonucleotide probes labelled with DAPI, FITC, Cy3, and Cy5 fluorophores – which match with each respective tested wavelengths, were then contact printed onto transparent food packaging films. These films were overlaid with the tested products to assess the visibility of fluorescently-labelled biomolecules when paired with these food backgrounds. Cy3-range fluorophores offered the most consistent visibility, with SNR values above 9 and CV values below 20% with all tested products. Meat products also showed compatibility with Cy5-range fluorophores, with SNR values above 5 and CV values below 20%. To confirm visibility of sensing-driven changes in fluorescence, RFDs were printed onto food packaging films for similar overlaid visualization. Importantly, contact printing was used to deposited RFDs – an approach not reported in prior literature. RFD cleavage-induced shifts in fluorescence were successfully detected in the presence of food backgrounds, with doubling SNR values obtained with all tested products, alongside CV value below 20%.

- II. In line with Objective 2, a platform technology coined *Lab-in-a-Package* was developed for the advancement of in-package, real-time food contamination monitoring. The developed platform consists of three key components: an inclined packaging tray with a cut-out for sensor integration, a reagent-immobilizing membrane, and a transparent optical sensor. The inclined packaging tray enables in-package representative test sample collection through the localization of fluids naturally released from the packaged product. The collected fluid is concentrated at the built-in sensor integration site. Incline angles of 45°, 60°, and 90° were evaluated, with the 45° offering the best fluid localization properties. The reagent-immobilizing membrane is placed directly adjacent to the sensing interface at the base of the tray, where it retains sensing reagents at the sensing site. Concurrently, the membrane limits the food-based fouling of the underlying sensor. Cotton, cotton-cellulose, cellulose, cellulose-polyester, and polyester membranes were evaluated in relation to their background fluorescence, porosity, fluid capacity, fluid retention, fluid diffusivity and microbial diffusivity

properties, wherein cotton was found to be best suited for the proposed application. To validate this platform, a novel *Salmonella*-responsive fNAP surface sensor was developed. Through the covalent immobilization of fNAP microarrays on food packaging films, a sensing platform with a *Salmonella* LOD of  $10^3$  CFU/mL was produced. The sensor also offered excellent specificity and good long-term stability. When integrated into the Lab-in-a-Package platform, the combined system offered  $10^3$  CFU/g detection of contaminated ready-to-eat chicken products. Even when pathogens were introduced through indirect mechanisms of contamination, detection sensitivity was retained. Finally, a handheld fluorescence reader was employed to demonstrate proof-of-concept industry-scale, in-package monitoring.

III. In line with Objective 3, a real-time spoilage sensor was developed for consumer-scale use. A novel microneedle needle material was developed for this objective, involving gelatin gelation, freezing, and dehydration. The resultant microneedles exhibited reversible rehydration when exposed to fluid-rich environments. This enabled their use in the real-time monitoring of already-sealed food products, where the mechanically robust initial state would penetrate through food packaging in a non-destructive manner, and subsequently rehydrated within food for biosensing applications. The gelatin concentration and dehydration time of the microneedles were optimized, wherein 15% w/v gelatin concentration and a 24 h dehydration time were found to be optimal based on mechanical force testing. These optimized needles exhibited excellent penetration of polyethylene food packaging films of diverse thicknesses, to a point where significant penetration was still observed after ten uses. Red cabbage anthocyanin was integrated into these microneedles as the sensing agent. Sensing efforts were enacted on fish because of its high safety risk and the correlation between its spoilage-induced pH changes and the pH conditions that induce red cabbage anthocyanin colour change. Here, the rehydration induced by fluids from the packaged fish would induce colorimetric monitoring of the products' state. Real-time monitoring of packaged fish samples showed effective spoilage monitoring in the form of a defined colour change in response to spoilage, as corroborated by concurrent pH measurements. Concurrently, rapid testing of spoiled fish



products that had been opened showed defined colour change within 45 minutes. Importantly, the mechanical integrity and pH responsiveness of the developed microneedle spoilage sensor was not decreased by long-term storage of diverse temperature storage conditions.

IV. In line with Objective 4, an improved mechanism for bacteriophage delivery into food was developed. It was noted that fluid-rich food products with a protective outer layer offer an excellent matrix to target, as overcoming the external barrier would invoke autonomous bacteriophage dissemination within the food. Recognizing that microneedles have been minimally applied towards on-food applications, gelatin, PVA, PDMS and PMMA were characterized to offer insights for future studies targeting unique food-related uses. This first involved assessing the mechanical integrity, reusability, resilience in response to varying storage time, pH, and temperature conditions, baseline penetrative ability and swelling. The candidate materials exhibited a wide range of performance profiles, suggesting use towards distinct on-food applications. Subsequent food-specific testing involved studies with mushrooms, peaches, fish, poultry, and cheese. Here, penetration and reusability were assessed following exposure to food-specific conditions, such as produce wash tumbling, chicken and fish microenvironment exposure, and vacuum packaging. PMMA was noted to be exceptionally resilient, inspiring its use towards in-food bacteriophage delivery. Here, *E. coli*-targeting bacteriophages loaded onto PMMA microneedles outperformed bacteriophage-loaded surface patches in pathogen reduction. Specifically, a near 3-log reduction was observed between the systems, when applied to contaminated RTE chicken breast products.

V. In line with Objective 5, extensive technical, commercial, and regulatory conversations were initiated with all relevant stakeholders throughout the course of the presented work. These discussions yielded a strong understanding of the operational landscape that defines progress in the smart food technology space. Recognizing that the smart packaging space is more developed than the in-food decontamination space, an industry-centric summary of barriers and opportunities for the real-world translation of smart food packaging was developed. Barriers were discussed through the lens of technical challenges that hinder effective sensor

development, corporate adaptation challenges, and consumer-level challenges. Opportunities for impact included the development of platform technologies, the translation of proven technologies from other spaces to food-related applications, the development of multifunctional technologies, and the concentration of efforts towards priority issues.

### **9.3 Contributions to the Field**

#### *I. Sensing-centric assessment of the fluorescence properties of contamination-prone foods*

While on-food fluorescence sensing has been reported extensively in prior literature, a gap existed in the baseline fluorescence profiling of contamination-prone foods. Some fluorescence analysis of food had been undertaken in prior works, but not in a manner that could be applied to biomolecule-driven on-food sensing. The detailed fluorescence profiles that are provided in Chapter 4 meet this gap, by offering valuable insights towards the design of future on-food sensing platforms. Particularly, through the assessment of fluorophore-labelled biomolecule microarray visibility on various food textures, the presented study informs future works towards the unsuitability of certain fluorophore-food pairings for on-food biosensing. With considerations made towards photobleaching activity and changes in fluorescence in food over time, the presented work offers a comprehensive assessment of the sensing-relevant fluorescence properties of food. The value-add of this work is corroborated by a subsequent review of literature that showed that several on-food sensing platforms have been employed suboptimal fluorophores, with consideration towards their target food.

#### *II. Contact printing of functional oligonucleotides*

While non-contact printing of functional oligonucleotides has been reported extensively in prior literature, contact printing-based approaches have not been reported. As contact printing largely relies on mechanisms of physical surface adsorption, depositing RFDs in a manner that sustains biomolecular activity would theoretically prove difficult. This barrier is overcome in Chapter 4, as an optimized contact printing protocol involving a biomolecule-crosslinker print solution was

employed. This approach was enacted within a controlled humidity environment, yielding fNAP sensors with responsiveness similar to that of non-contact printed microarrays. These findings are particularly relevant from a commercial standpoint, as contact printing can be easily employed towards rapid sensor fabrication *via* techniques such as roll-to-roll printing. Non-contact printing does not offer the same degree of mass fabrication capabilities, making sensor production more time-consuming and expensive.

### *III. Platform technology for the advancement of in-package food monitoring*

The developed *Lab-in-a-Package* system presented in Chapter 5 is not specific to the developed *Salmonella* sensor, rather acting as a platform technology that can be paired with any transparent optical sensor. The system's ability to enact in-package test sample localization stands to significantly improve sensing performance against large food products that have been contamination at localized sites. Most smart food detection platforms tested to date have employed small food samples with localized contamination right beneath the sensing interface. This is an approach that does not translate to real-world contamination monitoring. Concurrently, effective in-package immobilization of sensing-supporting reagents in a manner that is both stable, but accessible to the sensing moieties addresses a second oversight that has long been made in the food sensing space. Collectively, *Lab-in-a-Package* represents a tool in the smart food space that stand to improve the detection performance of pre-existing and emerging food contamination sensors.

### *IV. fNAP surface sensor for diverse sensing applications*

The fNAP surface sensor used in Chapter 5 to validate the performance of the *Lab-in-a-Package* platform holds significant value as a standalone sensors outside of in-package sensing. The sensor is composed of densely-packed, covalently attached functional oligonucleotides, which singlehandedly offer sensing and transducing capabilities. The only additive the sensor requires for functionality is a non-toxic  $\text{MgCl}_2$  ion-rich solution. The sensor offers an LOD of  $10^3$  CFU/mL within 8 hours, alongside exceptional specificity and stability. With its 8 hour detection timeline,

this sensor has potential applications in on-site food testing as an alternative to current overnight culturing strategies. Use can also be extended to clinical biosensing, where overnight culturing is commonly employed for pathogen detection. Moreover, this sensor can be used for environmental biosensing. Here, the sensor offers translational potential towards remote testing through its ease-of-use and simple readout involving only a handheld fluorescence reader and smartphone.

#### *V. Environment-responsive gelatin microneedles*

The development of stimuli-responsive microneedles is an active of research, enabled by a need for materials that offer induced activity. The fluid-responsive gelatin microneedles presented in Chapter 6 represent a new addition to this space, as a material that can reversibly transition between a dehydrated state characterized by high material integrity, and a hydrogel state characterized by high porosity. Without the presence of a fluid stimuli, the transition from its dehydrated state to hydrogel state is indefinitely inhibited, with strong performance stability maintained. While the presented study employed these microneedles towards in-food biosensing, their hydrating mechanism offers diverse potential applications. Most notably, as microneedle hydration induces a significant increase in microneedle porosity, these microneedles hold potential applications as agent delivery tools, wherein the dehydrated matrix would offer protective properties to the packaged agents until hydration-mediated delivery was enacted. With optimization of their size and composition, these microneedles may also be useful for clinical and environmental biosensing.

#### *VI. Inexpensive microneedle sensor for consumer-level spoilage monitoring*

The need for a spoilage sensor for consumer use is well-pronounced, as detailed in Chapters 1 and 2. With anthocyanin-embedded films offer limited real-world viability due to their low mechanical integrity and industry acceptance challenges, making accessible consumer-driven systems a high-impact alternative. The developed spoilage sensor presented in Chapter 6 offers such a system, by providing consumers with a safe, inexpensive mechanism for fish spoilage assessment. As a mechanism to alleviate societal reliance on static expiry dates, this sensor thus stands to both

improve food safety and reduce unnecessary food waste. The incorporation of microneedles is particularly intriguing for the field, as their application in food has been limited to date. Here, these three-dimensional sensing substrates introduce packaging penetration capabilities and increase sensing interface area to enact improvement in on-food monitoring. This highlights the benefits afforded by the translation of existing technology to the food-safe to inspire innovation.

#### *VII. Microneedle material assessment for on-food applications*

The use of microneedles for on-food applications has been minimally explored in literature. While there is extensive literature detailing the performance of diverse microneedle materials across parameters relevant to clinical use, such results are only partially translatable to food-based application. The food-centric assessment of four microneedle materials in Chapter 7 provides fills this gap, acting to educate future on-food microneedle works. The conditions in which the microneedles were tested were designed to be representative of diverse food products, ensuring that the presented results are beneficial to the food technology space at-large. Concurrently, the materials that were selected for evaluation varied greatly in their base properties, ensuring that a wide range of possible system designs could be represented. This includes potential on-food microneedle applications towards biosensing, agent delivery, and sample extraction. The presented study stands to inform future works regarding the benefits of employing particular material systems. For example, its high base mechanical integrity based with its fluid-driven dissolving nature makes PVA an excellent candidate for the high volume delivery of preservative agents.

#### *VIII. Mechanism for bacteriophage delivery into food and resultant benefits*

While bacteriophage suspensions for food decontamination are commercially available, their widespread adaptation has been limited by their limited efficacy. To date, deposition have largely involved surface treatment of food products through immersion, spraying and packaging with bacteriophage-embedded films. The bacteriophage microneedle system presented in Chapter 7 provides a simple, yet effective mechanism to improve the potency of such suspensions.

Specifically, PMMA microneedles loaded with pathogen-targeting bacteriophages enable the penetration of exterior food layers that otherwise hinder bacteriophage distribution within food. This direct delivery into fluid-rich interior food matrices enables autonomous movement towards effective pathogen reduction. With a defined improvement observed over surface-based deposition, the developed system presents the first effort that demonstrates the benefits afforded by bacteriophage delivery directly into certain foods.

## 9.4 Future Works

Significant strides were made in this dissertation towards breakthrough smart food technology platforms. While this has introduced a multitude of future directions, key objectives for subsequent works are detailed below.

### *I. Introducing multiplexed contamination sensing*

Prior works within our group have detailed *E. coli* RFD-based surface sensors with similar sensing performance.<sup>[17,24]</sup> Integrating both *E. coli* and *Salmonella* sensing onto single sensing substrates stand to increase the value proposition of the developed sensor dramatically. Such parallel detection would likely be enabled through two adjacent microarrays composed of differing RFDs, which would allow both systems to employ the optimal fluorophore for on-food sensing of a given food product. Validation of the developed multiplex sensor would follow the same approaches used to assess the *Salmonella* fNAP sensor in Chapter 4. Studies involving both bacterial species introduced simultaneously would also be performed to identify any inhibitory effects the microbes exhibit against the sensing of the opposing target. Such effects are not anticipated due to the high specificity of the developed probes but will nonetheless be assessed.

### *II. Improving the in-package sensitivity of RFD and fNAP sensors*

While the  $10^3$  CFU/g sensitivity of the developed in-package contamination sensors offers a strong proof-of-concept, real-world application for high-risk pathogens require much higher sensitivity. With regulatory thresholds ranging between 0 and 100 CFU/g,<sup>[13,14]</sup> improving detection

performance proves vital towards increasing the value-add of such platforms. For example, prior works by our group have reported on-food RFD sensors specific to *E. coli* that offer effective detection of bacterial loads of  $10^3$  CFU/g. Alongside integration into the *Lab-on-a-Package* platform, inducing a 1-log improvement in the sensor's detection sensitivity would yield a system that matches the regulatory safety threshold of 100 CFU/g. This would change the value proposition from a system capable of reporting high amounts of bacterial target, to one that reports safe versus unsafe status. A novel mechanism for the enacting of improved sensitivity involves the use of bacteriophages. Prior works have shown that lysing target bacteria induces an improvement in RFD sensor sensitivity, as the sensing agent.<sup>[206]</sup> As RFDs bind to a protein that is specific to the target bacteria, lysing events yield an increase in target availability. Bacteriophages represent an inexpensive, food-safe mechanism to enact such activity, alongside their induction of targeted antibacterial activity.

### *III. Integrating automated smartphone-mediated analysis of colorimetric systems*

With regards to colorimetric sensing of spoilage, the defined colour shift from purple to blue makes the sensors easily interpretable to the naked eye. However, recognizing that this shift is not instantaneous, detecting subtle changes at earlier timepoints would offer significant value. This is validated by the sensing studies performed in Chapter 6, where quantified values showed a gradual shift prior to what was considered a discernable optical signal. With regards to real-time spoilage monitoring, detecting earlier shifts in colour may offer effective detection of a “spoiling” state where the product is still edible but nearing spoilage. For product rapid testing, a shorter detection timeline may be accessible. The most effective means of enabling such shifts in a consumer-accessible manner is through the development of an artificial intelligence-driven application that classifies smartphone images of these food-sensing patches. Given the large quantity of smartphone images that were collected as a part of sensing performance analysis, such an effort should be an easily enacted future step for this work.

#### *IV. Embedding bacteriophages into microneedle matrices for pathogen elimination*

While the bacteriophage-loaded microneedles exhibited significant reduction in pathogen load within contaminated foods, full eradication was not enacted. One key mechanism towards improving antibacterial activity within food matrices would involve the introduction of larger quantities of bacteriophage into food products. To this end, successfully embedding bacteriophages throughout microneedle matrices stands to significantly improve delivery. While PMMA microneedles were selected for the work presented in Chapter 7 due to its their high penetrative ability necessary to effectively penetrate the targets food products, applications towards foods with softer external layers would enable the use of other candidate materials. Namely, the dehydrated gelatin microneedles presented in Chapter 6 stands to offer significant bacteriophage delivery if embedded with these agents, as its rehydrating nature may yield release from within its three-dimensional matrix.

#### **9.5 Final Remarks**

The overarching goal of this dissertation was to advance smart food technologies in a manner that enacts real-world reduction in the incidence of foodborne illness and the quantity of food waste. Efforts involved the development of novel food technology systems for contamination detection, spoilage detection, and food decontamination. Experience gathered through such efforts was employed towards the development of a comprehensive situational assessment of the smart food packaging space, with an emphasis on enacting real-world translation. While significant findings with real-world implications are presented, this work concurrently functions as a springboard for future innovations that seek to address the food insecurity crisis faced globally today.



## References

- [1] B. Devleesschauwer, J. A. Haagsma, M.-J. J. Mangen, R. J. Lake, A. H. Havelaar, in *Food Safety Economics: Incentives for a Safer Food Supply* (Ed.: T. Roberts), Springer International Publishing, Cham, **2018**, pp. 107–122.
- [2] W. H. Organization, **n.d.**
- [3] R. L. Scharff, *Journal of food protection* **2012**, *75*, 123.
- [4] R. L. Scharff, *Journal of Food Protection* **2015**, *78*, 1064.
- [5] R. A. Harris, C. Tchao, N. Prystajek, K. Weedmark, Y. Tcholakov, M. Lefebvre, J. W. Austin, *Emerging Infectious Diseases* **2023**, *29*, 1730.
- [6] S. Klopatek, T. R. Callaway, T. Wickersham, T. Sheridan, D. Nisbet, *Bacteriophages: Biology, Technology, Therapy* **2021**, 891.
- [7] Z. Dou, J. D. Toth, *Resources, Conservation and Recycling* **2021**, *168*, 105332.
- [8] S. Khan, J. K. Monteiro, A. Prasad, C. D. M. Filipe, Y. Li, T. F. Didar, *Advanced Materials* **2023**, 2300875.
- [9] H. Yousefi, H.-M. Su, S. M. Imani, K. Alkhaldi, C. D. M. Filipe, T. F. Didar, *ACS Sens.* **2019**, *4*, 808.
- [10] G. Comi, in *The Microbiological Quality of Food*, Elsevier, **2017**, pp. 179–210.
- [11] M. K. Thomas, R. Murray, L. Flockhart, K. Pintar, F. Pollari, A. Fazil, A. Nesbitt, B. Marshall, *Foodborne Pathogens and Disease* **2013**, *10*, 639.
- [12] M. K. Thomas, R. Murray, L. Flockhart, K. Pintar, A. Fazil, A. Nesbitt, B. Marshall, J. Tataryn, F. Pollari, *Foodborne Pathogens and Disease* **2015**, *12*, 820.
- [13] Government of Canada, **n.d.**
- [14] Government of Canada, **n.d.**
- [15] J. KOVAČEVIĆ, L. F. McINTYRE, S. B. HENDERSON, T. KOSATSKY, *Journal of Food Protection* **2012**, *75*, 216.
- [16] A. Prasad, S. Khan, J. K. Monteiro, J. Li, F. Arshad, L. Ladouceur, L. Tian, A. Shakeri, C. D. M. Filipe, Y. Li, T. F. Didar, *Advanced Materials* **2023**, *35*, 2302641.
- [17] H. Yousefi, M. M. Ali, H.-M. Su, C. D. M. Filipe, T. F. Didar, *ACS Nano* **2018**, *12*, 3287.
- [18] S. Shajil, A. Mary, C. E. Rani Juneius, *Microbial Biotechnology: Volume 2. Application in Food and Pharmacology* **2018**, *3*.
- [19] X.-Y. Xu, X. Lian, J.-N. Hao, C. Zhang, B. Yan, *Advanced Materials* **2017**, *29*, 1702298.
- [20] K. M. A. El-Nour, E. T. A. Salam, H. M. Soliman, A. S. Orabi, *Nanoscale Research Letters* **2017**, *12*, 231.
- [21] R. Becerril, C. Nerín, F. Silva, *Trends in Food Science & Technology* **2021**, *111*, 495.
- [22] J. G. de Oliveira Filho, A. R. C. Braga, B. R. de Oliveira, F. P. Gomes, V. L. Moreira, V. A. C. Pereira, M. B. Egea, *Food Research International* **2021**, *142*, 110202.
- [23] X. Zhang, B. B. Ismail, H. Cheng, T. Z. Jin, M. Qian, S. A. Arabi, D. Liu, M. Guo, *Carbohydrate Polymers* **2021**, *273*, 118616.
- [24] H. Yousefi, S. E. Samani, S. Khan, A. Prasad, A. Shakeri, Y. Li, C. D. Filipe, T. F. Didar, *ACS nano* **2021**, *16*, 29.
- [25] D. Kim, Y. Cao, D. Mariappan, M. S. Bono Jr., A. J. Hart, B. Marelli, *Advanced Functional Materials* **2021**, *31*, 2005370.
- [26] E. Sonwani, U. Bansal, R. Alroobaea, A. M. Baqasah, M. Hedabou, *Frontiers in Public Health* **2022**, *9*, 816226.
- [27] L. Gram, L. Ravn, M. Rasch, J. B. Bruhn, A. B. Christensen, M. Givskov, *Int. J. Food Microbiol* **2002**, *78*, 79.
- [28] Y. Jaguey-Hernandez, K. Aguilar-Arteaga, D. Ojeda-Ramirez, J. Anorve-Morga, L. G. González-Olivares, A. Castaneda-Ovando, *Food Research International* **2021**, *144*, 110341.
- [29] P. Jia, X. He, J. Yang, X. Sun, T. Bu, Y. Zhuang, L. Wang, *Sensors and Actuators B: Chemical* **2023**, *374*, 132803.
- [30] L. Maddalon, S. Grasso, L. De Gara, G. Pennazza, A. Zompanti, M. Rapa, R. Ruggieri, G. Vinci, M. Santonico, *Sensors and Actuators B: Chemical* **2021**, *347*, 130648.
- [31] S. Fang, Z. Guan, C. Su, W. Zhang, J. Zhu, Y. Zheng, H. Li, P. Zhao, X. Liu, *Food Control* **2022**, *138*, 109018.
- [32] H. Yong, J. Liu, *Food Packaging and Shelf Life* **2020**, *26*, 100550.
- [33] L. O'Sullivan, D. Bolton, O. McAuliffe, A. Coffey, *Annu. Rev. Food Sci. Technol.* **2019**, *10*, 151.
- [34] R. Pérez Pulido, M. J. Grande Burgos, A. Gálvez, R. Lucas López, **2016**.
- [35] A. Chibeu, L. Agius, A. Gao, P. M. Sabour, A. M. Kropinski, S. Balamurugan, *International Journal of Food Microbiology* **2013**, *167*, 208.
- [36] P. Zinno, C. Devirgiliis, D. Ercolini, D. Ongeng, G. Mauriello, *International Journal of Food Microbiology* **2014**, *191*, 69.
- [37] L. Tian, L. He, K. Jackson, A. Saif, S. Khan, Z. Wan, T. F. Didar, Z. Hosseini, *Nature Communications* **2022**, *13*, 7158.
- [38] L. Tian, K. Jackson, L. He, S. Khan, M. Thiruganasampanthar, M. Gomez, F. Bayat, T. F. Didar, Z. Hosseini, *Nature Protocols* **2024**, DOI 10.1038/s41596-024-00964-6.
- [39] Anany H., Chen W., Pelton R., Griffiths M. W., *Applied and Environmental Microbiology* **2011**, *77*, 6379.
- [40] I. Choi, D. S. Yoo, Y. Chang, S. Y. Kim, J. Han, *Food Chemistry* **2021**, *346*, 128883.
- [41] Z. D. Moye, J. Woolston, A. Sulakvelidze, *Viruses* **2018**, *10*.

- [42] G. G. GREER, *Journal of Food Protection* **2005**, 68, 1102.
- [43] G. G. GREER, *Journal of Food Protection* **1986**, 49, 104.
- [44] G. G. GREER, *Journal of Food Science* **1988**, 53, 1226.
- [45] S. M. Ali, M. A. Moktadir, G. Kabir, J. Chakma, M. J. U. Rumi, M. T. Islam, J., *Clean. Prod* **2019**, 228, 786.
- [46] R. Preka, S. Berjan, R. Capone, H. Bilali, M. S. Allahyari, P. Debs, F. Bottalico, V. Mrdalj, *Food, Agric. Soc* **2020**, 8, 1.
- [47] O. A. Odeyemi, O. O. Alegbeleye, M. Strateva, D. Stratev, *Compr, Rev. Food Sci. Food Saf* **2020**, 19, 311.
- [48] Y. Ma, W. Yang, Y. Xia, W. Xue, H. Wu, Z. Li, F. Zhang, B. Qiu, C., *Fu, Membranes* **2022**, 12, 477.
- [49] S. M. Abdel-Aziz, M. M. S. Asker, A. A. Keera, M. G. Mahmoud, *Microbes in Food and Health* **2016**, 239.
- [50] N. A. Abdul-Mutalib, A. N. Syafinaz, K. Sakai, Y. Shirai, *Int, J* **2015**, 22, 896.
- [51] S. J. Chai, D. Cole, A. Nisler, B. E. Mahon, *Epidemiol, Infect* **2017**, 145, 316.
- [52] A. Sulakvelidze, *J. Sci*, **2013**, 93.
- [53] F. R. Pinu, *Technol* **2016**, 54, 213.
- [54] K. S. Gracias, J. L. McKillip, *Can, J. Microbiol* **2011**, 50, 883.
- [55] M. S. Firouz, K. Mohi-Alden, M. Omid, *Int* **2021**, 141, 110113.
- [56] P. Müller, M. Schmid, *Foods* **2019**, 8, 16.
- [57] J. Zhang, H. Huang, G. Song, K. Huang, Y. Luo, Q. Liu, X. He, N. Cheng, *Biosensors and Bioelectronics* **2022**, 202, 114003.
- [58] M. Ghaani, C. A. Cozzolino, G. Castelli, S. Farris, *Trends in Food Science & Technology* **2016**, 51, 1.
- [59] J., **2022**, 85.
- [60] C. V. Garcia, G. H. Shin, J. T. Kim, *Technol* **2018**, 82, 21.
- [61] C. Dincer, R. Bruch, E. Costa-Rama, M. T. Fernández-Abedul, A. Merkoçi, A. Manz, G. A. Urban, F. Güder, *Adv, Mater* **2019**, 31, 1806739.
- [62] M. Frasconi, F. Mazzei, T. Ferri, *Anal, Bioanal. Chem* **2010**, 398, 1545.
- [63] Y. Li, H. J. Schluesener, S. Xu, W. G. Org, *Gold Bull* **2010**, 43, 29.
- [64] G. M. Das, S. Managò, M. Mangini, A. C., *Nanomaterials* **2021**, 11, 2679.
- [65] V. Pellas, D. Hu, Y. Mazouzi, Y. Mimoun, J. Blanchard, C. Guibert, M. Salmain, S., *Boujday, Biosensors* **2020**, 10, 146.
- [66] I. I. Suni, *Biosensors* **2021**, 11, 239.
- [67] P. Jamdagni, P. Khatri, J. S. Rana, *Int, Nano Lett* **2016**, 6, 139.
- [68] Y. Zhang, G. Wang, L. Yang, F. Wang, A. Liu, *Coord, Chem. Rev* **2018**, 370, 1.
- [69] S. M. Imani, R. Maclachlan, Y. Chan, A. Shakeri, L. Soleymani, T. F. Didar, *Small* **2020**, 16, 2004886.
- [70] S. Zeng, K. T. Yong, I. Roy, X. Q. Dinh, X. Yu, F. Luan, *Plasmonics* **2011**, 6, 491.
- [71] H. Hassan, P. Sharma, M. R. Hasan, S. Singh, D. Thakur, J. Narang, *Mater, Sci. Energy Technol* **2022**, 5, 375.
- [72] S. Pramanik, Y. Kumar, D. Gupta, V. K. Vashistha, A. Kumar, P. Karmakar, D. K., *Das, Mater. Sci. Eng., B* **2021**, 272, 115356.
- [73] G. Liu, M. Lu, X. Huang, T. Li, D., *Xu, Sensors* **2018**, 18, 4166.
- [74] M. Swierczewska, S. Lee, X. Chen, *Phys. Chem. Chem. Phys* **2011**, 13, 9929.
- [75] A. Sultangazyev, A. Ilyas, A. Dyussupova, R. Bukasov, **2022**, 12.
- [76] Y. Feng, D. Zhou, L. Gao, F. He, *Biosens, Bioelectron* **2020**, 168, 112527.
- [77] I. Ivanišević, S. Milardovic, P. Kassal, *Biotechnol* **2021**, 59, 216.
- [78] F. Faupel, V. Zaporozhchenko, T. Strunskus, M. Elbahri, *Adv, Eng. Mater* **2010**, 12, 1177.
- [79] A. Kausar, J., *Plast. Film Sheeting* **2019**, 35, 65.
- [80] C. I. Idumah, M. Zurina, J. Ogbu, J. U. Ndem, E. C. Igba, *Compos, Interfaces* **2019**, 27, 1.
- [81] L. E. Kreno, K. Leong, O. K. Farha, M. Allendorf, R. P. Duyne, J. T., *Hupp, Chem. Rev* **2012**, 112, 1105.
- [82] Y. Cui, B. Chen, G. Qian, *Coord, Chem. Rev* **2014**, 273.
- [83] P. L. Wang, L. H. Xie, E. A. Joseph, J. R. Li, X. O. Su, H. C., *Zhou, Chem. Rev* **2019**, 119, 10638.
- [84] V. Siracusa, P. Rocculi, S. Romani, M. D. Rosa, *Technol* **2008**, 19, 634.
- [85] S. Mangaraj, A. Yadav, L. M. Bal, S. K. Dash, N. K. Mahanti, J., *Packag. Technol. Res* **2018**, 3, 77.
- [86] I. R. S. Vieira, A. P. A. de de Carvalho, C. A. Conte-Junior, *Comprehensive Reviews in Food Science and Food Safety* **2022**, 21, 3673.
- [87] J. G. Oliveira Filho, A. R. C. Braga, B. R. Oliveira, F. P. Gomes, V. L. Moreira, V. A. C. Pereira, M. B. Egea, *Int* **2021**, 142, 110202.
- [88] E. Balbinot-Alfaro, D. V. Craveiro, K. O. Lima, H. L. G. Costa, D. R. Lopes, C. Prentice, *Rev* **2019**, 11, 235.
- [89] F. Mustafa, S. Andreescu, **2020**, 10.
- [90] T. K. O. Rosales, J. P. Fabi, *Colloids and Surfaces B: Biointerfaces* **2022**, 218, 112707.
- [91] R. Cunha, P. Trigueiro, M. D. Mar, O. Cuevas, S. Medina-Carrasco, T. M. Duarte, L. M. De, C. Honório, D. H. L. Damacena, M. G. Fonseca, E. C. Silva-Filho, J. A., *Osajima, Minerals* **2023**, 13, 268.
- [92] D. D. Liana, B. Raguse, J. J. Gooding, E. Chow, *Sensors* **2012**, 12, 11505.

- [93] R. Porta, M. Sabbah, P. Pierro, *Int. J. Mol. Sci* **2020**, *21*, 4942.
- [94] P. Makvandi, S. Iftekhhar, F. Pizzetti, A. Zarepour, E. N. Zare, M. Ashrafizadeh, T. Agarwal, V. V. T. Padil, R. Mohammadinejad, M. Sillanpaa, T. K. Maiti, G. Perale, A. Zarrabi, F. Rossi, *Environmental Chemistry Letters* **2021**, *19*, 583.
- [95] Q. K. Vu, Q. H. Tran, N. P. Vu, T. Anh, T. T. Dang, T. Matteo, T. H. H. Nguyen, *Mater. Today Commun* **2021**, *26*, 101726.
- [96] M. R. Hasan, T. Pulingam, J. N. Appaturi, A. N. Zifruddin, S. J. Teh, T. W. Lim, F. Ibrahim, B. F. Leo, K. L. Thong, *Anal. Biochem* **2018**, *554*, 34.
- [97] H. Dai, L. Gong, G. Xu, S. Zhang, S. Lu, Y. Jiang, Y. Lin, L. Guo, G. Chen, *Electrochim. Acta* **2013**, *111*, 57.
- [98] M. Pumera, *Mater. Today* **2011**, *14*, 308.
- [99] Y. Jung, J. K. Min, J. Choi, J. Bang, S. Jeong, K. R. Pyun, J. Ahn, Y. Cho, S. Hong, S. Hong, J. Lee, S. H. Ko, *Appl. Mater. Today* **2022**, *29*, 101589.
- [100] A. S. Sharma, S. Ali, D. Sabarinathan, M. Murugavelu, H. Li, Q. Chen, *Compr. Rev. Food Sci. Food Saf* **2021**, *20*, 5765.
- [101] J. Jiménez-López, E. J. Llorent-Martínez, P. Ortega-Barrales, A. RuizMedina, *Talanta* **2020**, *207*, 120344.
- [102] A. Halász, Á. Baráth, L. Simon-Sarkadi, W. Holzapfel, *Technol* **1994**, *5*, 42.
- [103] R. Torre, E. Costa-Rama, H. P. A. Nouws, C. Delerue-Matos, *Biosensors* **2020**, *10*, 139.
- [104] C. Ruiz-Capillas, A. M. Herrero, *Foods* **2019**, *8*, 62.
- [105] F. Barbieri, C. Montanari, F. Gardini, G. Tabanelli, *Foods* **2019**, *8*, 17.
- [106] D. Doeun, M. Davaatseren, M. S. Chung, *Biotechnol* **2017**, *26*, 1463.
- [107] P. Visciano, M. Schirone, A. Paparella, *Foods* **2020**, *9*, 1795.
- [108] L. Prester, *Food Addit. A, Conta*, **2011**.
- [109] N. Benkerroum, *Compr. Rev. Food Sci. Food Saf* **2016**, *15*, 801.
- [110] V. Ladero, M. Coton, M. Fernández, N. Buron, M. C. Martín, H. Guichard, E. Coton, M. A. Alvarez, **2011**, *28*.
- [111] G. Doria, J. Conde, B. Veigas, L. Giestas, C. Almeida, M. Assunção, J. Rosa, P. V. Baptista, *Sensors* **2012**, *12*, 1657.
- [112] H. Ahangari, S. Kurbanoglu, A. Ehsani, B. Uslu, *Technol* **2021**, *112*, 75.
- [113] A. Lapenna, M. Dell'Aglia, G. Palazzo, A. Mallardi, *Eng. Asp* **2020**, *600*, 124903.
- [114] E. Poyatos-Racionero, J. V. Ros-Lis, J. L. Vivancos, R. MartínezMáñez, J., *Clean. Prod* **2018**, *172*, 3398.
- [115] K. Miller, C. L. Reichert, M. Schmid, *Food Rev. Int* **2021**.
- [116] S. Gholampour, H. Jalali, R. Zhiani, H. Rashidi, A. Motavalizadehkakhky, *Inorg. Chem. Commun* **2021**, *123*, 108334.
- [117] H. Deng, Z. Lei, *Compos. B Eng* **2013**, *54*, 194.
- [118] S. Ben-Shabat, N. Kumar, A. J. Domb, *Macromol. Biosci* **2006**, *6*, 1019.
- [119] S. Y. Tseng, S. Y. Li, S. Y. Yi, A. Y. Sun, D. Y. Gao, D. Wan, *ACS Appl. Mater. Interfaces* **2017**, *9*, 17306.
- [120] D. Basavaraja, D. Dey, T. L. Varsha, C. T. F. Salfeena, M. K. Panda, S. B. Somappa, *ACS Appl. Bio. Mater* **2020**, *3*, 772.
- [121] X. N. Qi, Y. M. Zhang, H. Yao, Q. Lin, T. B. Wei, N. J., *Chem* **2021**, *45*, 11234.
- [122] Y. Duan, Y. Liu, H. Han, H. Geng, Y. Liao, T. Han, *Spectrochim. Acta A Mol. Biomol. Spectrosc* **2022**, *266*, 120433.
- [123] J. Wang, D. Li, Y. Ye, Y. Qiu, J. Liu, L. Huang, B. Liang, B. Chen, *Advanced Materials* **2021**, *33*, 2008020.
- [124] A. Sousaraei, C. Queirós, F. G. Moscoso, A. M. G. Silva, T. Lopes-Costa, J. M. Pedrosa, L. Cunha-Silva, J. Cabanillas-Gonzalez, *Advanced Materials Interfaces* **2021**, *8*, 2001759.
- [125] G. Meng, C. Zhang, P. Du, S. Sun, X. Zhang, B. Wang, X. Lu, *Sensors and Actuators B: Chemical* **2022**, *357*, 131435.
- [126] Y. Yao, J. Li, Y. Zhou, T. Gao, H. Li, P. Yan, *Dyes and Pigments* **2021**, *192*, 109441.
- [127] S. Jindal, V. K. Maka, J. N. Moorthy, *J. Mater. Chem. C* **2020**, *8*, 11449.
- [128] M. A. Sahudin, M. S. Su'ait, L. L. Tan, Y. H. Lee, N. H. A. Karim, *Anal Bioanal Chem* **2019**, *411*, 6449.
- [129] F. Lai, J. Yang, R. Huang, Z. Wang, J. Tang, M. Zhang, R. Miao, Y. Fang, *ACS Appl Nano Mater* **2021**, *4*, 2575.
- [130] Q. He, F. Zhan, H. Wang, W. Xu, H. Wang, L. Chen, *Materials Today Sustainability* **2022**, *17*, 100104.
- [131] K. L. Hong, L. J. Sooter, **2015**, DOI 10.1155/2015/419318.
- [132] S. Song, L. Wang, J. Li, C. Fan, J. Zhao, *TrAC Trends in Analytical Chemistry* **2008**, *27*, 108.
- [133] D. Li, L. Liu, Q. Huang, T. Tong, Y. Zhou, Z. Li, Q. Bai, H. Liang, L. Chen, *World J Microbiol Biotechnol* **2021**, *37*, 1.
- [134] O. Mukama, J. P. Sinumvayo, M. Shamoona, M. Shoaib, H. Mushimiyimana, W. Safdar, L. Bemena, P. Rwibasira, S. Mugisha, Z. Wang, *Food Analytical Methods* **2017**, *10*, 2549.
- [135] T. M. Lerga, M. Jauset-Rubio, V. Skouridou, A. S. Bashammakh, M. S. El-Shahawi, A. O. Alyoubi, C. K. O'Sullivan, *Anal Chem* **2019**, *91*, 7104.

- [136] T. M. Lerga, V. Skouridou, M. C. Bermudo, A. S. Bashammakh, M. S. El-Shahawi, A. O. Alyoubi, C. K. O'Sullivan, *Microchimica Acta* **2020**, 187, 1.
- [137] M. Dwidar, Y. Yokobayashi, *S. Reports*, **2019**, 9.
- [138] L. Zeng, X. Xu, L. Guo, Z. Wang, H. Ding, S. Song, L. Xu, H. Kuang, L. Liu, C. Xu, *J Hazard Mater* **2021**, 419, 126533.
- [139] K. Parate, C. C. Pola, S. Rangnekar, D. L. Mendivelso-Perez, E. A. Smith, M. C. Hersam, C. L. Gomes, J. C. Claussen, **2020**, 7.
- [140] C. Kaçar, P. E. Erden, B. Dalkiran, E. K. İnal, E. Kiliç, *Anal Bioanal Chem* **2020**, 412.
- [141] D. C. Vanegas, L. Patiño, C. Mendez, D. A. Oliveira, A. M. Torres, C. L. Gomes, E. S. McLamore, *Biosensors* **2018**, 8, Page 42, 42.
- [142] B. Bóka, N. Adányi, D. Virág, M. Sebela, A. Kiss, *Electroanalysis* **2012**, 24, 181.
- [143] Z. Mohammadi, S. M. Jafari, *Adv Colloid Interface Sci* **2020**, 286, 102297.
- [144] G. D. Betts, P. Linton, R. J. Betteridge, *Food Control* **1999**, 10, 27.
- [145] J. H. J. H. I, *Int J Food Microbiol* **1996**, 33, 1.
- [146] J. E. OWEN, R. A. LAWRIE, *Int J Food Sci Technol* **1975**, 10, 169.
- [147] V. Shukla, G. Kandeepan, M. R. Vishnuraj, A. Soni, *Agricultural Research* **2016**, 5, 205.
- [148] M. Weston, M. A. T. Phan, J. Arcot, R. Chandrawati, *Food Chem* **2020**, 326, 127017.
- [149] Y. Ma, S. Ding, Y. Fei, G. Liu, H. Jang, J. Fang, *Food Control* **2019**, 106, 106712.
- [150] R. Ullah, M. Khan, S. A. Shah, K. Saeed, M. O. Kim, *Nutrients* **2019**, 11, 11.
- [151] D. Neves, P. B. Andrade, R. A. Videira, V. Freitas, L. Cruz, *Food Hydrocoll* **2022**, 133, 107885.
- [152] L. Zhao, Y. Liu, L. Zhao, Y. Wang, *J Agric Food Res* **2022**, 9, 100340.
- [153] S. Roy, J.-W. Rhim, *Critical Reviews in Food Science and Nutrition* **2021**, 61, 2297.
- [154] T. Huang, Y. Qian, J. Wei, C. Zhou, *Polymers* **2019**, 11, DOI 10.3390/polym11030560.
- [155] H. Yong, J. Liu, *Food Packag Shelf Life* **2020**, 26, 100550.
- [156] N. Kanha, S. Osiriphun, K. Rakariyatham, W. Klangpetch, T. Laokuldilok, *J Sci Food Agric* **2022**, 102, 6804.
- [157] A. K. Rashwan, N. Karim, Y. Xu, J. Xie, H. Cui, M. R. Mozafari, W. Chen, **1080**, DOI 10.1080/10408398.2021.1987858.
- [158] A. R. C. Braga, D. C. Murador, L. M. Souza Mesquita, V. V. Rosso, *Journal of Food Composition and Analysis* **2018**, 68, 31.
- [159] M. Alizadeh-Sani, M. Tavassoli, E. Mohammadian, A. Ehsani, G. J. Khaniki, R. Priyadarshi, J. W. Rhim, *Int J Biol Macromol* **2021**, 166, 741.
- [160] B. Kuswandi, N. P. N. Asih, D. K. Pratoko, N. Kristiningrum, M. Moradi, *Packaging Technology and Science* **2020**, 33, 321.
- [161] T. V. Vo, T. H. Dang, B. H. Chen, *Polymers* **2019**, 11, 1088.
- [162] N. Aliabbasi, M. Fathi, Z. Emam-Djomeh, *J Environ Chem Eng* **2021**, 9, 105520.
- [163] K. Zhang, T. S. Huang, H. Yan, X. Hu, T. Ren, *Int J Biol Macromol* **2020**, 145, 768.
- [164] F. N. Eze, T. J. Jayeoye, S. Singh, *Food Chem* **2022**, 366, 130574.
- [165] Y. Wen, J. Liu, L. Jiang, Z. Zhu, S. He, S. He, W. Shao, *Food Packag Shelf Life* **2021**, 29, 100709.
- [166] X. Qin, D. Yuan, Q. Wang, Z. Hu, Y. Wu, J. Cai, Q. Huang, S. Li, G. Liu, *J Agric Food Chem* **2018**, 66, 9556.
- [167] X. Zhang, Q. Zeng, Y. Liu, Z. Cai, *Food Hydrocoll* **2021**, 118, 106668.
- [168] M. K. Lauer, R. C. Smith, *Compr Rev Food Sci Food Saf* **2020**, 19, 3031.
- [169] L. Liu, W. Wu, L. Zheng, J. Yu, P. Sun, P. Shao, *Food Chem* **2022**, 387, 132908.
- [170] Y. Qin, D. Yun, F. Xu, D. Chen, J. Kan, J. Liu, *Food Hydrocoll* **2021**, 119, 106850.
- [171] M. Cheng, Y. Cui, X. Yan, R. Zhang, J. Wang, X. Wang, *Food Hydrocoll* **2022**, 124, 107225.
- [172] S. H. Othman, *Agriculture and Agricultural Science Procedia* **2014**, 2, 296.
- [173] J. Pires, C. D. Paula, V. G. L. Souza, A. L. Fernando, I. Coelho, *Polymers* **2021**, 13.
- [174] R. R. Koshy, J. T. Koshy, S. K. Mary, S. Sadanandan, S. Jisha, L. A. Pothan, *Food Control* **2021**, 126, 108039.
- [175] W. Wang, J. Jung, Y. Zhao, *Carbohydr Polym* **2017**, 157, 1246.
- [176] J. Ge, P. Yue, J. Chi, J. Liang, X. Gao, *Food Hydrocoll* **2018**, 74, 23.
- [177] X. Zhang, Y. Liu, H. Yong, Y. Qin, J. Liu, J. Liu, *Food Hydrocoll* **2019**, 94, 80.
- [178] D. Kim, S. Lee, K. Lee, S. Baek, J. Seo, *Food Science and Biotechnology* **2017**, 26, 37.
- [179] L. Chen, Y. Li, L. Miao, X. Pang, T. Li, Y. Qian, H. Li, *Biosens Bioelectron* **2021**, 188, 113308.
- [180] L. Pathak, A. Kanwal, Y. Agrawal, *J Food Sci Technol* **2015**, 52, 6143.
- [181] M. Duan, S. Yu, J. Sun, H. Jiang, J. Zhao, C. Tong, Y. Hu, J. Pang, C. Wu, *Int J Biol Macromol* **2021**, 187, 332.
- [182] P. Ezati, J. W. Rhim, *Food Hydrocoll*, **2020**, 102.
- [183] A. Etxabide, P. A. Kilmartin, J. I. Maté, *Food Control* **2021**, 121, 107645.
- [184] F. E. Tirtashi, M. Moradi, H. Tajik, M. Forough, P. Ezati, B. Kuswandi, *Int J Biol Macromol* **2019**, 136, 920.
- [185] S. Eyvazi, B. Baradaran, A. Mokhtarzadeh, M. Guardia, *Trends Food Sci Technol* **2021**, 114, 712.
- [186] Md. Fakruddin, K. S. B. Mannan, S. Andrews, *ISRN Microbiology* **2013**, 2013, 703813.

- [187] M. A. Morales, J. M. Halpern, *Bioconjug Chem* **2018**, *29*, 3231.
- [188] A. Singh, S. Poshtiban, S. Evoy, *Sensors*, **2013**, *13*.
- [189] Bayat F., Didar T. F., Hosseinidoust Z., *Environ Sci Nano* **2021**, *8*, 367.
- [190] Z. A. Ahovan, A. Hashemi, L. M. Plano, M. Gholipourmalekabadi, A. Seifalian, *Nanomaterials* **2020**, *10*, Page 501, 501.
- [191] P. A. Quiton, B. M. Carreon, D. May, D. Cruz-Papa, *J. Bergantin, Sensors & Transducers n.d n.d.*, *28*, 38.
- [192] J. Wang, H. Li, C. Li, Y. Ding, Y. Wang, W. Zhu, J. Wang, Y. Shao, H. Pan, X. Wang, *Food Research International* **2022**, *158*, 111479.
- [193] O. Zolti, B. Suganthan, R. Maynard, H. Asadi, J. Locklin, R. P. Ramasamy, *J Electrochem Soc* **2022**, *169*, 067510.
- [194] L. O'Connell, P. R. Marcoux, Y. Roupiez, *ACS Biomater Sci Eng* **2021**, *7*.
- [195] K. S. Sultan, T. A. Ali, N. A. Fahmy, A. El-Shibiny, *Engineering Reports* **2019**, *1*, 12026.
- [196] N. Wisuthiphaet, X. Yang, G. M. Young, N. Nitin, *AMB Express* **2019**, *9*, 1.
- [197] M. M. Nguyen, J. Gil, M. Brown, E. C. Tondo, N. S. M. Aquino, M. Eisenberg, S. Erickson, *Scientific Reports* **2020**, *10*, 1.
- [198] J. Tsonos, D. Vandenheuvel, Y. Briers, H. Greve, J. P. Hernalsteens, R. Lavigne, *Vet Microbiol* **2014**, *171*, 460.
- [199] Q. Emslander, K. Voge, P. Braun, J. Stender, C. Willy, M. Joppich, J. A. Hammerl, M. Abele, C. Meng, A. Pichlmair, C. Ludwig, J. J. Bugert, F. C. Simmel, G. G. Westmeyer, *Cell Chem Biol* **2022**, *29*,.
- [200] S. Khan, B. Burciu, C. D. M. Filipe, Y. Li, K. Dellinger, T. F. Didar, *ACS Nano* **2021**, *15*, 13943.
- [201] H. Yousefi, H.-M. Su, M. Ali, C. D. M. Filipe, T. F. Didar, *Advanced Materials Interfaces* **2018**, *5*, 1800659.
- [202] B. B. Tasbasi, B. C. Guner, M. Sudagidan, S. Ucak, M. Kavruk, V. C. Ozalp, *Anal Biochem* **2019**, *587*, 113449.
- [203] Y. Tian, X. Li, R. Cai, K. Yang, Z. P. Gao, Y. Yuan, T. Yue, Z. Wang, *Food Control* **2021**, *126*, 108060.
- [204] X. Ma, W. Ding, C. Wang, H. Wu, X. Tian, M. Lyu, S. Wang, *Sens Actuators B Chem* **2021**, *331*, 129422.
- [205] M. Qin, X. Ma, S. Fan, H. Wu, W. Yan, X. Tian, J. Lu, M. Lyu, S. Wang, *Food Sci Nutr* **2021**, *9*, 3873.
- [206] M. M. Ali, C. L. Brown, S. Jahanshahi-Anbuhi, B. Kannan, Y. Li, C. D. M. Filipe, J. D. Brennan, *Scientific Reports* **2017**, *7*, 12335.
- [207] X. Ma, C. wang, M. Qin, X. Tian, S. Fan, H. Zu, M. Lyu, S. Wang, *Food Control* **2021**, *123*, 107829.
- [208] H. Yousefi, S. E. Samani, S. Khan, A. Prasad, A. Shakeri, Y. Li, C. D. M. Filipe, T. F. Didar, *ACS Nano* **2022**, *16*, 29.
- [209] A. Shakeri, N. A. Jarad, J. Terryberry, S. Khan, A. Leung, S. Chen, T. F. Didar, *Small* **2020**, *n/a*, 2003844.
- [210] S. M. Imani, M. Badv, A. Shakeri, H. Yousefi, D. Yip, C. Fine, T. F. Didar, *Lab Chip* **2019**, *19*, 3228.
- [211] E. Kasapgil, M. Badv, C. A. Cantú, S. Rahmani, H. Y. Erbil, I. A. Sakir, J. I. Weitz, Z. Hosseini-Doust, T. F. Didar, *ACS Biomater Sci Eng* **2021**, *7*, 541.
- [212] M. Villegas, Y. Zhang, M. Badv, C. Alonso-Cantu, D. Wilson, Z. Hosseinidoust, T. F. Didar, *Scientific Reports* **2022**, *12*, 1.
- [213] E. Afonso, F. Bayat, L. Ladouceur, S. Khan, A. Martínez-Gómez, J. I. Weitz, Z. Hosseinidoust, P. Tiemblo, N. García, T. F. Didar, *ACS Appl. Mater. Interfaces* **2022**, *14*, 53535.
- [214] Z. Liu, Y. Yuan, X. Wu, Q. Ning, S. Wu, L. Fu, *Sens Actuators B Chem* **2020**, *322*, 128646.
- [215] L. Zeng, X. Xu, H. Ding, S. Song, L. Xu, C. Xu, H. Kuang, *J Mater Chem B* **2022**, *10*, 909.
- [216] D. Kim, Y. Cao, D. Mariappan, M. S. Bono Jr, A. J. Hart, B. Marelli, D. Kim, Y. Cao, B. Marelli, D. Mariappan, M. S. Bono Jr, A. J. Hart, *Adv Funct Mater* **2021**, *31*, 2005370.
- [217] M. S. Chiriaco, I. Parlange, F. Sirsi, P. Poltronieri, E. Primiceri, *Electronics* **2018**, *7*, Page 347, 347.
- [218] R. S. Riaz, M. Elsherif, R. Moreddu, I. Rashid, M. U. Hassan, A. K. Yetisen, H. Butt, *ACS Omega* **2019**, *4*, 21792.
- [219] S. Chen, M. Wu, P. Lu, L. Gao, S. Yan, S. Wang, *Int J Biol Macromol* **2020**, *149*, 271.
- [220] P. Mustafa, M. B. K. Niazi, Z. Jahan, G. Samin, A. Hussain, T. Ahmed, S. R. Naqvi, *J Food Saf* **2020**, *40*, 12725.
- [221] X. Wang, Y. Bouzembrak, A. G. J. M. O. Lansink, H. J. Fels-Klerx, *Compr Rev Food Sci Food Saf* **2022**, *21*, 416.
- [222] M. Yang, X. Liu, Y. Luo, A. J. Pearlstein, S. Wang, H. Dillow, K. Reed, Z. Jia, A. Sharma, B. Zhou, D. Pearlstein, H. Yu, B. Zhang, *Nature Food* **2021**, *2*, 110.
- [223] X. Deng, S. Cao, A. L. Horn, **1146**, *12*.
- [224] M. Liu, Q. Zhang, J. D. Brennan, Y. Li, *MRS Communications* **2018**, *8*, 687.
- [225] D. Wynn, N. Raut, S. Joel, P. Pasini, S. K. Deo, S. Daunert, *Analyst* **2018**, *143*, 4774.
- [226] W. Hussain, M. W. Ullah, U. Farooq, A. Aziz, S. Wang, *Biosens Bioelectron* **2021**, *177*, 112973.
- [227] T. H. Begley, **1080**, *14*.
- [228] S. A. Siddiqui, O. Zannou, N. A. Bahmid, H. Fidan, A. F. Alamou, A. A. Nagdalian, A. Hassoun, I. Fernando, S. A. Ibrahim, M. Arsyad, *Future Foods* **2022**, *6*, 100191.
- [229] N. Bumbudsanpharoke, S. Ko, *J. F. Sci*, **2015**, *80*.
- [230] K. Aschberger, S. Gottardo, V. Amenta, M. Arena, F. B. Moniz, H. Bouwmeester, P. Brandhoff, A. Mech, L. Q. Pesudo, H. Rauscher, R. Schoonjans, M. V. Vettori, R. Peters, *J Phys Conf Ser* **2015**, *617*, 012032.

- [231] S. T. Odonkor, T. Mahami, *Int J Microbiol* **2020**, DOI 10.1155/2020/2534130.
- [232] “International Microbiological Criteria – Scientific Criteria to Ensure Safe Food – NCBI Bookshelf”, can be found under, <https://www.ncbi.nlm.nih.gov/books/NBK221566/> (accessed: Mar 2023).
- [233] G. D. Betts, *Nutr Food Sci* **2000**, *30*, 183.
- [234] B. Malorny, C. Löfström, M. Wagner, N. Krämer, J. Hoorfar, A. E. Microbiol, **2008**, *74*.
- [235] M. Weston, S. Geng, R. Chandrawati, M. Weston, S. Geng, R. Chandrawati, *Adv Mater Technol* **2021**, *6*, 2001242.
- [236] C. A. Lázaro, C. A. Conte-Júnior, F. L. Cunha, E. T. Mársico, S. B. Mano, R. M. Franco, *Food Anal Methods* **2013**, *6*, 1024.
- [237] S. Neethirajan, V. Ragavan, X. Weng, R. Chand, *Biosensors*, **2018**, *8*.
- [238] A. Bieberstein, J. Roosen, S. Marette, S. Blanchemanche, F. Vandermoere, *European Review of Agricultural Economics* **2013**, *40*, 73.
- [239] G. Nocella, J. Wu, S. Cerroni, *Int J Consum Stud* **2023**, *47*, 249.
- [240] N. H. C. Hamzah, N. A. M. Shaidi, M. S. Merai, N. Khairuddin, *IOP Conf Ser Earth Environ Sci* **2021**, *733*, 012030.
- [241] L. X. Mei, A. M. Nafchi, F. Ghasemipour, A. M. Easa, S. Jafarzadeh, A. A. Al-Hassan, *Int J Biol Macromol* **2020**, *164*, 4603.
- [242] G. Barandun, M. Soprani, S. Naficy, M. Grell, M. Kasimatis, K. L. Chiu, A. Ponzoni, F. Güder, *ACS Sens.* **2019**, *4*, 1662.
- [243] “BlakBear – Make Food Efficient”, can be found under, <https://www.blakbear.com/> (accessed: Mar 2023).
- [244] “CheckPack | Pack4Food”, can be found under, <https://www.pack4food.be/en/projects/checkpack> (accessed: Mar 2023).
- [245] M. Vanderroost, P. Ragaert, F. Devlieghere, B. Meulenaer, *Trends Food Sci Technol* **2014**, *39*, 47.
- [246] “Detect Food Spoilage with Sensors | Concepts & Innovations”, can be found under, <https://www.electronicsforu.com/technology-trends/detect-food-spoilage-sensors> (accessed: Nov 2017).
- [247] “To Eat, Or Not To Eat, Science Has an Answer | Discover Mag-azine”, can be found under, <https://www.discovermagazine.com/technology/to-eat-or-not-to-eat-science-has-an-answer> (accessed: Jan 2016).
- [248] J. A. Covington, S. Marco, K. C. Persaud, S. S. Schiffman, H. T. Nagle, *IEEE Sens J* **2021**, *21*, 12969.
- [249] K. B. Beć, J. Grabska, N. Plewka, C. W. Huck, *Molecules* **2021**, DOI 10.3390/MOLECULES26216390.
- [250] “McMaster and Toyota Tsusho Canada collaborate to move pathogen-detecting food wrap from lab to market – BrighterWorld”, can be found under, <https://www.brighterworld.mcmaster.ca/articles/mcmaster-and-toyota-tsusho-canada-collaborate-to-move-pathogen-detecting-food-wrap-from-lab-to-market/> (accessed: July 2020).
- [251] “Products — Kraken Sense”, can be found under, <https://www.krakensense.com/products> (accessed: Mar 2023).
- [252] “Toronto Airport Authority Partners with Kraken Sense, a Leading Canadian Tech Company, as Part of Study to Combat COVID-19 | Business Wire”, can be found under, <https://www.businesswire.com/news/home/20230131005114/en/Toronto-Airport-Authority-Partners-with-Kraken-Sense-a-Leading-Canadian-Tech-Company-as-Part-of-Study-to-Combat-COVID-19> (accessed: January 2023).
- [253] “VPCIR Technology”, can be found under, <https://www.vpcir.com/pages/vpcir-technology> (accessed: Mar 2023).
- [254] “Food Tech Startup Combatting Food Safety Scandals Raises \$8.9m for Testing Device – AFN”, can be found under, <https://www.agfundernews.com/food-tech-startup-combatting-food-safety-scandals-raises-8-9m-for-testing-device> (accessed: June 2016).
- [255] “Ancera,” can be found under, <https://www.ancera.com/#platform> (accessed: Mar 2023).
- [256] “SnapDNA – Technology,” can be found under, <https://www.snapdna.com/technology/> (accessed: Dec 2020).
- [257] “Food pathogen detection startup wins IFT FIRST pitch competition | 2021-07-22 | Food Business News”, can be found under, <https://www.foodbusinessnews.net/articles/19161-food-pathogen-detection-startup-wins-ift-first-pitch-competition> (accessed: July 2021).
- [258] E. Mohebi, L. Marquez, *J Food Sci Technol* **2015**, *52*, 3947.
- [259] M. Ghaani, C. A. Cozzolino, G. Castelli, S. Farris, *Trends Food Sci Technol* **2016**, *51*, 1.
- [260] R. R. Breaker, G. F. Joyce, *Chemistry & Biology* **1994**, *1*, 223.
- [261] D. Morrison, M. Rothenbrocker, Y. Li, *Small Methods* **2018**, *2*, 1700319.
- [262] S. K. Silverman, *Nucleic Acids Research* **2005**, *33*, 6151.
- [263] D. A. Baum, S. K. Silverman, *Cellular and Molecular Life Sciences* **2008**, *65*, 2156.
- [264] P.-J. J. Huang, M. Liu, J. Liu, *Reviews in Analytical Chemistry* **2013**, *32*, 77.
- [265] R. Hu, T. Liu, X.-B. Zhang, Y. Yang, T. Chen, C. Wu, Y. Liu, G. Zhu, S. Huan, T. Fu, W. Tan, *Anal. Chem.* **2015**, *87*, 7746.
- [266] S. Petralia, S. Conoci, *ACS Sens.* **2017**, *2*, 876.
- [267] Y. Yamamoto, *Clin Diagn Lab Immunol* **2002**, *9*, 508.
- [268] M. Darmostuk, S. Rimpelova, H. Gbelcova, T. Ruml, *Biotechnology Advances* **2015**, *33*, 1141.

- [269] S. Kumar, S. Jain, N. Dilbaghi, A. S. Ahluwalia, A. A. Hassan, K.-H. Kim, *Trends in Biochemical Sciences* **2019**, *44*, 190.
- [270] J. Wu, Y. Zhu, F. Xue, Z. Mei, L. Yao, X. Wang, L. Zheng, J. Liu, G. Liu, C. Peng, *Microchimica Acta* **2014**, *181*, 479.
- [271] C. B. Swearingen, D. P. Wernette, D. M. Cropek, Y. Lu, J. V. Sweedler, P. W. Bohn, *Anal. Chem.* **2005**, *77*, 442.
- [272] T. S. Dalavoy, D. P. Wernette, M. Gong, J. V. Sweedler, Y. Lu, B. R. Flachsbar, M. A. Shannon, P. W. Bohn, D. M. Cropek, *Lab Chip* **2008**, *8*, 786.
- [273] J. Liu, L. Tian, Y. Qiao, S. Zhou, A. J. Patil, K. Wang, M. Li, S. Mann, *Angewandte Chemie International Edition* **2020**, *59*, 6853.
- [274] W. Cai, S. Xie, J. Zhang, D. Tang, Y. Tang, *Biosensors and Bioelectronics* **2017**, *98*, 466.
- [275] P. Wu, K. Hwang, T. Lan, Y. Lu, *J. Am. Chem. Soc.* **2013**, *135*, 5254.
- [276] L. Zhang, H. Deng, R. Yuan, Y. Yuan, *Microchimica Acta* **2019**, *186*, 709.
- [277] M. Wang, S. Zhang, Z. Ye, D. Peng, L. He, F. Yan, Y. Yang, H. Zhang, Z. Zhang, *Microchimica Acta* **2015**, *182*, 2251.
- [278] L. He, Y. Zhang, S. Liu, S. Fang, Z. Zhang, *Microchimica Acta* **2014**, *181*, 1981.
- [279] M. Wang, S. Zhai, Z. Ye, L. He, D. Peng, X. Feng, Y. Yang, S. Fang, H. Zhang, Z. Zhang, *Dalton Trans.* **2015**, *44*, 6473.
- [280] L. Wang, F. Zhu, M. Chen, Y. Zhu, J. Xiao, H. Yang, X. Chen, *Food Chemistry* **2019**, *271*, 581.
- [281] B. Mondal, B. N. S. Ramlal, J. Kingston, *J. Agric. Food Chem.* **2018**, *66*, 1516.
- [282] S. Li, Y. Zhang, J. Tian, W. Xu, *Food Chemistry* **2020**, *324*, 126859.
- [283] T. Lee, S. Y. Park, H. Jang, G.-H. Kim, Y. Lee, C. Park, M. Mohammadniaei, M.-H. Lee, J. Min, *Materials Science and Engineering: C* **2019**, *99*, 511.
- [284] M. M. Ali, M. Wolfe, K. Tram, J. Gu, C. D. M. Filipe, Y. Li, J. D. Brennan, *Angewandte Chemie International Edition* **2019**, *58*, 9907.
- [285] N. Alizadeh, R. Hallaj, A. Salimi, *Biosensors and Bioelectronics* **2017**, *94*, 184.
- [286] Y. Wen, Y. Yuan, L. Li, D. Ma, Q. Liao, S. Hou, *Microchimica Acta* **2017**, *184*, 3909.
- [287] E. Azuaje-Hualde, S. Arroyo-Jimenez, G. Garai-Ibabe, M. M. de Pancorbo, F. Benito-Lopez, L. Basabe-Desmonts, *Analytica Chimica Acta* **2020**, *1123*, 1.
- [288] C. Zong, D. Zhang, H. Yang, S. Wang, M. Chu, P. Li, *Microchimica Acta* **2017**, *184*, 3197.
- [289] D. Wang, R. Guo, Y. Wei, Y. Zhang, X. Zhao, Z. Xu, *Biosensors and Bioelectronics* **2018**, *122*, 247.
- [290] G. Liang, Y. Man, A. Li, X. Jin, X. Liu, L. Pan, *Microchemical Journal* **2017**, *131*, 145.
- [291] B. Shlyahovsky, D. Li, E. Katz, I. Willner, *Biosensors and Bioelectronics* **2007**, *22*, 2570.
- [292] W. Hu, X. Min, X. Li, S. Yang, L. Yi, L. Chai, *RSC Adv.* **2016**, *6*, 6679.
- [293] J. Kosman, J. Jatschka, A. Csaki, W. Fritzsche, B. Juskowiak, O. Stranik, *Sensors (Basel)* **2017**, *17*, 849.
- [294] Y. Okumoto, T. Ohmichi, N. Sugimoto, *Biochemistry* **2002**, *41*, 2769.
- [295] Y. Yang, Z. Yuan, X.-P. Liu, Q. Liu, C.-J. Mao, H.-L. Niu, B.-K. Jin, S.-Y. Zhang, *Biosensors and Bioelectronics* **2016**, *77*, 13.
- [296] Q. Han, F. Mo, J. Wu, C. Wang, M. Chen, Y. Fu, *Sensors and Actuators B: Chemical* **2020**, *302*, 127191.
- [297] S. Xu, B. Dai, J. Xu, L. Jiang, H. Huang, *Electroanalysis* **2019**, *31*, 2330.
- [298] J. Wu, Y. Lu, N. Ren, M. Jia, R. Wang, J. Zhang, *Sensors (Basel)* **2019**, *19*, 2732.
- [299] J. Wang, S. Mao, H.-F. Li, J.-M. Lin, *Analytica Chimica Acta* **2018**, *1027*, 76.
- [300] T. F. Didar, M. Tabrizian, *Lab Chip* **2012**, *12*, 4363.
- [301] T. F. Didar, K. Bowey, G. Almazan, M. Tabrizian, *Advanced Healthcare Materials* **2014**, *3*, 253.
- [302] A. Shakeri, D. Yip, M. Badv, S. M. Imani, M. Sanjari, T. F. Didar, *Materials* **2018**, *11*, DOI 10.3390/ma11061003.
- [303] M. Amouzadeh Tabrizi, J. Ferré-Borrull, L. F. Marsal, *Sensors and Actuators B: Chemical* **2020**, *321*, 128314.
- [304] W. Chen, B. Li, C. Xu, L. Wang, *Biosensors and Bioelectronics* **2009**, *24*, 2534.
- [305] N. Hughes, N. Nguyen, D.-K. Daley, J. Grennell, A. Gee, M. F. Ali, *MRS Adv* **2018**, *3*, 1491.
- [306] M. Liu, X. Lou, J. Du, M. Guan, J. Wang, X. Ding, J. Zhao, *Analyst* **2012**, *137*, 70.
- [307] Y. Wu, Z. Cai, G. Wu, M. Rong, Y. Jiang, C. J. Yang, X. Chen, *Sensors and Actuators B: Chemical* **2014**, *191*, 60.
- [308] Z. Yu, N. Li, X. Hu, Y. Dong, Y. Lin, H. Cai, Z. Xie, D. Qu, X. Li, *Synthetic Metals* **2019**, *254*, 164.
- [309] Z. Ye, G. Li, L. Xu, Q. Yu, X. Yue, Y. Wu, B. Ye, *Talanta* **2020**, *209*, 120611.
- [310] H. Wang, Y. Liu, G. Liu, *Nanomaterials (Basel)* **2018**, *8*, 258.
- [311] H. Wang, Y. Liu, J. Wang, B. Xiong, X. Hou, *Microchimica Acta* **2020**, *187*, 207.
- [312] A. Niazov, R. Freeman, J. Girsh, I. Willner, *Sensors* **2011**, *11*, DOI 10.3390/s111110388.
- [313] J. Zhuang, L. Fu, M. Xu, Q. Zhou, G. Chen, D. Tang, *Biosensors & bioelectronics* **2013**, *45*, 52.
- [314] D. Tang, B. Xia, Y. Tang, J. Zhang, Q. Zhou, *Microchimica Acta* **2019**, *186*, 318.
- [315] T. T. Nguyen, K. L. Sly, J. C. Conboy, *Anal. Chem.* **2012**, *84*, 201.

- [316] A. Jain, A. Barve, Z. Zhao, W. Jin, K. Cheng, *Mol. Pharmaceutics* **2017**, *14*, 1517.
- [317] M. I. Pividori, A. Lermo, E. Zacco, S. Hernández, S. Fabiano, S. Alegret, *Thin Solid Films* **2007**, *516*, 284.
- [318] C. Ocaña, N. Malashikhina, M. del Valle, V. Pavlov, *Analyst* **2013**, *138*, 1995.
- [319] W. Song, J. Li, Q. Li, W. Ding, X. Yang, *Analytical Biochemistry* **2015**, *471*, 17.
- [320] J. Y. Do, J. Y. Jeong, C. A. Hong, *Talanta* **2021**, *233*, 122505.
- [321] S. E. Samani, D. Chang, E. M. McConnell, M. Rothenbroker, C. D. M. Filipe, Y. Li, *ChemBioChem* **2020**, *21*, 632.
- [322] L. Gu, W. Yan, H. Wu, S. Fan, W. Ren, S. Wang, M. Lyu, J. Liu, *Anal. Chem.* **2019**, *91*, 7887.
- [323] R. Ji, W. Niu, S. Chen, W. Xu, X. Ji, L. Yuan, H. Zhao, M. Geng, J. Qiu, C. Li, *Biosensors and Bioelectronics* **2019**, *144*, 111560.
- [324] T.-J. Yim, J. Liu, Y. Lu, R. S. Kane, J. S. Dordick, *J. Am. Chem. Soc.* **2005**, *127*, 12200.
- [325] X. Gong, X. Li, T. Qing, P. Zhang, B. Feng, *Analyst* **2019**, *144*, 1948.
- [326] J. Liu, Y. Lu, *J. Am. Chem. Soc.* **2003**, *125*, 6642.
- [327] J. Liu, Y. Lu, *J. Am. Chem. Soc.* **2004**, *126*, 12298.
- [328] H. Zhang, X. Cheng, L. Chen, F. Mo, L. Xu, F. Fu, *Analytica Chimica Acta* **2017**, *956*, 63.
- [329] W. Wu, C. Yu, J. Chen, Q. Yang, *null* **2020**, *100*, 324.
- [330] Y. Sun, Y. Lin, R. Han, X. Wang, C. Luo, *Talanta* **2019**, *200*, 57.
- [331] H. G. Hanstock, J. P. Edwards, N. P. Walsh, *Frontiers in Immunology* **2019**, *10*, 1178.
- [332] Abdul-Salam Vahitha B., Ramrakha Punit, Krishnan Unni, Owen David R., Shalhoub Joseph, Davies Alun H., Tang Tjun Y., Gillard Jonathan H., Boyle Joseph J., Wilkins Martin R., Edwards Robert J., *Arteriosclerosis, Thrombosis, and Vascular Biology* **2010**, *30*, 1027.
- [333] D. Santoriello, L. M. Andal, R. Cox, V. D. D'Agati, G. S. Markowitz, *Kidney Int Rep* **2016**, *2*, 84.
- [334] J. Jin, D. Zhang, E. C. Alocilja, D. L. Grooms, *IEEE Sensors Journal* **2008**, *8*, 891.
- [335] C. Y. Hui, M. Liu, Y. Li, J. D. Brennan, *Angewandte Chemie International Edition* **2018**, *57*, 4549.
- [336] M. M. Ali, A. Slepkin, E. Peterson, W. Zhao, *ChemBioChem* **2019**, *20*, 906.
- [337] M. R. N. Monton, E. M. Forsberg, J. D. Brennan, *Chem. Mater.* **2012**, *24*, 796.
- [338] A. GAO, Y.-R. WANG, X.-W. HE, X.-B. YIN, *Chinese Journal of Analytical Chemistry* **2012**, *40*, 1471.
- [339] S. K. Silverman, *Trends in Biochemical Sciences* **2016**, *41*, 595.
- [340] I. Willner, B. Shlyahovsky, M. Zayats, B. Willner, *Chem. Soc. Rev.* **2008**, *37*, 1153.
- [341] Y. Guo, Y. Wang, S. Liu, J. Yu, H. Wang, Y. Wang, J. Huang, *Biosensors and Bioelectronics* **2016**, *75*, 315.
- [342] Z. Zhou, Y. Zhang, M. Guo, K. Huang, W. Xu, *Biosensors and Bioelectronics* **2020**, *167*, 112475.
- [343] M. Liu, C. Y. Hui, Q. Zhang, J. Gu, B. Kannan, S. Jahanshahi-Anbuhi, C. D. M. Filipe, J. D. Brennan, Y. Li, *Angewandte Chemie International Edition* **2016**, *55*, 2709.
- [344] L. Zheng, P. Qi, D. Zhang, *Sensors and Actuators B: Chemical* **2018**, *276*, 42.
- [345] X. Ma, C. wang, M. Qin, X. Tian, S. Fan, H. Zu, M. Lyu, S. Wang, *Food Control* **2021**, *123*, 107829.
- [346] Z. Liu, C. Yao, Y. Wang, C. Yang, *Anal. Methods* **2018**, *10*, 848.
- [347] Z. Liu, Y. Yuan, X. Wu, Q. Ning, S. Wu, L. Fu, *Sensors and Actuators B: Chemical* **2020**, *322*, 128646.
- [348] Y. Sun, N. Duan, P. Ma, Y. Liang, X. Zhu, Z. Wang, *J. Agric. Food Chem.* **2019**, *67*, 2313.
- [349] M. Rothenbroker, E. M. McConnell, J. Gu, M. L. Urbanus, S. E. Samani, A. W. Ensminger, C. D. M. Filipe, Y. Li, *Angewandte Chemie International Edition* **2021**, *60*, 4782.
- [350] K. Setlem, B. Mondal, R. Shylaja, M. Parida, *Analytical Biochemistry* **2020**, *608*, 113874.
- [351] X. Yu, Y. Lin, X. Wang, L. Xu, Z. Wang, F. Fu, *Microchimica Acta* **2018**, *185*, 259.
- [352] Z. Shen, Z. Wu, D. Chang, W. Zhang, K. Tram, C. Lee, P. Kim, B. J. Salena, Y. Li, *Angewandte Chemie International Edition* **2016**, *55*, 2431.
- [353] H. Xi, M. Juhas, Y. Zhang, *Biosensors and Bioelectronics* **2020**, *167*, 112494.
- [354] A. M. Foudeh, T. Fatanat Didar, T. Veres, M. Tabrizian, *Lab Chip* **2012**, *12*, 3249.
- [355] C. E. McGhee, K. Y. Loh, Y. Lu, *Curr Opin Biotechnol* **2017**, *45*, 191.
- [356] H. S. Kim, Y. J. Kim, Y. R. Seo, *J Cancer Prev* **2015**, *20*, 232.
- [357] P. B. Tchounwou, C. G. Yedjou, A. K. Patlolla, D. J. Sutton, *Exp Suppl* **2012**, *101*, 133.
- [358] I. Cozma, E. M. McConnell, J. D. Brennan, Y. Li, *Biosensors and Bioelectronics* **2021**, *177*, 112972.
- [359] K. Hwang, Q. Mou, R. J. Lake, M. Xiong, B. Holland, Y. Lu, *Inorg Chem* **2019**, *58*, 13696.
- [360] R. J. Lake, Z. Yang, J. Zhang, Y. Lu, *Acc. Chem. Res.* **2019**, *52*, 3275.
- [361] World Health Organization, *Copper in Drinking-Water: Background Document for Development of WHO Guidelines for Drinking-Water Quality*, **2004**.
- [362] W. Xu, J. Tian, Y. Luo, L. Zhu, K. Huang, *Scientific Reports* **2017**, *7*, 43362.
- [363] H.-B. Wang, L.-H. Ma, B.-Y. Fang, Y.-D. Zhao, X.-B. Hu, *Colloids and Surfaces B: Biointerfaces* **2018**, *169*, 305.
- [364] W. Diao, G. Wang, L. Wang, L. Zhang, S. Ding, T. Takarada, M. Maeda, X. Liang, *ACS Appl. Bio Mater.* **2020**, *3*, 7003.



- [365] G. Flora, D. Gupta, A. Tiwari, *Interdisciplinary Toxicology* **2012**, 5, 47.
- [366] T. Lan, K. Furuya, Y. Lu, *Chem. Commun.* **2010**, 46, 3896.
- [367] K. M. Rice, E. M. Walker Jr, M. Wu, C. Gillette, E. R. Blough, *J Prev Med Public Health* **2014**, 47, 74.
- [368] G. Chen, Z. Guo, G. Zeng, L. Tang, *Analyst* **2015**, 140, 5400.
- [369] C. Wu, G. Gao, K. Zhai, L. Xu, D. Zhang, *Food Chemistry* **2020**, 331, 127208.
- [370] A. Ravikumar, P. Panneerselvam, K. Radhakrishnan, *Microchimica Acta* **2017**, 185, 2.
- [371] W. Yun, H. Zhong, S. Zheng, R. Wang, L. Yang, *Sensors and Actuators B: Chemical* **2018**, 277, 456.
- [372] C. Li, Z. Wang, L. Wang, C. Zhang, *Biosensors and Bioelectronics* **2019**, 144, 111695.
- [373] S. Lv, K. Zhang, Z. Lin, D. Tang, *Biosensors and Bioelectronics* **2017**, 96, 317.
- [374] X. Li, J. Li, C. Zhu, X. Zhang, J. Chen, *Talanta* **2018**, 182, 292.
- [375] H. Peng, A. M. Newbigging, Z. Wang, J. Tao, W. Deng, X. C. Le, H. Zhang, *Anal. Chem.* **2018**, 90, 190.
- [376] N. Alizadeh, A. Salimi, R. Hallaj, in *Catalytically Active Nucleic Acids* (Eds.: H. Seitz, F. Stahl, J.-G. Walter), Springer International Publishing, Cham, **2020**, pp. 85–106.
- [377] S. Chen, P. Liu, K. Su, X. Li, Z. Qin, W. Xu, J. Chen, C. Li, J. Qiu, *Biosensors and Bioelectronics* **2018**, 99, 338.
- [378] R. Ren, Q. Bi, R. Yuan, Y. Xiang, *Sensors and Actuators B: Chemical* **2020**, 304, 127068.
- [379] G. Peng, Y. Yuan, S. Wu, F. He, Y. Hu, B. Luo, *Translational Stroke Research* **2015**, 6, 437.
- [380] M. Satoh, Y. Minami, Y. Takahashi, T. Tabuchi, M. Nakamura, *Journal of Cardiac Failure* **2011**, 17, 923.
- [381] N. Balakathiresan, M. Bhomia, R. Chandran, M. Chavko, R. M. McCarron, R. K. Maheshwari, *Journal of Neurotrauma* **2012**, 29, 1379.
- [382] F. Biamonte, G. Santamaria, A. Sacco, F. M. Perrone, A. Di Cello, A. M. Battaglia, A. Salatino, A. Di Vito, I. Aversa, R. Venturella, F. Zullo, F. Costanzo, *Scientific Reports* **2019**, 9, 5668.
- [383] D. M. Aly, N. A.-H. Gohar, A. A. Abd El-Hady, M. Khairy, M. M. Abdullatif, *Asian Pac J Cancer Prev* **2020**, 21, 555.
- [384] D. Sun, X. Lin, J. Lu, P. Wei, Z. Luo, X. Lu, Z. Chen, L. Zhang, *Biosensors and Bioelectronics* **2019**, 142, 111578.
- [385] Z. Luo, D. Sun, Y. Tong, Y. Zhong, Z. Chen, *Microchimica Acta* **2019**, 186, 374.
- [386] C. Zhu, W. Zhu, L. Xu, X. Zhou, *Analytica Chimica Acta* **2019**, 1047, 21.
- [387] L. Kong, D. Wang, Y. Chai, Y. Yuan, R. Yuan, *Anal. Chem.* **2019**, 91, 10289.
- [388] Y. Sun, X. Wang, H. Xu, C. Ding, Y. Lin, C. Luo, Q. Wei, *Analytica Chimica Acta* **2018**, 1043, 132.
- [389] X. Wang, D. Sun, Y. Tong, Y. Zhong, Z. Chen, *Microchimica Acta* **2017**, 184, 1791.
- [390] D. Kwapisz, *Ann Transl Med* **2017**, 5, 46.
- [391] Y. Zhou, H. Xu, H. Wang, B.-C. Ye, *Analyst* **2020**, 145, 107.
- [392] Q. Zhang, W. Wang, S. Huang, S. Yu, T. Tan, J.-R. Zhang, J.-J. Zhu, *Chem. Sci.* **2020**, 11, 1948.
- [393] X. Mao, S. Pan, D. Zhou, X. He, Y. Zhang, *Sensors and Actuators B: Chemical* **2019**, 285, 385.
- [394] P. Li, M. Wei, F. Zhang, J. Su, W. Wei, Y. Zhang, S. Liu, *ACS Appl. Mater. Interfaces* **2018**, 10, 43405.
- [395] C. Alix-Panabières, H. Schwarzenbach, K. Pantel, *Annu. Rev. Med.* **2012**, 63, 199.
- [396] D. Sun, J. Lu, D. Chen, Y. Jiang, Z. Wang, W. Qin, Y. Yu, Z. Chen, Y. Zhang, *Sensors and Actuators B: Chemical* **2018**, 268, 359.
- [397] J. W. Shay, Y. Zou, E. Hiyama, W. E. Wright, *Human Molecular Genetics* **2001**, 10, 677.
- [398] C. B. Harley, *Nature Reviews Cancer* **2008**, 8, 167.
- [399] E. Hiyama, K. Hiyama, *Cancer Letters* **2003**, 194, 221.
- [400] L. Wang, F. Ma, B. Tang, C. Zhang, *Chem. Sci.* **2017**, 8, 2495.
- [401] C. Xu, F. Zhang, K. Wang, E. Xu, Y. Liu, W. Wei, S. Liu, *Sensors and Actuators B: Chemical* **2019**, 298, 126930.
- [402] Y. Wang, L. Yang, Y. Wang, W. Liu, B. Li, Y. Jin, *Analyst* **2019**, 144, 5959.
- [403] K. B. Reddy, *Cancer Cell International* **2015**, 15, 38.
- [404] J. Cacheux, A. Bancaud, T. Leichlé, P. Cordelier, *Frontiers in Chemistry* **2019**, 7, 815.
- [405] M. Mahdiannasser, Z. Karami, *Biosensors and Bioelectronics* **2018**, 107, 123.
- [406] K. Chen, Q. Huang, T. Fu, G. Ke, Z. Zhao, X. Zhang, W. Tan, *Anal. Chem.* **2020**, 92, 7404.
- [407] Q. Yao, H. Xu, Q.-Q. Zhang, H. Zhou, L.-H. Qu, *Biochemical and Biophysical Research Communications* **2009**, 388, 539.
- [408] Y. Wu, J. Huang, X. Yang, Y. Yang, K. Quan, N. Xie, J. Li, C. Ma, K. Wang, *Anal. Chem.* **2017**, 89, 8377.
- [409] M. Liu, Q. Zhang, B. Kannan, G. A. Botton, J. Yang, L. Soleymani, J. D. Brennan, Y. Li, *Angewandte Chemie International Edition* **2018**, 57, 12440.
- [410] A. Hosseini, M. Villegas, J. Yang, M. Badv, J. I. Weitz, L. Soleymani, T. F. Didar, *Advanced Materials Interfaces* **2018**, 5, 1800617.
- [411] M. Osborne, A. Aryasomayajula, A. Shakeri, P. R. Selvaganapathy, T. F. Didar, *ACS sensors* **2019**, 4, 687.
- [412] M. Badv, I. H. Jaffer, J. I. Weitz, T. F. Didar, *Scientific Reports* **2017**, 7, 11639.
- [413] M. Badv, S. M. Imani, J. I. Weitz, T. F. Didar, *ACS Nano* **2018**, 12, 10890.

- [414] M. Badv, C. Alonso-Cantu, A. Shakeri, Z. Hosseinidoust, J. I. Weitz, T. F. Didar, *ACS Biomaterials Science & Engineering* **2019**, *5*, 6485.
- [415] M. Villegas, C. Alonso-Cantu, S. Rahmani, D. Wilson, Z. Hosseinidoust, T. F. Didar, *ACS Appl. Mater. Interfaces* **2021**, *13*, 27774.
- [416] Y. Zhang, M. Villegas, M. Badv, C. Alonso-Cantu, D. Wilson, Z. Hosseinidoust, T. Didar, **2021**, DOI 10.21203/rs.3.rs-624942/v1.
- [417] T. F. Didar, M. Badv, Z. Cetinic, A. Shakeni, **2020**.
- [418] M. Badv, J. I. Weitz, T. F. Didar, *Small* **2019**, *15*, 1905562.
- [419] D. Mazumdar, T. Lan, Y. Lu, in *Biosensors and Biodetection: Methods and Protocols Volume 1: Optical-Based Detectors* (Eds.: A. Rasooly, B. Prickril), Springer New York, New York, NY, **2017**, pp. 389–406.
- [420] Y. Shen, G. Mackey, N. Rupcich, D. Gloster, W. Chiuman, Y. Li, J. D. Brennan, *Anal. Chem.* **2007**, *79*, 3494.
- [421] Y. Li, S. Liu, Q. Deng, L. Ling, *Journal of Medical Virology* **2018**, *90*, 699.
- [422] Y. Sun, Y. Chang, Q. Zhang, M. Liu, *Micromachines (Basel)* **2019**, *10*, 531.
- [423] N. Zaouri, Z. Cui, A. S. Peinetti, Y. Lu, P.-Y. Hong, *Environ. Sci.: Water Res. Technol.* **2019**, *5*, 2260.
- [424] X. Song, Y. Wang, S. Liu, X. Zhang, J. Wang, H. Wang, F. Zhang, J. Yu, J. Huang, *Microchimica Acta* **2019**, *186*, 559.
- [425] Y. Wang, G. Zhao, G. Zhang, Y. Zhang, H. Wang, W. Cao, T. Li, Q. Wei, *Sensors and Actuators B: Chemical* **2020**, *319*, 128313.
- [426] H. Wu, S. Wang, S. F. Y. Li, Q. Bao, Q. Xu, *Analytical and Bioanalytical Chemistry* **2020**, *412*, 7525.
- [427] X. Chen, X. Wang, Z. Lu, H. Luo, L. Dong, Z. Ji, F. Xu, D. Huo, C. Hou, *Sensors and Actuators B: Chemical* **2020**, *311*, 127898.
- [428] X.-L. Du, T.-F. Kang, L.-P. Lu, S.-Y. Cheng, *Analytical Methods* **2018**, *10*, 51.
- [429] X. Liao, J. Luo, J. Wu, T. Fan, Y. Yao, F. Gao, Y. Qian, *Journal of Electroanalytical Chemistry* **2018**, *829*, 129.
- [430] T. Zhang, C. Liu, W. Zhou, K. Jiang, C. Yin, C. Liu, Z. Zhang, H. Li, *Journal of Analytical Methods in Chemistry* **2019**, *2019*, 3528345.
- [431] W. Yun, J. Jiang, D. Cai, X. Wang, G. Sang, J. Liao, T. Lu, K. Yan, *RSC Adv.* **2016**, *6*, 3960.
- [432] S. Xue, P. Jing, W. Xu, *Biosensors and Bioelectronics* **2016**, *86*, 958.
- [433] Y. Shi, H. Wang, X. Jiang, B. Sun, B. Song, Y. Su, Y. He, *Anal. Chem.* **2016**, *88*, 3723.
- [434] P. Zhang, X. Wu, R. Yuan, Y. Chai, *Anal. Chem.* **2015**, *87*, 3202.
- [435] B. Zhang, B. Liu, J. Zhuang, D. Tang, *Bioconjugate Chem.* **2013**, *24*, 678.
- [436] L. Zhang, A. Kan, S. Wang, X. Xu, N. Zhang, W. Jiang, *Sensors and Actuators B: Chemical* **2021**, *333*, 129551.
- [437] L. Hong, F. Zhou, D. Shi, X. Zhang, G. Wang, *Biosensors and Bioelectronics* **2017**, *95*, 152.
- [438] B. Zhang, B. Liu, J. Zhou, J. Tang, D. Tang, *ACS Appl. Mater. Interfaces* **2013**, *5*, 4479.
- [439] H. Lee, Y. Yoon, *Food Sci of Anim Resour* **2021**, *41*, 1.
- [440] B. B. Calley, C. Meyers, C. Gibson, E. Irlbeck, *Journal of Applied Communications* **2019**, *103*.
- [441] O. M. Olanya, A. K. Hoshide, O. A. Ijabadeniyi, D. O. Ukuku, S. Mukhopadhyay, B. A. Niemira, O. Ayeni, *Food Control* **2019**, *102*, 231.
- [442] C. Cicatiello, S. Franco, B. Pancino, E. Blasi, L. Falasconi, *Resources, Conservation and Recycling* **2017**, *125*, 273.
- [443] K. Venkat, *International Journal on Food System Dynamics* **2011**, *2*, 431.
- [444] A. D. Cuéllar, M. E. Webber, *Environmental science & technology* **2010**, *44*, 6464.
- [445] B. Kuswandi, M. Moradi, P. Ezati, *Packaging Technology and Science* **2022**.
- [446] Y. Wang, T. V. Duncan, *Current Opinion in Biotechnology* **2017**, *44*, 74.
- [447] Q. Ma, X. Lu, W. Wang, M. A. Hubbe, Y. Liu, J. Mu, J. Wang, J. Sun, O. J. Rojas, *Food Packaging and Shelf Life* **2021**, *28*, 100634.
- [448] M. Liu, D. Chang, Y. Li, *Acc. Chem. Res.* **2017**, *50*, 2273.
- [449] H.-Y. Li, W.-N. Jia, X.-Y. Li, L. Zhang, C. Liu, J. Wu, *Emerging Microbes & Infections* **2020**, *9*, 1671.
- [450] J. Khang, D. Kim, K. W. Chung, J. H. Lee, *Talanta* **2016**, *147*, 177.
- [451] R. Liu, S. A. Haruna, S. Ali, J. Xu, Y. Zhang, P. Lü, H. Li, Q. Chen, *Sensors and Actuators B: Chemical* **2022**, *355*, 131311.
- [452] Y. Zhang, P. Zuo, B.-C. Ye, *Biosensors and Bioelectronics* **2015**, *68*, 14.
- [453] X. Ma, W. Ding, C. Wang, H. Wu, X. Tian, M. Lyu, S. Wang, *Sensors and Actuators B: Chemical* **2021**, *331*, 129422.
- [454] M. Dwidar, Y. Yokobayashi, *Scientific Reports* **2019**, *9*, 16659.
- [455] R. Karoui, C. Blecker, *Food and Bioprocess Technology* **2011**, *4*, 364.
- [456] K. Nishi, S.-I. Isobe, Y. Zhu, R. Kiyama, *Sensors* **2015**, *15*, 25831.
- [457] M. A. Costa Angeli, T. Cramer, B. Fraboni, L. Magagnin, D. Gastaldi, P. Vena, *MRS Communications* **2019**, *9*, 129.
- [458] P. Ihalainen, A. Määttänen, N. Sandler, *International Journal of Pharmaceutics* **2015**, *494*, 585.

- [459] S. A. Lange, V. Benes, D. P. Kern, J. K. H. Hörber, A. Bernard, *Anal. Chem.* **2004**, 76, 1641.
- [460] A. Krishan, P. D. Dandekar, *Journal of Histochemistry & Cytochemistry* **2005**, 53, 1033.
- [461] G. Hungerford, J. Benesch, J. F. Mano, R. L. Reis, *Photochemical & Photobiological Sciences* **2007**, 6, 152.
- [462] J. E. Berlier, A. Rothe, G. Buller, J. Bradford, D. R. Gray, B. J. Filanoski, W. G. Telford, S. Yue, J. Liu, C.-Y. Cheung, W. Chang, J. D. Hirsch, J. M. Beechem Rosaria P. Haugland, R. P. Haugland, *J Histochem Cytochem.* **2003**, 51, 1699.
- [463] C. Buschmann, *Photosynthesis Research* **2007**, 92, 261.
- [464] C.-N. Lai, M. A. Butler, T. S. Matney, *Mutation Research/Genetic Toxicology* **1980**, 77, 245.
- [465] M. Lingvay, P. Akhtar, K. Sebök-Nagy, T. Páli, P. H. Lambrev, *Frontiers in Plant Science* **2020**, 11, DOI 10.3389/fpls.2020.00849.
- [466] L. Fu, Y. Qian, J. Zhou, L. Zheng, Y. Wang, *Comprehensive Reviews in Food Science and Food Safety* **2020**, 19, 3343.
- [467] M. Asnaashari, R. E. Kenari, S. M. Taghdisi, K. Abnous, R. Farahmandfar, *Journal of Fluorescence* **2023**, 1.
- [468] J. Li, S. Khan, J. Gu, C. D. Filipe, T. F. Didar, Y. Li, *Angewandte Chemie* **2023**, 135, e202300828.
- [469] C. Thibault, C. Séverac, A.-F. Mingotaud, C. Vieu, M. Mauzac, *Langmuir* **2007**, 23, 10706.
- [470] B. Mosadegh, H. Tavana, S. C. Leshner-Perez, S. Takayama, *Lab Chip* **2011**, 11, 738.
- [471] K. Glasmästar, J. Gold, A.-S. Andersson, D. S. Sutherland, B. Kasemo, *Langmuir* **2003**, 19, 5475.
- [472] D. M. Mayder, C. M. Tonge, G. D. Nguyen, M. V. Tran, G. Tom, G. H. Darwish, R. Gupta, K. Lix, S. Kamal, W. R. Algar, S. A. Burke, Z. M. Hudson, *J. Am. Chem. Soc.* **2021**, 143, 16976.
- [473] X. Zhou, H. Xu, J. Cheng, N. Zhao, S.-C. Chen, *Scientific Reports* **2015**, 5, 10402.
- [474] W. H. Organization, *World Health Organization* **2015**.
- [475] E. Scallan, R. M. Hoekstra, F. J. Angulo, R. V. Tauxe, M.-A. Widdowson, S. L. Roy, J. L. Jones, P. M. Griffin, *Emerg Infect Dis* **2011**, 17, 7.
- [476] S. Hoffmann, J.-W. Ahn, *Natural Resources, and Rural America* **2021**.
- [477] B. A. Smith, A. Fazil, **2019**, 45.
- [478] O. Ehuwa, A. K. Jaiswal, S. Jaiswal, *Foods* **2021**, 10, 907.
- [479] G. Ekici, E. Dümen, in *The Universe of Escherichia Coli, IntechOpen*, **2019**.
- [480] M. Kurpas, K. Wieczorek, J. Osek, *J Vet Res* **2018**, 62, 49.
- [481] M. S. Chiriaco, I. Parlangeli, F. Sirsi, P. Poltronieri, E. Primiceri, *Electronics*, **2018**, 7.
- [482] P. A. Quiton, B. M. Carreon, D. M. D. Cruz-Papa, J. Bergantin Jr, *Sensors & Transducers* **2018**, 28, 38.
- [483] C. Bou-Mitri, M. Abdessater, H. Zgheib, Z. Akiki, *Nutr Food Sci* **2020**, 51, 71.
- [484] S. Jafarzadeh, A. M. Nafchi, A. Salehabadi, N. Oladzad-Abbasabadi, S. M. Jafari, *Adv Colloid Interface Sci* **2021**, 291, 102405.
- [485] B. Nemat, M. Razzaghi, K. Bolton, K. Rousta, *Sustainability* **2019**, 11, 4350.
- [486] N. Lavoine, V. Guillard, I. Desloges, N. Gontard, J. Bras, *Carbohydr Polym* **2016**, 149, 40.
- [487] Yan M. R., Hsieh S., Ricacho N., *Processes* **2022**, 10, 747.
- [488] **2016**.
- [489] R. Farag, Y., *Elmogahzy, in Handbook of Tensile Properties of Textile and Technical Fibres*, Woodhead Publishing, **2009**.
- [490] T. Thamae, S. Aghedo, C. Baillie, D., in *Handbook of Tensile Properties of Textile and Technical Fibres* (Ed.: A. R. B. Ed.), Woodhead Publishing, **2009**, pp. 73–99.
- [491] E. Pinho, G. Soares, J. M. C. B, **2018**.
- [492] B., *L*, Woodhead Publishing, **2015**.
- [493] M. Riley, in *Size Limits of Very Small Microorganisms: Proceedings of a Workshop*, National Academies Press, Washington, DC, **1999**, p. 21.
- [494] A. Andino, I. Hanning, *The Scientific World Journal* **2015**.
- [495] S. Khan, A. Shakeri, J. Monteiro, S. Tariq, A. Prasad, J. Gu, C. Filipe, Y. Li, T. Didar, **2023**.
- [496] M. Canali, P. Amani, L. Aramyan, M. Gheoldus, G. Moates, K. Östergren, K. Silvennoinen, K. Waldron, M. Vittuari, *Sustainability* **2017**, 9, DOI 10.3390/su9010037.
- [497] S. Hoffman, B. Maculloch, M. Batz, **2015**.
- [498] J. Kameník, *Maso International—Journal of Food Science and Technology.—2013.—P* **2013**, 1.
- [499] A. Raposo, E. Pérez, C. T. de Faria, M. A. Ferrús, C. Carrascosa, *Foodborne pathogens and antibiotic resistance* **2016**, 41.
- [500] S. Khan, J. K. Monteiro, A. Prasad, C. D. M. Filipe, Y. Li, T. F. Didar, *Advanced Materials* **2024**, 36, 2300875.
- [501] A. B. Snyder, N. Martin, M. Wiedmann, *Nature Reviews Microbiology* **2024**, 1.
- [502] E. Balbinot-Alfaro, D. V. Craveiro, K. O. Lima, H. L. G. Costa, D. R. Lopes, C. Prentice, *Food engineering reviews* **2019**, 11, 235.
- [503] M. I. Shaik, M. F. Azhari, N. M. Sarbon, *Foods* **2022**, 11, 3797.
- [504] Q. Luo, M. A. Hossen, Y. Zeng, J. Dai, S. Li, W. Qin, Y. Liu, *Journal of Food Engineering* **2022**, 313, 110762.

- [505] S. Rawdkuen, A. Faseha, S. Benjakul, P. Kaewprachu, *Food Bioscience* **2020**, *36*, 100603.
- [506] K. A. Barrett, J. H. Nakao, E. V. Taylor, C. Eggers, L. H. Gould, *Foodborne Pathogens and Disease* **2017**, *14*, 537.
- [507] D.-Y. Kim, S.-W. Park, H.-S. Shin, *Foods* **2023**, *12*, 1801.
- [508] J. Zou, L. Wang, G. Sun, *ACS Sustainable Chem. Eng.* **2021**, *9*, 15365.
- [509] M. Nadi, S. M. A. Razavi, D. Shahrapour, *Food Science & Nutrition* **2023**, *11*, 6360.
- [510] World Health Organization, *WHO Estimates of the Global Burden of Foodborne Diseases: Foodborne Disease Burden Epidemiology Reference Group 2007-2015*, World Health Organization, **2015**.
- [511] H. Lee, Y. Yoon, *Food Science of Animal Resources* **2021**, *41*, 1.
- [512] A. Prasad, S. Khan, J. K. Monteiro, J. Li, F. Arshad, L. Ladouceur, L. Tian, A. Shakeri, C. D. M. Filipe, Y. Li, *Advanced Materials* **2023**, 2302641.
- [513] R. L. Scharff, *Journal of Food Protection* **2015**, *78*, 1064.
- [514] D. Knüsli, R. Friedli, J. Busenhar, *Food Safety in a Globalised World*, Swiss Re, **2015**.
- [515] S. Ahmed, D. E. Sameen, R. Lu, R. Li, J. Dai, W. Qin, Y. Liu, *Research Progress on Antimicrobial Materials for Food Packaging*, **2022**.
- [516] A. Istiqola, A. Syafiuddin, *Journal of the Chinese Chemical Society* **2020**, *67*, 1942.
- [517] J. R. Xavier, S. T. Babusha, J. George, K. V. Ramana, *Applied Biochemistry and Biotechnology* **2015**, *176*, 1498.
- [518] N. Wrońska, N. Katir, K. Miłowska, N. Hammi, M. Nowak, M. Kędzierska, A. Anouar, K. Zawadzka, M. Bryszewska, A. El Kadib, K. Lisowska, *International Journal of Molecular Sciences* **2021**, DOI 22.
- [519] H. M. Fahmy, R. E. Salah Eldin, E. S. Abu Serea, N. M. Gomaa, G. M. AboElmagd, S. A. Salem, Z. A. Elsayed, A. Edrees, E. Shams-Eldin, A. E. Shalan, *RSC Adv* **2020**, *10*, 20467.
- [520] Z. D. Moye, J. Woolston, A. Sulakvelidze, *Viruses* **2018**, *10*, 205.
- [521] B. Kim, E. S. Kim, Y.-J. Yoo, H.-W. Bae, I.-Y. Chung, Y.-H. Cho, *Viruses* **2019**, *11*, DOI 10.3390/v11030268.
- [522] T. Huang, Y. Qian, J. Wei, C. Zhou, *Polymers* **2019**, *11*, DOI 10.3390/polym11030560.
- [523] S. Sharma, S. Barkauskaite, A. K. Jaiswal, S. Jaiswal, *Food Chemistry* **2021**, *343*, 128403.
- [524] B. Guttman, R. Raya, E. Kutter, *Bacteriophages: Biology and applications* **2005**, *4*, 30.
- [525] A. Campbell, *Nat Rev Genet* **2003**, *4*, 471.
- [526] G. G. Greer, *Journal of food protection* **2005**, *68*, 1102.
- [527] C. Desplats, H. M. Krisch, *Research in Microbiology* **2003**, *154*, 259.
- [528] H.-W. Ackermann, *Research in Microbiology* **2003**, *154*, 245.
- [529] L. O'Sullivan, D. Bolton, O. McAuliffe, A. Coffey, *Annu. Rev. Food Sci. Technol* **2019**, *10*, 151.
- [530] C. Lee, H. Kim, S. Ryu, *Recent Advances and Future Trends* **2022**, *1*.
- [531] X. Zhang, Y. D. Niu, Y. Nan, K. Stanford, R. Holley, T. McAllister, C. Narváez-Bravo, *International Journal of Food Microbiology* **2019**, *305*, 108250.
- [532] L. Tian, L. He, K. Jackson, A. Saif, S. Khan, Z. Wan, T. F. Didar, Z. Hosseinidoust, *Nature Communications* **2022**, *13*, 7158.
- [533] A. E. Liana, C. P. Marquis, C. Gunawan, J. Justin Gooding, R. Amal, *Journal of Colloid and Interface Science* **2018**, *514*, 227.
- [534] E. Pinho, G. Soares, *Journal of Materials Chemistry B* **2018**, *6*, 1887.
- [535] A. Duconseille, T. Astruc, N. Quintana, F. Meersman, V. Sante-Lhoutellier, *Food hydrocolloids* **2015**, *43*, 360.
- [536] Q. Du, F. Liu, Q. Lei, *Applied Sciences* **2023**, *13*, 8640.
- [537] L. S. Peixoto, P. A. Melo, M. Nele, J. C. Pinto, *Macromolecular materials and engineering* **2009**, *294*, 463.
- [538] S.-J. Lee, S. C. Ung, C.-L. Kim, *Physica Scripta* **2024**, *99*, 055942.
- [539] Y.-T. Wang, H.-B. Zhao, K. Degracia, L.-X. Han, H. Sun, M. Sun, Y.-Z. Wang, D. A. Schiraldi, *ACS applied materials & interfaces* **2017**, *9*, 42258.
- [540] J. Gu, J. Huang, G. Chen, L. Hou, J. Zhang, X. Zhang, X. Yang, L. Guan, X. Jiang, H. Liu, *ACS Applied Materials & Interfaces* **2020**, *12*, 40815.
- [541] S. K. Mallapragada, N. A. Peppas, *Journal of Polymer Science Part B: Polymer Physics* **1996**, *34*, 1339.
- [542] C. Milampure, D. Jawale, S. Shingate, P. Mahala, U. Kulshrestha, S. B. Ghosh, S. Bandyopadhyay-Ghosh, *Materials Today: Proceedings* **2024**.
- [543] K. Afsana, S. P. Jolly, F. Akhter, in *Handbook of Global Health*, Springer, **2022**, pp. 1–28.
- [544] S. Hogan, J. Kerry, *Smart packaging technologies for fast moving consumer goods* **2008**, 33.
- [545] P. R. Ghosh, D. Fawcett, S. B. Sharma, G. E. J. Poinern, *International Journal of Food Science* **2016**, *2016*, 3563478.
- [546] F. Mustafa, S. Andreescu, *RSC advances* **2020**, *10*, 19309.
- [547] A. Lacombe, I. A. Quintela, Y.-T. Liao, V. C. Wu, *Frontiers in Food Science and Technology* **2022**, *2*, 1068690.